NASA CR- 166630

OCEAN DATA SYSTEMS, INC.

odsi

OCEAN DATA SYSTEMS, INC.
2400 GARDEN ROAD, MONTEREY, CALIFORNIA 93940 • 408/649-1133

Submitted to:
GODDARD SPACE FLIGHT CENTER
Greenbelt Road
Greenbelt, Maryland 20771

ADVANCED DEVELOPMENT OF ATMOSPHERIC MODELS

Final Technical Report

Prepared Under:
NASA-GSFC Contract No. NAS5-24468

June 1979

Prepared by:
Philip G. Kesel
Rodger A. Langland
Pamela L. Stephens
Robert E. Wellck
Paul M. Wolff
OCEAN DATA SYSTEMS, INC.
Monterey, California

TABLE OF CONTENTS

TABLE OF CONTENTS (Continued)

LIST OF CHARTS

LIST OF CHARTS (Continued)

LIST OF CHARTS (Continued)

LIST OF CHARTS (Continued)

LIST OF TABLES

LIST OF FIGURES

EXECUTIVE SUMMARY

Ocean Data Systems, Inc. has performed advanced development of a set of atmospheric analysis and prediction models in support of the SEASAT Program of NASA under Contract NAS5-24468 to Goddard Space Flight Center.

Analysis Model Development

The task objectives were to devise, implement and test modifications (to existing NASA-ODSI objective analysis models) to: (1) facilitate the use, distribution and coupling of ocean-area surface winds in the analysis models; and (2) examine satellite data dependencies in the analysis models.

The analysis models, which utilize a 125x125 polar stereographic grid of the Northern Hemisphere, have been modified in order to incorporate and assess the impact of (real or simulated) satellite data in the analysis of a two-day meteorological scenario in January 1979. Such program/procedural changes include:

- a provision to utilize winds in the sea level pressure and multi-level height analyses (1000-100 MBS);
- the capability to perform a pre-analysis at two "control levels" (1000 MBS and 250 MBS);
- a greater degree of wind- and mass-field coupling, especially at these control levels;
- an improved facility to bogus the analyses based on results of the pre-analysis; and
- a provision to utilize (SIRS) satellite thickness values and cloud-motion vectors in the multi-level height analysis.

Once modified, the analysis models were tested (and adjusted further) using observations for January 1979 to establish workable procedures and parameter settings. Only the 19-21 January period is highlighted in this Final Report.

Two types of experiments were conducted (and documented) to determine the potential impact of real (or simulated) satellite data on this set of models:

- an ocean-area surface wind experiment to determine the extent to which SASS winds might be used to enhance the specification of sea-level pressure (and low-level flows, generally) during a two-day analysis sequence, and

- an upper-level satellite information experiment to assess the impact of cloud-motion vectors and SIRS soundings during a two-day analysis sequence.

In the surface wind experiment, suitably-adjusted ship winds (used in lieu of unavailable SASS winds) were used, while associated ship pressures were withheld, in specified octants of the hemisphere. Location of octants (for withholding pressure reports) depended on the analysis time. This analysis sequence ran from 0000Z 19-21 January and led to Chart Set C. A second sequence for the same period in which both wind and pressure reports were withheld in the same time-dependent octants (Chart Set D) was executed to provide an upper bound on analysis error. The same upper-air data base was used in both sequences. Any differences between corresponding charts in Sets A, C and/or D are attributable to changes in the sea-level pressure analyses (and the set of twelve-hour forecasts used to bootstrap each analysis sequence). Chart Set A is the baseline analysis sequence which used all available observations.

Results from such tests indicate that the surface winds had a positive impact on the SLP analyses, and reduced the potential analysis error by about 25% in the two-day sequence. Such effects are propagated vertically into the entire troposphere through the distribution and coupling mechanisms in the models. The differences between Set C and Set A analyses tend to take on the

spatial scales peculiar to the number and locations of withheld pressure reports (as would be expected). But, since SASS wind sets would be quite large (compared to the number and distribution of ship reports), we would expect that: (1) the differences would be of meteorological scale; and (2) the "potential" analysis error would be greatly reduced.

Prediction Model Development

The task objectives were: (1) to implement and test an iterative procedure (based on the Temperton scheme) in order to dynamically condition the initial state specification; (2) to modify that procedure and examine the effects on model behavior and program efficiency; (3) to modify the program to ingest new data at a second time origin and to dynamically condition the new state (at the second time origin); and (4) to produce short-range forecasts to assess the impact of dynamic initialization.

The (program) context for carrying out these task objectives was prepared and tested. A version of the five-layer, coarse-mesh (63x63) prediction model (PECHCV) was modified to permit the dynamic conditioning/adjustment [using an iterative procedure devised by Temperton (1973) and tested in a multi-layered model by Kesel and Wellck (1975)] of any state specification (i.e., the specification of model variables at any time origin). The new version, referred to as DYNMOD, has been coded to permit the selection (via data cards) of any number of iterations ("orbits") of any orbital length. For this study, the length consists of five (time) steps forward and five steps backward (about some time origin) per orbit. Even the "static initialization" case (zero orbits) can be handled by DYNMOD, since all of the dynamic initialization runs begin with static initialization.

Analysis model outputs (for 19/0000Z, 19/1200Z, and 20/0000Z January 1979) were used for the static initialization phase of the forecasts. In some forecasts this static initialization was augmented by a specified number of Temperton-style orbits before commencing the two-day forecasts (dynamic initialization at a single time origin). In still other forecasts, gridded values (for

a pie-shaped region in the Pacific) from an analysis of conditions twelve hours into the forecast period were ingested/assimilated and dynamically adjusted using additional orbits before completing the remainder of the two-day forecast (i.e., dynamic conditioning at <u>two</u> time origins with data assimilation at the second). Identifiers for these forecasts are as follows:

Run Type	Number of Orbits	Initial Conditions for		
		19/0000Z	19/1200Z	20/0000Z
static initialization only	0	E	-	-
dynamic conditioning at a single time origin	6	F	-	-
	12	G1	G2	G3
dynamic conditioning at two time origins plus data assimilation	12+12=24	H1	H2	H3

All forecasts were compared to the appropriate analyses within the "baseline" analysis sequence (which used all available observations). Additionally, model behavior was monitored via a set of diagnostics computed each forecast hour. The most useful measure of dynamic conditioning of model variables is the (squared) mass divergence (at each model level).

The results from these forecasts are described in terms of program efficiency, model behavior and forecast quality.

- <u>Program Efficiency</u>

The FTN (Fortran) program DYNMOD is modular, quite general, and substantially transportable. It was executed on both a CDC CYBER 175 (using NOS/BE) and a CYBER 74 (using SCOPE). Central memory (user) requirement is

65K (decimal) words. No Extended Core Storage (ECS) was used. About three million words of mass storage are needed for each two-day forecast.

Dynamic initialization may be performed using any number of orbits (including zero orbits) of any orbit length. Data assimilation in a specified geographical region and dynamic conditioning at a second time origin are "hardwired" in the code at present. With only minor changes thereto, other regions and/or other time origins could be handled.

On a CYBER 74, static initialization takes 3,770 CP-seconds and 7,460 seconds of I/O. There is a substantial overlap of CP and I/O during model integrations, but not during initialization and output preparation. Each orbit adds about 190 CP-seconds and 400 I/O-seconds to these totals.

- Model Behavior

Dynamic adjustment/conditioning of any state specification does not enhance the validity of that specification. Rather, it enhances the quality of the relationships between the mass fields and winds, especially in the numerical sense. Through numerical/dynamic consistency, initialization shock is reduced and modeling of secondary physical effects is improved (in the first several forecast hours).

Examination of the (squared) mass divergence statistic in Forecasts E, F, and G1 shows that: (1) the reduction of initialization shock is proportional to the number of orbits made; (2) dynamic initialization greatly accelerates the geostrophic adjustment process in the model -- a task which would take the model itself from one to two forecast days to accomplish with its own "adjustive" powers; (3) the use of twelve orbits was satisfactory for this study.

Dynamic conditioning appears to have less impact on the layer-mean kinetic energy (in these two-day forecasts). The differences noted between the static and dynamic (initialization) cases tend to be small (at the outset) and remain small throughout the forecasts. The adjustments noted tended to be in the right direction (i.e., closer to values the forecast ultimately produces).

There is an impact on the model's precipitation mechanism. Convective precipitation tends to be reduced (i.e., the size of the affected area and the average amounts). Large-scale precipitation appears to be increased by about 10-20 percent. (Vertical velocity patterns become more mature during the adjustment process -- giving rise to more precipitation in the first forecast day.)

- Forecast Quality

Differences in the type/complexity of the initialization did not lead to large differences in the two-day forecasts which were produced. This appears to be true in spite of the numerical/physical benefits just discussed.

Forecast Runs E, F and G1 (which all used initial conditions for 0000Z 19 January) produced RMSE scores at 500 MBS of 46.2 - 46.4 meters, and 4.97 - 4.99 MBS at sea level. Forecast H1, which ingested new (analysis) data for 19/1200Z, had 46.4 meters and 5.01 MBS at 500 MBS and sea level, respectively. Data ingestion did not improve the forecast error.

Forecasts G2 and H2, initialized at 19/1200Z, differed in RMSE scores by only 0.05 MBS and 0.9 meters at sea level and 500 MBS, respectively. Thus, data assimilation produced a positive, but small impact on the forecast.

Forecasts G3 and H3, initialized at 20/0000Z, differed in RMSE scores by only 0.06 MBS and 1.4 meters -- with data assimilation producing a positive but small impact.

An examination of the central pressures and pressure profiles of major low-pressure systems (handled by these forecasts) indicates a minor (and mixed) impact when using dynamic conditioning and/or data assimilation. Some features benefitted and others did not benefit.

We have tentatively concluded that the computational expense is difficult to justify under the conditions of this study. The lack of precise knowledge of initial conditions over the world's oceans is a much larger problem than problems related to numerical consistency.

I. INTRODUCTION

Ocean Data Systems, Inc. (ODSI) has designed, developed and tested atmospheric analysis and prediction models of varying (grid) resolution in support of the SEASAT Program of the National Aeronautics and Space Administration (NASA): (1) under Contract NASW-2558 to Econ, Inc.; and (2) under Contract No. 954668 to the Jet Propulsion Laboratory (JPL). Some advanced development of these models was performed under Contract No. NAS5-24469 to Goddard Space Flight Center (GSFC). In the latter effort, procedures for enhancing the computational viability of SEASAT-type data were identified and tested. Specifically, the effects of three discretionary procedures in objective analysis were studied: (1) varying the weights in the Pattern Conserving Technique; (2) varying the influence functions for observations: and (3) examining the effects of using wind information in analyses of mass-structure variables.

Finally, this Technical Report covers additional advanced development of the models under Contract No. NAS5-24468 to GSFC. The effort consisted of: (1) modifying the analysis programs and determining the impact of (real or simulated) satellite observations on the analysis of a meteorological scenario in January 1979; and (2) developing and testing a primitive-equation prediction model which is initialized using dynamic methods, and which is capable of both data assimilation and dynamic re-initialization at a second time origin. These advanced development efforts have focused on ways to prepare a better "model context" for assessing the utility of SEASAT-type observations in analysis and prediction. Ways were sought to ingest and to distribute such information into (spatial) scales which are less likely to get "washed out" in the adjustment period of a short-range prediction using a primitive-equation model. The objective analysis program sequence was modified rather extensively in order to facilitate the use of both satellite-sourced winds and temperature profiles, as well as the coupling of wind and mass-structure information.

The testing of the analysis and prediction models was carried out with a real data set for January 1979 made available to ODSI by Fleet Numerical Weather Central, Monterey. For purposes of this Final Report, however, only the observations and computer runs for the period 19-22 January were used.

FNWC also provided some computer support in the early phases of this contractual effort under an agreement between FNWC and NASA. As the work progressed to those phases requiring more frequent turnaround and longer production runs, it became necessary to shift the data base and computer programs to other computational facilities. This led to delays and to additional work. Nevertheless, the work has been successfully completed. This transition to other computer systems was facilitated, in part, by FNWC which provided to ODSI (through NASA) some of the system software peculiar to the FNWC system environment.

Section II pertains to analysis model development. There is a description of the models, and the descriptions and test results of a marine-wind experiment and an upper-level satellite-information experiment. Section III provides the descriptions of and test results from use of prediction models initialized using conventional (static) and dynamic methods. Comparative results for one- and two-time-origin dynamic initialization model executions are provided. Sections IV, V and VI contain the charts, tables and figures, respectively. Five appendices are also provided. Appendices A and B provide a ready reference for readers interested in the use of PCT in scalar and vector analyses, respectively. The derivation of the Mass-Structure Linear Transformations is provided in Appendix C. Appendix D describes the procedure used to merge/check mandatory and significant level radiosonde data. A brief description of the procedure used to obtain temperatures and heights above the 100 MB level is contained in Appendix E.

II. ANALYSIS MODEL DEVELOPMENT

The objective analysis models developed by ODSI for the SEASAT studies employ the Pattern Conserving Technique (PCT). The models and procedures were modified rather extensively in order to accomplish the proposed objectives in this effort. The description of PCT is provided in Part A, as well as in Appendices A and B to this Report. Part A also: (1) outlines the program sequence used to complete the several analysis production tests; and (2), describes the modifications to models and procedures necessary to accomplish study objectives. Part B describes the impact of real (and/or simulated) satellite observations on the analyses from a two-day scenario in January 1979. Part B is presented in three parts. Part 1 introduces the "baseline" analysis sequence produced using all available data. Part 2 describes a marine-wind experiment in which shipboard surface winds (used in lieu of SASS winds) are employed to determine the extent to which ocean-area surface winds may be used to help maintain the sea-level pressure specification in a two-day sequence. Part 3 describes an upper-level satellite information experiment in which the impact of cloud-motion vectors and SIRS reports is determined (in the same scenario).

A. Description of Models

1. The Pattern Conserving Technique

The procedure/method used by ODSI for all analysis modeling in support of SEASAT is called the Pattern Conserving Technique (PCT). It has been used by ODSI to analyze sea-surface temperature; sea level pressure; and the multi-level temperatures, heights and winds (from 1000-100 MBS). It is a multi-cycle procedure in which each cycle consists of:

- Assembling the observations to grid points.
- Solving the PCT minimization equation.
- Re-evaluating the weight of each observation.
- Adjusting the influence function for each observation.

The method lends itself very well to the "engineering adjustments" which have to be accomplished in operational analysis. With an appropriate selection of weights, control can be exercised over which of the characteristics will be emphasized in the final analysis. In the assembly stage, one exercises control over the spatial scales being affected by each datum. The relative importance of each observation -- as it changes in each cycle -- may also be controlled. The complexity of the minimization equation may be tailored to the purpose of the analysis. (In this contract effort, for example, the pressure and height analyses were modified to use wind information.) Filtering may be adjusted as desired, even though the "perfect filter" does not exist.

A rather complete description of the models (the PCT method; relevant equations; computer program descriptions) is available in Volume II of the ODSI Final Report to the Jet Propulsion Laboratory (dated 30 September 1977) under Contract 954668. Additional model discussion/description is contained in the ODSI Final Report to Goddard Space Flight Center (dated November 1978) under Contract NAS5-24469. Appendices A and B to this report explain the use of PCT in the analysis of scalars and vectors, respectively, for readers without access to the aforementioned references.

2. Analysis Program Sequence

All of the analysis results presented in this report were generated using a 125x125 grid-point polar stereographic projection. This grid has a resolution of 190.5 kilometers at 60° latitude. This resolution should be better able to accommodate the spatial scales observed by SEASAT, yet is not as computationally burdensome as the 187x187 grid used by ODSI previously.

Figure II-1 depicts the order of execution of the jobs required to complete one analysis sequence. The jobs are executed serially since the output from one program is often required input for the next program in the sequence. The sequence is initiated every 12 hours with the analysis date and hour specified as the current "date-time group" (DTG). Once the DTG is set and the required data records are made available, a first guess field for a -6 hour (6 hours before

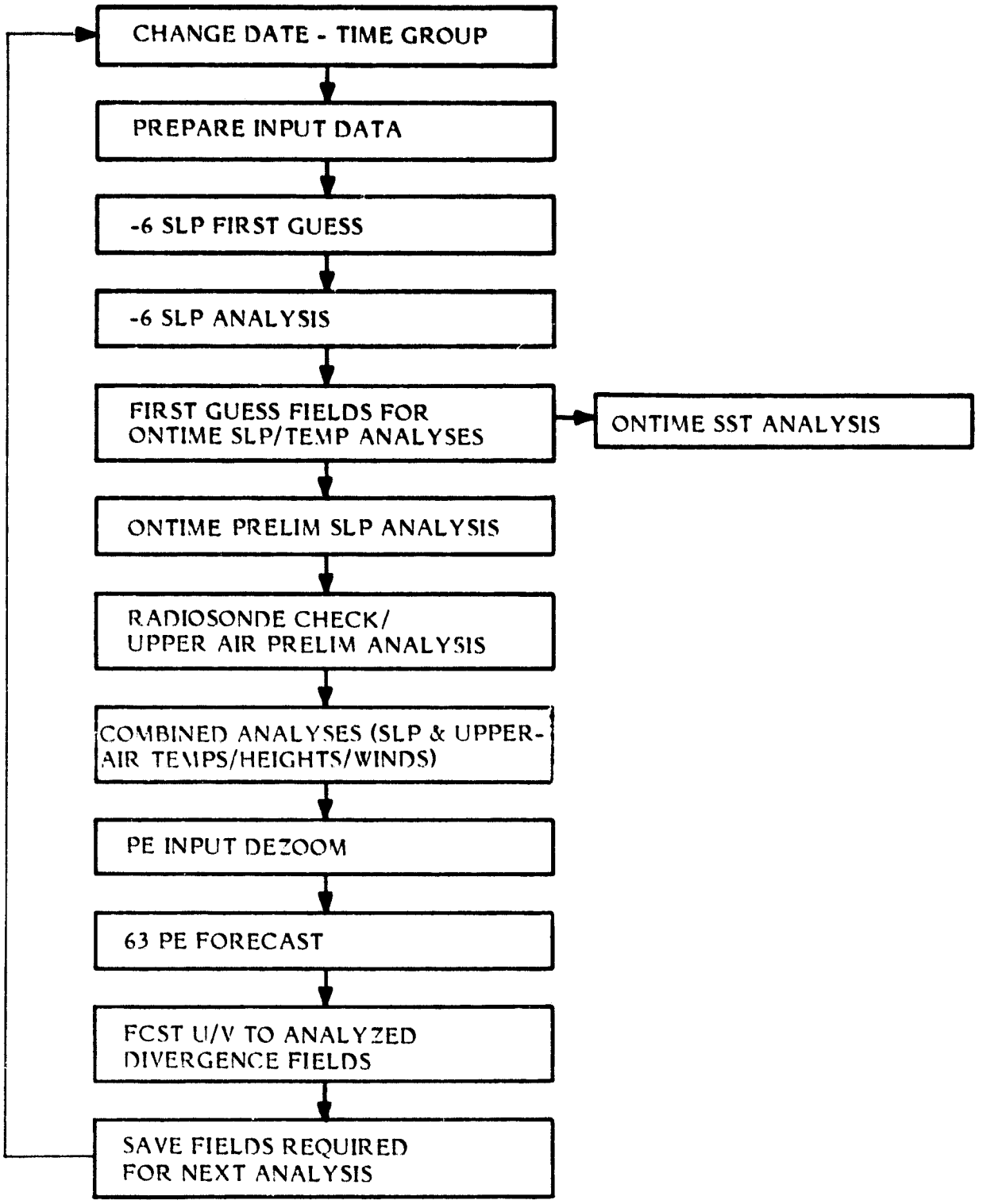

FIGURE II-1: ANALYSIS/PREDICTION SEQUENCE

the current DTG) sea level pressure (SLP) analysis is generated. To prevent time lag, this guess field is time-centered, combining the 12 hour old SLP analysis and the 12 hour SLP forecast from the last sequence run. With this guess field, the -6 hour SLP analysis is performed using the PCT as described in Appendix A. The resulting field serves as the major input for the ontime SLP guess field which is produced in the next program. At the same time, the guess fields are generated for the preliminary upper air temperature analysis. The time-centered temperature guess fields represent a blend of the 12 hour old temperature analyses and the previous run's 24 hour forecast temperature fields. While the guess program is executing, the sea surface temperature (SST) analysis can also be run since its execution is independent of other analyses. With the completion of the guess field program, the preliminary ontime SLP analysis is initiated. This is followed by a program which checks the validity of the radiosonde data. (This radiosonde checking program is described in Appendix D). Next, the preliminary upper air analysis is performed. [The preliminary upper air analysis produces upper air temperature and height guess fields for the final analysis which are consistent with two "control" levels. The 1000 MB and 250 MB levels were selected because they generally have the best data coverage. The 1000 MB level is derived from the data-rich sea level pressure analysis, and 250 MB is the level where both aircraft reports and satellite cloud-motion vectors are concentrated. Deriving the other guess fields from the analyses at these two levels provides a consistent and vertically coupled guess field structure.] There is now a complete set of guess fields and the final combined analysis (final SLP and upper air temperature, height, and wind analyses) can be performed. To review, the key steps in the upper air analyses, preliminary and final, are:

- The 1000 MB height guess is generated using the "preliminary" SLP analysis and the preliminary 1000 MB temperature guess.

- The 1000 MB height analysis is performed.

- The preliminary first-guess height fields (8) for the 950-250 MB levels are generated using the 1000 MB height and a hydrostatic integration of the preliminary first-guess temperatures.

- The preliminary 250 MB height analysis is performed, using the bogus capability as necessary.

- The preliminary D-values for the seven (7) pressure levels between 1000 and 250 MBS are computed by using a ln p interpolation of the preliminary D-values at 1000 and 250 MBS.

- The twelve (12) preliminary heights (1000-100 MBS) are then "transformed" into ten (10) static stability values -- which are then adjusted as necessary.

[Note: The reader should see Appendix C for details of the Mass Structure Linear Transformations being used. In order to retrieve twelve heights (or temperatures) from these static stabilities, two additional conditions must be specified: we have chosen the 1000 MB height and the 1000-250 MB thickness.]

- The twelve (12) first-guess temperature fields are retrieved from the static stabilities, 1000 MB height and 1000-250 MB thicknesses.

- The final SLP analysis is performed, bogusing as necessary.

- The upper-air temperature analysis is completed using guess fields just retrieved.

- A 1000 MB first-guess is generated from the final SLP and the 1000 MB temperature fields.

- The height analysis is performed one level/layer at a time, using the heights at the level just analyzed and the final analyzed temperatures (for the given layer) in a hydrostatic integration to produce the guess heights for the next level to be analyzed.

- Using regression equations described in Appendix E, the temperature/height values are extended above 100 MBS (to 10 MBS).

- The winds at twelve (12) levels are analyzed using the PCT method described in Appendix B.

A five-level 63x63 grid-point primitive equation forecast model is used to bootstrap the analysis sequences. To initialize the forecast model, the required 125x125 analysis fields must be "dezoomed" to 63x63 fields. The model (without dynamic initialization) is integrated to 24 hours to produce the required forecast input fields for the next analysis. Since forecast velocity divergence is required as a constraint in the wind analysis, a separate program is run to create these fields.

3. Program/Procedural Modifications

A considerable amount of time and thought was given to possible approaches to the proposed analysis model modifications. The design which was selected provided the following essential features: (1) it was capable of utilizing all available satellite (and conventional) observations; (2) it emphasized the use of ocean-area surface winds, of cloud-motion vectors in the 300-200 MB layer, and of satellite temperature profiles; (3) it was capable of using wind information in the sea-level pressure and multi-level height analyses; (4) its complexity was numerically and dynamically consistent with the requirements and characteristics of the prediction model; (5) it was computationally economical; (6) the work could be successfully accomplished within project resource limitations; (7) it had the potential for fulfilling the task objectives, i.e., to distribute the reported information and to couple the estimates of the winds and mass-structure parameters.

Several types of analysis program/procedural modifications were incorporated for this contractual effort. Brief descriptions are listed below. In subsequent paragraphs, each modification will be described more fully.

- analysis model re-design allowing for a pre-analysis at the 1000 MB and 250 MB control levels -- with a facility for bogusing as necessary.

- provision to utilize wind information (gradients) in the sea-level pressure and multi-level height analyses.

- changes in the (data) assembly procedure and in the number of analysis cycles (in the sea-level pressure and multi-level temperature analyses) to better accommodate and distribute observed information.

- provision to return (functional values) to long-term climatology in regions of few or no recent observations -- in order to control the analyses.

- time-centered blending of first-guess fields, using a recent-past analysis and a short-range (PE) forecast.

- changes in the type and degree of filtering (of model outputs).

The most significant modification of the analysis program set involved a major re-design which permits a pre-analysis at the 1000 MB and 250 MB "control levels" (new feature). At the control levels, which tend to be data rich anyway, use of the bogusing capability is encouraged and facilitated in order to arrive at the best possible specification of analysis variables. The thickness values from satellite (height) observations are relied upon to produce the (important) 250 MB height pre-analysis. The 1000 MB height first-guess field is generated from a (very) data-rich sea-level pressure analysis. Very often, the final 1000 MB heights are subject to change with the addition of 500-600 radiosondes and with the (different) procedures that are embedded in the upper-air analysis programs. Winds are allowed to strongly influence the height patterns at both control levels. The D-values produced at the control levels in the pre-analysis are then distributed to remaining (intermediate) pressure levels

using ln p interpolation. Consistent temperatures are generated from this height structure using the linear transformations described in Appendix C.

Second, the PCT approach proved to be very useful when it was decided that wind information had to be incorporated in pressure and (multi-level) height analyses. Each wind report is checked against a gross tolerance which is similar to that being used in the wind analysis. If accepted, the velocities are then converted to height/pressure gradients. These gradients are substituted for the (height/pressure) guess-field gradients at the nine grid points (3x3) closest to the wind observation. In this manner, the gradients act as a constraint on the solution of the PCT minimization equation(s). (The calculations are made in the subroutine BKGRND.) The (3x3) stencil of grid points mentioned above could not be enlarged without a major recoding effort because of the central memory limitation. Otherwise, the spatial scales being influenced in this way might have been quite different.

The assembly procedure (used to get the observed values to the grid points) was also modified: (1) to better distribute observed information; and (2) to make the procedure more efficient and still meet the computer resource limitations. For the most part, the procedure which was used (previously) with the 63x63 models still applies. The exceptions are noted below:

- Observations south of 5°N are not used (they cause more problems than they solve).

- For the 125x125 grid, observations are sorted according to the "J-row" (J=1,I), and then grouped into five-row sets for inclusion/assembly. The central memory restriction dictates that only one such five-row set can be assembled at a time.

- The region influenced by each observation (now) depends upon: data density; cycle number; analysis type; and (in the SLP and SST) the differential properties of the guess field. Generally, a datum doesn't affect grid points very much if such points are already affected by closer and/or more

densely-spaced observations. The influence region gets smaller with each cycle through the analysis. The region being affected by a report is larger in the upper-air analyses than at sea-level, other factors being the same. Regions with strong gradients and/or curvature cause the influence radius to be reduced according to the magnitudes of such gradients and/or Laplacians, but the provision applies only to the analysis of sea-level pressure and sea-surface temperature. Finally, the toss-out criterion also depends (now) on latitude - with the tolerance being reduced as the latitude decreases.

- Each analysis (except for the wind analysis) now returns to long-term climatology in regions for which there are few or no recent observations. North of 20°N, the specification returns at a 5% rate each analysis time. Below 20°N the rate of return is inversely proportional to latitude. The information density, of course, is the primary consideration in the calculation.

The analysis programs have been modified so that they may be re-started from a given DTG -- but with slightly altered procedures and constants for the first such DTG in the new analysis sequence. Such alterations consist of:

- an increase in the data reject limits.
- extra smoothing and filtering of outputs (since the first guess for the re-start is climatology).
- altered PCT weights in the sea-level pressure and height analyses (these analyses use wind gradients which enter via the PCT equations).
- data weights are not re-evaluated after each analysis cycle.
- the PCT stage is by-passed in the U/A temperature analyses.

B. Impact of Satellite Observations on Analysis Structures

After describing the "baseline" analysis sequence, the remaining material is presented in two major parts: (1) an ocean-area surface wind experiment; and (2) an upper-level satellite information experiment. Each type of result may be compared to that obtained in the baseline analysis sequence.

In the part of the study involving objective analysis, there were two proposed objectives: (1) to implement and test an analysis procedure to distribute surface information vertically into the lower troposphere, and to couple the winds and mass-structure variables; and (2) to examine satellite data dependencies in the analysis models. These experiments were conducted in order to demonstrate the proposed objectives.

Four separate two-day analysis sequences were produced. Each sequence is presented with its own chart set. The key features of each analysis chart set are defined below:

Set A: Baseline analyses made using all available data.

Set B: Analyses made without cloud-motion vectors and SIRS reports.

Set C: Analyses in which shipboard pressure reports are withheld (in specified octants) but associated ship winds are used.

Set D: Analyses in which entire ship reports are withheld (in specified octants).

1. Baseline Analyses

The set of ODSI-NASA objective analysis models (programs) was used to produce analyses for a scenario extending from 0000Z, 19 January, through 0000Z, 22 January 1979. The "baseline" set of analyses utilized all

available observations. This included: sea surface temperature; sea level pressure; and the temperatures, heights and winds at twelve constant-pressure levels from 1000 to 100 MBS. The heights and temperatures at 50 MBS, used to initialize the prediction model, are produced using regression equations described in Appendix E. Winds are derived from the heights at the 50 MB level.

Although Versatec charts were produced for most analysis parameters and levels, only a portion of them is included in this report. Charts IV-1 through IV-26, referred to as Chart Set A, contain the relevant information in the baseline analysis set. These should be examined by the reader in order to understand the meteorological context in which the experiments were conducted.

Charts IV-20 through IV-22 contain the 48-hour analysis change patterns at sea level and 500 MBS. In this scenario one can see some very large (and interesting) changes occurring everywhere except in southeast Asia and central Europe. In IV-20, for example, there are many change centers with magnitudes greater than thirty (30) millibars in this two-day period. The chart discussion will tend to focus on the Pacific area. Thus, the reader should examine the evolution of pressure systems shown in Charts IV-1, IV-8, IV-10, and IV-12, in that region.

In Section II, the emphasis is placed on sea level pressure, and the temperature and wind at both 900 MBS and 250 MBS, levels at which cloud-motion vectors seem to be most plentiful. In Section III, the emphasis is placed on sea level pressure and 500 MB height, levels at which prediction models are often evaluated. Thus, Chart Set A includes analyses which will be used to discuss the results of both the analysis and prediction tasks.

2. Marine-Wind Experiment

The discussion is presented in two parts. First, there is a description of the experiment and the (additional) special modifications made in order to accomplish the proposed objectives. Then, the results of the analysis test demonstration are presented.

a. Description

In this analysis task, the objective was to devise, implement and test appropriate modifications to the objective analysis models (under development for NASA by ODSI) so that SASS winds (and other satellite data) could be utilized to enhance the specification of the initial conditions (in ocean areas) for short-range atmospheric prediction. Specifically, ODSI proposed to devise and test a method for distributing surface-level information vertically, into the lower troposphere and for coupling the available (estimates of) wind and mass-structure parameters. In addition, ODSI proposed to examine what may be termed "data dependencies" in this particular set of analysis programs/models.

Having referred (earlier) to limitations on project resources, it is important to note that the initially-envisioned comprehensive data set (containing SASS winds) did not materialize. Thus, ODSI decided to simulate SASS winds with ship (surface) winds -- and to design an experiment to determine the extent to which ocean-area surface winds may be used to maintain/enhance the sea-level pressure specification (as well as the flows in the lower troposphere). Ship winds and pressures had to be withheld (say) from certain octants to define an "upper bound" on analysis error in one two-day analysis sequence; but only ship pressures would be withheld from the same octants in a second analysis sequence for the same two-day period. The octant(s) in which the ship reports were handled in this manner represented a simulation of the time-varying areal coverage of satellite data. Finally, the ship winds had to be "adjusted" in an appropriate way to make them more acceptable to the experiment.

In the sea-level pressure analysis, for example, the geostrophic wind law was altered in order to simulate the reduction of speed due to friction and the turning of the wind across the isobars. The coefficients, R and S, control the speed and direction, respectively, in the final version of the wind law shown below:

$$u = -\frac{1}{M}\left(f\frac{\partial p}{\partial y} + S\frac{\partial p}{\partial x}\right) \qquad [II.1]$$

$$v = \frac{1}{M}\left(f\frac{\partial p}{\partial x} - S\frac{\partial p}{\partial y}\right) \qquad [II.2]$$

where $M = R\rho (f^2 + S^2)$. Wind observations must first pass a gross-error check in which they are compared to winds derived from the first-guess pressure distribution using [II.1] and [II.2]. If the speed difference exceeds a specified fraction of the guess-field speed, the observation is not used. If it is accepted, the pressure gradients at the nearest grid point(s) are set to the values implied by that observation. If more than one observation influences a grid point, the implied values from the (several) reports are averaged. With appropriate tuning of the PCT equation constants, an optimum mix of assembled (functional) values and differential properties may be obtained.

b. Results of Tests

Chart Sets C and D will be referred to in this discussion. Chart Set C contains selected charts from the sequence of analyses in which ship winds were used -- but associated ship pressures were withheld in specified octants. The objective was to simulate the extent to which SASS winds might be used to assist in the specification of the sea-level pressure. Through coupling mechanisms in the three-dimensional analysis, effects should also be discernible at and above 900 MBS. In Chart Set D, both the pressures and winds were withheld in the same specified octants. This analysis set may provide an upper bound to the analysis error in this scenario which runs from 0000Z 19 January through 0000Z 21 January 1979. Thus, there were nine (9) sea-level pressure analyses (spaced every six hours) and five (5) upper-level analyses (spaced every twelve hours) in each of the two sequences (Set C and Set D). Finally, it is also possible to assess the interactive/cumulative effects within each analysis sequence since each sequence is connected by its own set of (12-hour) PE forecasts which produce the necessary first-guess fields.

Chart IV-47 (from Set C) contains the sea-level pressure analysis for 0000Z 19 January. About 280 (ship) pressure reports (6% of total) were withheld from this analysis. From these 280, there were 232 wind observations accepted by the analysis. This analysis should be compared to the corresponding (Set A) baseline analysis provided as Chart IV-1. The difference

between these Set C and Set A analyses is provided as Chart IV-53. At 0000Z, the octants being affected are in the eastern Atlantic and western Pacific. In the Atlantic the differences are generally smaller than three (3) millibars -- but in the Pacific they tend to be much larger (8 millibars in one place).

Charts IV-48 and IV-49 contain the (Set C) 900 MB Temperature and Wind Analyses, respectively, for 0000Z 19 January. Compare these to Charts IV-2 and IV-3 in the baseline sequence and examine the differences. Charts IV-54 and IV-55 actually contain the corresponding differences for the 900 MB temperatures and winds, respectively.

Next, we will discuss the charts two days into the (interactive) analysis sequence. Chart IV-50 (Set C) contains the sea-level pressure analysis for 0000Z 21 January. About 314 ship pressure reports (6.7% of total) were withheld from this analysis. Of these 314 reports, there were 236 wind observations accepted into the analysis. Compare this analysis to the corresponding analysis from the baseline analysis set shown in Chart IV-12. The difference between the Set C and Set A analyses is shown in Chart IV-56. Although it is difficult to determine visually, the (RMS) differences on 21 January are slightly smaller than on 19 January (0.55 vs. 0.62). Indeed, whatever cumulative differences there might be are not discernible in either the difference charts or statistics. The differences at each analysis time are primarily related to the number/location of pressure values being withheld, as well as to the viability of spatial scales portrayed in each analysis.

Charts IV-51 and IV-52 (from Set C) contain the 900 MB Temperature and Wind Analyses, respectively, for 0000Z 21 January. Compare these to the corresponding baseline analyses shown in Charts IV-14 and IV-15. The differences between corresponding 900 MB analyses are provided as Charts IV-57 and IV-58. Table V-1 contains the RMS differences between Set C and Set A analyses in the sequence. The RMS temperature difference at 900 MBS varied from 0.02-0.04 degrees Celsius during the two-day sequence; and the corresponding RMS height difference at 900 MBS varied from 2.1-3.4 meters. Also, the RMS wind component difference varied from 0.46-0.71 meters per second. Note that the differences extend to the 250 MB level, where they are about half as large as at 900 MBS, generally.

The charts in Set D may be used as a control — an upper bound on the analysis error in that analysis sequence from which entire ship reports (pressures and winds) were withheld in the same octants used in Set C.

Chart IV-59 (Set D) shows the sea-level pressure analysis for 0000Z 19 January. Compare this to Chart IV-47 (from Set C) and to Chart IV-1 (from Set A). Chart IV-65 contains the difference between the Set D and Set A sea level pressure analyses at this time. This may be compared to Chart IV-53 containing the difference between Set C and Set A. Or, finally, examine Charts IV-71 and IV-72 which show the differences between Set D and Set C analyses on 19 and 21 January, respectively. The spatial scale of these differences reflects the number and location of withheld reports, primarily.

Charts IV-60 and IV-61 (Set D) show the 900 MB Temperature and Wind Analyses, respectively, for 0000Z 19 January. Compare these to the corresponding charts in the baseline analyses (Charts IV-2 and IV-3), as well as to the corresponding charts in Set C (Charts IV-48 and IV-49). The differences between Set D and Set A analyses are contained in Charts IV-66 and IV-67.

Next, we will introduce and discuss the (Set D) analyses two days into the (interactive) sequence. Chart IV-62 contains the sea-level pressure analysis for 0000Z 21 January. The difference between this analysis and the baseline analysis is shown in Chart IV-68. Table V-2 contains the RMS differences between Set D and Set A analyses for several parameters/levels. [Generally, one would expect that the (Set D-Set A) differences would be greater than the (Set C-Set A) differences. A comparison of Table V-2 with Table V-1 shows that such an expectation is realized in two-thirds of the parameters/levels tabulated.] The sea-level pressure (RMS) values in the two tables indicate the use of the winds reduced the analysis error by about 25 per cent. The greater number of SASS winds, however, would lead us to expect a much greater impact on (operational) sea-level pressure analyses. Secondly, there is little indication of cumulative effects in these sequences. Had the (initial) differences been in larger spatial scales (as they would be with SASS winds), we would expect to see more cumulative (interactive) effects.

Charts IV-63 and IV-64 contain the 900 MB Temperature and Wind Analyses, respectively, for 0000Z 21 January. Compare these analyses to the corresponding charts in Set A (Charts IV-14 and IV-15) and in Set C (Charts IV-51 and IV-52). The 900 MB temperature and wind differences (Set D minus Set A) are provided as Charts IV-69 and IV-70, respectively.

3. Upper-Level Satellite Information Experiment

As discussed previously, model modifications were made which set the stage for this sensitivity study employing the three-dimensional temperature, height and wind analysis codes. In this experiment, the main objective was to assess the impact of satellite temperature/height profiles and cloud-motion vectors on a two-day analysis sequence.

a. Description

The January 19-21 period was not only meteorologically interesting, but one in which the numbers of observations were greater than usual. Table V-3 shows that the numbers of radiosonde/rawinsonde soundings available for the upper-air analyses varied from 550 to 590, with an additional 50 to 85 SIRS profiles. Table V-4 contains the numbers of cloud-motion vectors, which varied from about 110 to 260 with the typical concentrations both at 900 MBS and in the 300-200 MB zone. (The level of each wind value is specified to the nearest ten millibars.) Table V-5 indicates the even larger numbers of aircraft wind reports. These were useful for proper specification of high-level flows, generally, but extremely so at the 250 MB control level. Although the impact of cloud-motion vectors was both measurable and positive (in this experiment), it would probably have been greater were it not for the fact that aircraft winds had already played such a large role in specifying flows at high levels.

SIRS soundings presently contain heights from 850 MBS through 100 MBS. Since these heights are referenced to a NOAA control field, the absolute heights are of less value to these (ODSI) analyses than the implied thickness values. The ODSI 850 MB height, therefore, is employed to compute heights which are consistent.

b. Results of Tests

Chart Sets A and B will be referred to in this discussion. Chart Set A contains selected charts from the baseline analysis sequence -- produced using all available observations. Chart Set B contains corresponding analyses from the separate analysis sequence from which both SIRS soundings and satellite cloud-motion vectors were withheld. The two-day sequence began with observations for 0000Z 19 January. During this sequence, the corresponding sea-level pressure analyses for Sets A and B will be more or less identical. But, the upper-air temperature, height and wind analyses for the two sequences will diverge. The following discussion will concentrate on the differences at 900 MBS and 250 MBS.

Charts IV-27 and IV-28 contain the (Set B) 900 MB Temperature and Wind Analyses, respectively, for 0000Z 19 January. Compare these to Charts IV-2 and IV-3, respectively, in the baseline analysis sequence. The differences between Sets B and A are provided as Charts IV-38 and IV-39. On Chart IV-38, note three areas where the 900 MB temperatures differed by more than one degree Celsius. These patterns are of meteorological scale. There are two additional places where differences exceed 0.5 degrees Celsius. On Chart IV-39, the wind differences tend to be less than ten knots.

Charts IV-32 and IV-33 contain the (Set B) 900 MB Temperature and Wind Analyses, respectively, for 0000Z 21 January. Compare these to Charts IV-14 and IV-15, respectively, in the baseline sequence. The Set B-Set A corresponding differences are provided as Charts IV-43 and IV-44. The magnitudes of temperature difference patterns on IV-43 are in excess of two degrees Celsius in the central and eastern Pacific. The wind differences shown on IV-44, however, do not appear to have increased beyond those on 19 January discussed on Chart IV-39.

Table V-6 contains the RMS differences between Set B and Set A for several analysis times and parameters. The RMS temperature difference at 900 MBS is 0.17 degrees on 19 January -- and increases to 0.32 degrees on 20 January. No further increase occurred on 21 January. (The same

result was observed at 250 MBS wherein the RMS temperature difference doubled (to 0.22 degrees) after one day, but did not increase much beyond that amount in the second day.) Table V-6 also shows that the RMS wind differences at 900 MBS did not increase beyond 0.6 m/sec and 0.3 m/sec for the u-and v-components, respectively, as shown on the first day.

Chart IV-29 contains the 250 MB Height Analysis for 0000Z 19 January (from Set B). Compare this to Chart IV-5 containing the corresponding analysis from Set A. The differences between these analyses are shown in Chart IV-37. Note the two regions with differences in excess of ninety (90) meters -- on the first analysis in the sequence. Table V-6 indicates an RMS height difference of about fifteen meters at 250 MBS -- throughout the two-day sequence. Chart IV-34 contains the 250 MB Height Analysis for 0000Z 21 January. Compare this to Chart IV-17 in Set A. And note the height differences for 21 January on Chart IV-42. Although the differences have grown in the eastern Pacific (to 120 meters in one place), the RMS difference has increased only slightly (from 13.7 to 15.8 meters).

Charts IV-30 and IV-31 contain the (Set B) 250 MB Temperature and Wind Analyses, respectively, for 0000Z 19 January. Compare these to Charts IV-6 and IV-7 which show the corresponding baseline analyses. The (Set B-Set A) differences for these parameters are shown in Charts IV-40 and IV-41. The temperature differences are minor -- but the wind differences are as great as fifty knots at one spot (20N 140W)! In Table V-6 one notes the RMS temperature difference of 0.11 degrees, and the RMS wind differences of 2.55 and 1.78 m/sec for the u- and v-components, respectively. Thus, the wind differences at 250 MBS are about five (5) times greater than at 900 MBS.

Charts IV-35 and IV-36 contain the 250 (Set B) MB Temperature and Wind Analyses, respectively, for 0000Z 21 January. Compare these to Charts IV-18 and IV-19 which show the corresponding baseline analyses. The (Set B-Set A) differences for these parameters are shown in Charts IV-45 and IV-46. In the Pacific the temperature differences exceed one degree Celsius in three

regions -- and two degrees in one of them. Compare IV-45 with IV-40, noting that the cumulative temperature differences have become increasingly significant. In terms of RMS, the differences doubled between 19 and 20 Januarv. On Chart IV-46, the wind speed difference is 35 knots at only one location (35N 145W), but evident in the entire Pacific and Atlantic oceans to one degree or another.

III. PREDICTION MODEL DEVELOPMENT

A. Description of Models

The basic primitive equation atmospheric prediction model employed in this study uses a northern hemisphere polar stereographic grid in the horizontal and a sigma coordinate in the vertical. This model (PECHCV) has five sigma layers and a 63x63 horizontal grid (381 km at 60°N). PECHCV was developed by ODSI in support of the SEASAT Program and was described in detail by Wellck (1977). A very brief description is given here.

Conservation forms of the difference equations based on the Arakawa technique are integrated using a twelve-minute time step. Pressure-gradient-force terms are replaced by a single geopotential gradient on local pressure surfaces to reduce inconsistent truncation error [Kurihara (1968)]. A nonlinear pressure smoother is used along with momentum and temperature diffusion to control model behavior and computational noise. The horizontal boundary conditions are a persistence region below 5°N, a blend region from 5° to 20°N, and a fully-active region above 20°N. Centered time differencing with time averaging of the pressure-gradient-force term in the momentum equations is used. Robert (1966) time filtering of the temperature and moisture solutions is used for computational stability with a larger-than-usual integration time step.

The moisture and heat source/sink terms are modeled in a manner similar to those in the (early) Mintz and Arakawa general circulation model as described by Langlois and Kwok (1969). Terms representing evaporation and large-scale condensation, sensible heat exchange, parameterized cumulus convection and precipitation, and solar and terrestial radiation are included. Dry convective adjustment precludes hydrostatic instability. Stress is applied at the lowest level.

The objectives of the prediction modeling task were as follows:

- to implement and test an iterative procedure (based on the work of Temperton) to dynamically condition the initial state specification for the forecast model.

- to modify the forecast model (initialization and integration sections) to permit data ingestion and dynamic conditioning at a second time origin (intermittent assimilation).

- vary the iterative procedure to study model behavior and to determine a practical number of Temperton "orbits" for dynamic conditioning.

- compare the behavior, efficiency, and results of each forecast model execution using the initial conditions being produced by the analysis models.

These objectives were translated into three types of forecast model test demonstrations:

- a "static initialization" baseline forecast (Chart Set E).

- forecasts which dynamically conditioned the initial state (using a specified number of Temperton "orbits") prior to commencing the prediction, where

  - Chart Set F pertains to the case in which six (6) orbits were made.

  - Chart Sets G1, G2 and G3 pertain to the cases in which twelve (12) orbits were made.

- forecasts which dynamically conditioned the initial state (using twelve orbits), then integrated forward for twelve forecast hours and ingested new (analyzed) values at specified grid points; then

dynamically conditioned the (new) state prior to completing the remainder of the forecast. These gave rise to Chart Sets H1, H2 and H3.

Forecasts E, F, G1 and H1 were initialized with analyses for 0000Z 19 January. Use 0000Z 21 January analyses for verification. Forecasts G2 and H2 were initialized with analyses for 1200Z 19 January. Verify these at 1200Z 21 January. Forecasts G3 and H3 were initialized using analyses for 0000Z 20 January. These verify at 0000Z 22 January.

Table V-7 contains the central processor (CP) and input/output (I/O) times (in seconds) for the various types of forecast runs in this study. All production test runs were made using a CDC CYBER 74 System. Note that the basic model (static initialization) takes just over an hour of CP time for a two-day forecast, but the I/O time is twice as large. Each Temperton orbit adds about 190 CP-seconds and 400 I/O seconds to these amounts. Both the model energetics and the dynamic conditioning of the initial state specification improve as the number of such orbits (taken) increases.

1. Static Initialization

The forecast model requires an initial state specification (of model variables) at each grid point in the three-dimensional lattice. Usually, this initial-state specification is obtained from a set of analysis model outputs or is derived therefrom. The analysis models output gridded values of sea-level pressure and sea-surface temperature, as well as the temperatures, heights and winds at twelve (12) pressure levels from 1000 to 100 MBS. Heights and temperatures above 100 MBS are produced using regression equations. Winds above 100 MBS are derived from these heights. The moisture variable is derived from the (normalized) vorticity distribution at each pressure level using a procedure suggested/used by Kesel and Lewit (1974).

The forecast model requires its initial values on its terrain-following "sigma" surfaces [Phillips (1957)] rather than on pressure surfaces. This means that the analysis model outputs (and fields derived therefrom) must

be interpolated to sigma surfaces and rearranged into suitable arrays and/or formats. Thus, the quality of the relationships between the variables suffers considerably in the process. This approach to initialization shall be referred to as "static initialization" in this Final Report.

Having completely specified the initial state of the atmosphere in terms of grid point values in the forecast model, this specification is then numerically marched forward in time according to the primitive equations to obtain a forecast of the state of the atmosphere at some later time.

2. Dynamic Initialization

No attempt is made in the static initialization process to ensure that the specification of initial conditions for the forecast model results in a set of conditions that are numerically and dynamically consistent with the forecast model equations. If the mass and wind fields are not dynamically conditioned, gravity waves will be excited. However, when starting from a static initial state, it is assumed that the relationships are fairly good, and that the various numerical devices will bring the model trauma under control within the first six to twelve forecast hours with little damage to the forecast.

An early approach to specifying suitably conditioned initial fields, carried over from the days of filtered models, was to assume that the required "balance" could be expressed as a diagnostic relationship between the mass and wind fields. The simplest such relationship is the geostrophic approximation; and more sophisticated diagnostic relationships lead to a hierarchy of balance equations for the rotational component of the wind and to various forms of the ω-equation for the divergent component.

Although the diagnostic relationships could be used to produce a reasonable set of initial winds on pressure surfaces, problems cited earlier still had to be overcome. Specifically, we refer to: (1) the requirement for numerical and dynamic consistency with the forecast model; (2) the need to reduce initialization shock; (3) the desire to account for secondary physical

effects in the relationships (e.g., convection, heating, diffusion, friction). Such considerations have led to an alternative approach to initialization --to employ the forecast model itself to arrive at a set of numerically and dynamically consistent winds. The two main approaches to dynamic initialization are described below.

In Miyakoda and Moyer's (1968) initialization scheme, the first and second time derivatives of the divergence are constrained to be zero, as in the derivation of the ω-equation; but, instead of solving explicitly a diagnostic equation, the primitive equations are used in an iterative fashion to alter the wind field slowly until the constraints on the divergence are satisfied. The principal computational drawback to this scheme is that it involves the solution of Poisson equations, repeated many times.

In the scheme proposed by Nitta and Hovermale (1969), no constraints are placed on the divergence; instead, the forecast model equations are used to integrate backwards and forwards (around the initial time) using a scheme designed to damp the high-frequency gravity modes while retaining the lower-frequency balanced meteorological modes. Besides lifting the restrictions imposed by the Miyakoda-Moyer scheme, the Nitta-Hovermale scheme is more adaptable since provision can be made for the mass field to adjust to the wind field. The main disadvantage of the scheme is the somewhat slow rate of convergence towards the required solution.

The dynamic initialization scheme used in this study is a variation of the Nitta-Hovermale scheme proposed by Temperton (1973), and implemented and tested in a multi-layer (PE) model by Kesel and Wellck (1975). One iteration (or "orbit") of this scheme is carried out as follows: beginning at a central time level, τ_o, integrate forward to $(\tau_o + N\Delta t)$, and then integrate backward from τ_o to $(\tau_o - N\Delta t)$. To obtain the <u>new</u> estimate of the wind fields at time level τ_o, <u>restore</u> the mass fields and <u>replace</u> the wind fields by

$$u' = \tfrac{1}{2}\left[u(\tau_o+N\Delta t) - u(\tau_o-N\Delta t)\right]$$

and

$$v' = \tfrac{1}{2}\left[v(\tau_o+N\Delta t) + v(\tau_o-N\Delta t)\right]$$

This process may be repeated for "N" orbits until successive wind sets differ from one another by less than epsilon. As a practical matter, we have chosen to use the layer-mean squared mass divergence as the measure for assessing the quality of the conditioning. For this, we define mass divergence as

$$M \sim \frac{\partial}{\partial x} (\Phi u) + \frac{\partial}{\partial y} (\Phi v)$$

where Φ is the geopotential-height.

A version of the northern hemisphere primitive equation atmospheric forecast model PECHCV which includes Temperton-style dynamic initialization was constructed for this study. This version of the forecast model, known as DYNMOD, has provision for a varying number of orbits of variable length to be performed (after the static initialization) in order to dynamically condition the initial state. The orbit length used for this study was $N\Delta t$ = 1 hour or five time steps. Thus, each orbit was computationally equal to two forecast hours (roughly).

3. Data Assimilation Method: Dynamic Conditioning at Two Time Origins

A data assimilation experiment using the DYNMOD forecast model was designed to simulate the effect of ingesting off-time satellite data on a forecast. This experiment combines dynamic initialization with the (intermittent) assimilation of data during the course of the forecast. The steps involved in the data assimilation experiment are listed below:

- static initialization
- dynamic balancing with twelve orbits
- the first twelve hours of the forecast
- ingestion of mass field data over a limited geographic region
- dynamic balancing with twelve orbits
- continuation of the forecast to 48 hours

Data was ingested into the forecast model in a pie-shaped wedge over the Pacific extending from 130W to 155E. In order to avoid boundary

discontinuities created by the data ingestion process, the 75^{o} wedge was divided into two blend zones of 25^{o} each and a center zone in which data was directly substituted. Only mass field data (sea level pressure, temperatures and geopotentials) were ingested. The winds from their twelve-hour forecast values were forced to adjust during the dynamic conditioning that followed the data ingestion.

B. Test Results

Three types of forecasts were made in the test demonstration task: (1) static initialization; (2) dynamic initialization using a varying number of Temperton orbits; (3) dynamic initialization at two time origins with data assimilation. Selected charts will be introduced and discussed in order to allow the reader to determine the validity of the forecasts, as well as the comparative performance. Graphs that contain plots of sensitive model parameters (RMS mass divergence; kinetic energy; number of precipitating grid points) for forecasts initialized with either zero, six or twelve Temperton orbits will be presented.

1. Static Initialization (Forecast E)

Forecast Run E (Static Initialization) was initialized using analysis model outputs for 0000Z 19 January. Charts IV-1 and IV-5 contain the starting sea-level pressure and 500 MB height analyses, respectively. The verification analyses for 0000Z 21 January are provided as Charts IV-12 and IV-16, respectively, for the SLP and Z500 analyses.

The Run E outputs are provided as Charts IV-73 and IV-74, the 48-hour SLP and Z500 forecasts, respectively. Run E deepened the low near Japan from 976 MBS to 960 MBS, and moved it to 53N 180. It actually verified at 956 MBS slightly north of the forecast position. Run E also deepened the low near Newfoundland from 996 MBS to 988 MBS and moved it northeastward to 44N50W. It verified about 350 miles further north and slightly deeper than predicted (at 984 MBS). An intense low south of Novaya Zemyla (984 MBS) was predicted to

deepen slightly to 980 MBS, but it actually filled a little to 988 MBS. Over the United States, Run E predicted a 1004 MB low over Illinois -- but it verified in northern Mississippi at 992 MBS.

Error statistics for Run E were encouraging, however. The RMSE was 4.99 MBS in the sea-level pressure forecast. Compare this to an RMS actual change (between the initial and verification analyses) of 8.36 MBS during the 48-hour period. At 500 MBS, Run E had an RMSE of 46.4 meters compared to an RMS actual change of 69.7 meters. Thus, Run E exhibited good skill when compared to persistence.

2. Dynamic Initialization (Forecasts F and G1)

a. Geostrophic Adjustment Study

The prediction model DYNMOD (which stands for "dynamic initialization model") was used to produce 48-hour forecasts after first completing six (6) Temperton orbits (Forecast Run F) and twelve (12) Temperton orbits (Forecast Run G1). Each of these forecasts may be compared to the Run E forecast discussed earlier, since all three used the same initial conditions (for 0000Z 19 January).

To measure the degree of geostrophic adjustment (dynamic conditioning) in each forecast, statistical measures of sensitive model parameters were produced each forecast hour. Perhaps the most useful measure is the RMS mass divergence at each model level. Figures VI-1 through VI-5 show the effect of "orbital integrations" at each of the five model levels, respectively. On each figure, there are three curves: Curve A depicts the static initialization forecast (Run E); Curve B depicts Run F which employed six Temperton orbits. Curve C depicts Run G1 which employed twelve orbits (before commencing the forecast).

From an examination of these figures, it is obvious that dynamic initialization has a beneficial effect on the balance between the mass

and motion fields estimates. (It remains to be seen if the forecasts are any better.) At the sigma=0.9 level (shown in Figure VI-1), the mass divergence parameter increases from five to twelve units (on Curve A) within the first twelve forecast hours -- but settles back to about six units toward the end of the forecast. Curve B (six Temperton orbits) shows less trauma. And Curve C (twelve orbits) shows even less trauma. Observe, also, that the "envelope" described by the three curves "narrows" appreciably after the first 24-36 forecast hours. This particular effect (narrowing of the envelope) is even more pronounced at other model levels. The suggestion is that the model itself has the adjustive power to accomplish the job, but it would take the model longer! One detects a slight computational "edge" to the task of accomplishing an acceptable degree of geostrophic adjustment through the iterative process being tested, rather than let the model do it at the same time the forecast solution is evolving.

Thus, our experience compels us to say that dynamic conditioning of an initial state specification can be substantially accomplished before the forecast commences, thereby eliminating or reducing harmful, spurious physical effects.

Recall, however, that two general types of Temperton orbits can be employed. The first type has been demonstrated herein. The second type has not been discussed. In the second type, the winds are restored and the mass-field variable estimates are averaged at the end of each orbit. From geostrophic theory, both types probably should be done -- perhaps in an alternating manner. And the two solutions could be combined according to the latitude (since the winds oscillate about the mass-field gradients poleward of about 30^{o} latitude, and vice versa equatorward of 30^{o} latitude. The second type of orbits, however, was not tried in this study.

Figures VI-6 through VI-10 show the effect of initialization (type) on the layer-mean kinetic energy. These show that dynamic initialization has far less effect on mean kinetic energy (than on mass divergence), which is as expected. The "envelopes" tend to be quite narrow in these figures as well.

Even so, by taking the orbits the model commences the forecast (generally) with KE values closer to the values the forecast ultimately produces.

Figures VI-11 and VI-12 show the effect of initialization on the precipitation mechanisms in this model. Two types of precipitation are modeled: large-scale and convective. Note that here (too) the envelope narrows as the forecast lengthens. Thus, the impact on convective precipitation is to reduce the affected areas and amounts in the first forecast day, with little impact after the adjustment has matured. In Figure VI-12, however, the effect of dynamic initialization is to increase the large-scale precipitation area and amounts by about 10-20%. A reasonable explanation is that the vertical velocity patterns become rather well developed in the orbital integration period. Improvements in modeling of "secondary" physical effects such as precipitation may be one of the more important motivations to dynamically condition the initial state of a (PE) prediction model.

b. Chart Discussion

(1) Forecast Run F

Run F was dynamically initialized with only six Temperton orbits. Even so, the alterations in the wind fields were large. The resulting forecasts should be compared to Run E (static initialization) and/or to Run G1 (twelve orbits).

Charts IV-75 and IV-76 show the 48-hour sea-level pressure and 500 MB height forecasts (for Run F), respectively. The corresponding verification analyses are provided as Charts IV-12 and IV-16.

Run F tended to produce lows which were 1-2 millibars weaker than in Run E. The Japan low was 1-2 millibars weaker than in Run E. With the Asian low Run F was actually better than Run E by not deepening it as much. The differences between the two forecasts for both the U.S. and Newfoundland lows were negligible. At 500 MBS, Run F and Run E look almost identical. If anything, the major low centers appear to be slightly weaker in Run F.

Statistically, Run F was slightly better than Run E. At sea-level, the Run F RMSE was 4.97 millibars compared to 4.99 for Run E. At 500 MBS, Run F was 46.2 meters compared to 46.4 meters. Strictly speaking, the differences are not statistically significant.

(2) Forecast Run G1

R in G1 was dynamically initialized using twelve (12) Temperton orbits. When the results are compared to other forecasts (E,F) in the same initialization class, it is difficult to see any significant differences. The pressures of the major storm centers are identical to Run F. And, as with Run F, Run G1 seems to predict lows which are slightly weaker than in the static initialization forecast (Run E). The same generalization holds at 500 MBS, where it is difficult to detect differences between Runs E, F and G1 except to say that the centers of lows seem to get progressively weaker as the number of orbits is increased (before commencing the forecast).

Charts IV-77 and IV-78 contain the 48-hour sea-level pressure and 500 MB height forecasts, respectively. Compare these to Charts IV-75 and IV-76, respectively, for Run F; and to Charts IV-73 and IV-74, respectively, for Run E.

Statistically, Run G1 produced RMSE values nearly identical to those produced by Runs E and F.

In summary, it has been demonstrated that the quality of the mass-motion parameter relationships is improved as the number of orbits is increased. Further, one detects an impact on the large-scale precipitation mechanism. Yet, the differences between the static and dynamic initialization two-day forecasts were not significant.

3. Data Assimilation: Dynamic Conditioning at Two Time Origins

a. Run H1 vs. Run G1

In Forecast Run H1, the sequence of events was as follows: (1) static initialization; (2) twelve orbits; (3) forward integrations for twelve forecast hours; (4) data assimilation in a 75° (longitude) band in the central Pacific; (5) twelve orbits; (6) forward integrations for last thirty-six hours.

Run H1 was initialized with 0000Z 19 January data, a time at which the data base is best (generally) in the Pacific area. The ingested data came from an analysis for 1200Z 19 January -- a time at which the data base in the Pacific is not very rich. Thus, we may have introduced a problem by updating our forecast solution with values that may not be as valid as those in the forecast solution. If this is so, Run H2 may be helpful -- since it was initialized at 19/1200Z and was updated using 20/0000Z analysis values.

The 48-hour sea-level pressure and 500 MB height forecasts for Run H1 are shown in Charts IV-79 and IV-80, respectively. The verification analyses are provided as Charts IV-12 and IV-16. They may also be compared to Forecast Run G1 which was dynamically initialized with twelve orbits also -- but which did not assimilate new values at a second time origin. The G1 charts are IV-77 and IV-78.

The biggest difference between G1 and H1 is in the western Pacific -- where H1 produced a low of about 966 MBS, whereas G1 deepened it to 961 MBS. For the other major features, Runs H1 and G1 produced nearly identical solutions. The RMS statistics support this assessment. The 48-hour 500 MB height RMSE values differed by only 0.1 meter; and the sea-level pressure RMSE values differed by only 0.03 millibars. Thus, the only major difference occurred at the upstream edge of the assimilation region.

b. Run H2 vs. Run G2

Another pair of forecasts was initialized using 19/1200Z analyses. These are Runs G2 and H2. G2 employed twelve orbits at the initial time origin only. H2 was also conditioned this way at the initial time origin, but assimilated updated values in the 75^{o} band in the central Pacific twelve hours into the 48-hour forecast. In this comparison, H2 did produce a slightly better forecast. At 500 MBS, H2 had an RMSE of 49.2 meters while G2 had 50.1 meters. At sea level, H2 had an RMSE of 5.21 millibars while G2 had 5.26 millibars.

The SLP and Z500 48-hour forecasts for Run H2 are provided as Charts IV-83 and IV-84, respectively. Compare these outputs to Run G2 outputs contained in Charts IV-81 and IV-82. (The initial conditions for both runs are shown in Charts IV-8 and IV-9. The verification analyses are provided as Charts IV-23 and IV-24.)

Neither H2 nor G2 handled (well) the Japan low (which moved to the Aleutians during the period). H2 filled it from 972 MBS to 974 MBS, even though it deepened to 960 MBS by 21/1200Z. Run G2, in contrast, kept the central pressure about the same. Neither forecast deepened the system.

During this period, a major low evolved in the eastern U.S. Both H2 and G2 produced 998 MB lows near Chicago. The system actually deepened to 984 MBS.... from a 1007 MB low near northeastern Nebraska on 19/1200Z.

The 980 MB low (at 19/1200Z) just south of Newfoundland filled to about 1000 MBS during the period. Both G2 and H2 only filled it to 992 MBS (about half as much as it did in fact).

Although the H2 forecast was slightly better than the G2 forecast (statistically), one is hard pressed to detect it with an examination of the output charts.

c. Run H3 vs. G3

Here are two more runs from the "G" and "H" series. (Recall that data assimilation takes place in the "H" series.) Runs H3 and G3 were initialized using analyses for 0000Z 20 January (Charts IV-10 and IV-11). The verification analyses are provided as Charts IV-25 and IV-26.

Once again, H3 appears to be better statistically. Its RMSE at 500 MBS was 48.6 meters, compared to 50.0 meters for Run G3. At sea level, H3 had 5.27 MBS compared to 5.33 MBS for G3.

The H3 forecasts are shown in Charts IV-87 and IV-88. Compare these to the G3 outputs in Charts IV-85 and IV-86.

Clearly, the only difference at sea level takes place in the northwest Pacific, where H3 produces a 970 MB low and G3 produces a 974 MB low. It actually verified at 968 MBS.

In the eastern U.S., both H3 and G3 predicted the low to be 988 MBS -- and it verified about ten millibars deeper than that.

4. Comparative Performance Summary

Table III-8 shows the error statistics for all production test runs. The most striking aspect of the statistics is that the differences are quite small. For all four forecasts made from 19/0000Z, for example, the RMSE ranges were from 4.97-5.01 millibars at sea level, and from 46.2-46.4 meters at 500 MBS. For the two forecasts initialized at 19/1200Z, as well as for the two forecasts initialized at 20/0000Z, one can detect slight superiority in the H2 and H3 forecasts.

Table III-9 shows comparative model performance at sea level for the four forecast runs initialized at 19/0000Z. The central pressures for four systems are tabulated. The entries in parentheses represent our best estimates

of the actual central pressures, whereas the associated entries (without parentheses) indicate the value of the last closed isobar. The Japan low (which moved to the Aleutians) is most relevant to this study -- since data ingestion occurred there (in Run H1). For Runs F and G1, which were initialized with six and twelve orbits, respectively, the low appears to be slightly weaker (1-2 MBS) than in Run E (static initialization). In Run H1, dynamic conditioning at two time origins (with data ingestion, too) produced a low which was even weaker. With the other features, the differences were extremely minor. But, we still detect a slight "flattening" of the pressure profiles through the major lows when dynamic initialization takes place.

On the basis of the small number of forecasts made, we are hesitant to draw strong conclusions about the benefits of dynamic initialization and/or data assimilation. On the basis of these tests it is tempting to conclude that the impact of dynamic initialization on the forecasts is minor -- even though it improves the quality of the coupling in the initial state specification and impacts on secondary physical effects (the number of precipitation grid points, for example).

Data assimilation was tried in three forecasts (H1, H2, H3). We detect slightly better statistics at 500 MBS. In the sea level pressure forecasts we are not sure we detect any improvement in the forecasts. Since the computational burden was so much greater in the G-series and H-series forecasts, one must carefully consider the cost-to-benefit ratio. Perhaps the data assimilation issue can (only) be resolved when large quantities of accurate, representative data are available for the assimilation. It doesn't make sense to ingest values from a later analysis -- if such an analysis is based on an equally-poor data base.

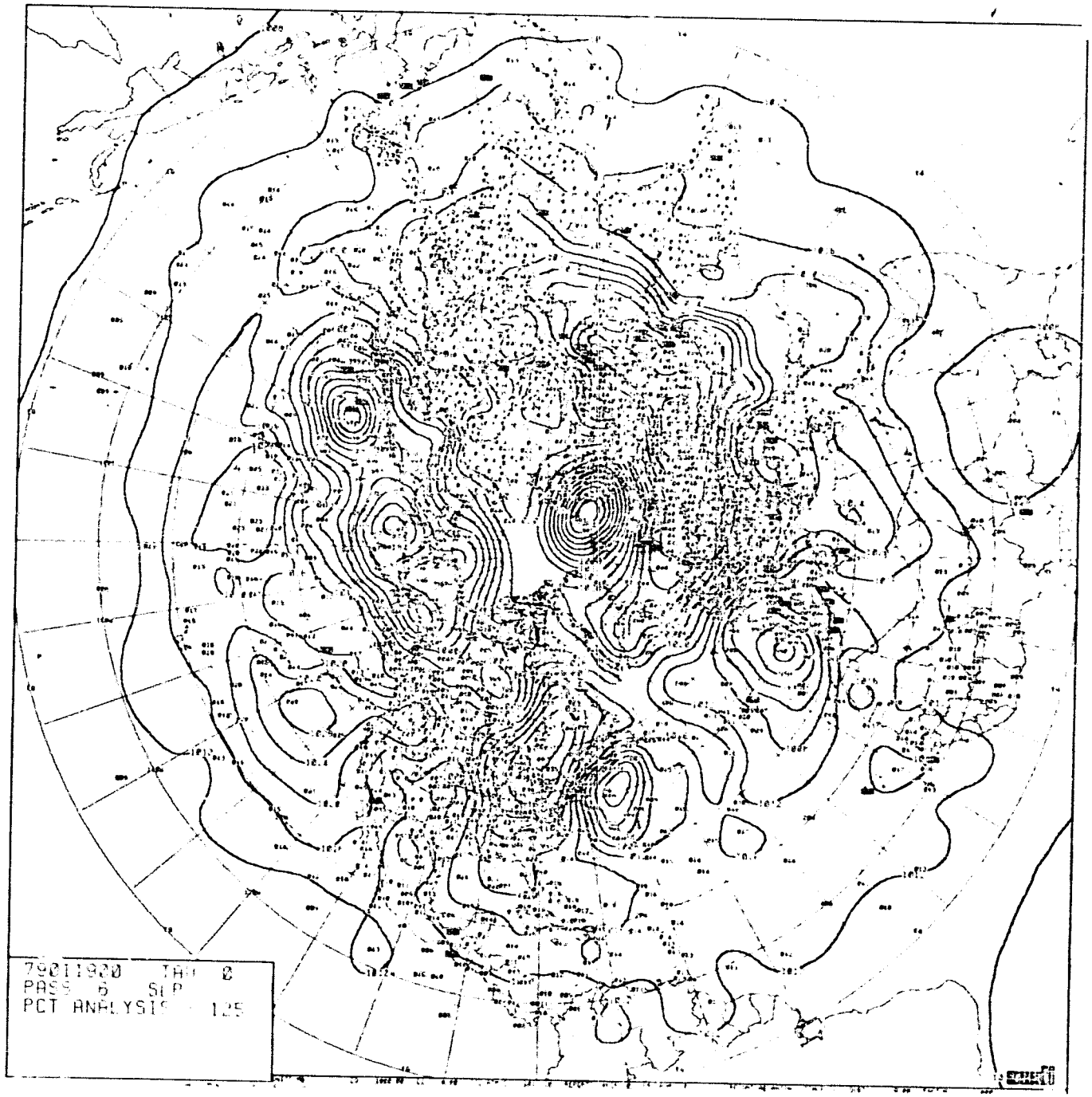

CHART IV-1: Surface Pressure Analysis, 0000Z 19 January 1979. Chart Set A.

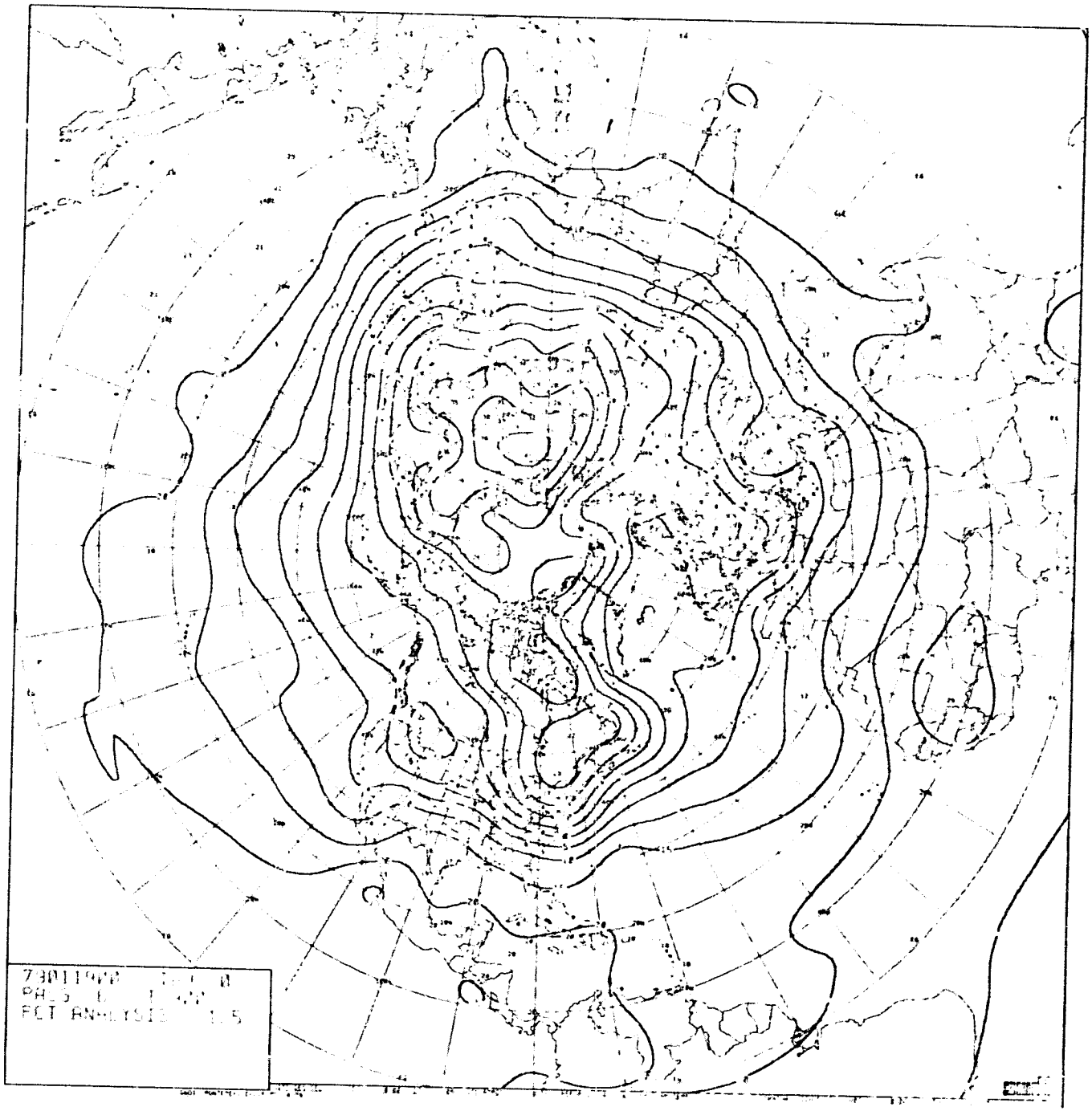

CHART IV-2: 900MB Temperature Analysis, 0000Z 19 January 1979. Chart Set A.

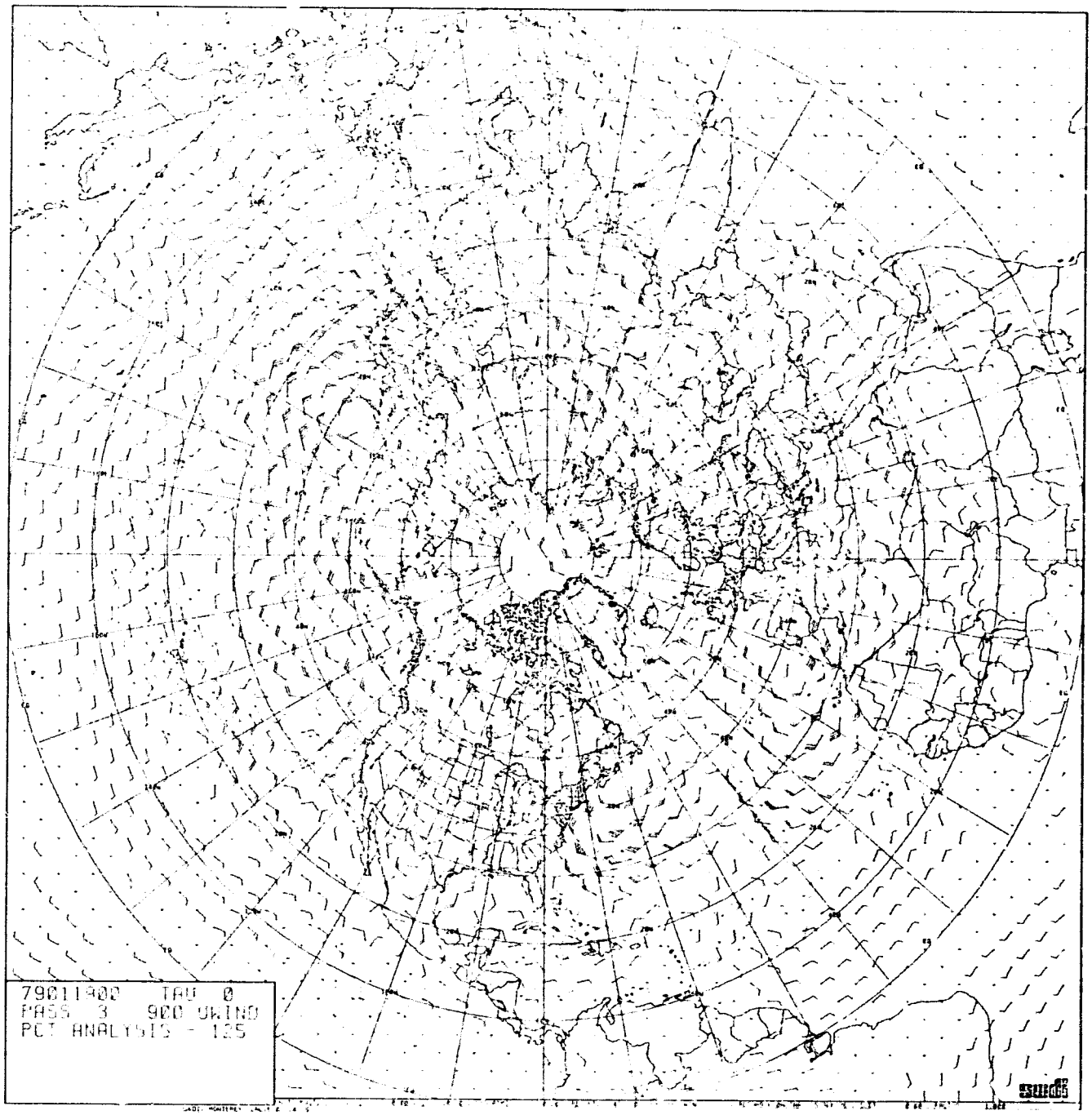

CHART IV-3: 900MB Wind Analysis, 0000Z 19 January 1979. [illegible]rt Set A.

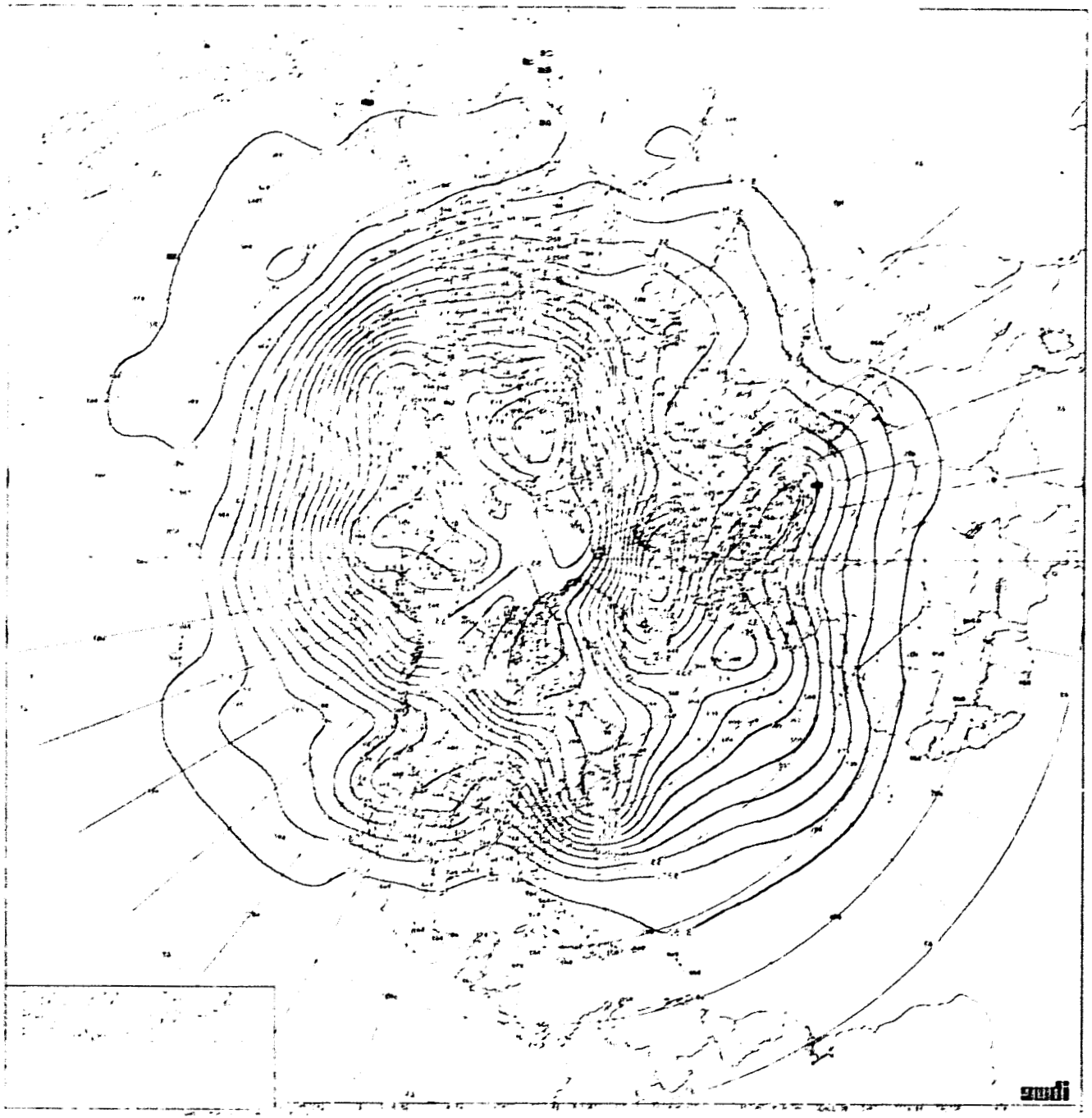

CHART IV-4: 500MB Height Analysis, 0000Z 19 January 1979. Chart Set A.

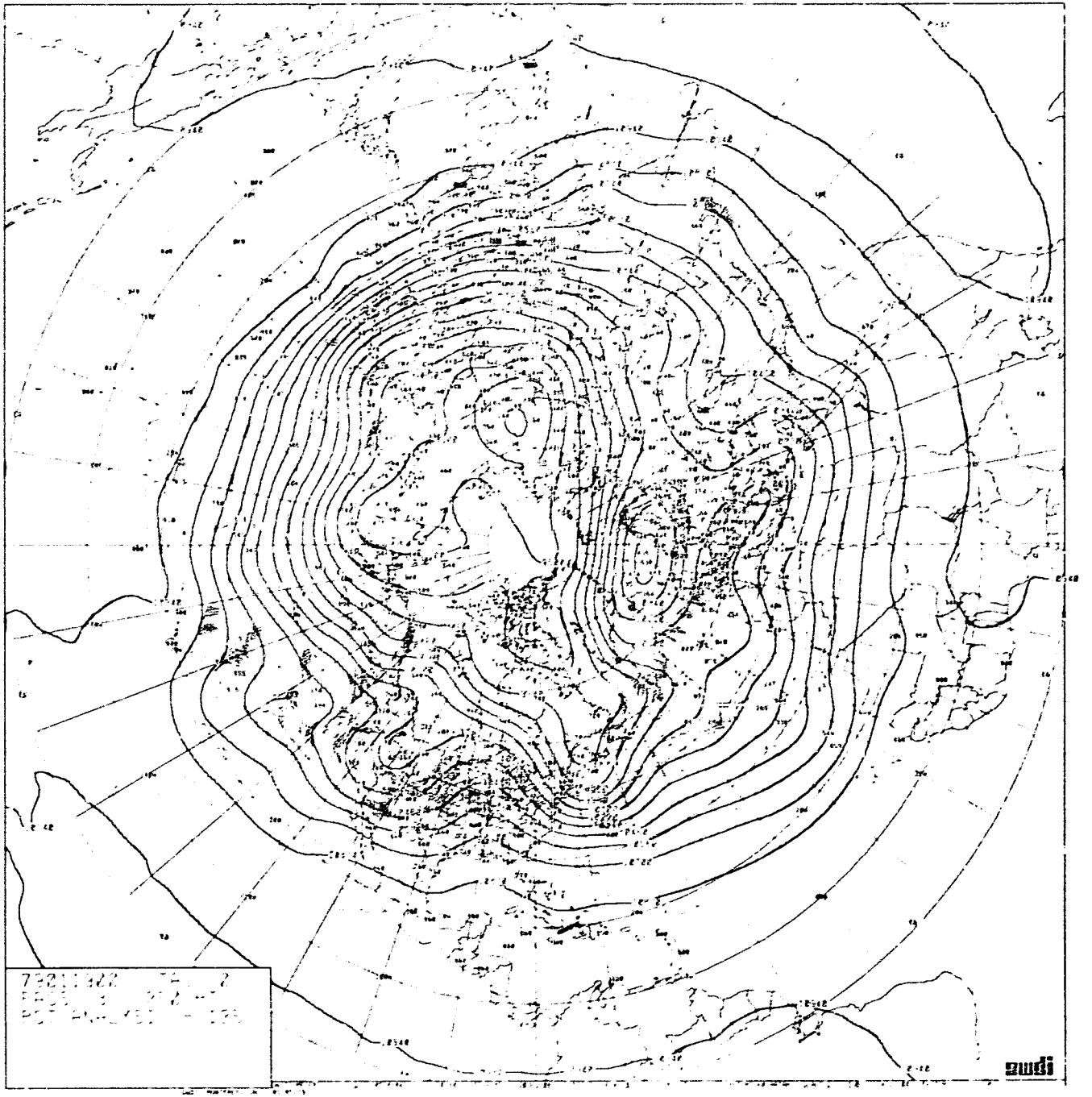

CHART IV-5: 250MB Height Analysis, 0000Z 19 January 1979. Chart Set A.

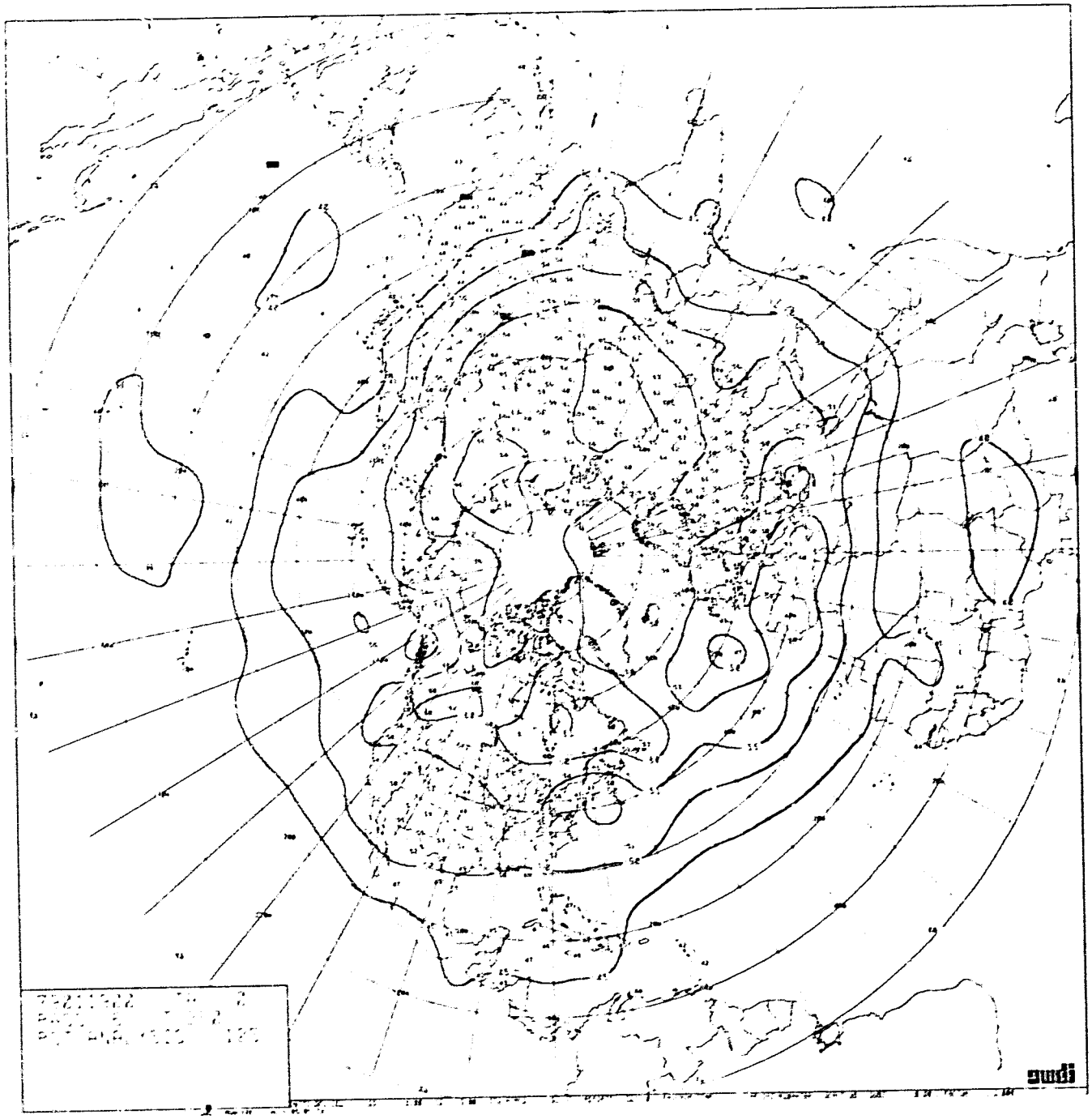

CHART IV-6: 250MB Temperature Analysis, 0000Z 19 January 1979. Chart Set A.

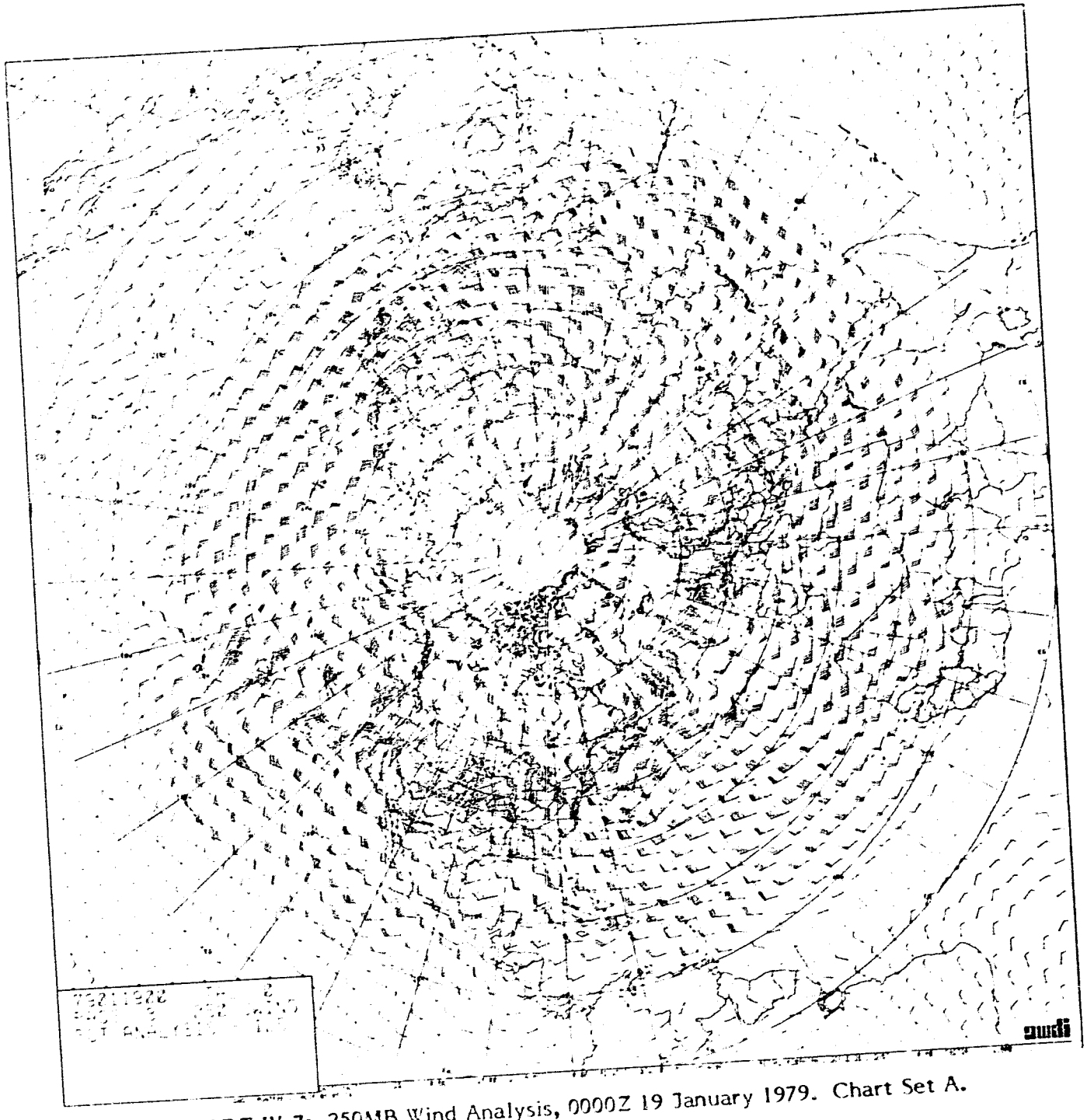

CHART IV-7: 250MB Wind Analysis, 0000Z 19 January 1979. Chart Set A.

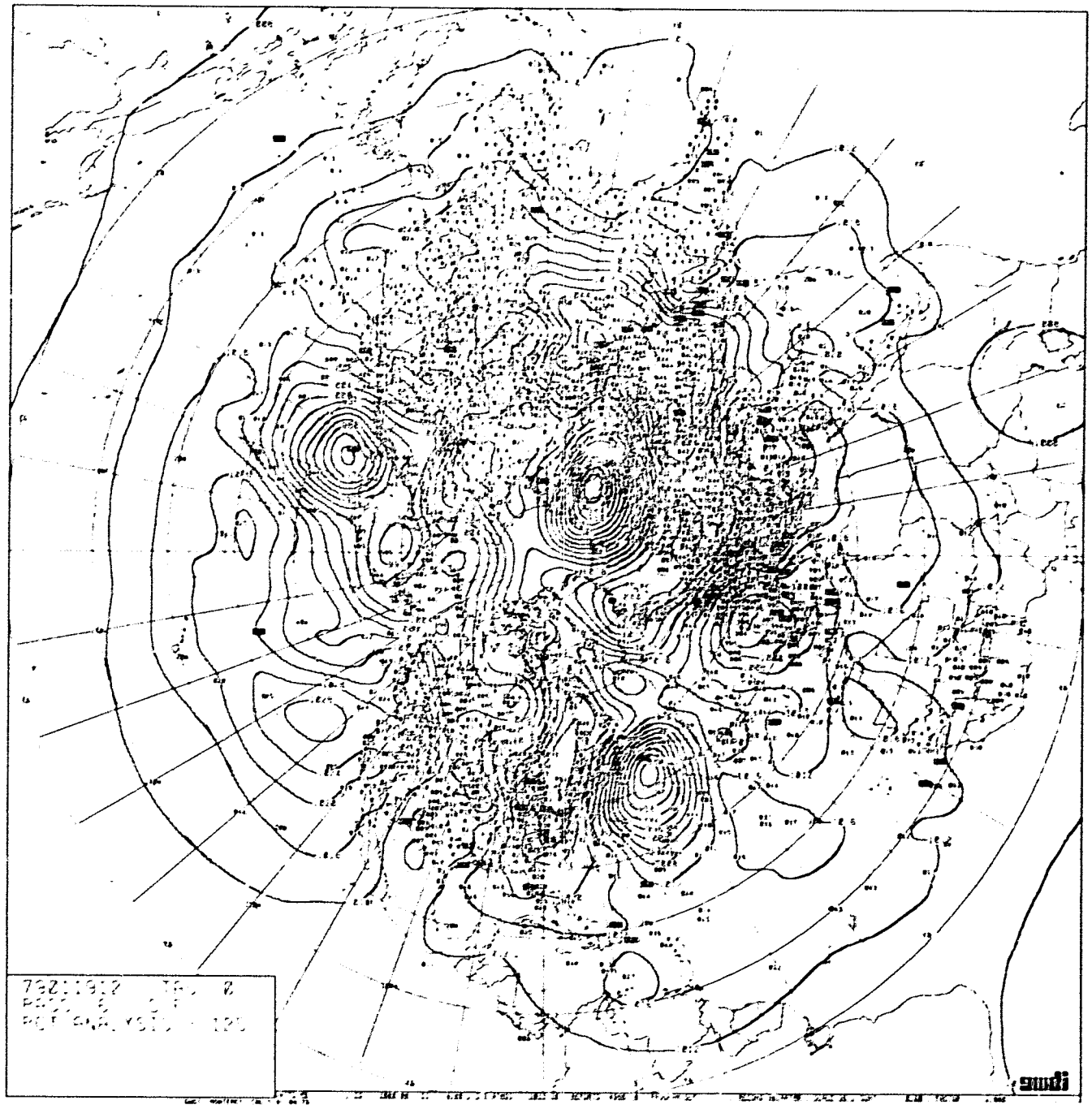

CHART IV-8: Surface Pressure Analysis, 1200Z 19 January 1979. Chart Set A.

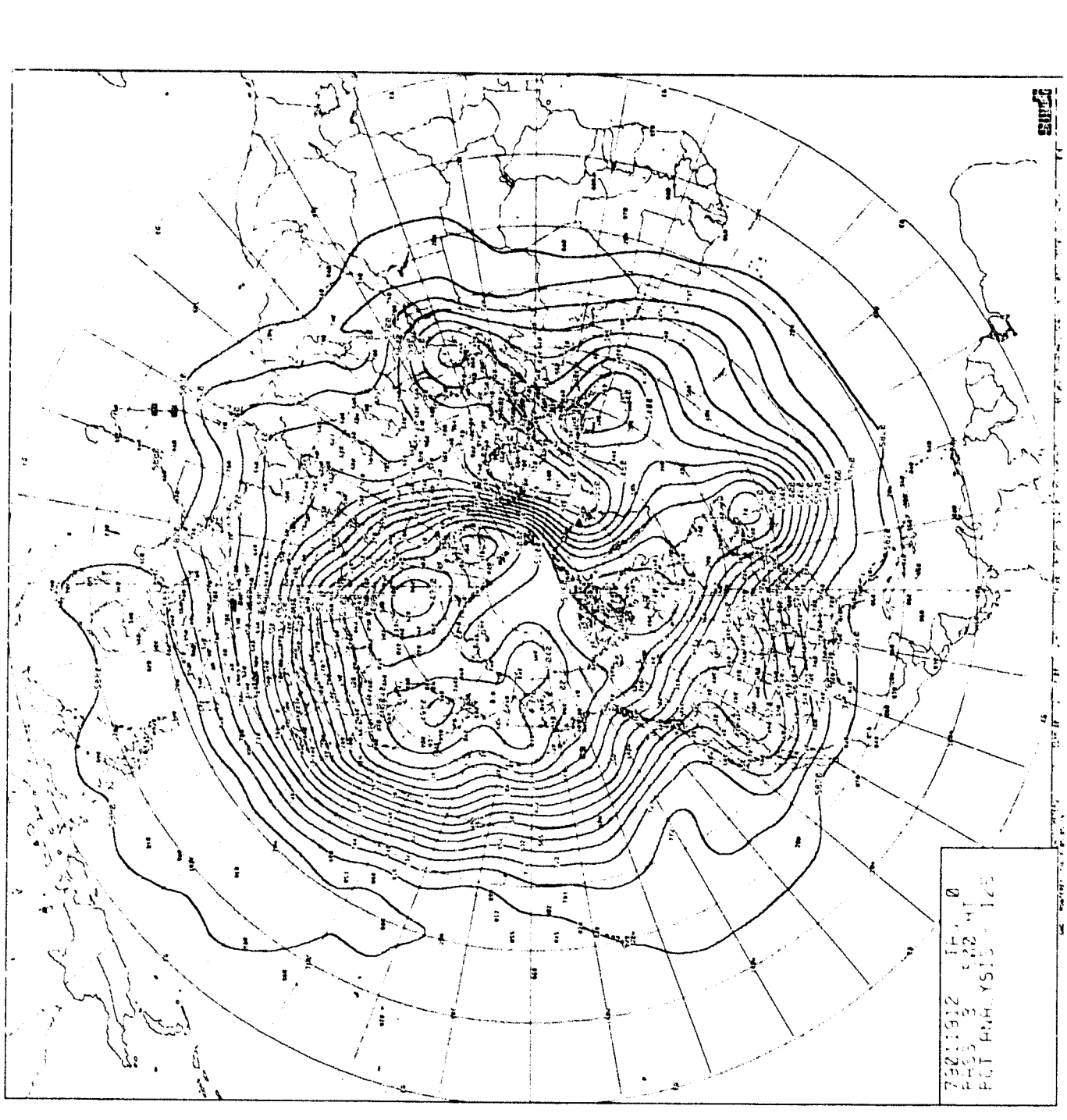

CHART IV-9: 500MB Height Analysis, 1200Z 19 January 1979. Chart Set A.

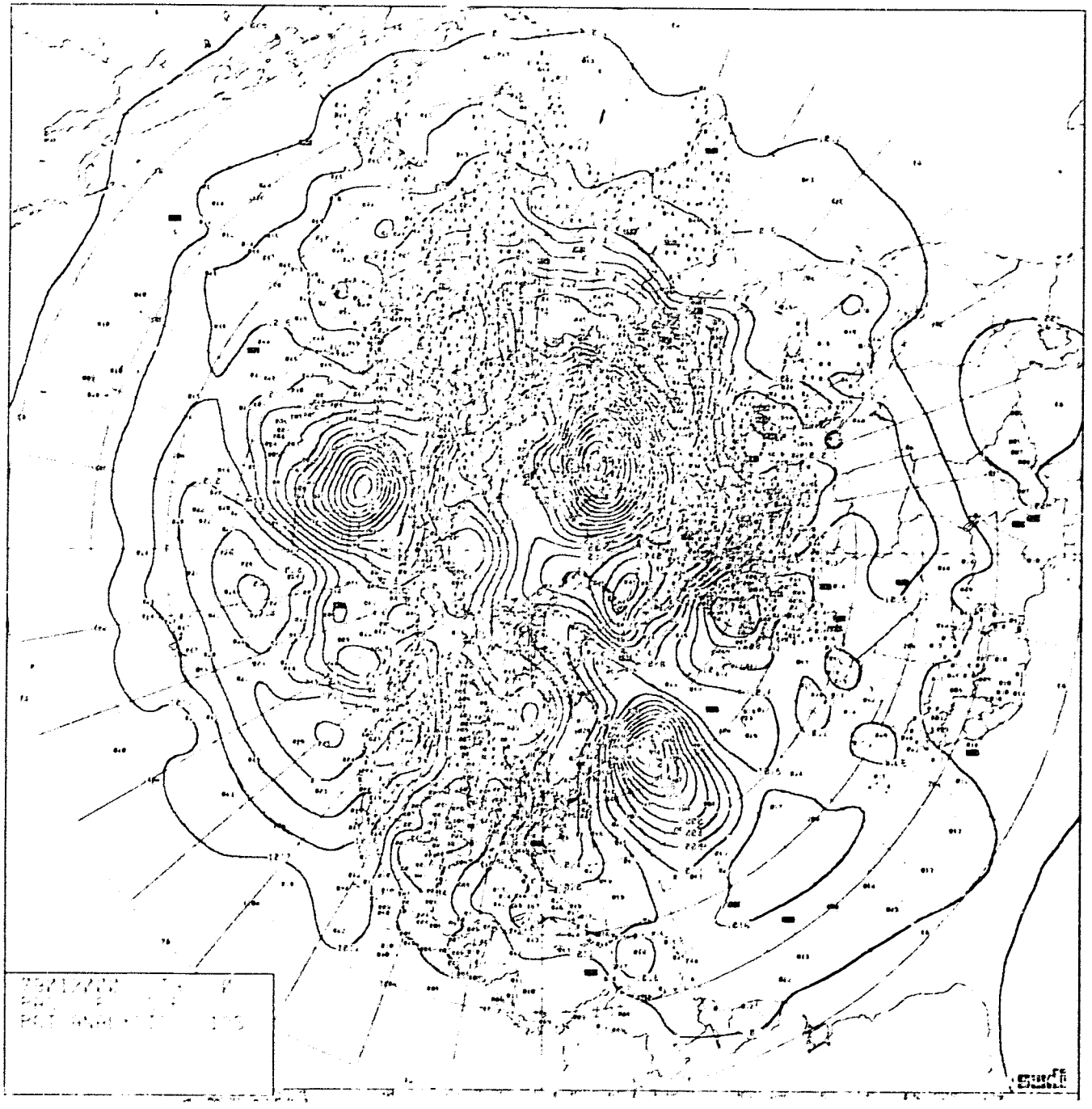

CHART IV-10: Surface Pressure Analysis, 0000Z 20 January 1979. Chart Set A.

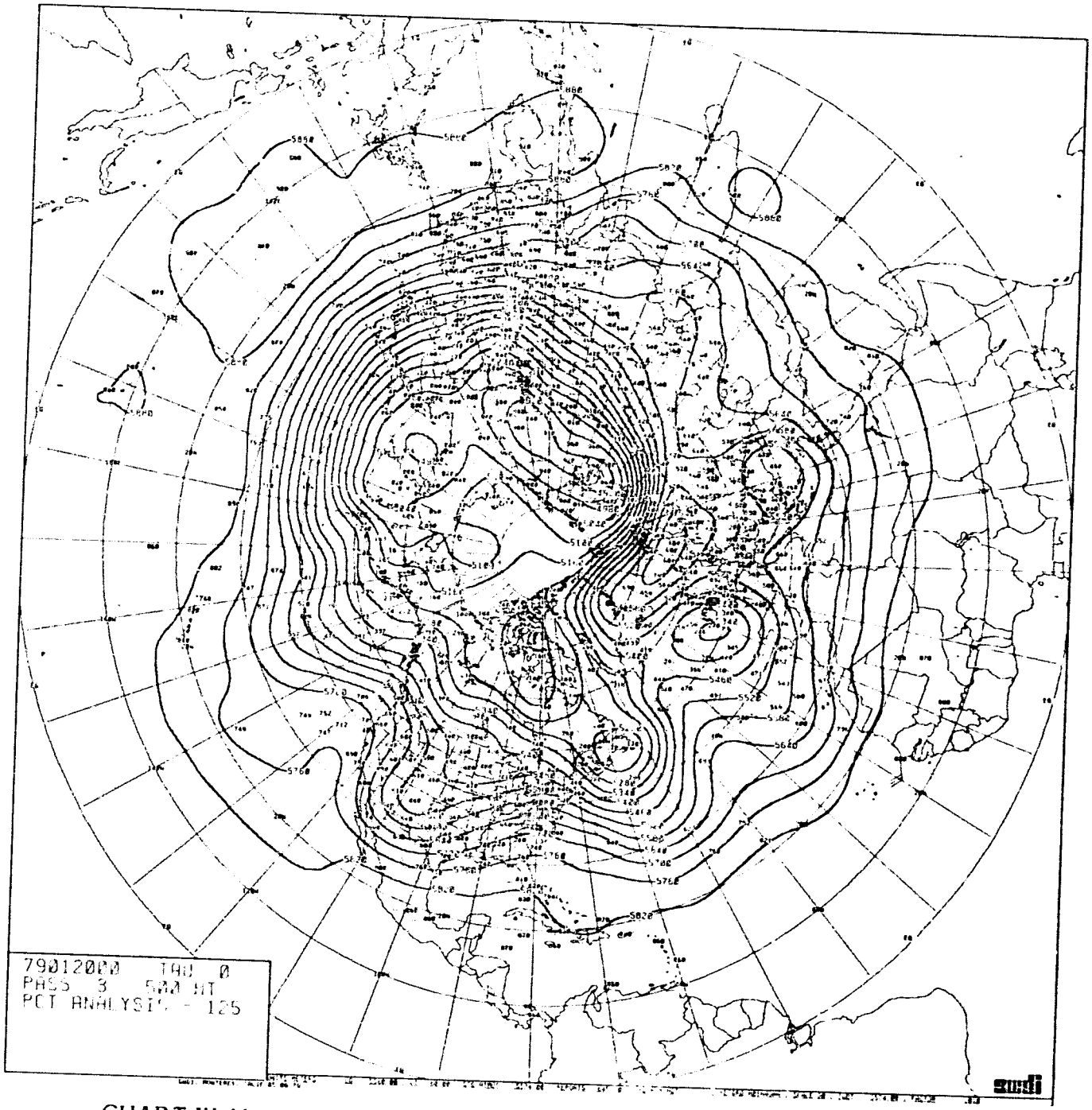

CHART IV-11: 500MB Height Analysis, 0000Z 20 January 1979. Chart Set A.

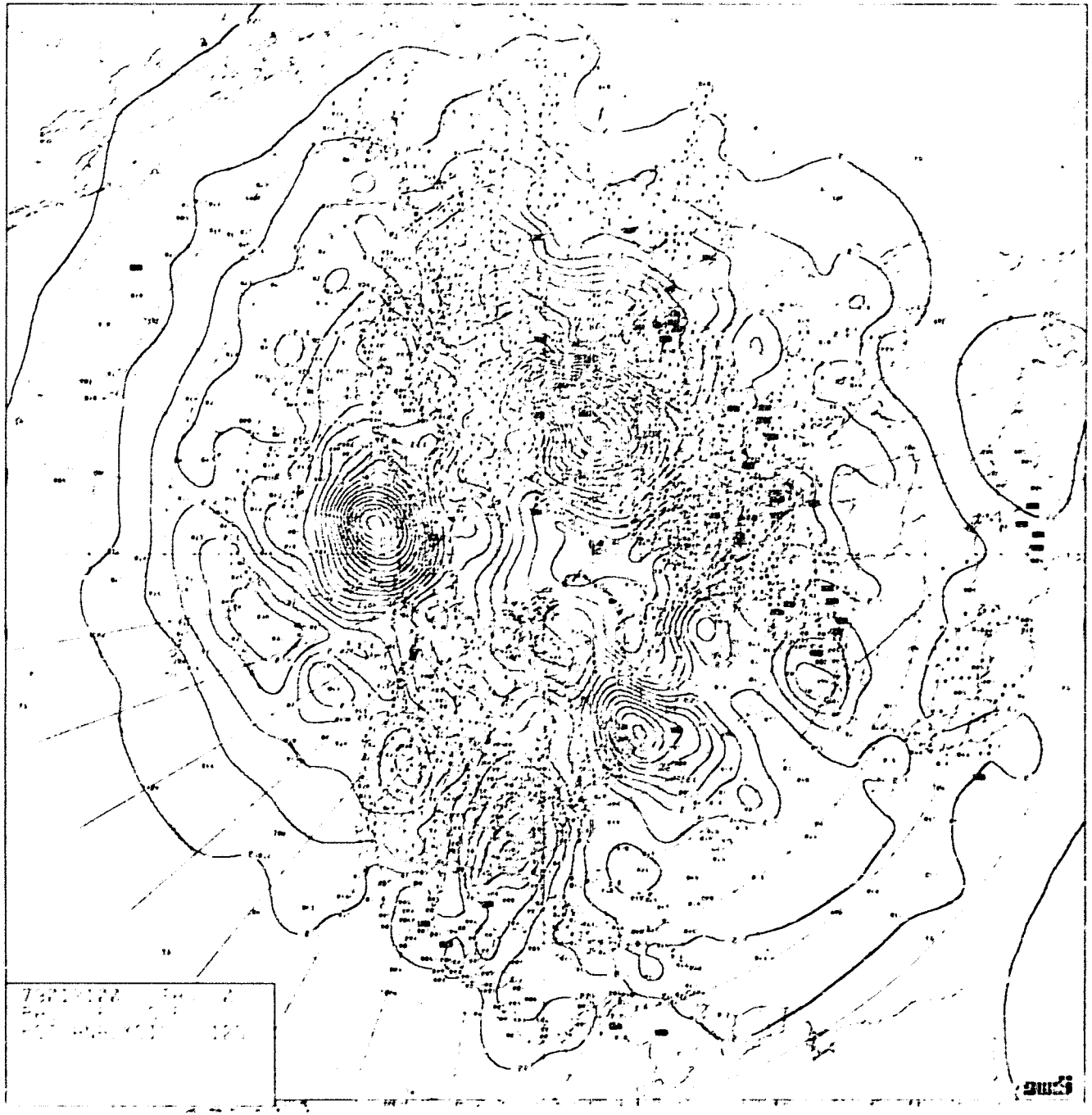

CHART IV-12: Surface Pressure Analysis, 0000Z 21 January 1979. Chart Set A.

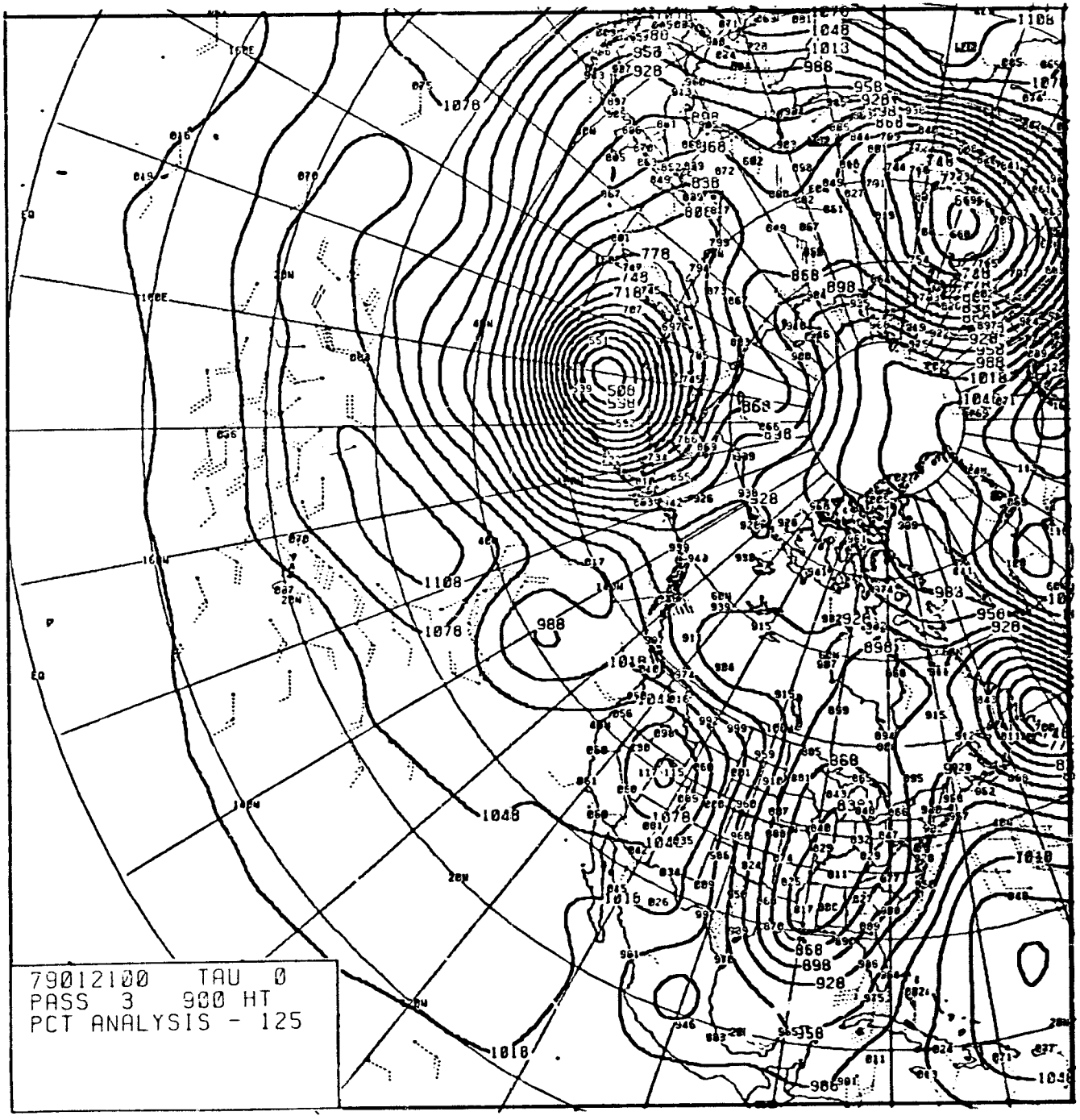

CHART IV-13: 900MB Height Analysis, 0000Z 21 January 1979. Chart Set A.

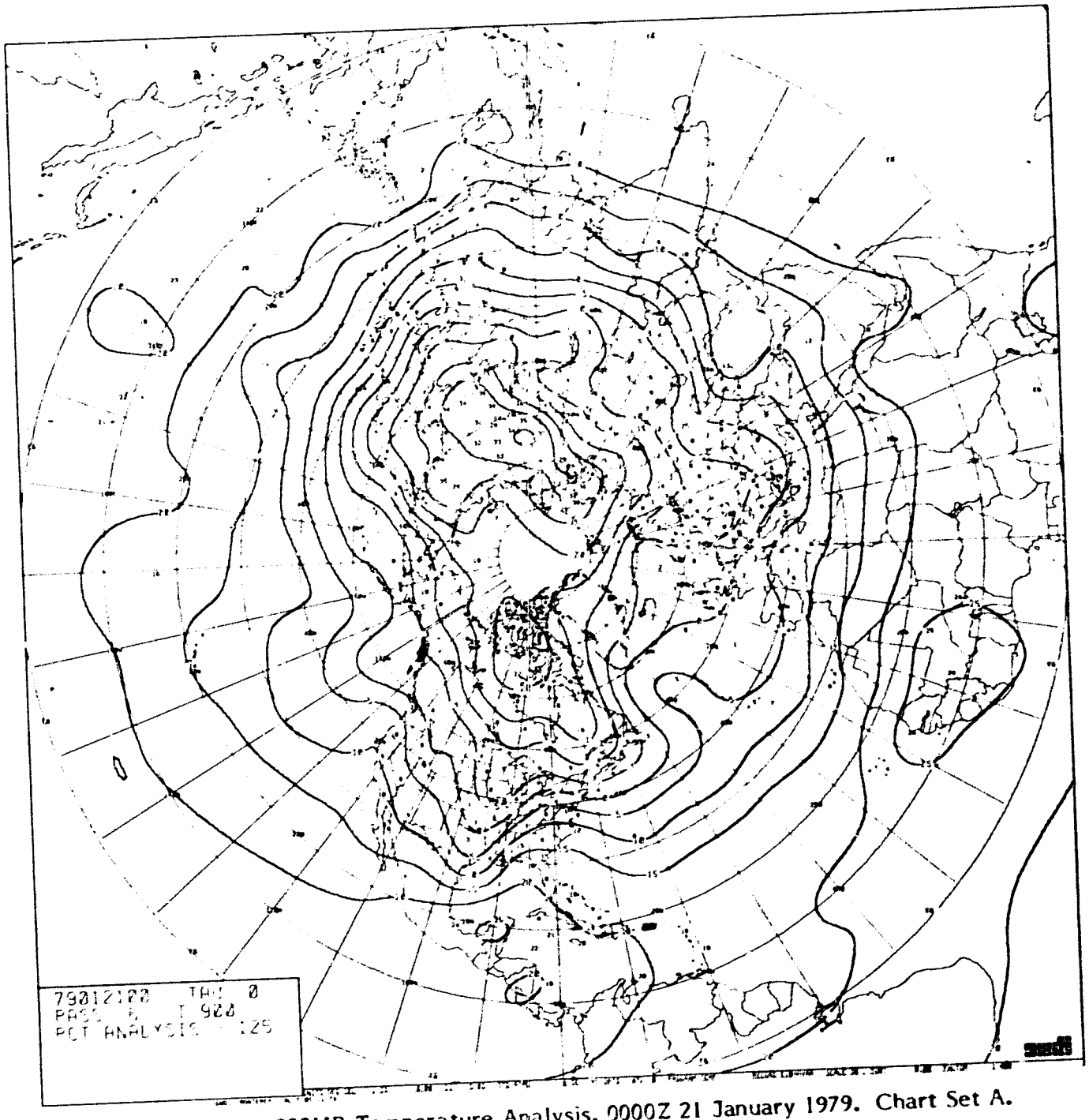

CHART IV-14: 900MB Temperature Analysis, 0000Z 21 January 1979. Chart Set A.

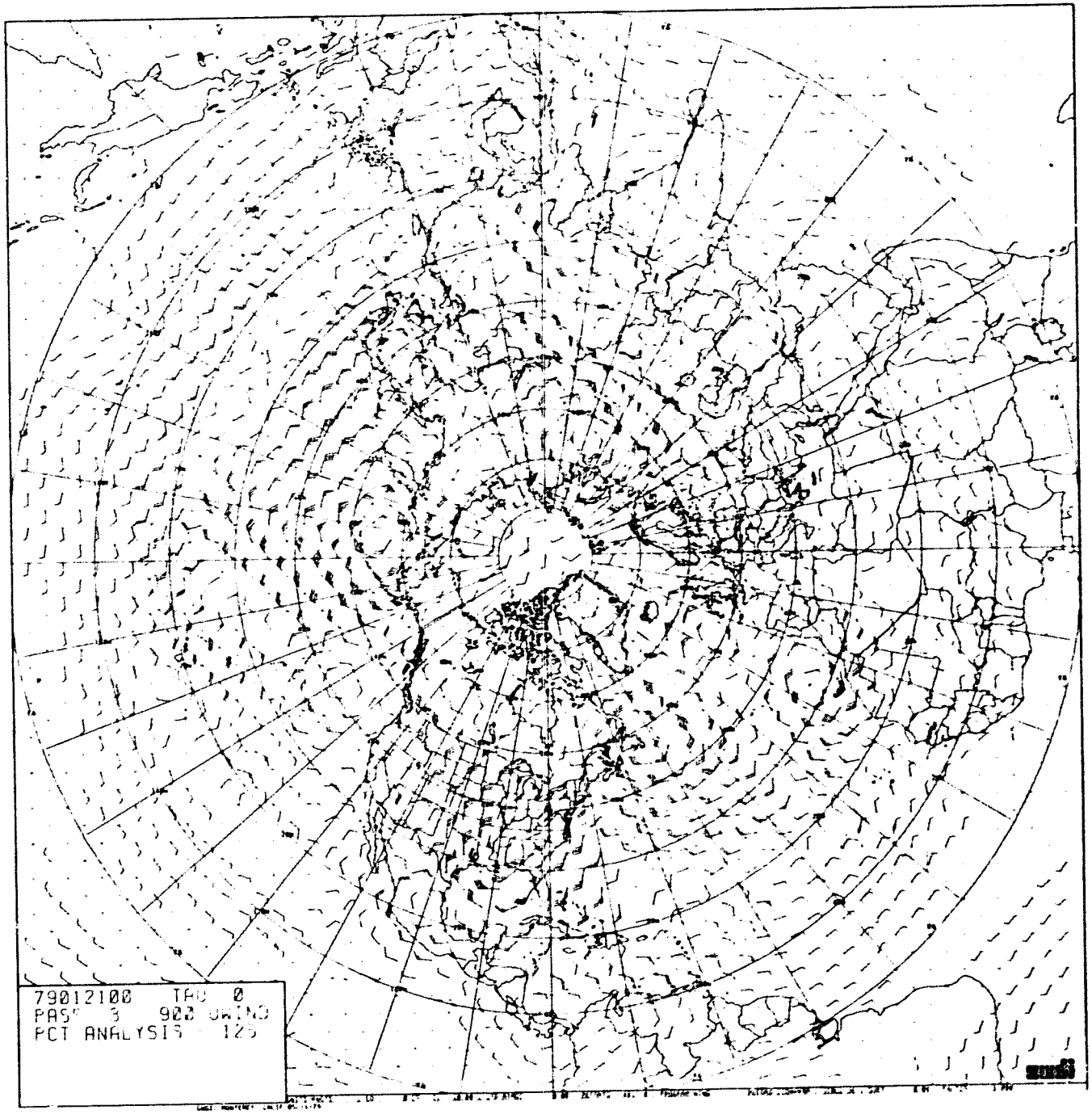

CHART IV-15: 900MB Wind Analysis, 0000Z 21 January 1979. Chart Set A.

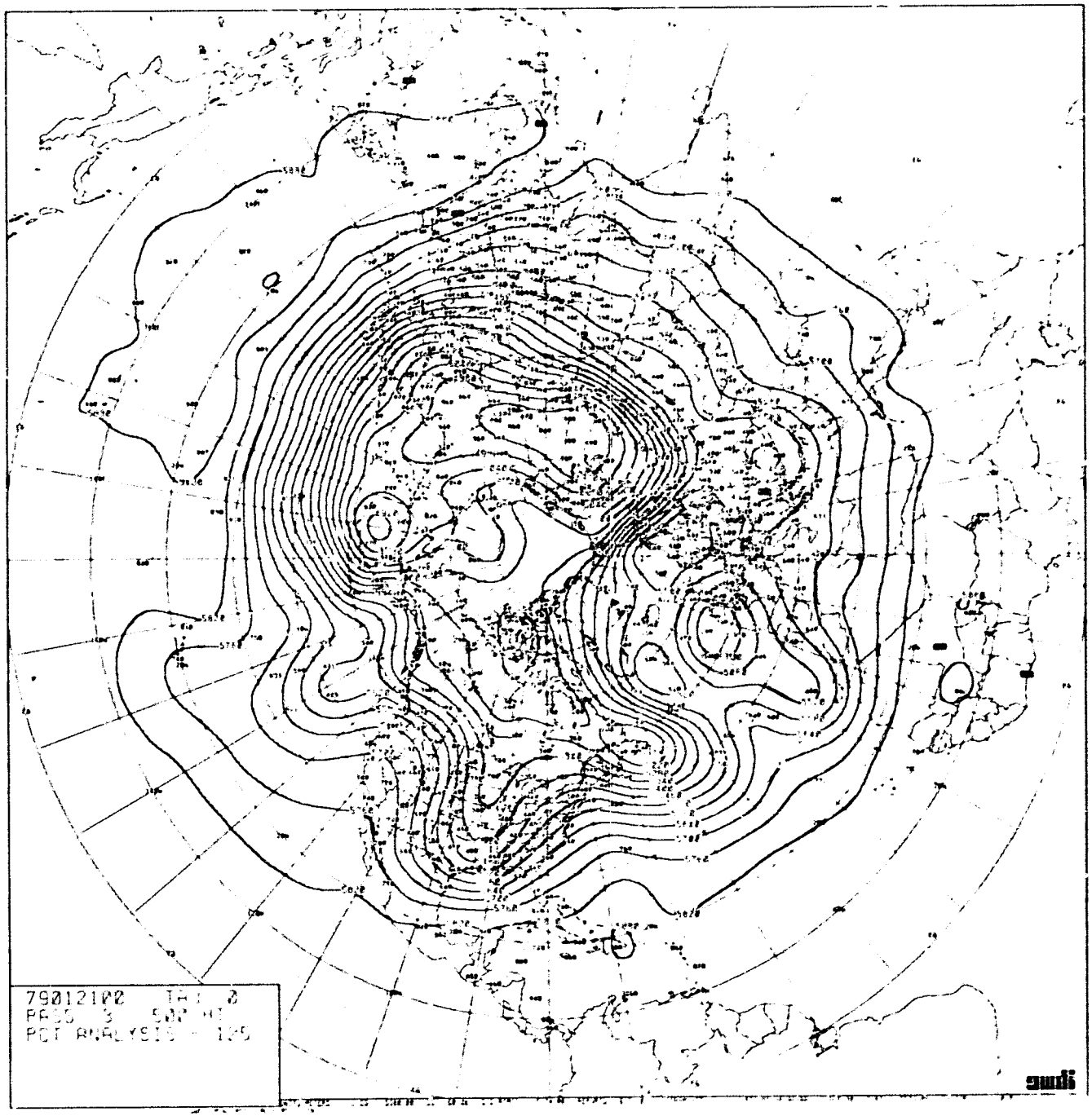

CHART IV-16: 500MB Height Analysis, 0000Z 21 January 1979. Chart Set A.

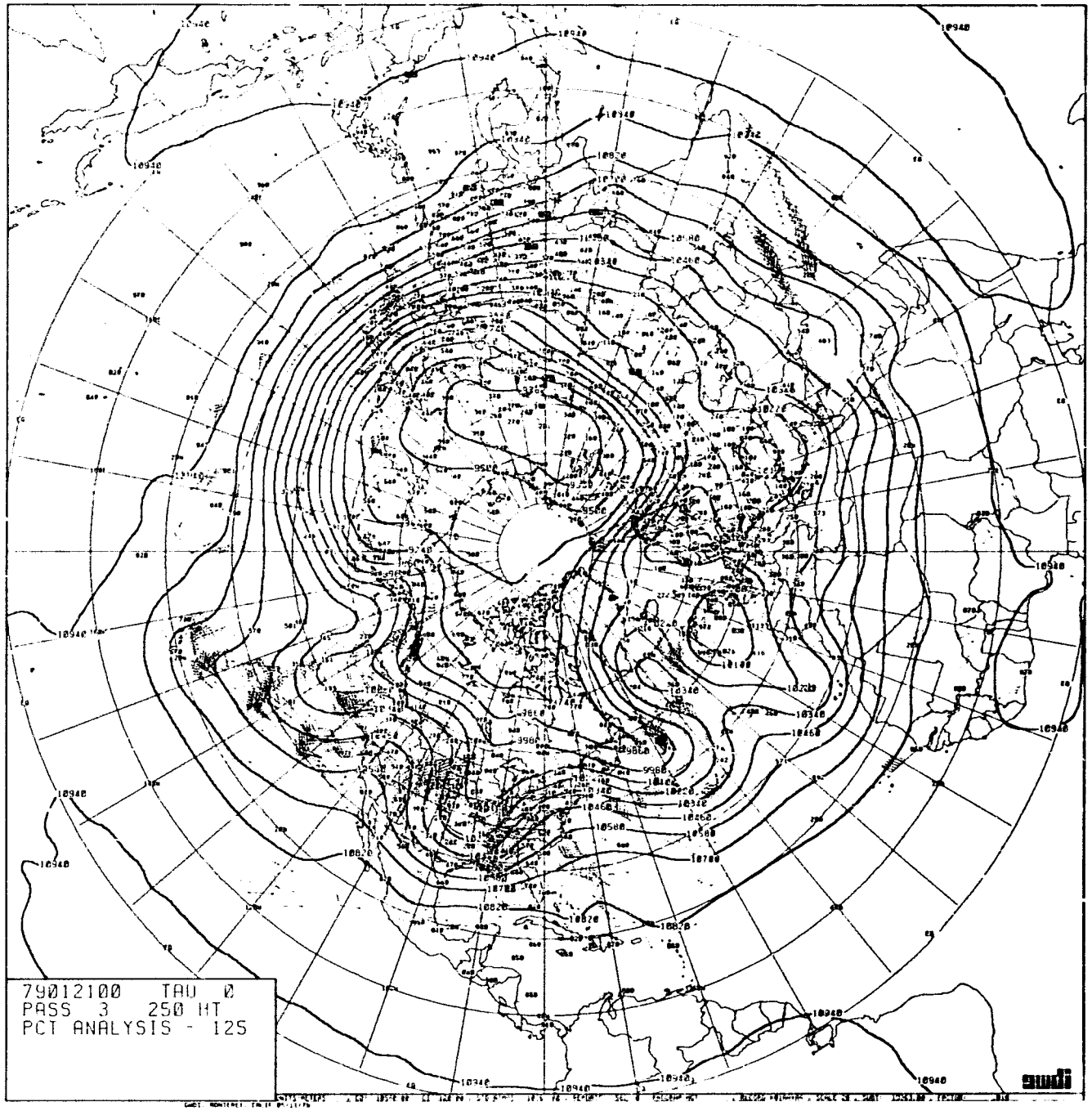

CHART IV-17: 250MB Height Analysis, 0000Z 21 January 1979. Chart Set A.

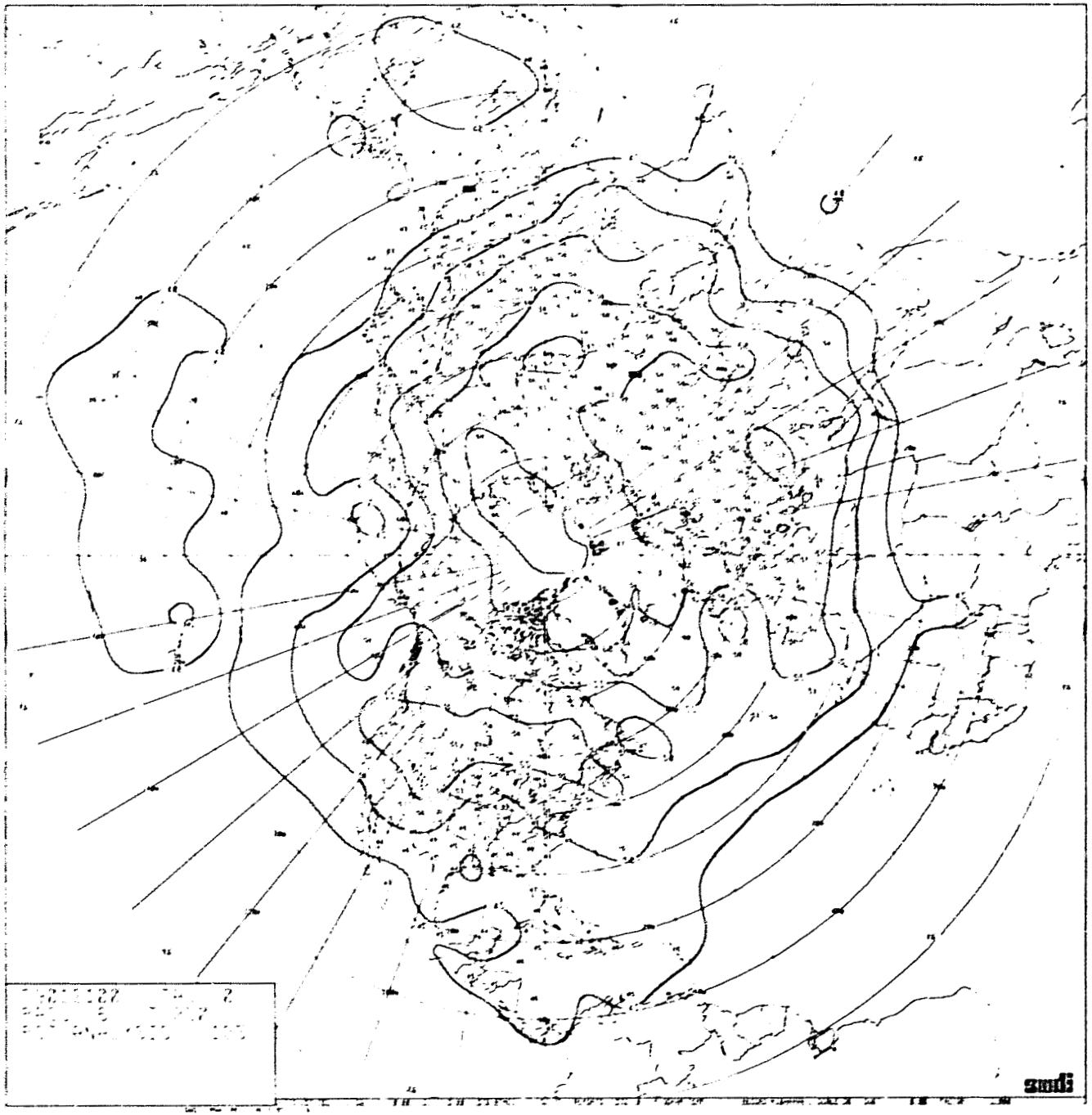

CHART IV-18: 250MB Temperature Analysis, 0000Z 21 January 1979. Chart Set A.

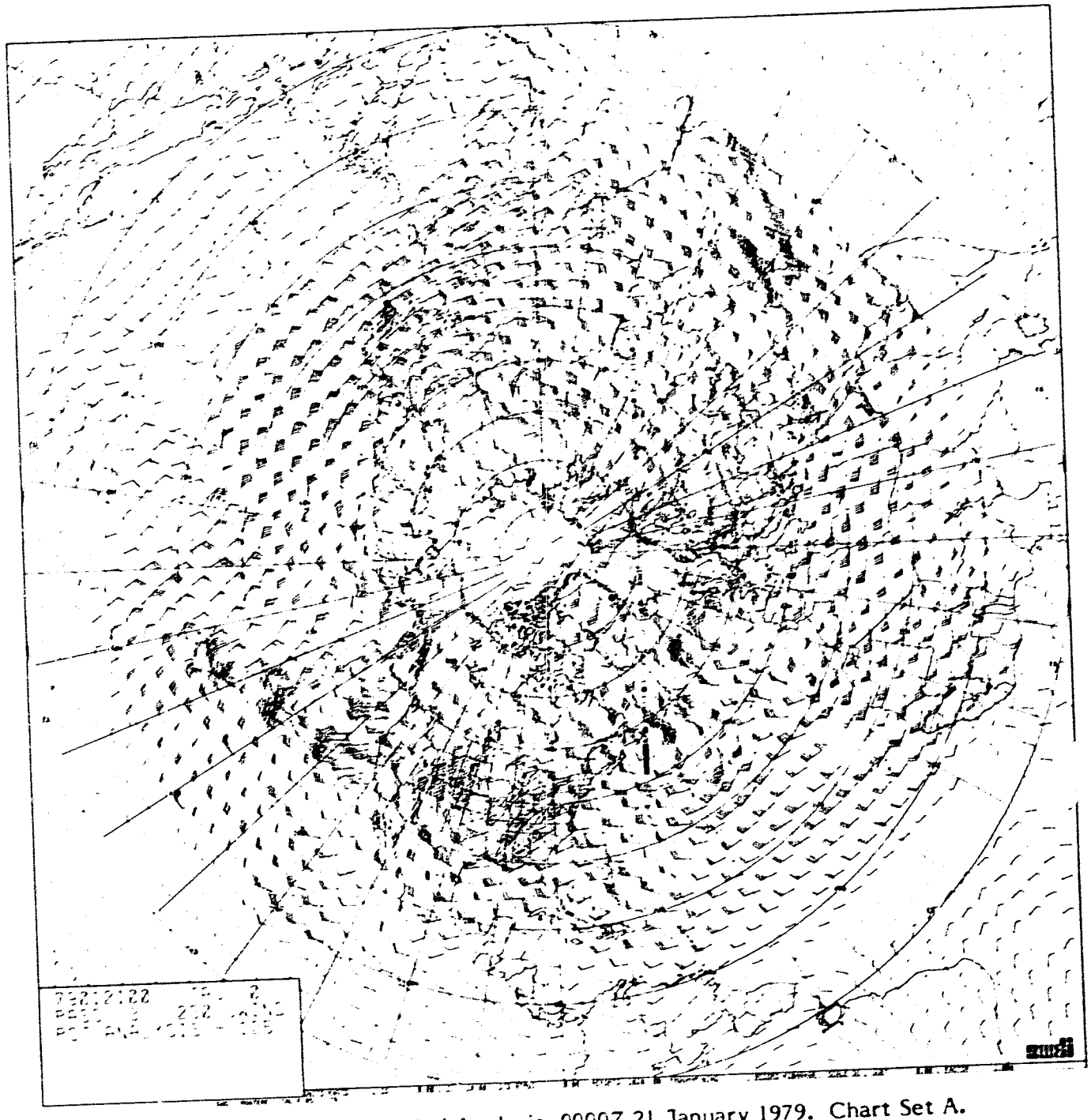

CHART IV-19: 250MB Wind Analysis, 0000Z 21 January 1979. Chart Set A.

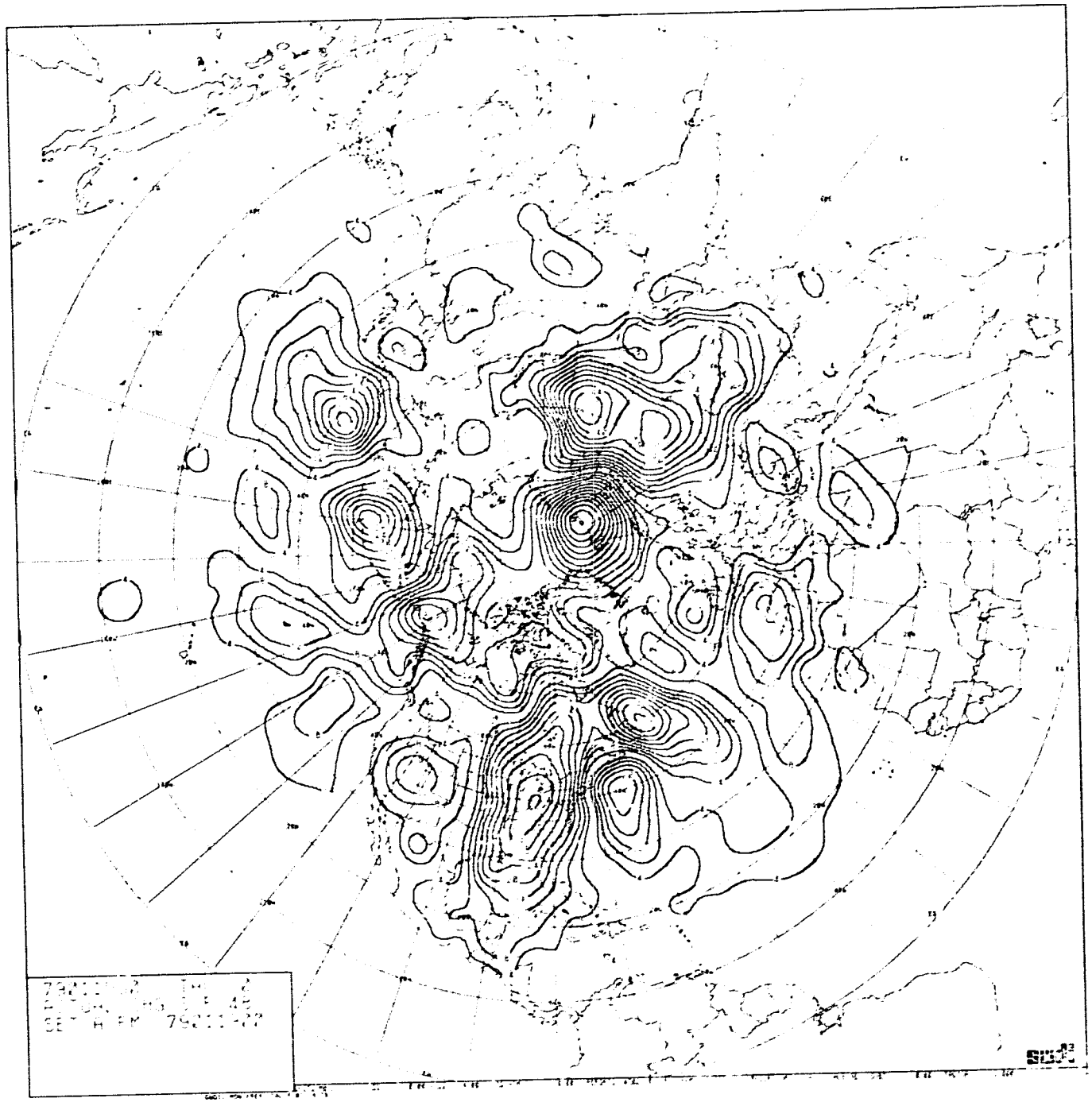

CHART IV-20: 48-Hour Surface Pressure Change, period ending 0000Z 21 January 1979. Chart Set A.

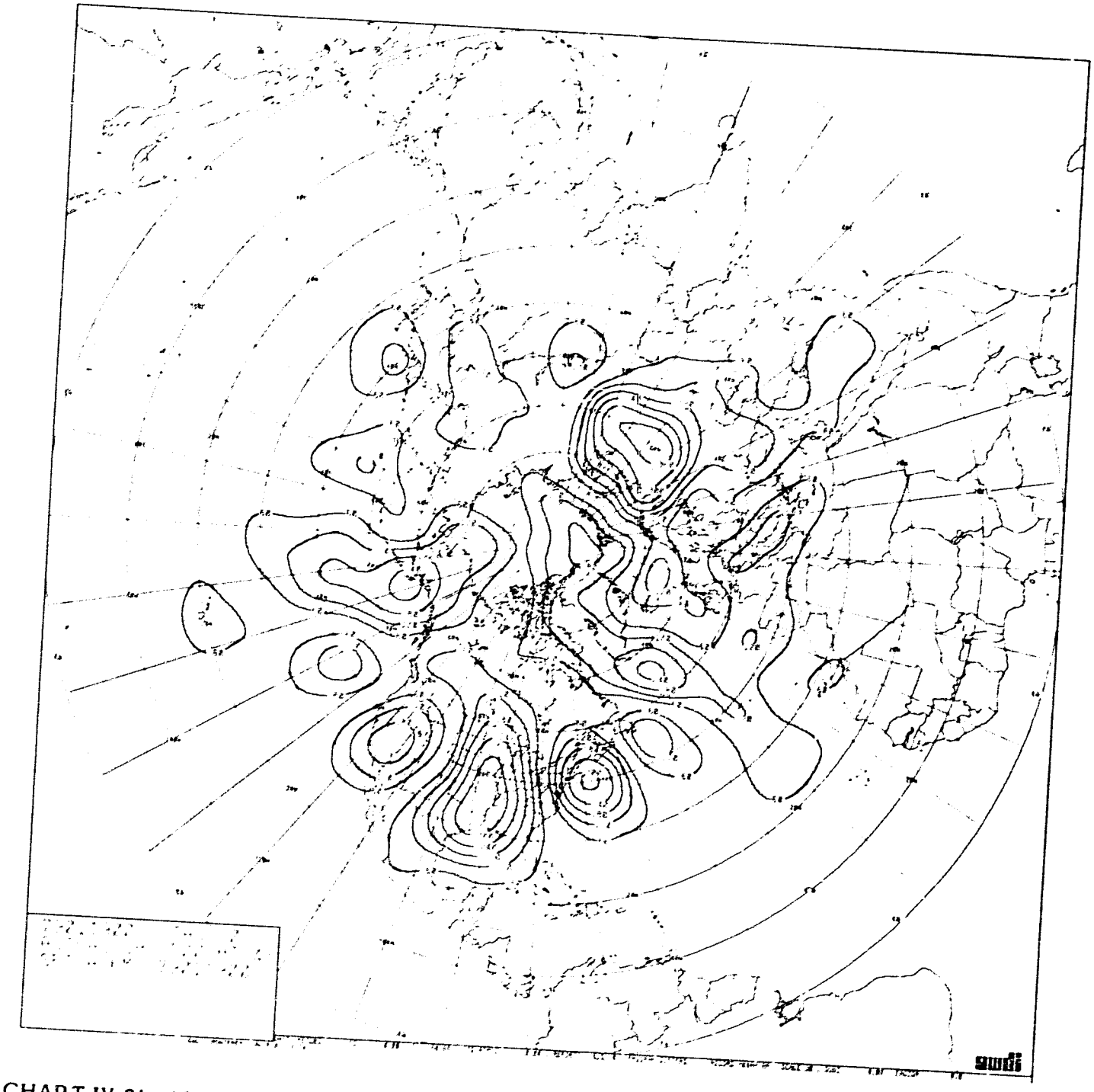

CHART IV-21: 48-Hour 500MB Height Change, period ending 0000Z 21 January 1979. Chart Set A.

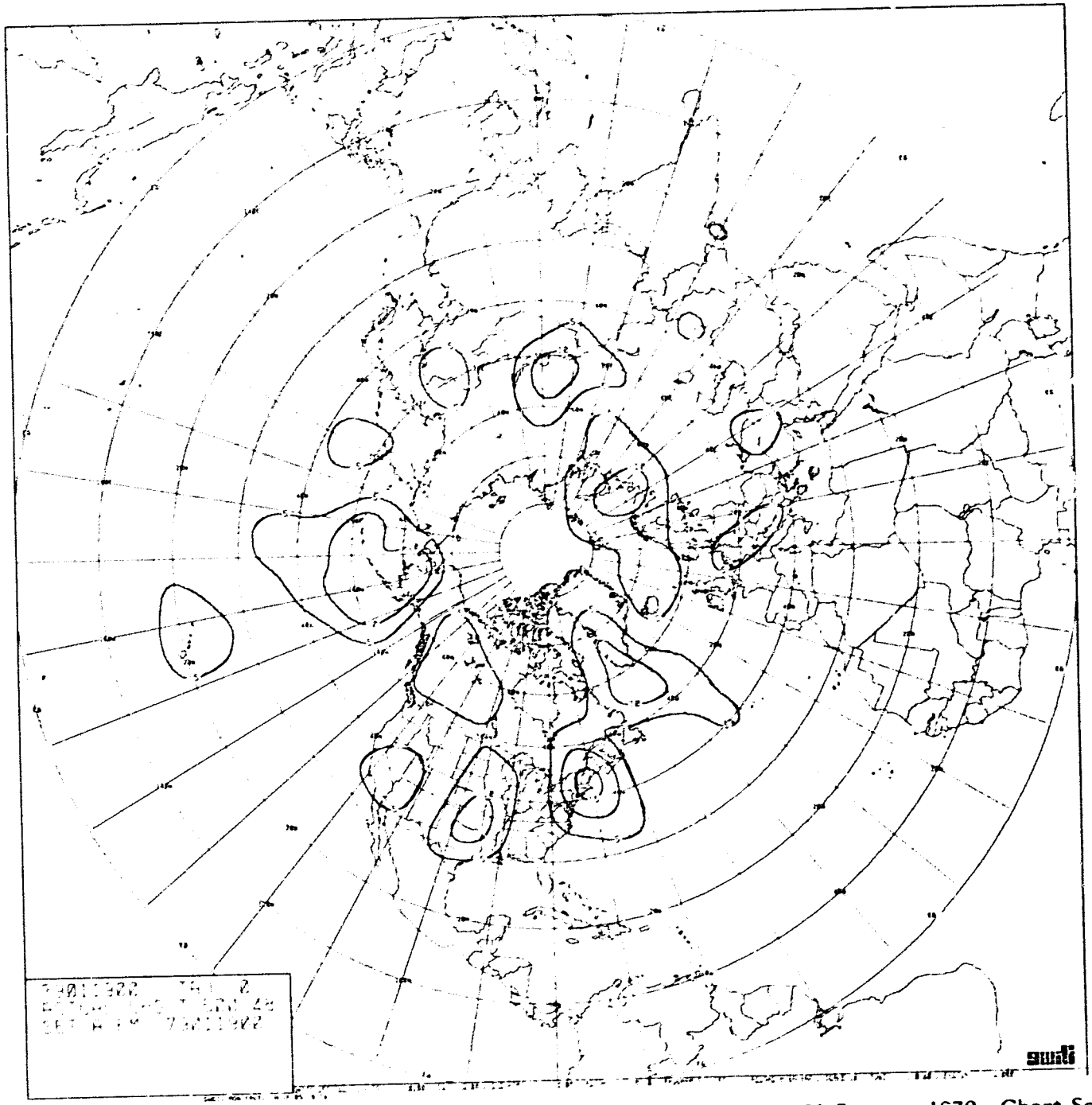

CHART IV-22: 48-Hour 500MB Temperature Change, period ending 0000Z 21 January 1979. Chart Set A.

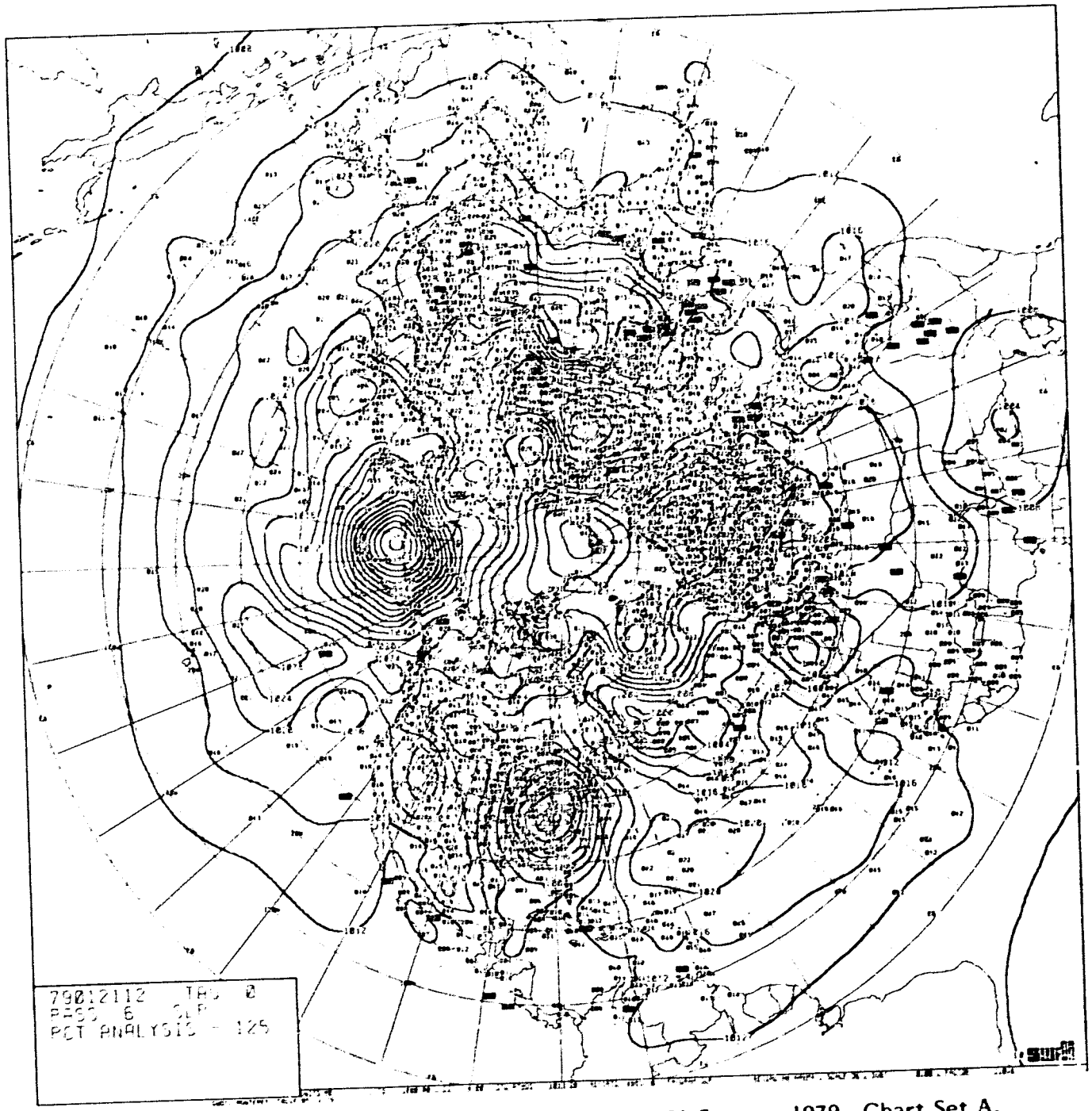

CHART IV-23: Surface Pressure Analysis, 1200Z 21 January 1979. Chart Set A.

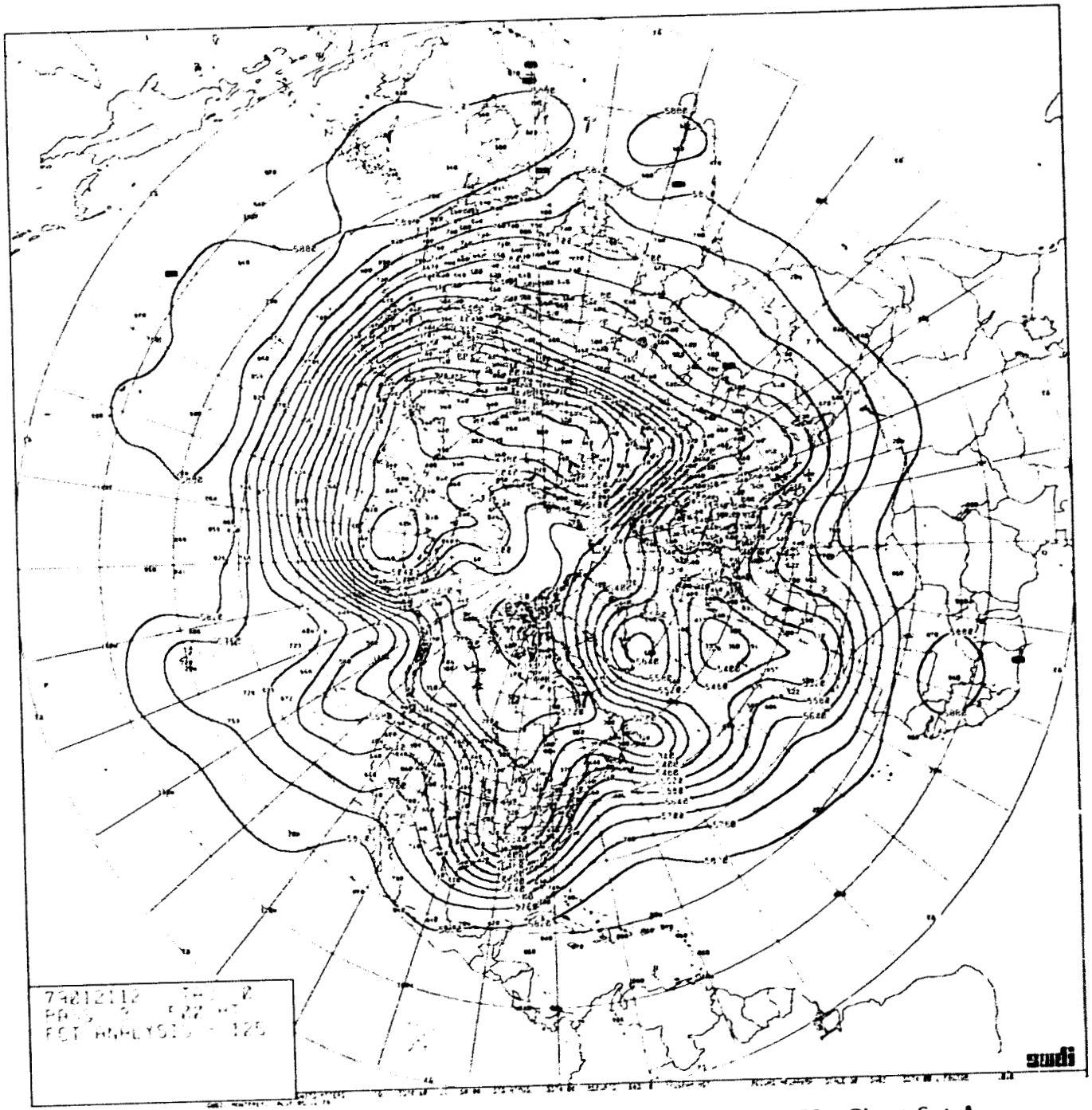

CHART IV-24: 500MB Height Analysis, 1200Z 21 January 1979. Chart Set A.

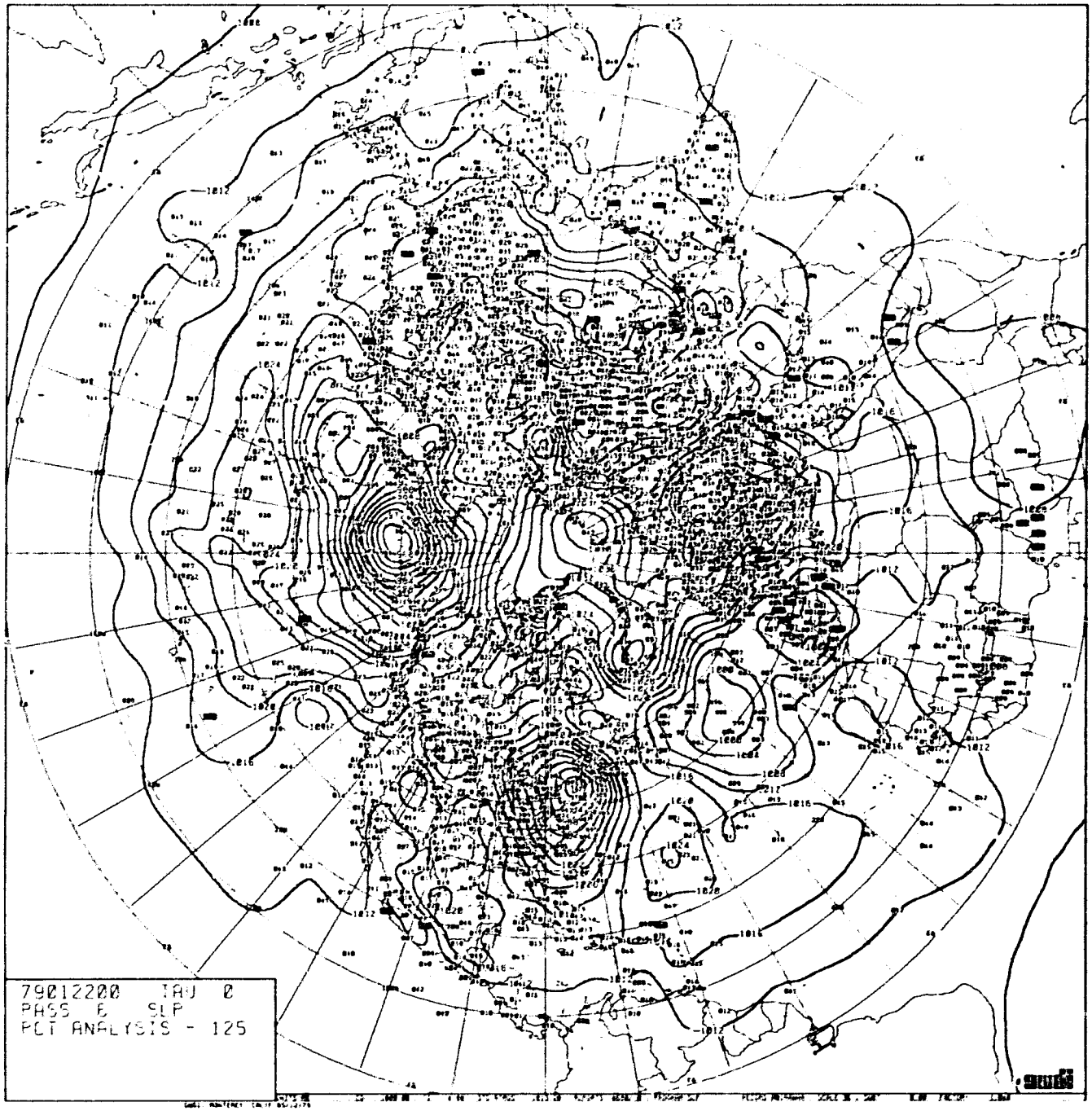

CHART IV-25: Surface Pressure Analysis, 0000Z 22 January 1979. Chart Set A.

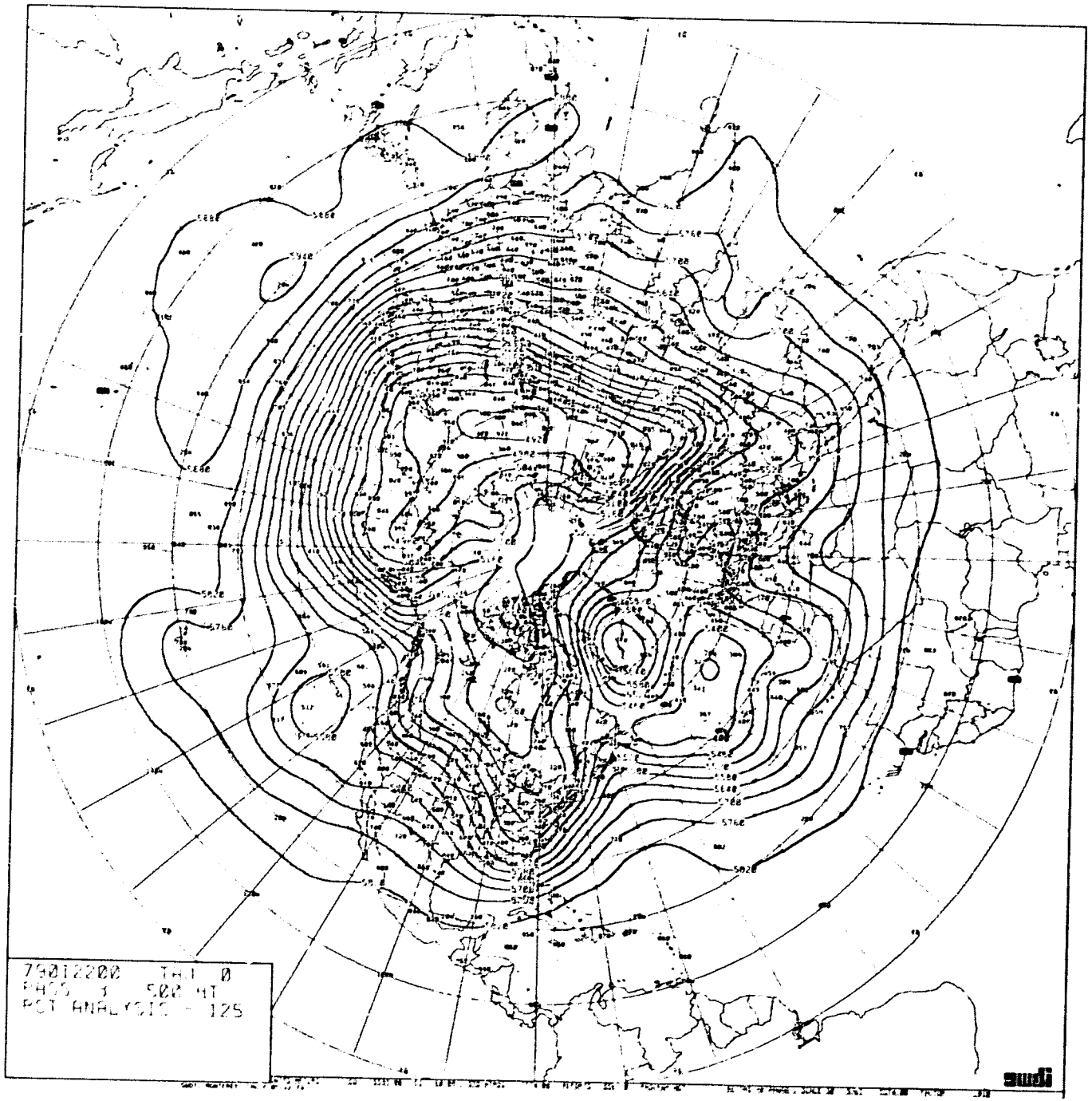

CHART IV-26: 500MB Height Analysis, 0000Z 22 January 1979. Chart Set A.

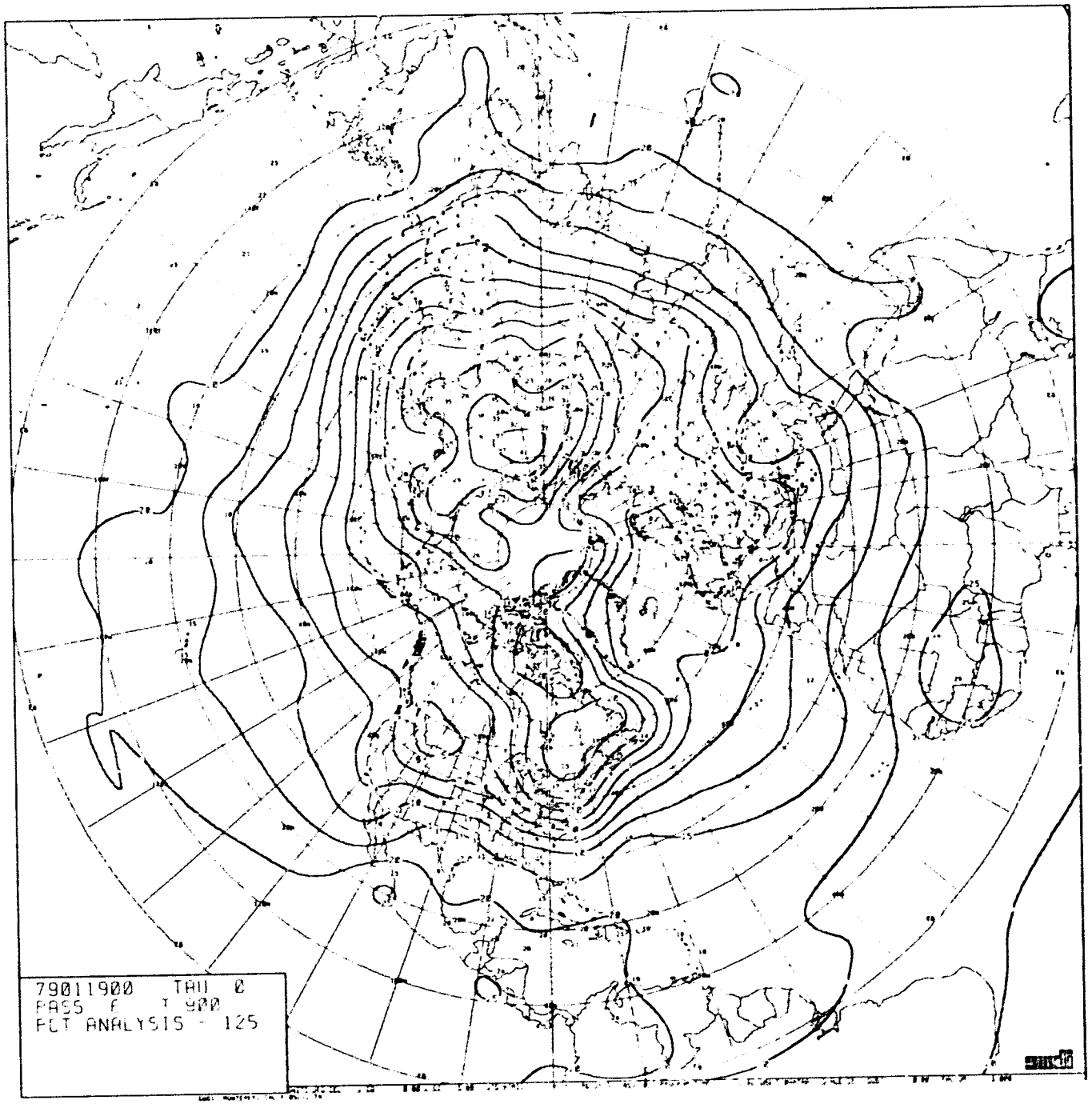

CHART IV-27: 900MB Temperature Analysis, 0000Z 19 January 1979. Chart Set B.

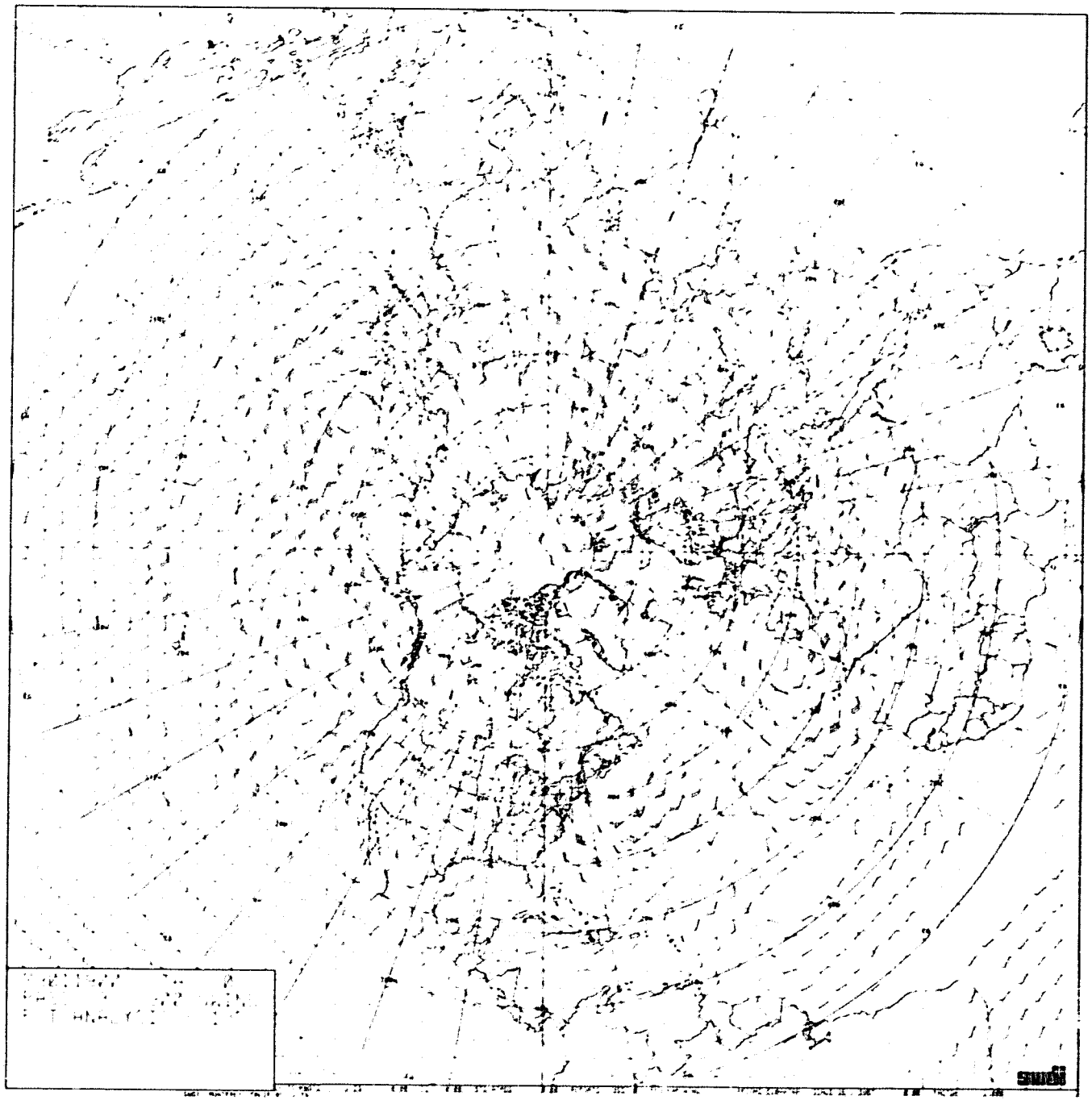

CHART IV-28: 900MB Wind Analysis, 0000Z 19 January 1979. Chart Set B.

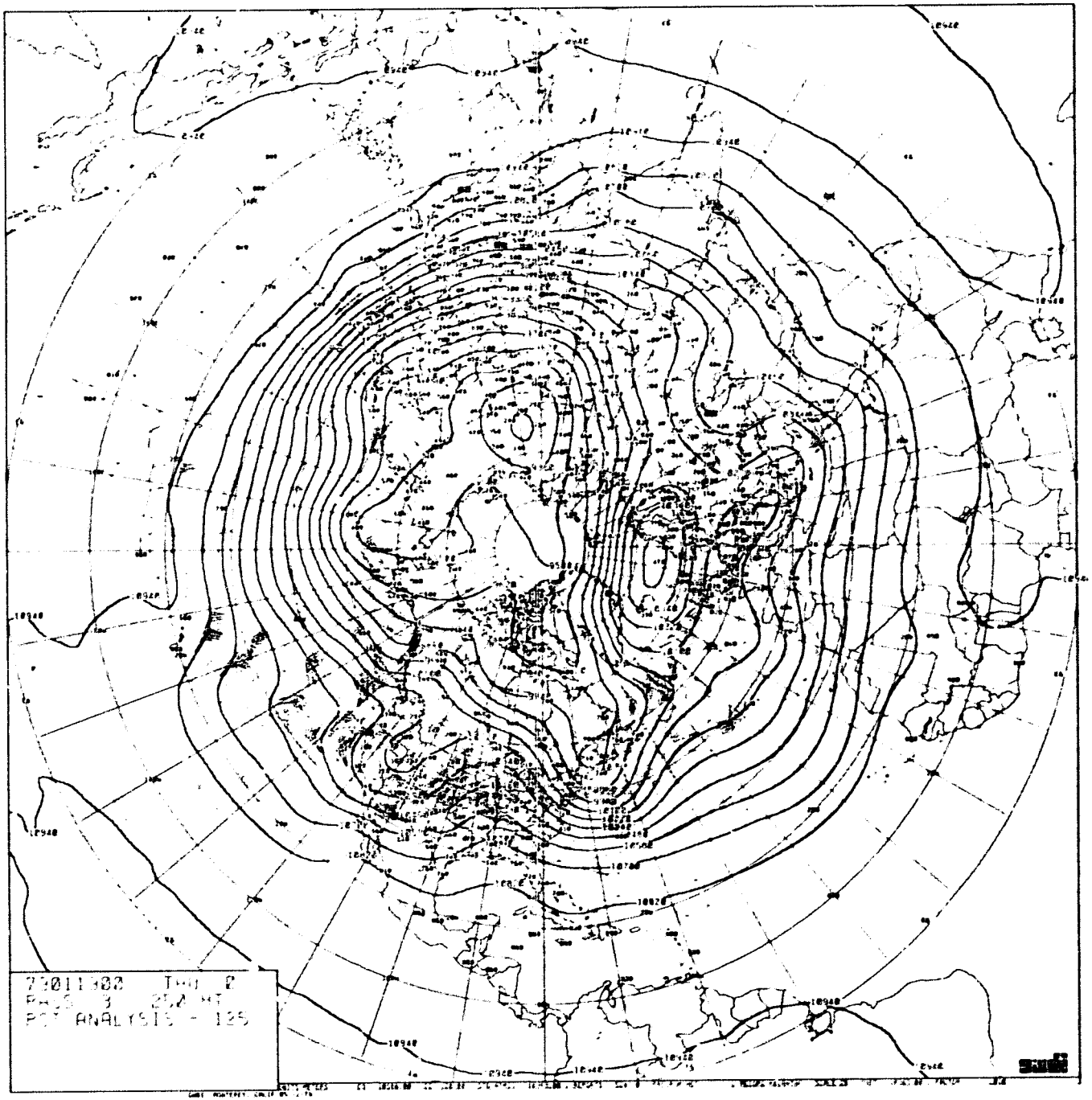

CHART IV-29: 250MB Height Analysis, 0000Z 19 January 1979. Chart Set B.

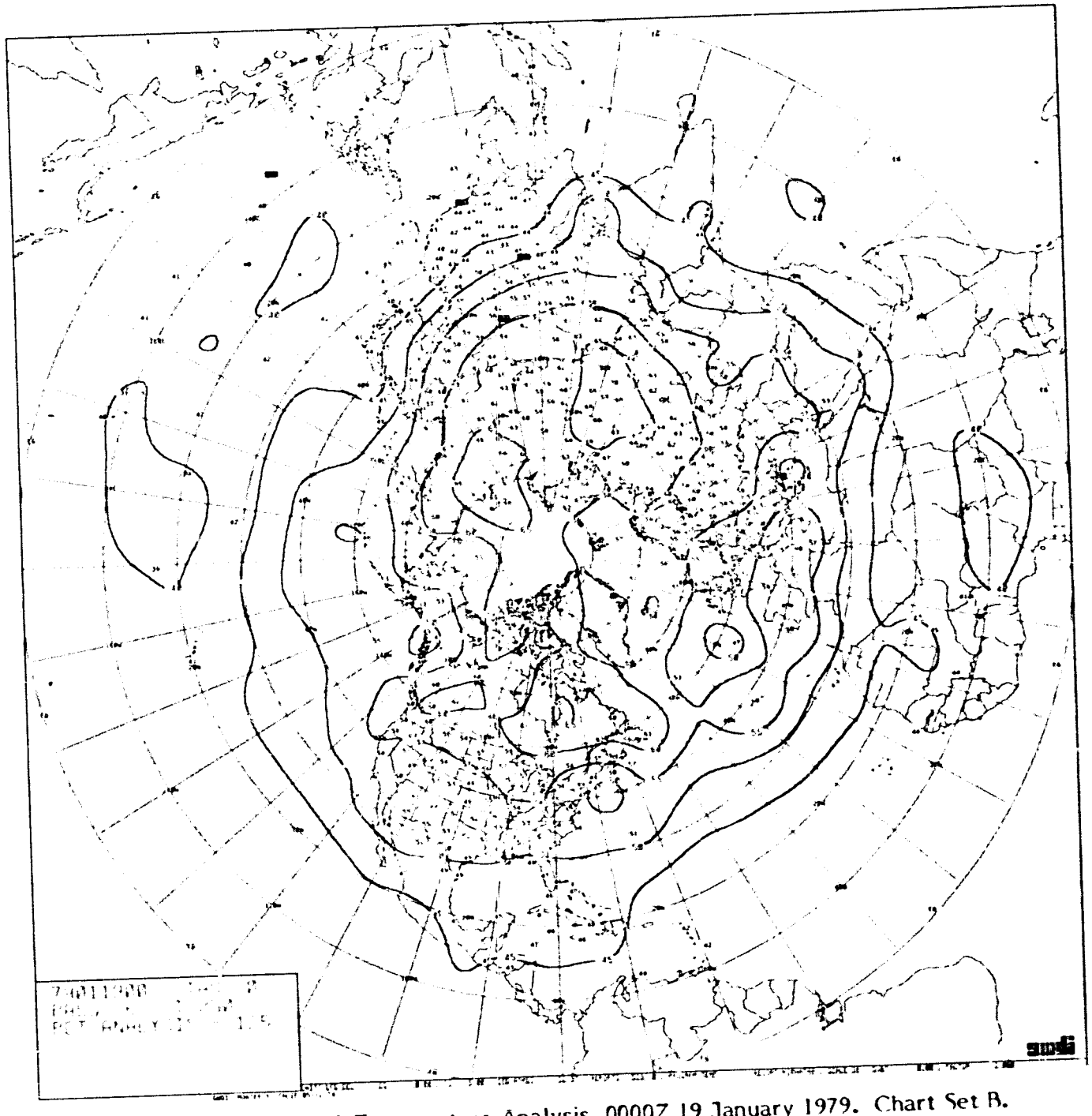

CHART IV-30: 250MB Temperature Analysis, 0000Z 19 January 1979. Chart Set B.

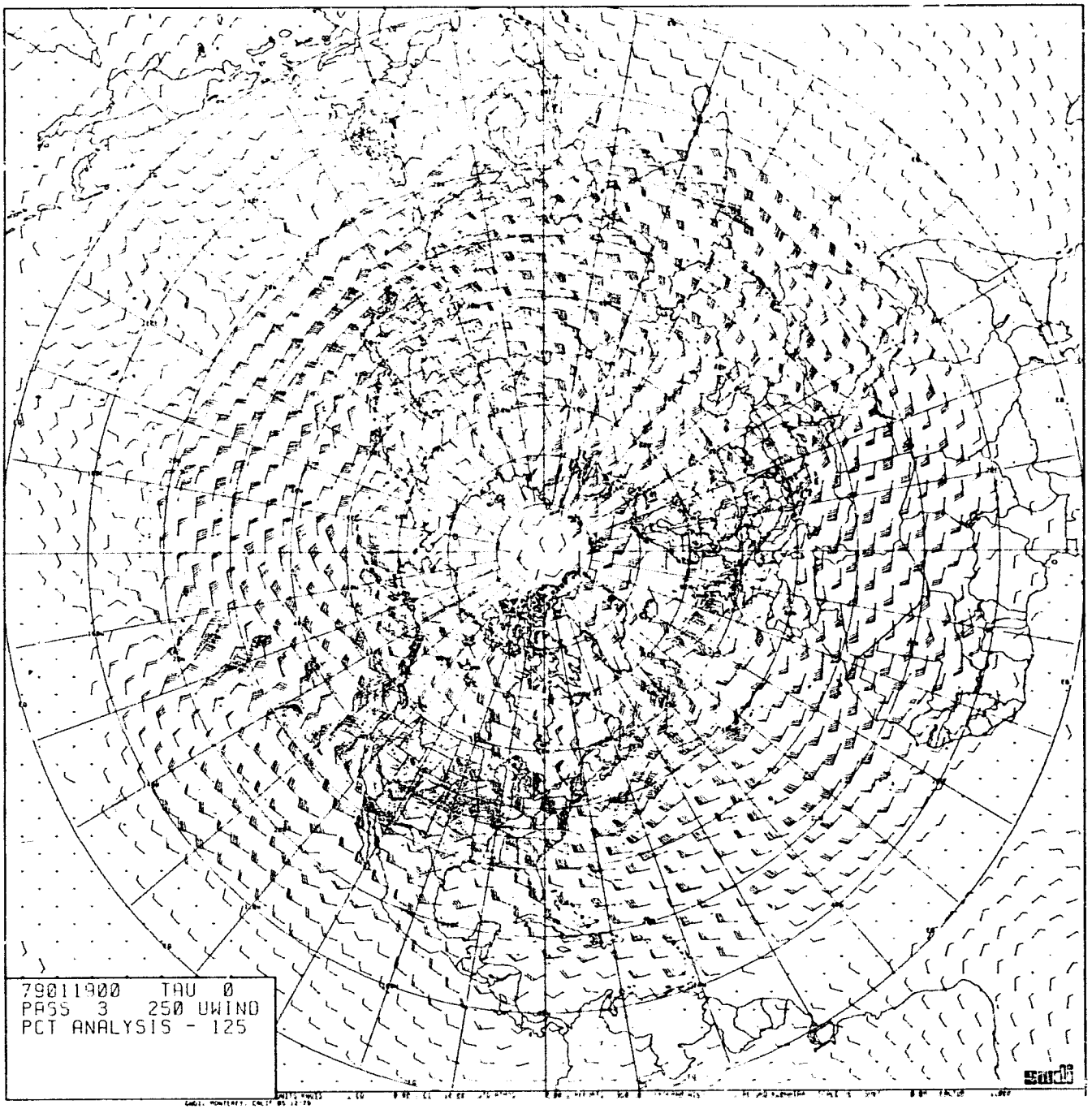

CHART IV-31: 250MB Wind Analysis, 0000Z 19 January 1979. Chart Set B.

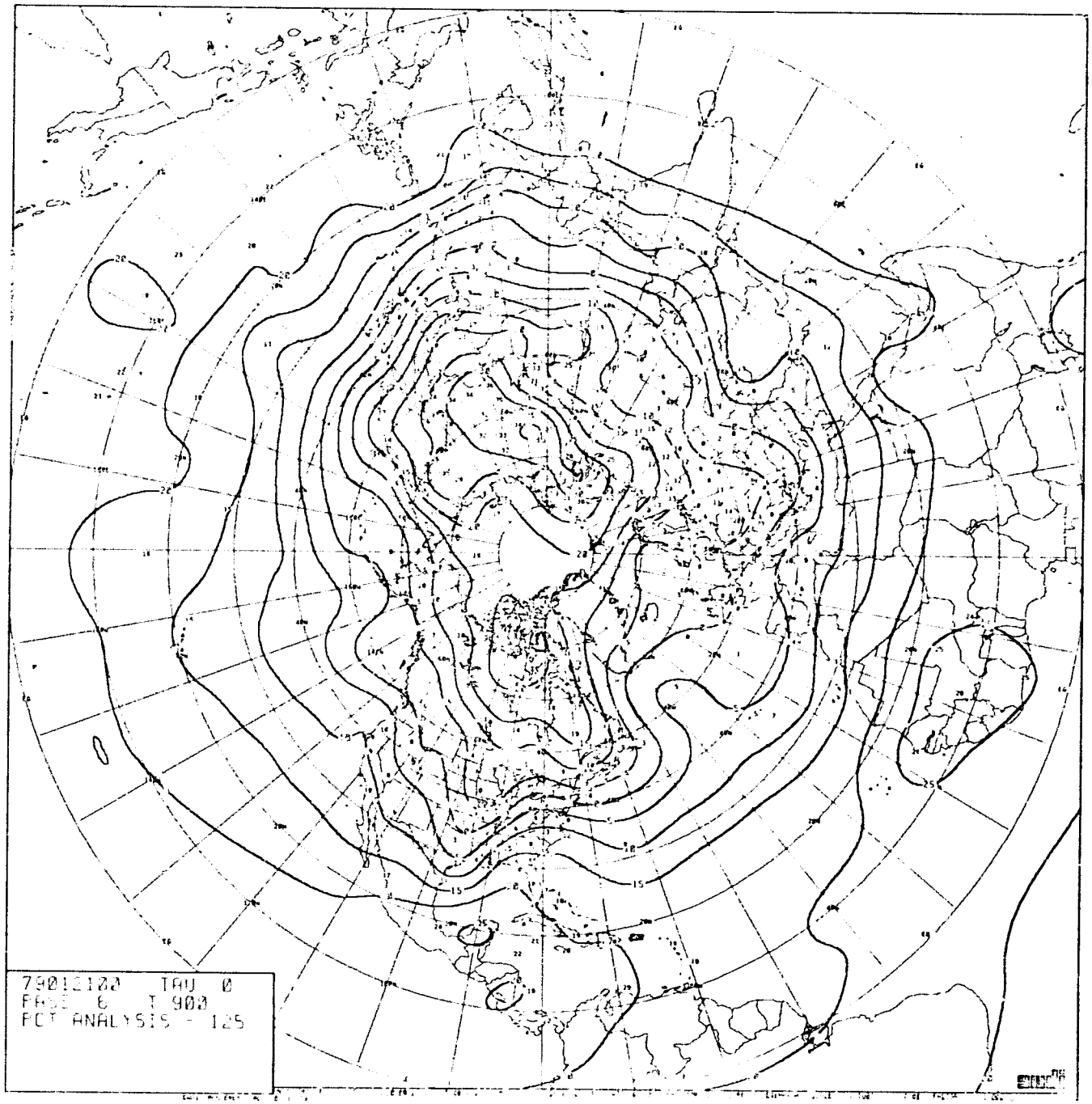

CHART IV-32: 900MB Temperature Analysis, 0000Z 21 January 1979. Chart Set B.

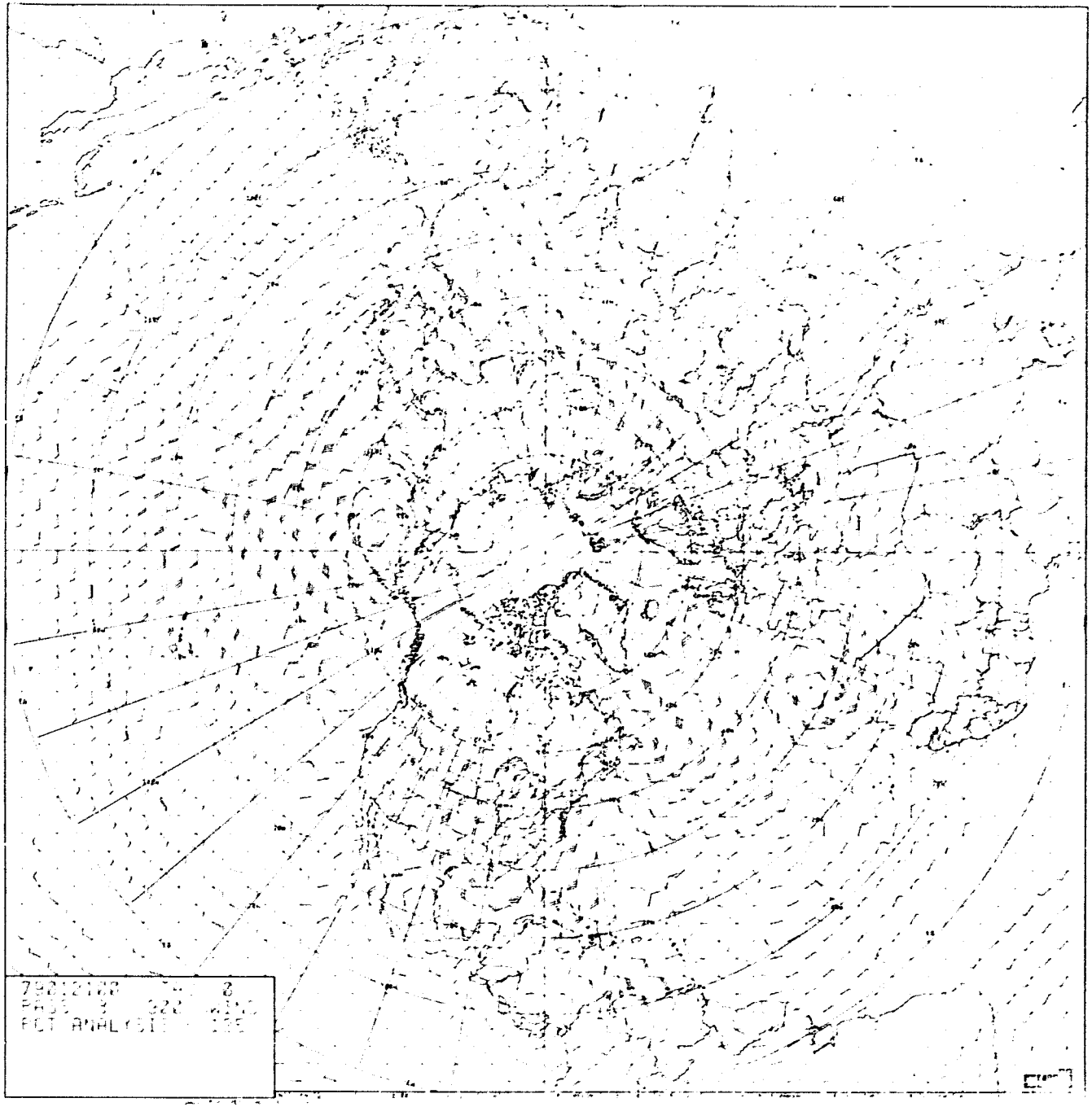

CHART IV-33: 900MB Wind Analysis, 0000Z 21 January 1979. Chart Set B.

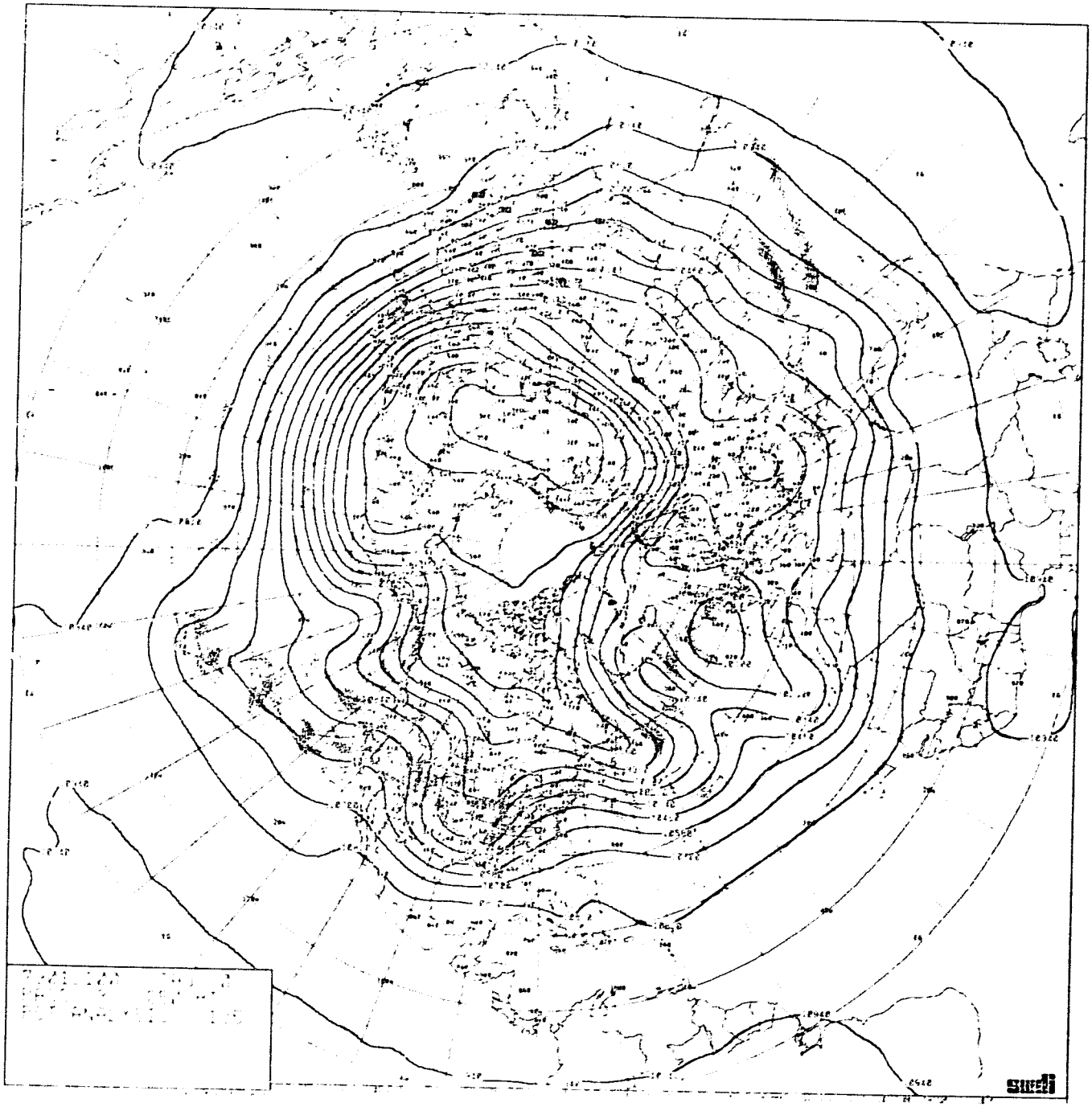

CHART IV-34: 250MB Height Analysis, 0000Z 21 January 1979. Chart Set B.

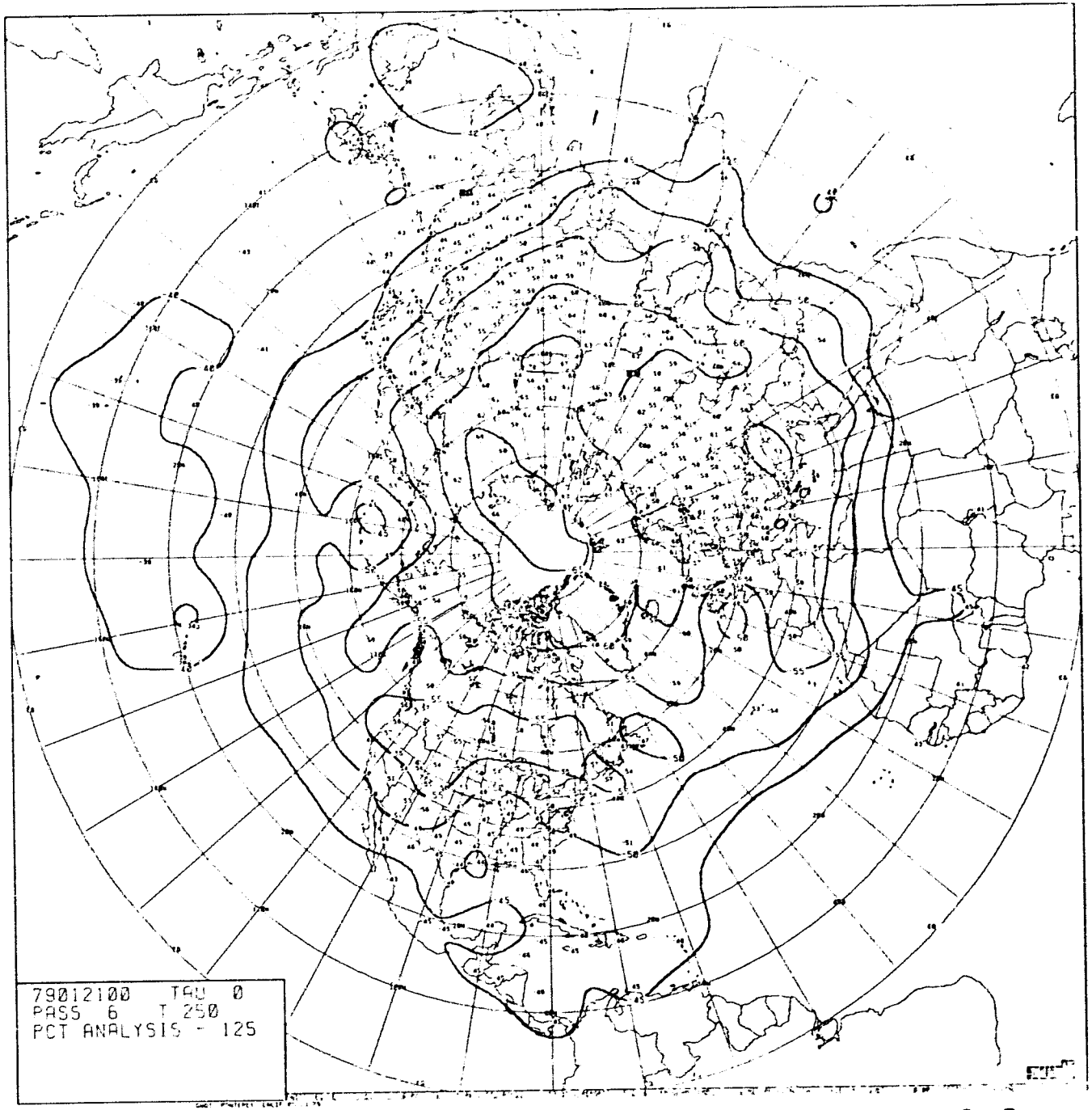

CHART IV-35: 250MB Temperature Analysis, 0000Z 21 January 1979. Chart Set B.

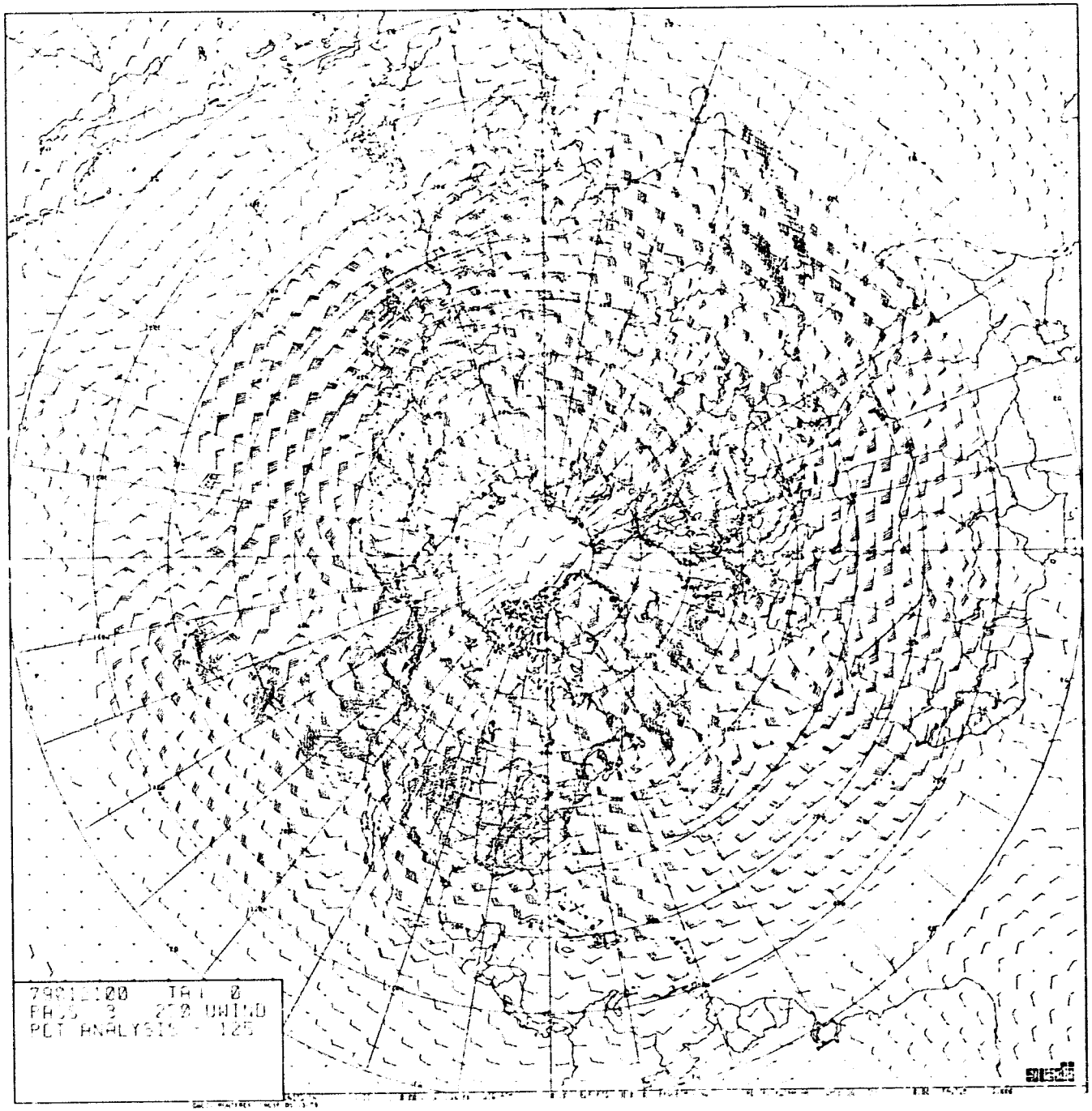

CHART IV-36: 250MB Wind Analysis, 0000Z 21 January 1979. Chart Set B.

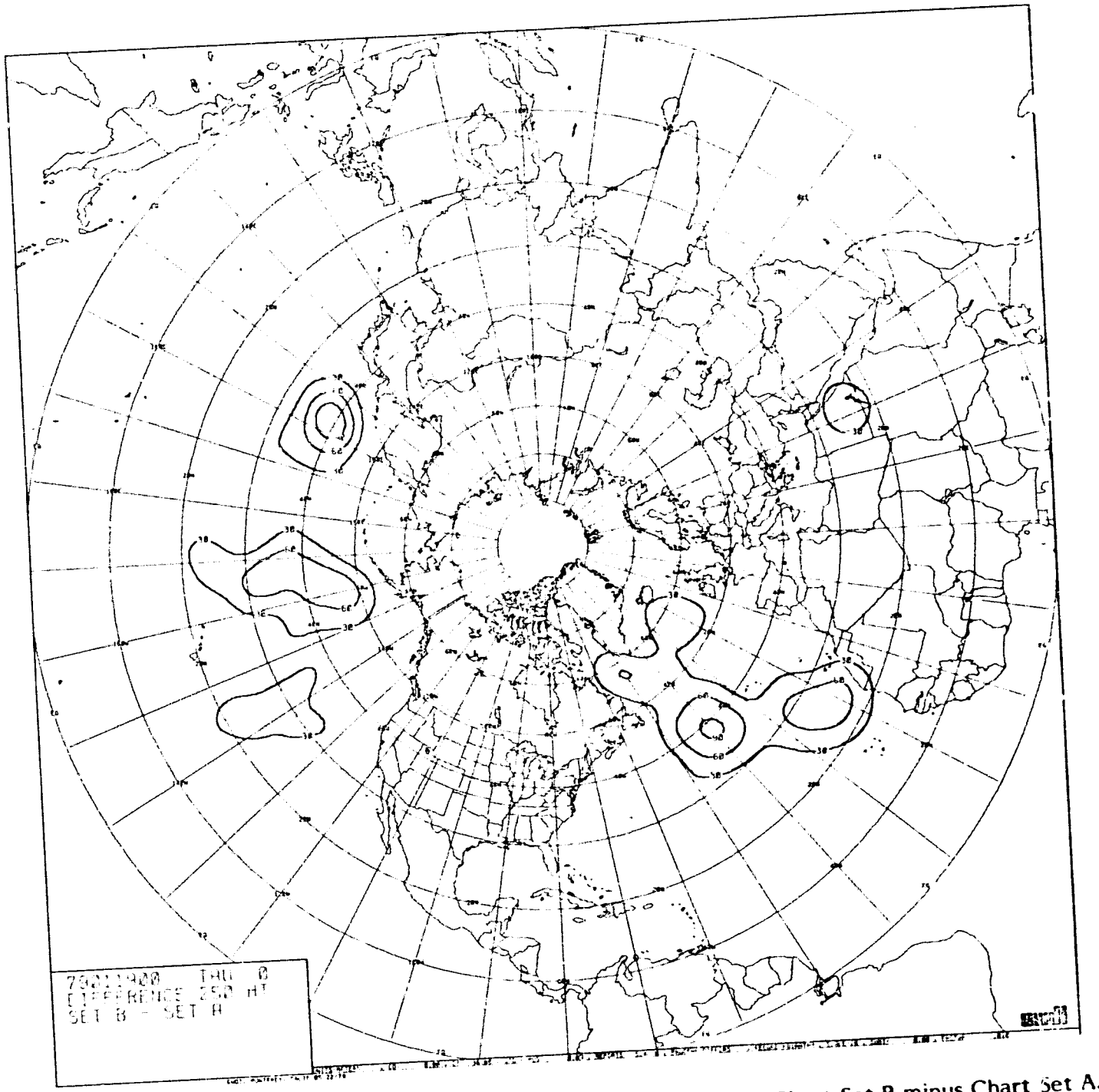

CHART IV-37: 250 MB Height Difference, 0000Z 21 January 1979. Chart Set B minus Chart Set A.

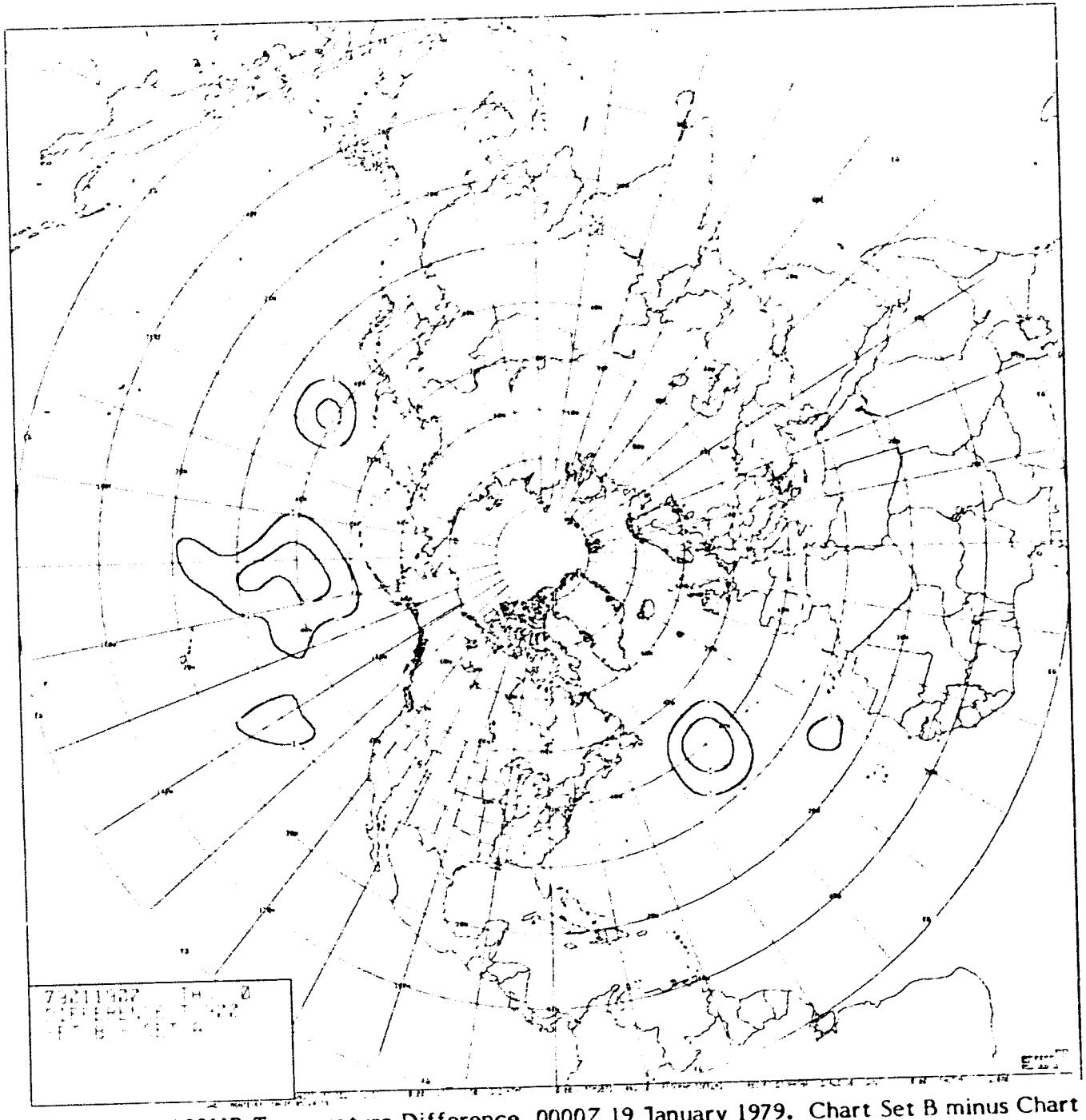

CHART IV-38: 900MB Temperature Difference, 0000Z 19 January 1979. Chart Set B minus Chart Set A.

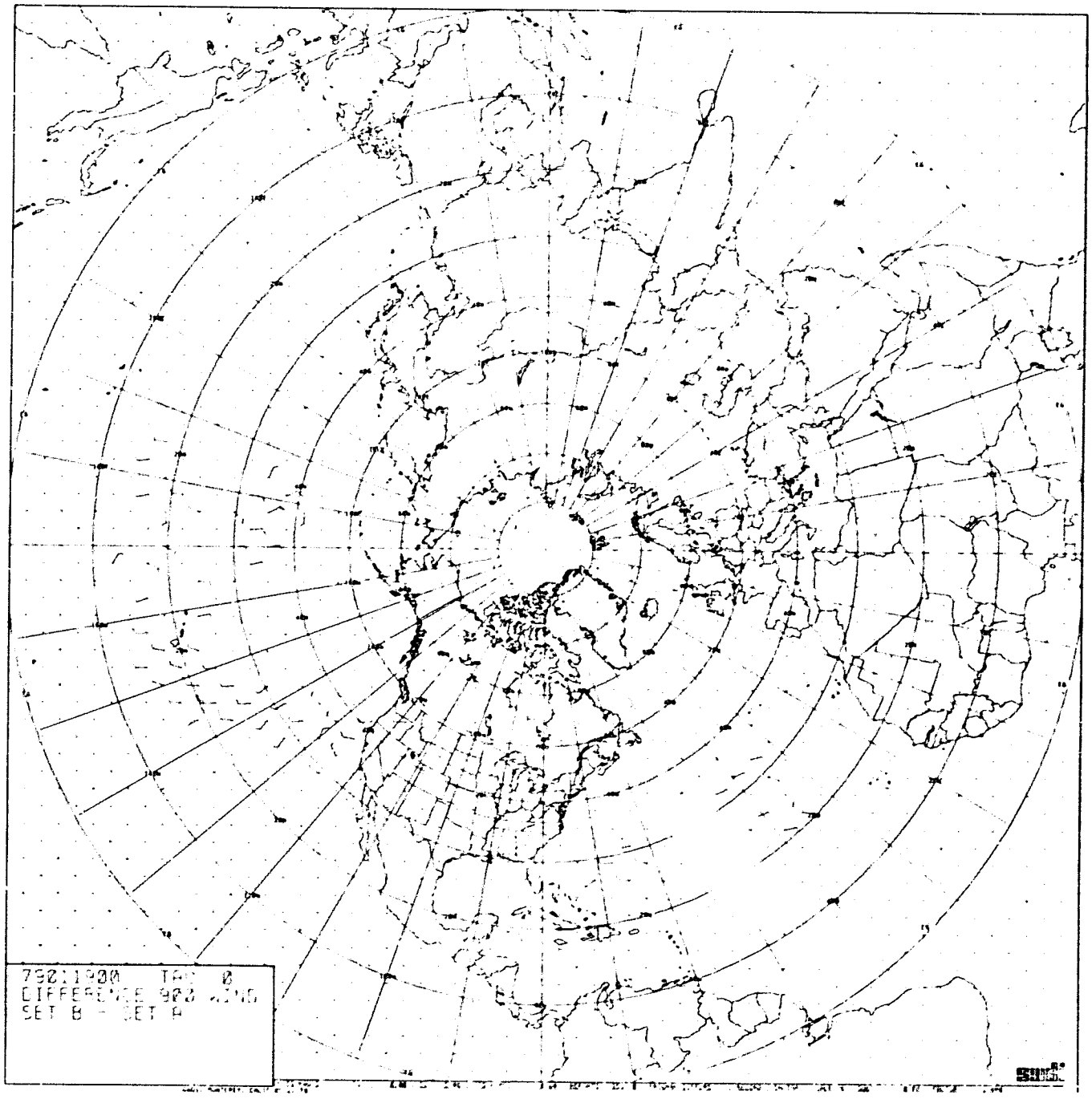

CHART IV-39: 900MB Wind Difference, 0000Z 19 January 1979. Chart Set B minus Chart Set A.

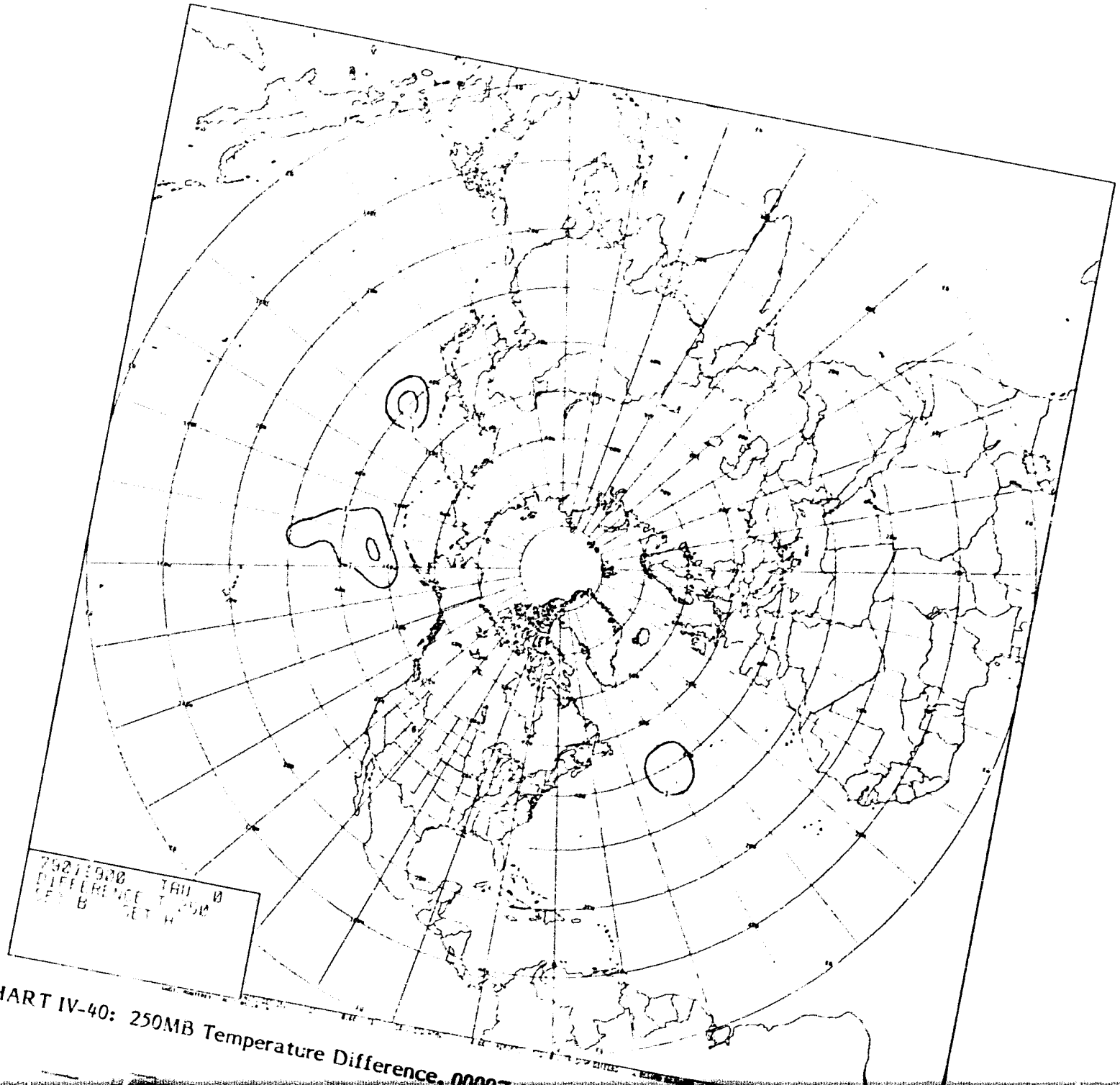

CHART IV-40: 250MB Temperature Difference, 0000

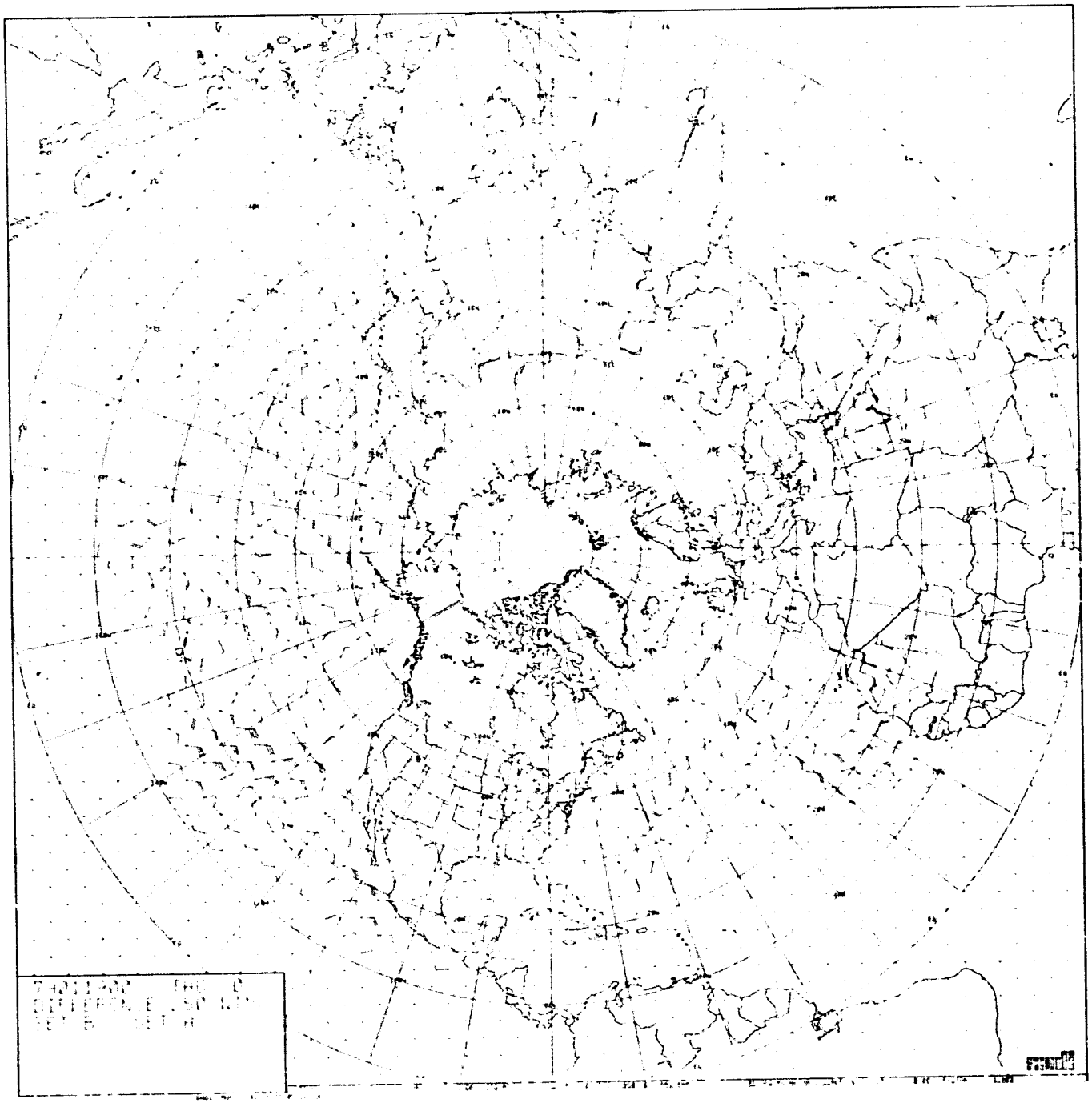

CHART IV-41: 250MB Wind Difference, 0000Z 19 January 1979. Chart Set B minus Chart Set A.

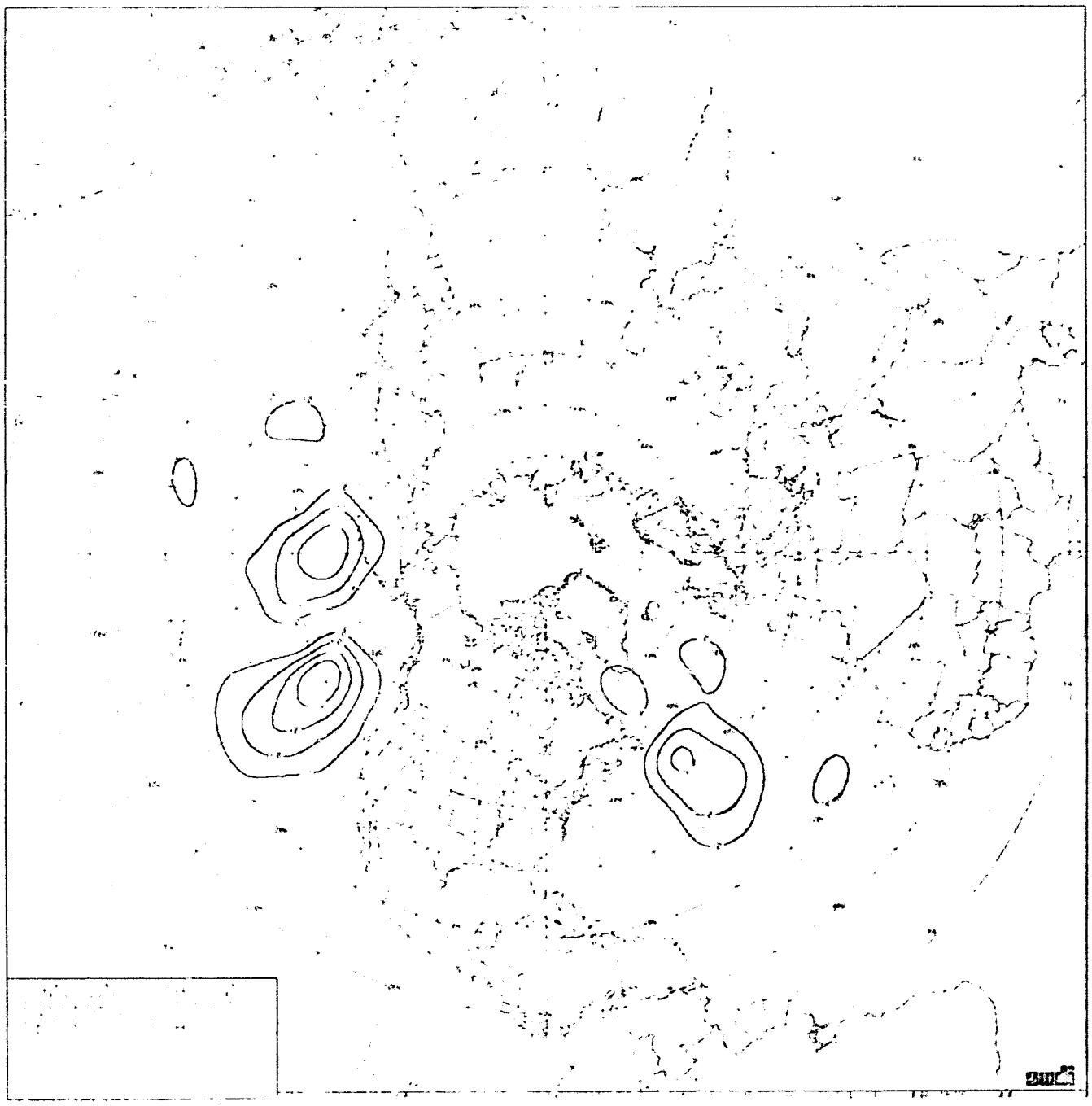

CHART IV-42: 250 MB Height (Cumulative) Difference, 0000Z 21 January 1979. Chart Set B minus Chart Set A.

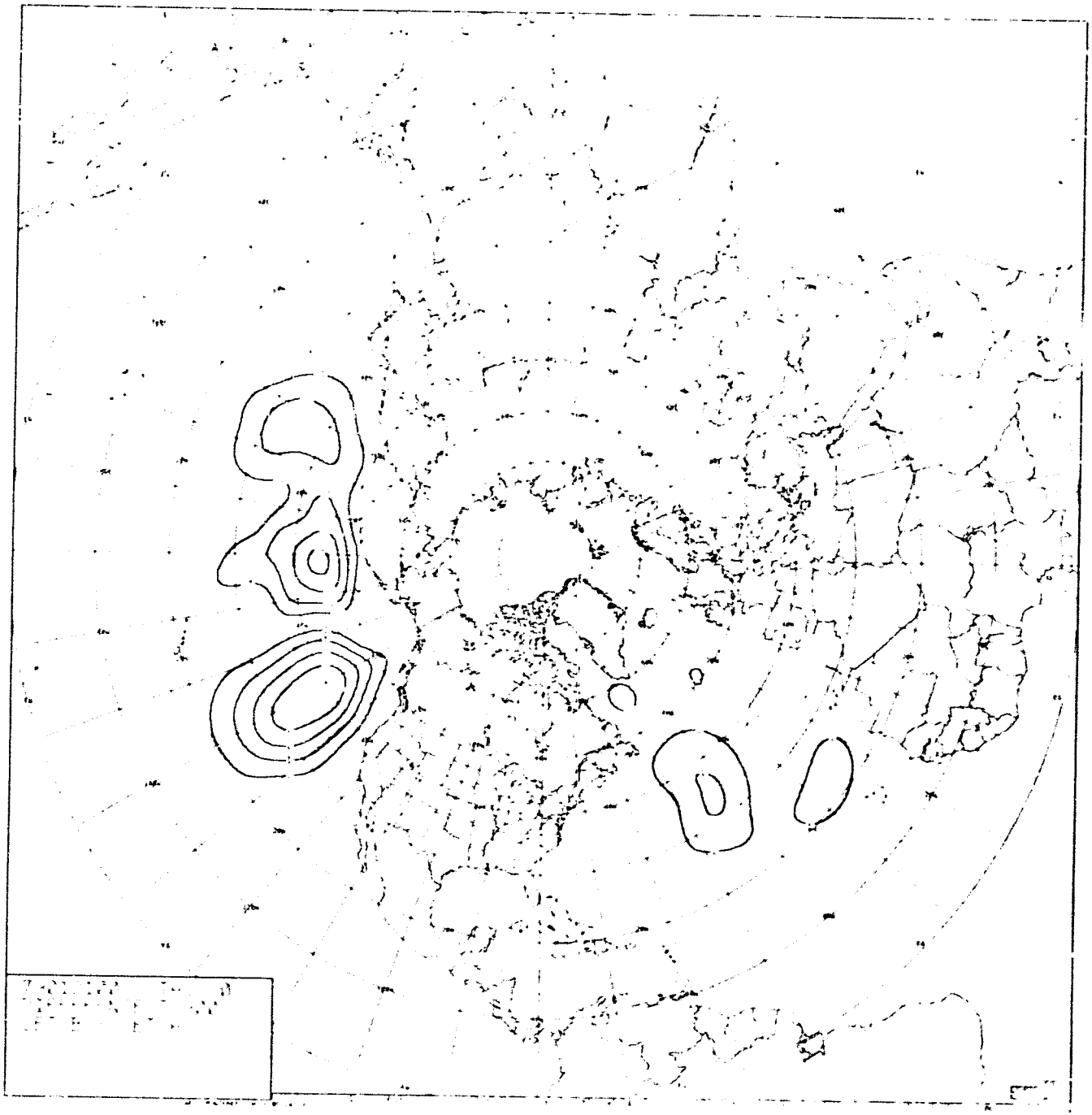

CHART IV-43: 900MB Temperature (Cumulative) Difference, 0000Z 21 January 1979. Chart Set B minus Chart Set A.

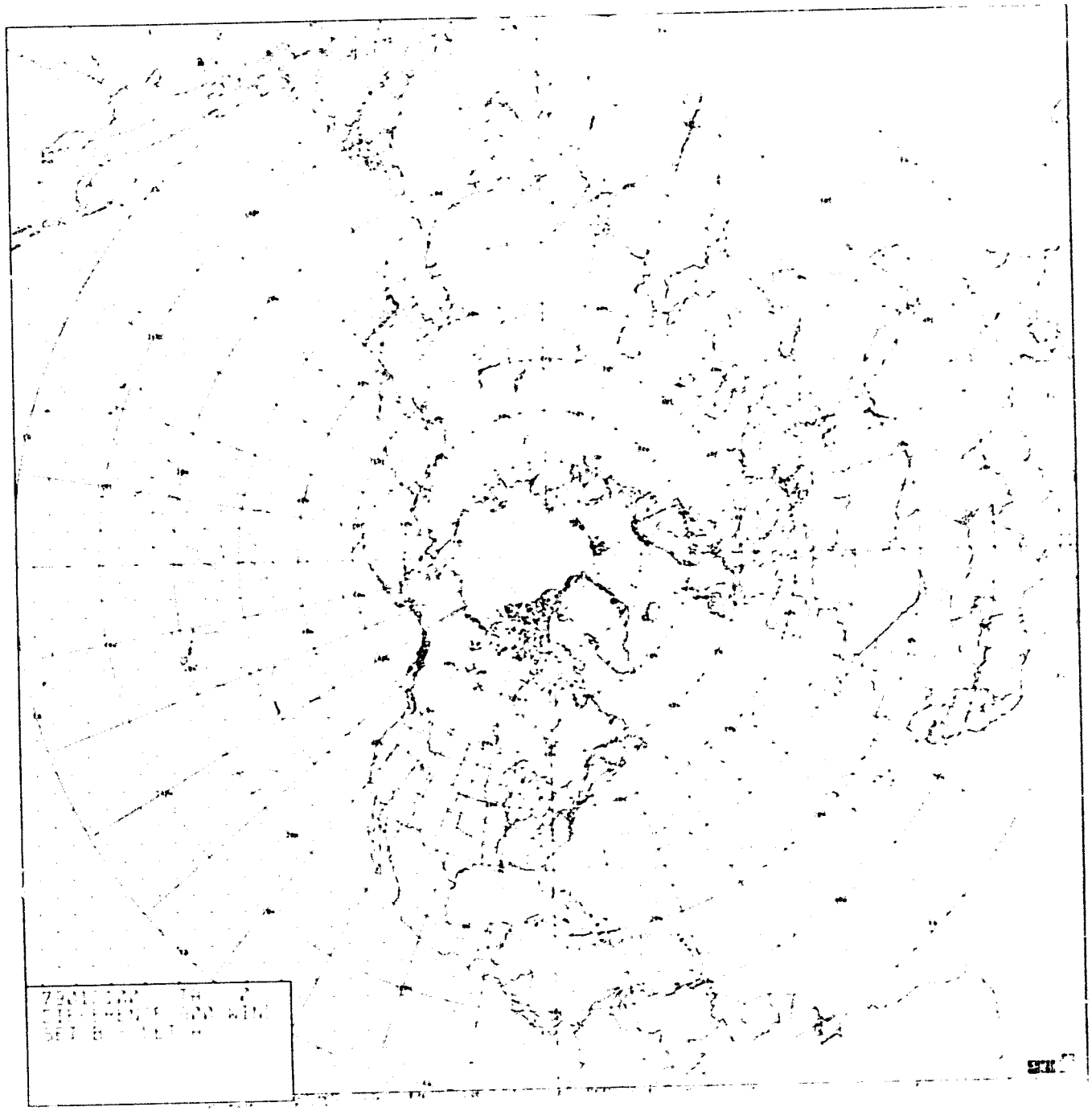

CHART IV-44: 900MB Wind (Cumulative) Difference, 0000Z 21 January 1979. Chart Set B minus Chart Set A.

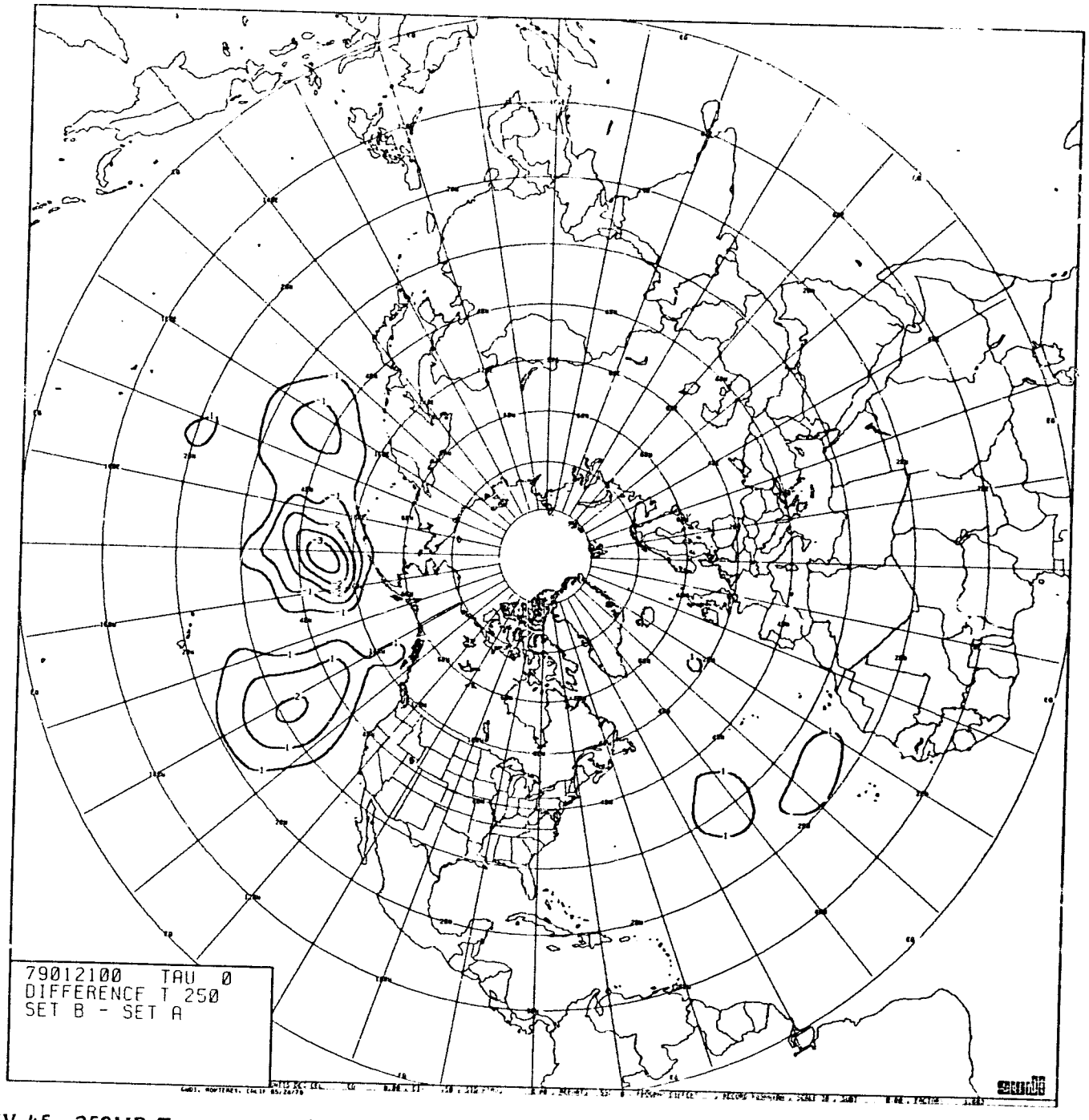

CHART IV-45: 250MB Temperature (Cumulative) Difference, 0000Z 21 January 1979. Chart Set B minus Chart Set A.

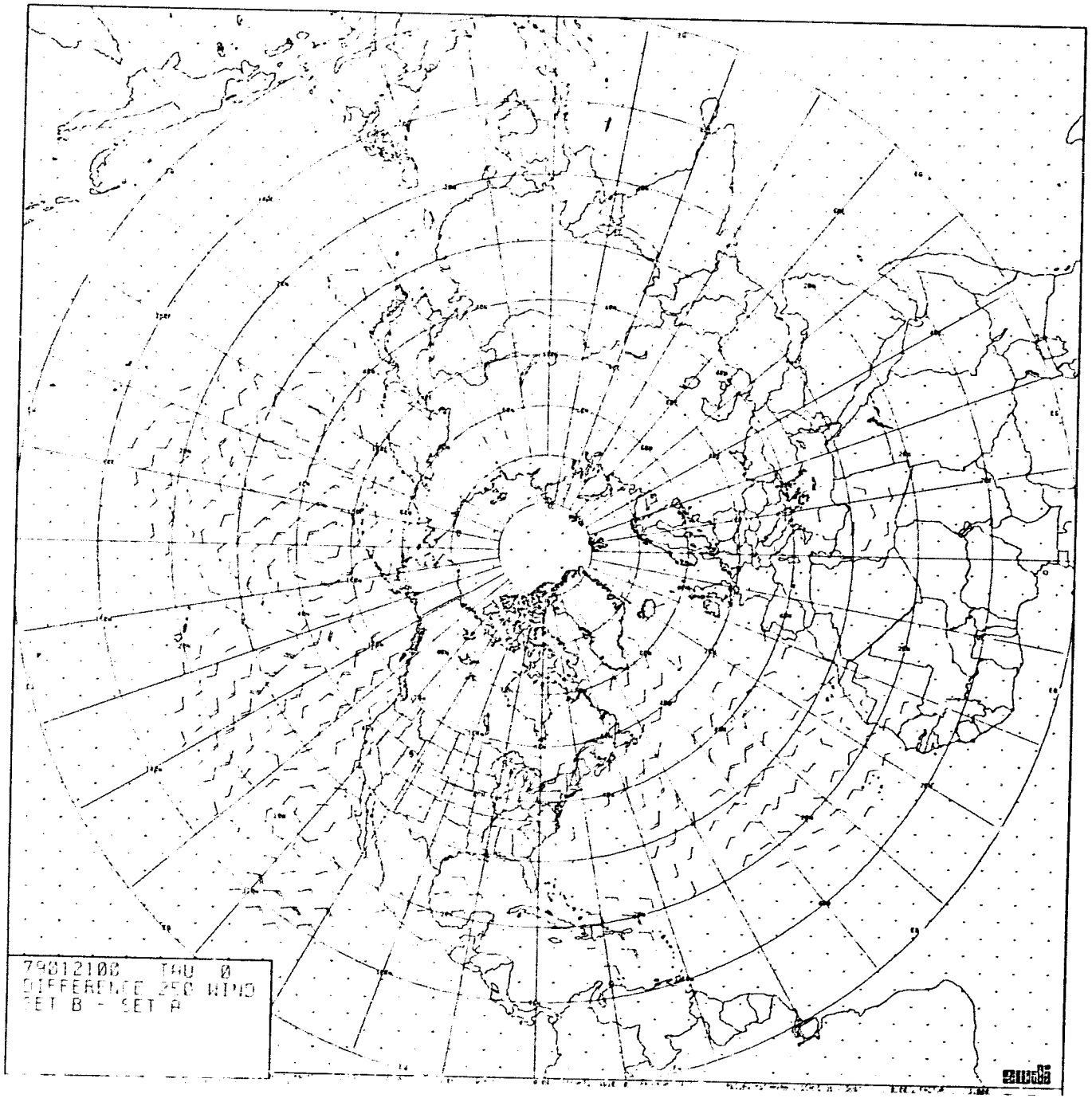

CHART IV-46: 250MB Wind (Cumulative) Difference, 0000Z 21 January 1979. Chart Set B minus Chart Set A.

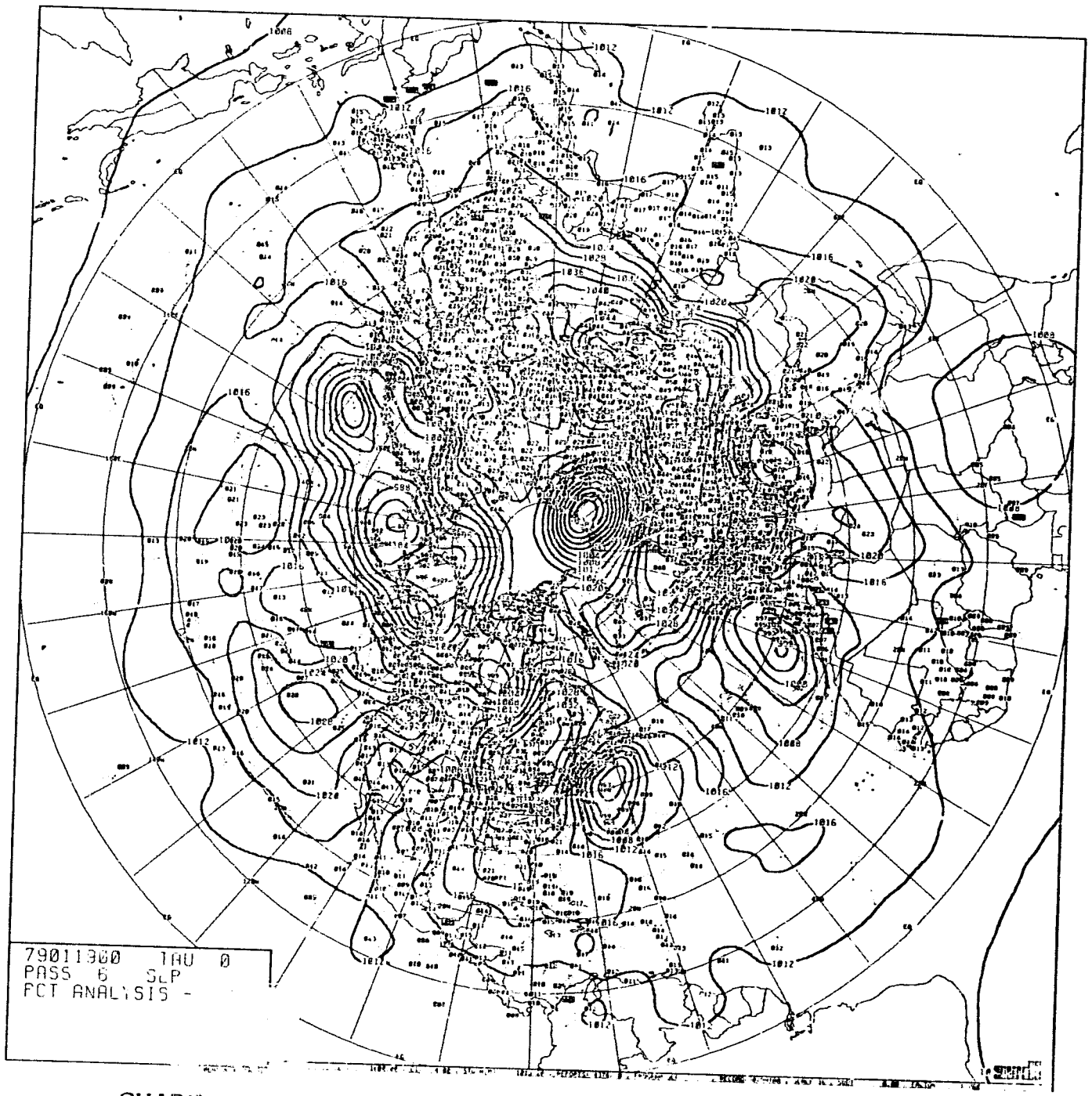

CHART [illegible]. Surface Pressure Analysis, 0000Z 19 January 1979. Chart Set C.

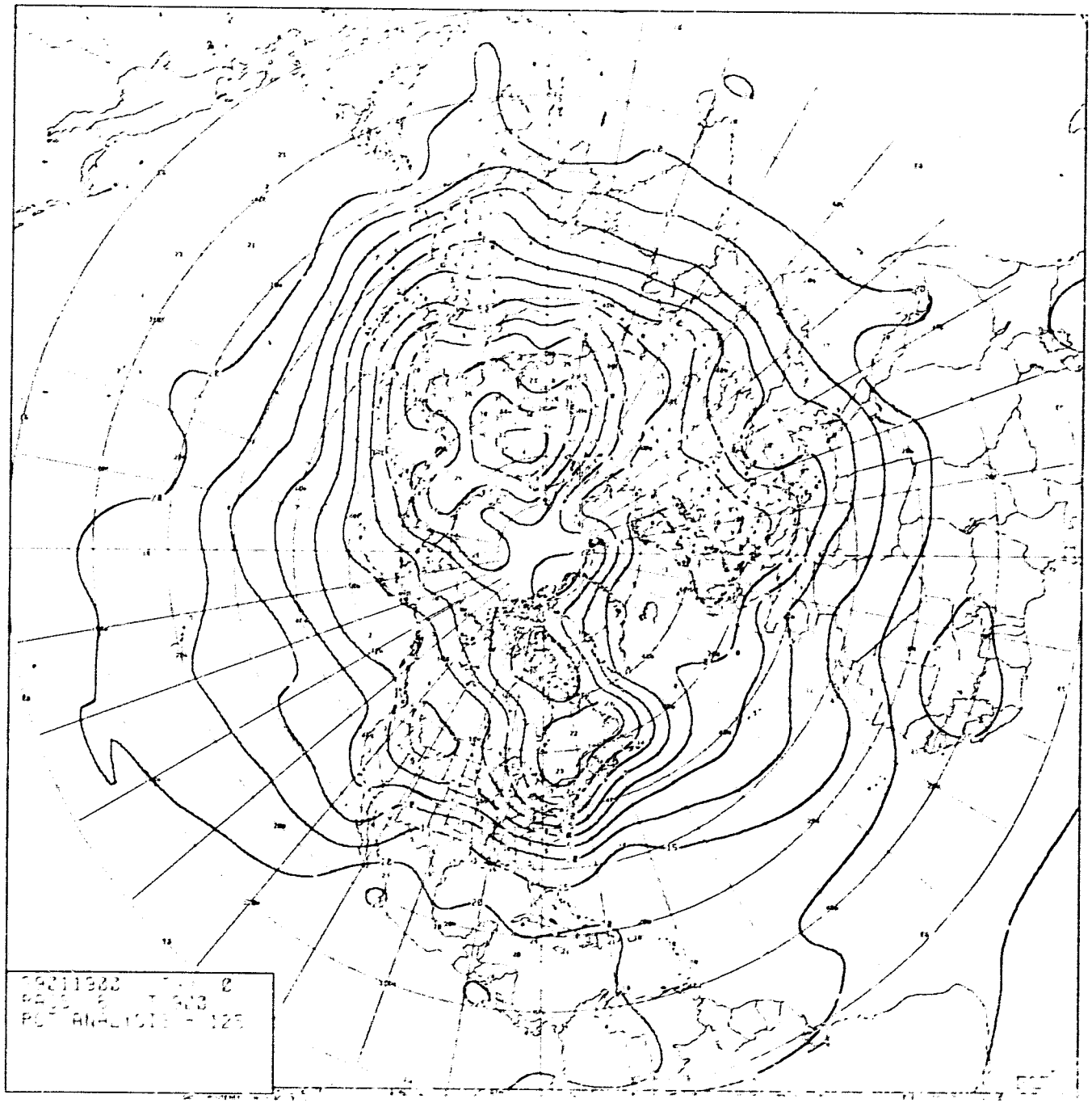

CHART IV-48: 900MB Temperature Analysis, 0000Z 19 January 1979. Chart Set C.

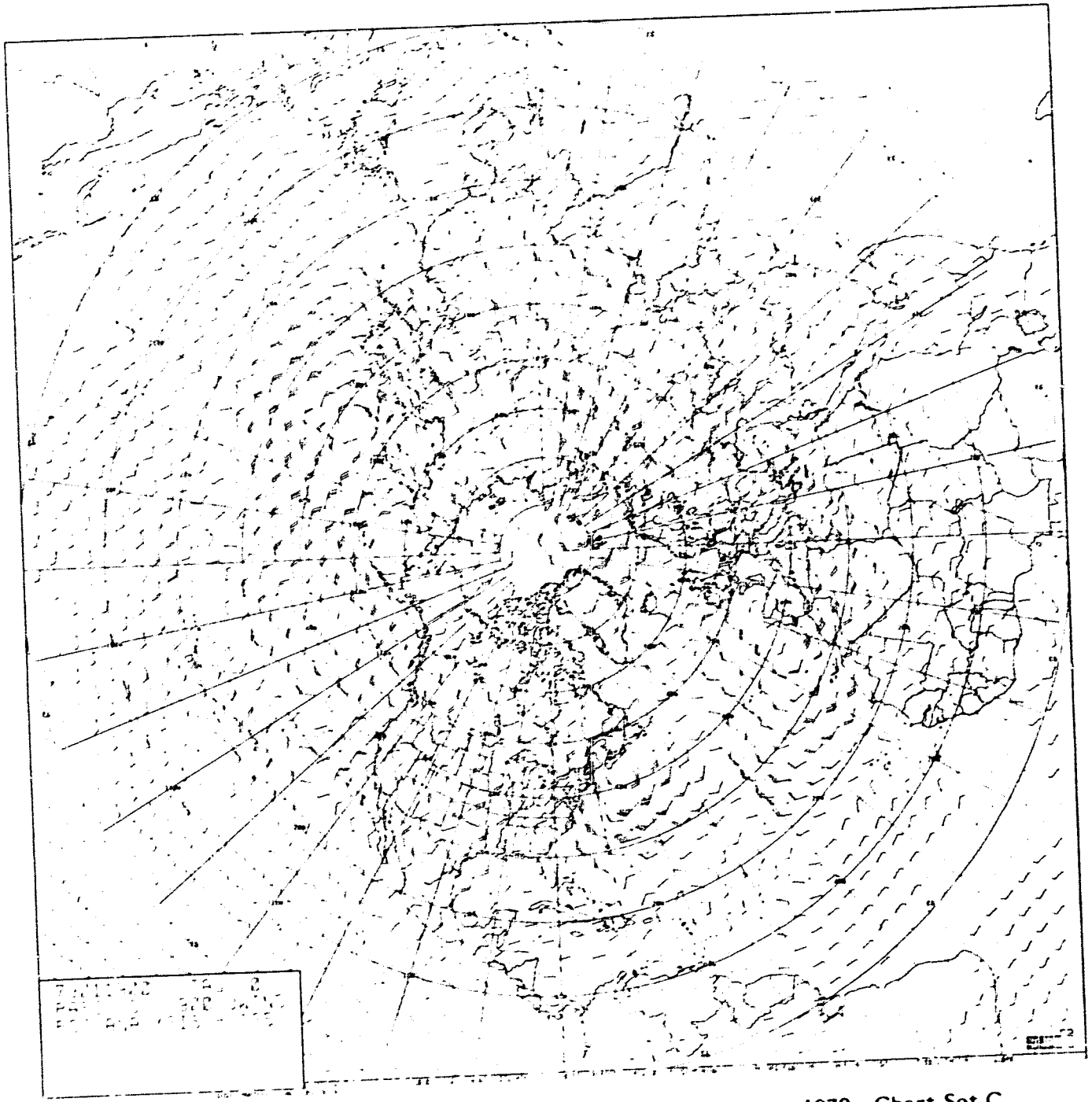

CHART IV-49: 900MB Wind Analysis, 0000Z 19 January 1979. Chart Set C.

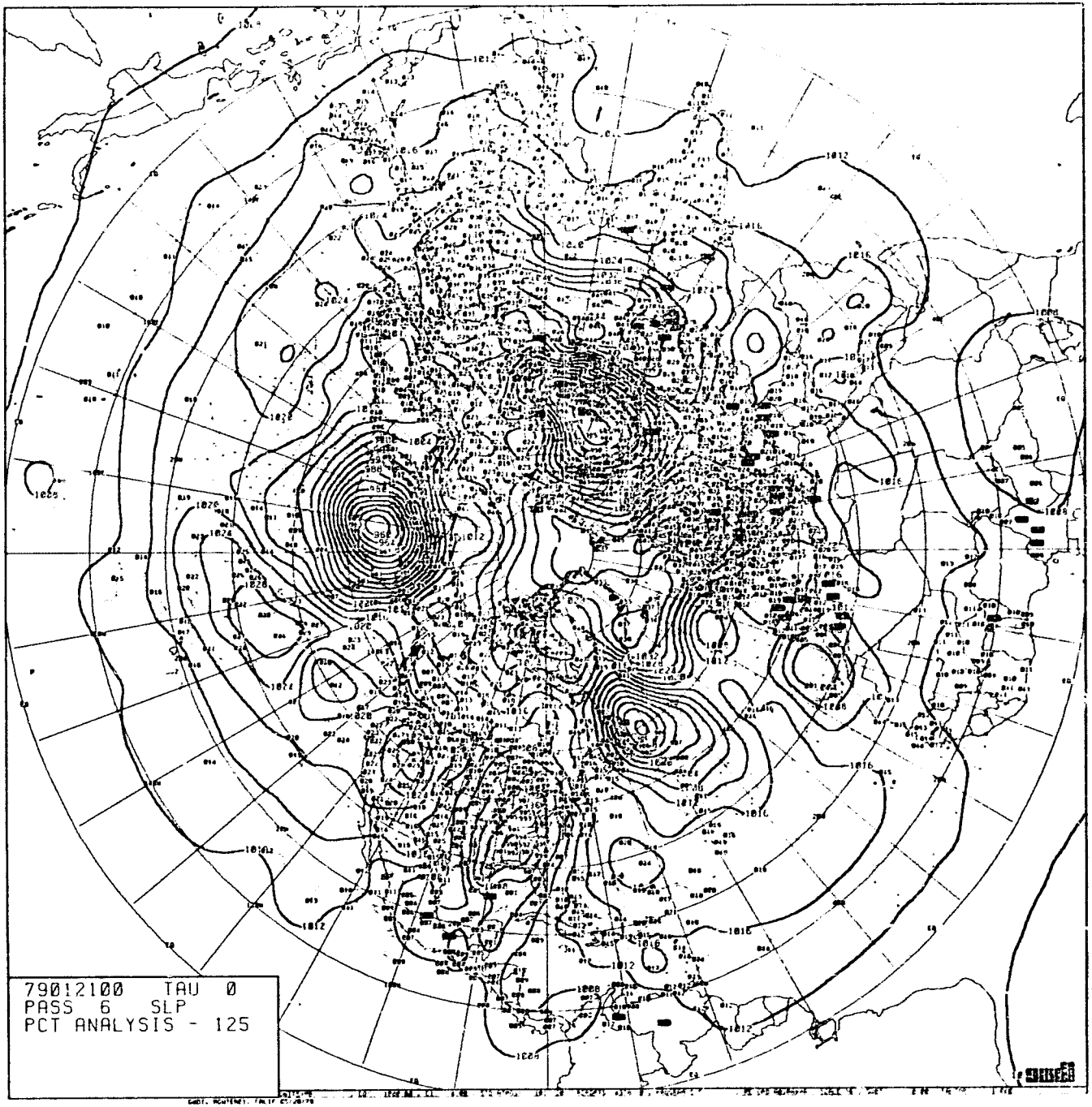

CHART IV-50: Surface Pressure Analysis, 0000Z 21 January 1979. Chart Set C.

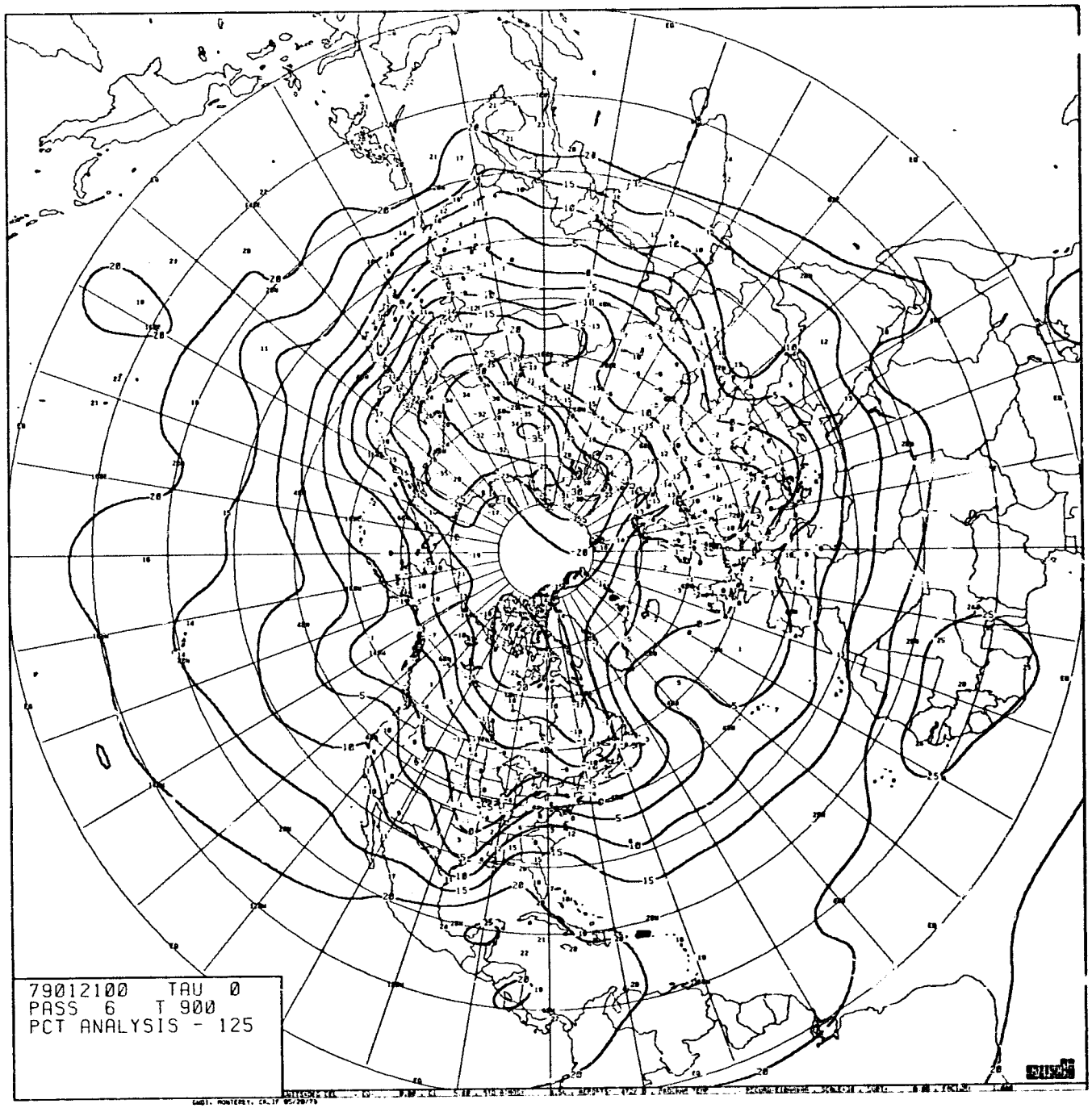

CHART IV-51: 900MB Temperature Analysis, 0000Z 21 January 1979. Chart Set C.

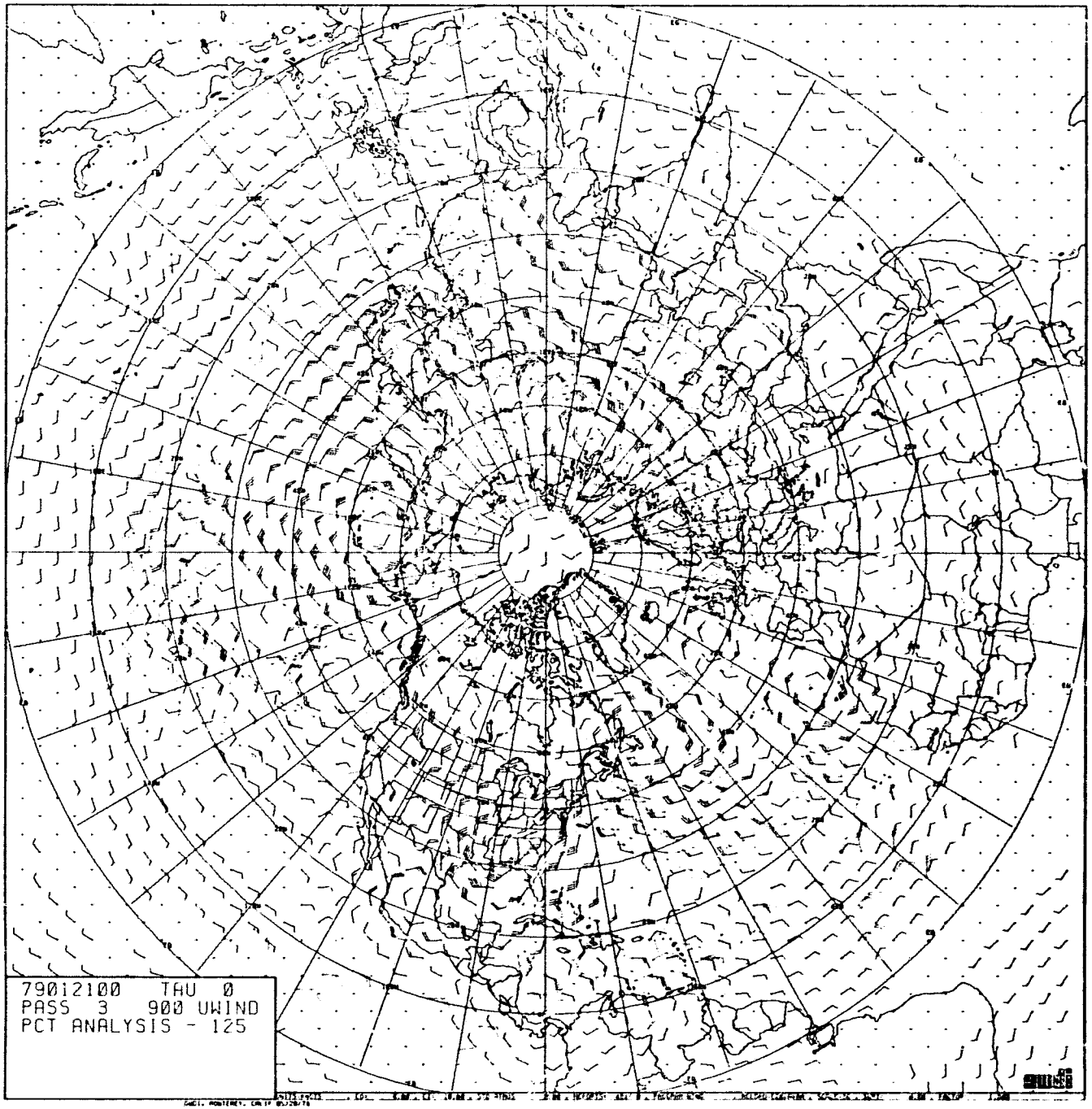

CHART IV-52: 900MB Wind Analysis, 0000Z 21 January 1979. Chart Set C.

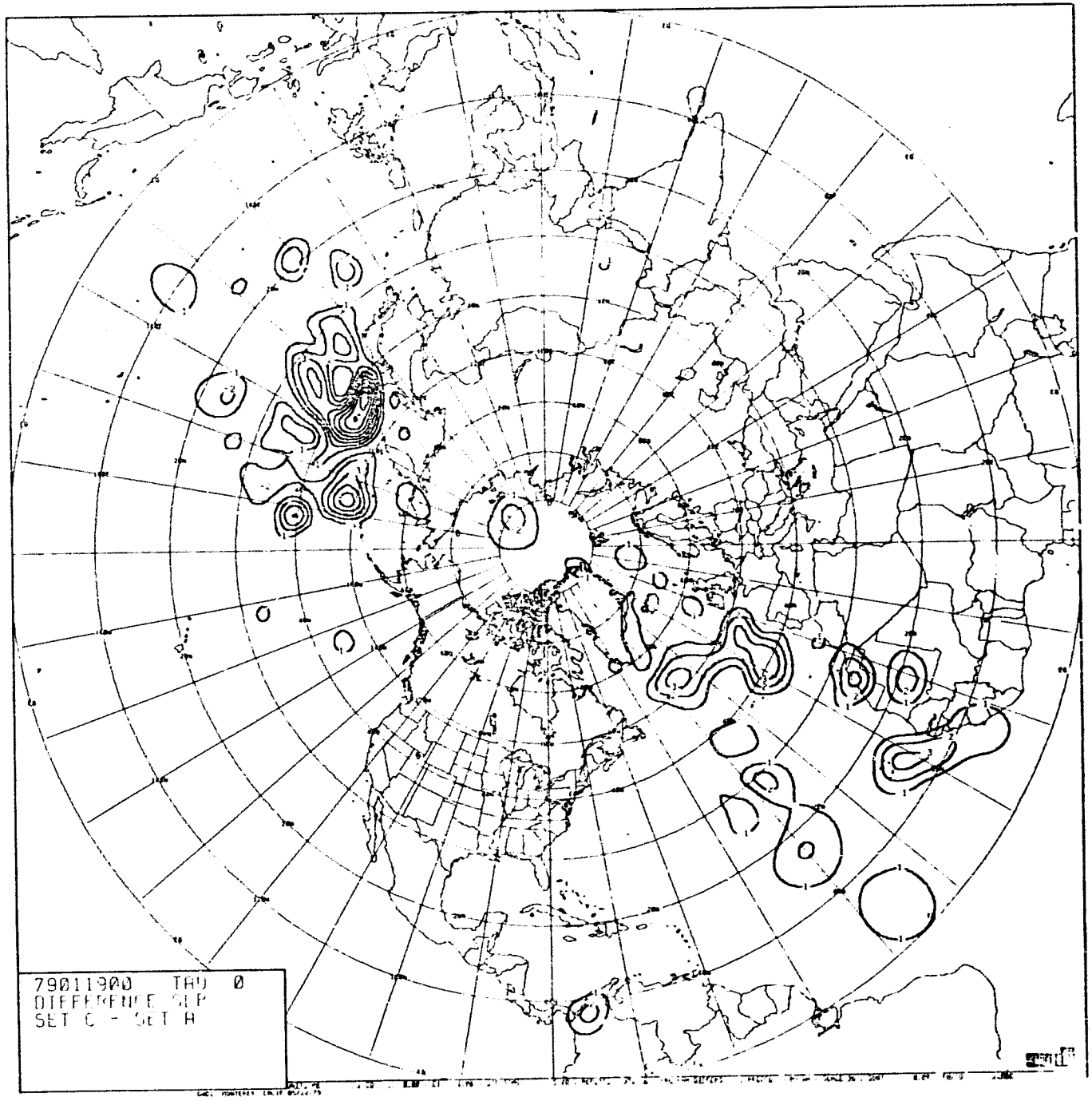

CHART IV-53: Surface Pressure Difference, 0000Z 19 January 1979. Chart Set C minus Chart Set A.

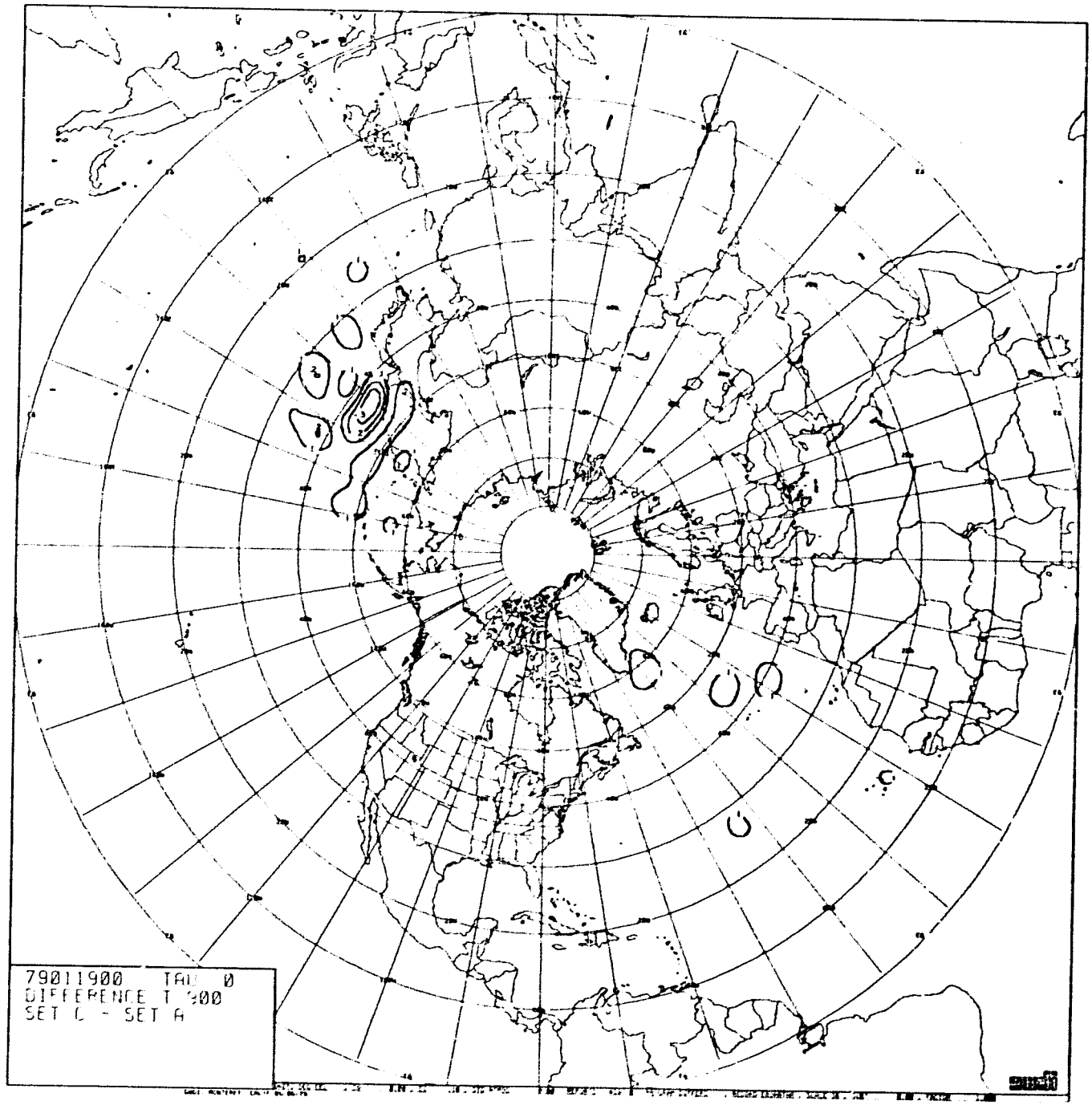

CHART IV-54: 900MB Temperature Difference, 0000Z 19 January 1979. Chart Set C minus Chart Set A.

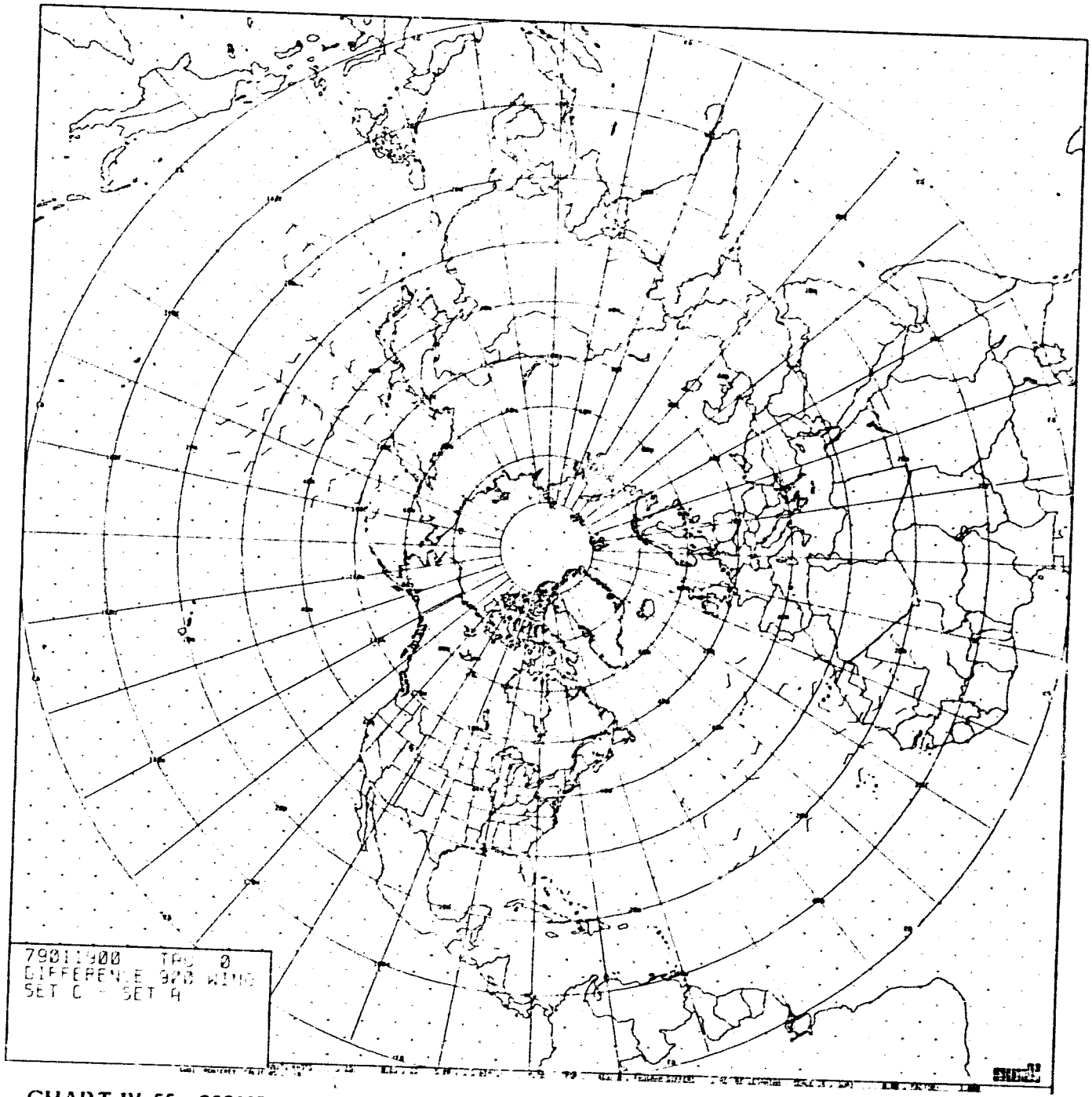

CHART IV-55: 900MB Wind Difference, 0000Z 19 January 1979. Chart Set C minus Chart Set A.

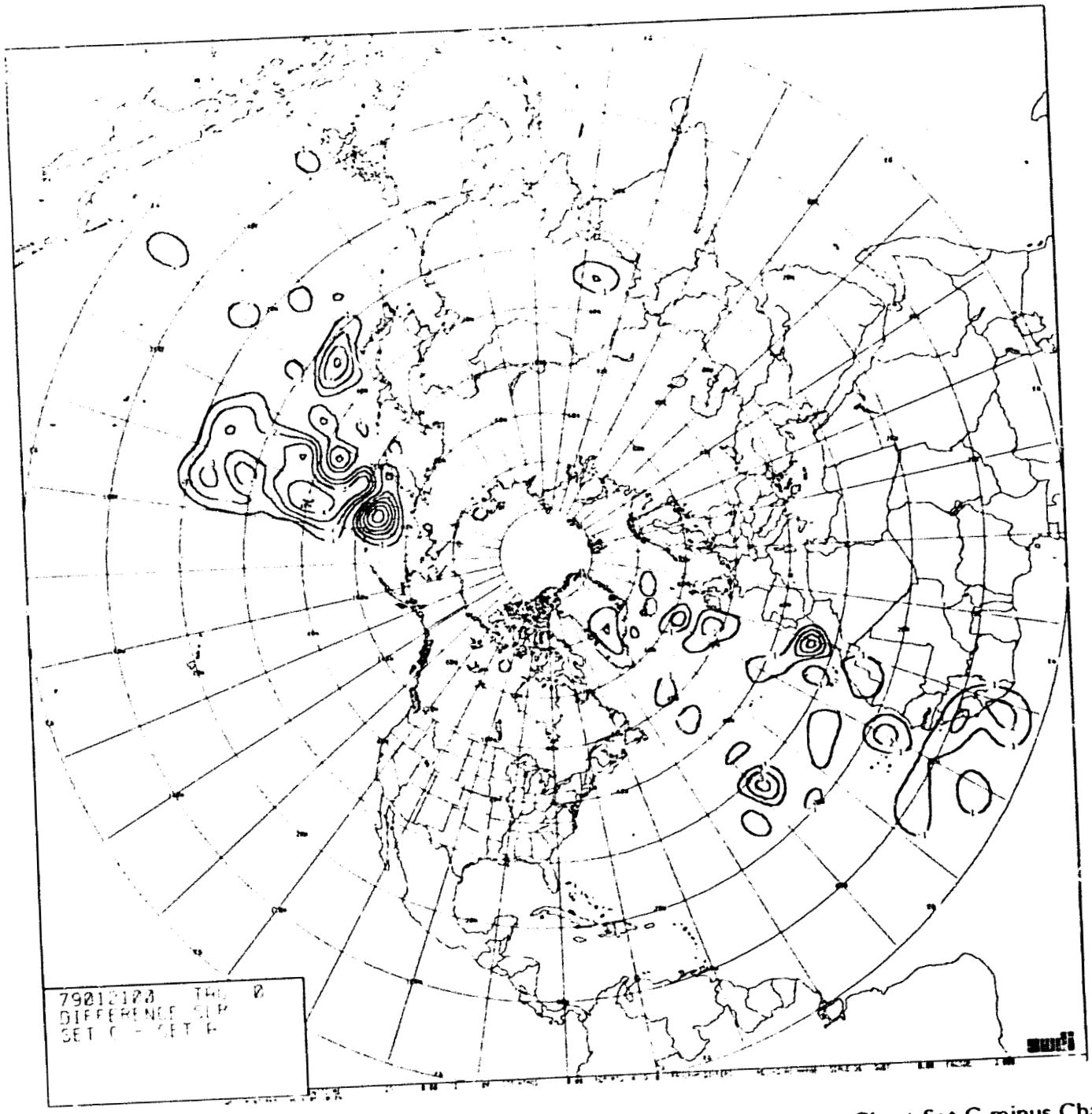

CHART IV-56: Surface Pressure (Cumulative) Difference, 0000Z 21 January 1979. Chart Set C minus Chart Set A.

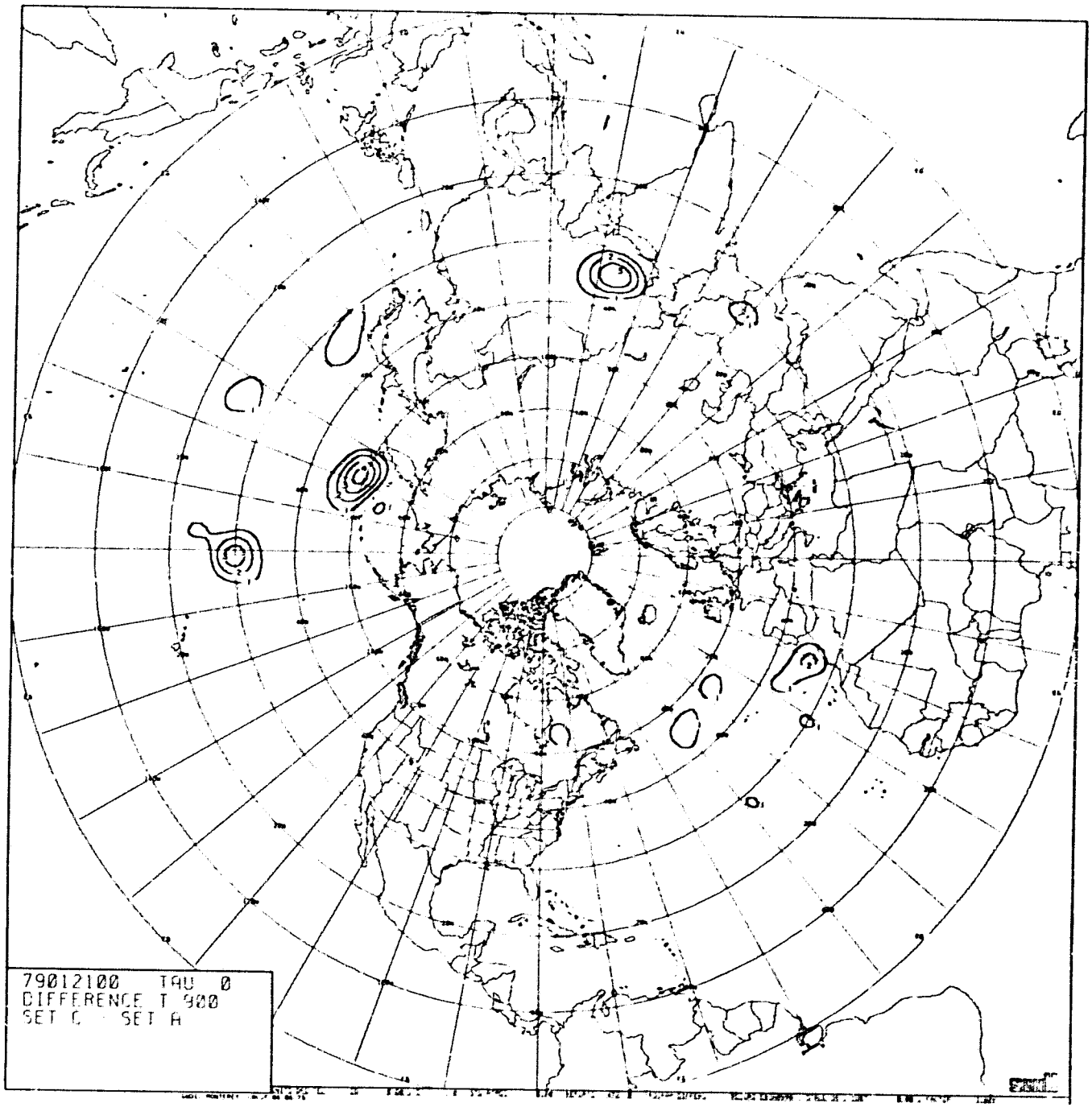

CHART IV-57: 900MB Temperature (Cumulative) Difference, 0000Z 21 January 1979. Chart Set C minus Chart Set A.

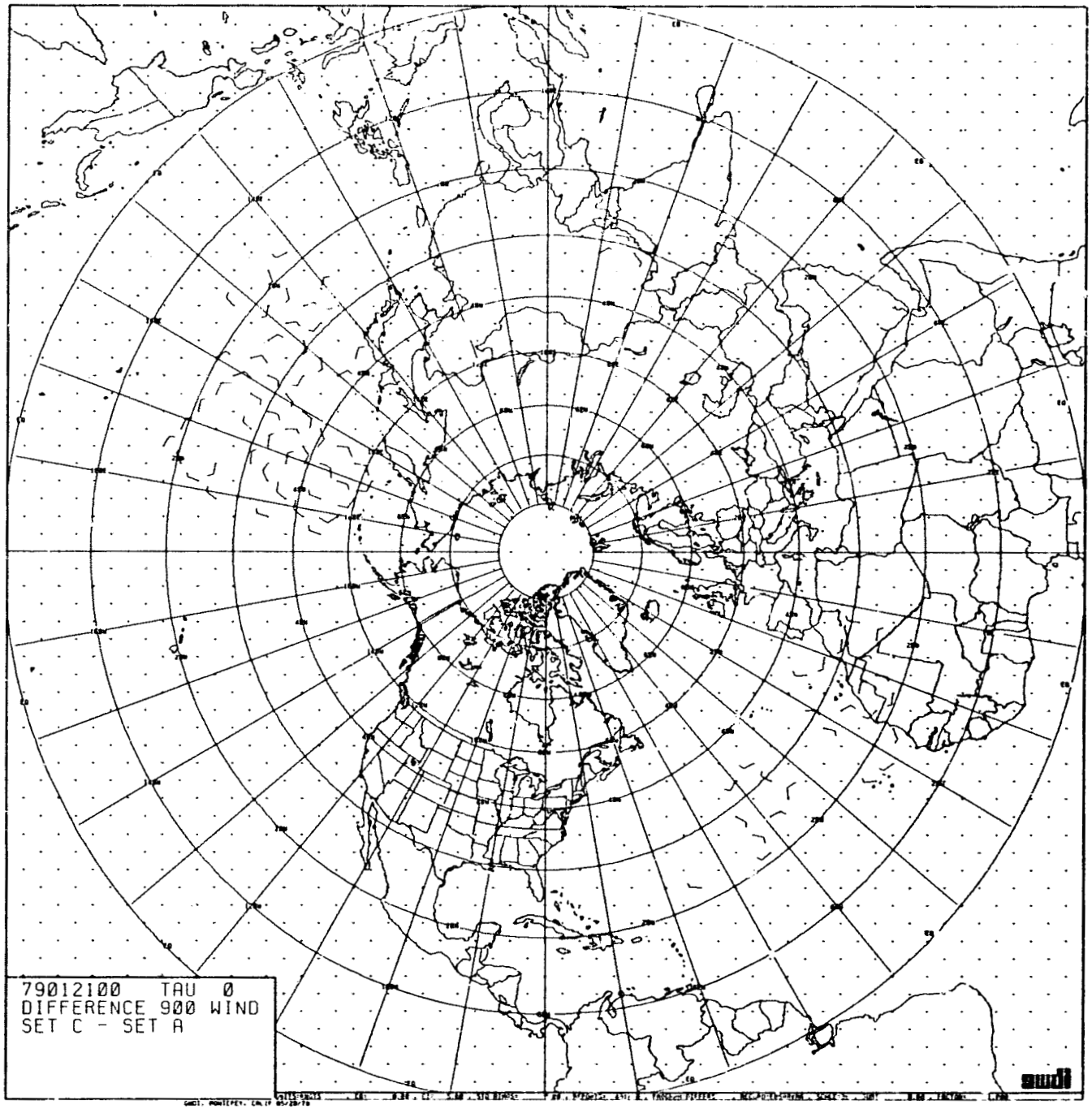

CHART IV-58: 900MB Wind (Cumulative) Difference, 0000Z 21 January 1979. Chart Set C minus Chart Set A.

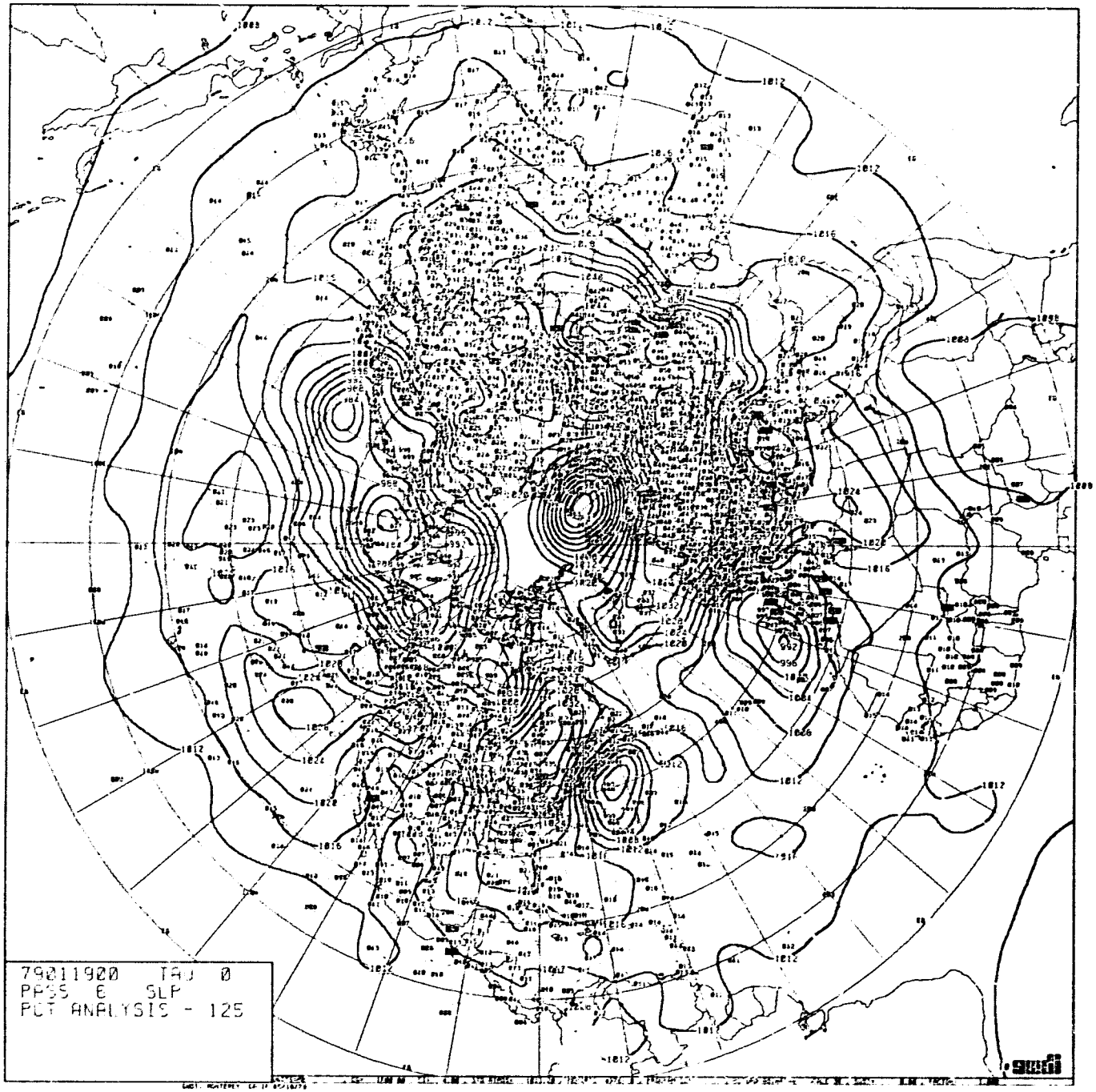

CHART IV-59: Surface Pressure Analysis, 0000Z 19 January 1979. Chart Set D.

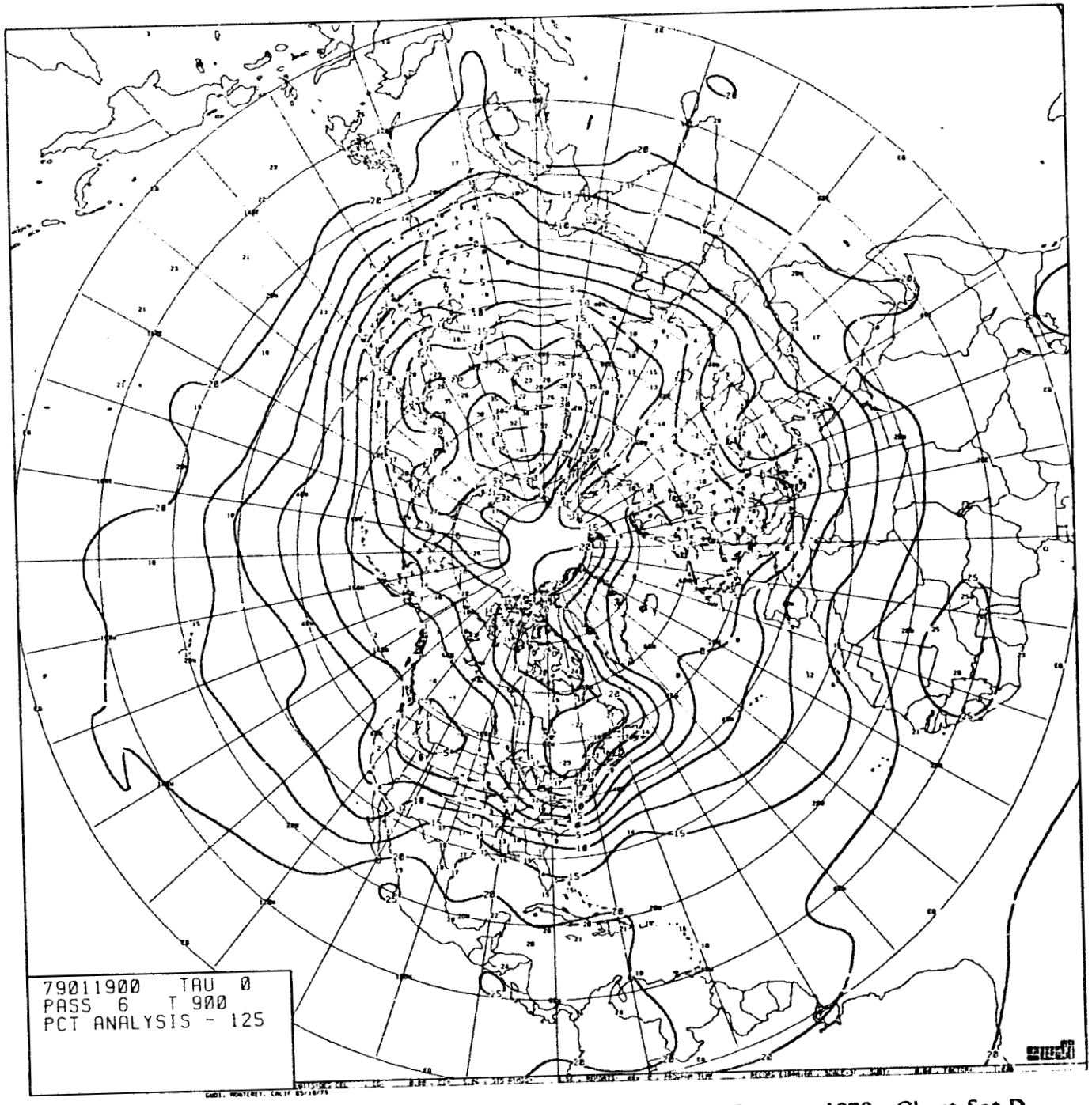

CHART IV-60: 900MB Temperature Analysis, 0000Z 19 January 1979. Chart Set D.

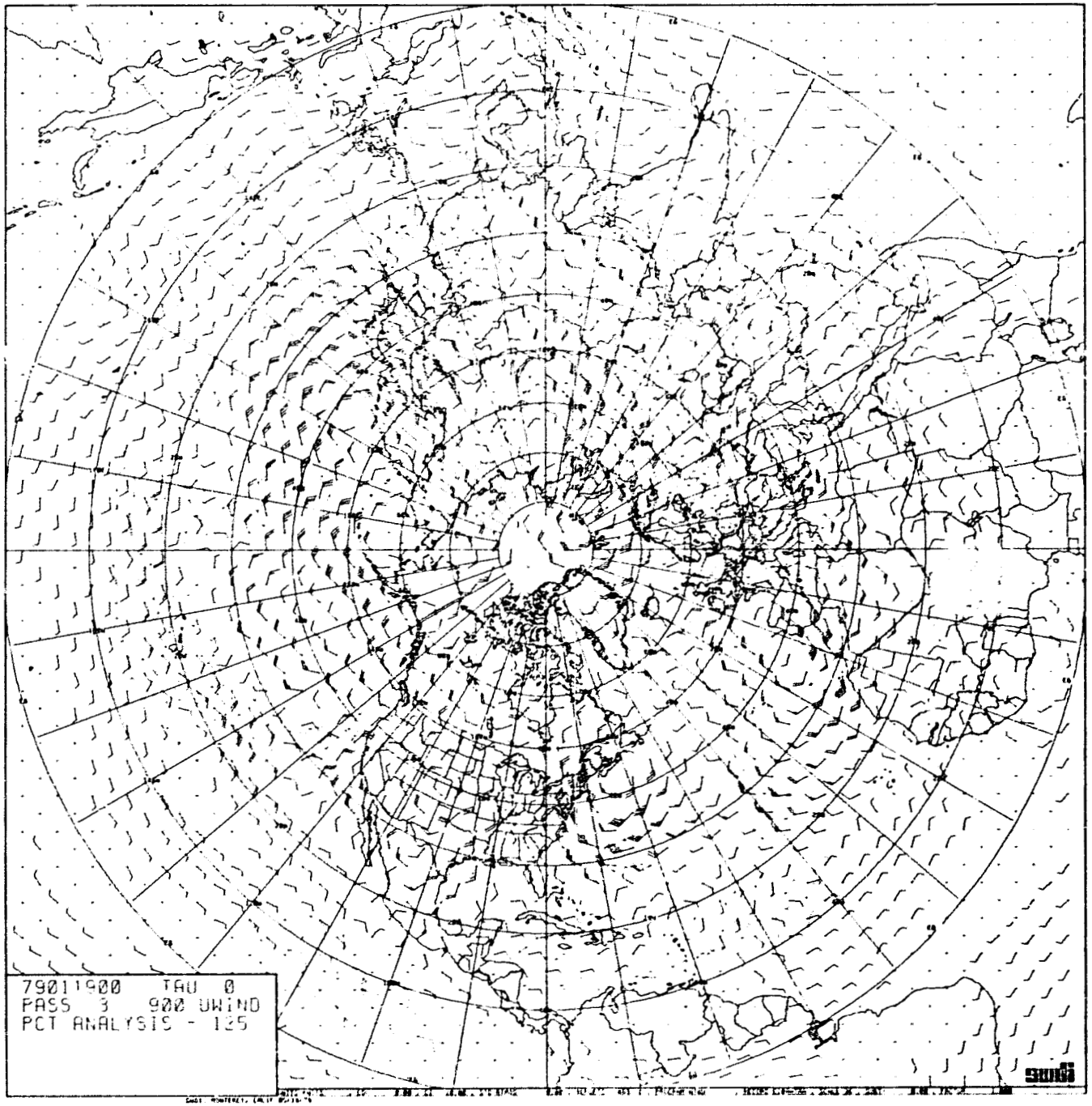

CHART IV-61: 900MB Wind Analysis, 0000Z 19 January 1979. Chart Set D.

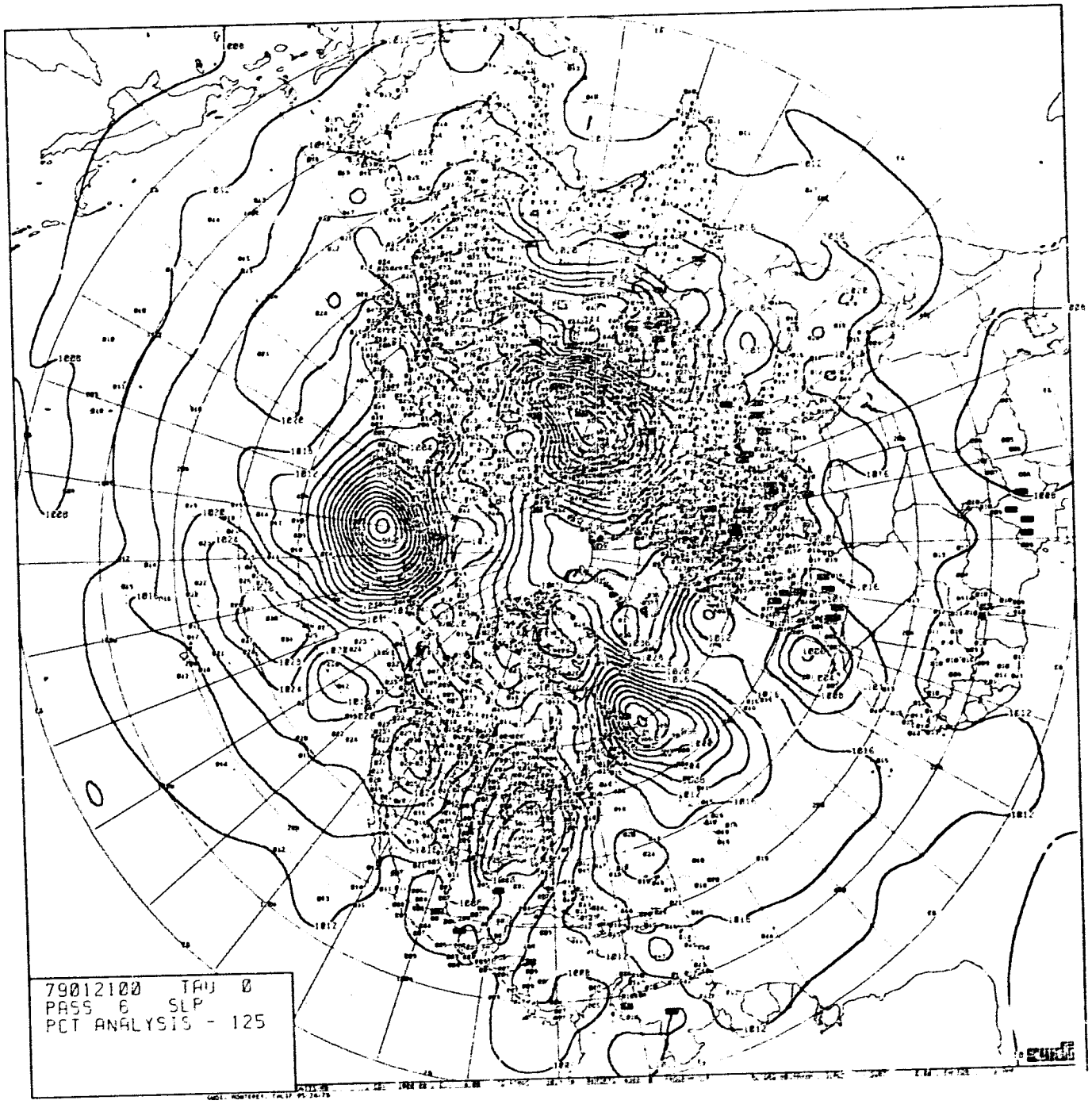

CHART IV-62: Surface Pressure Analysis, 0000Z 21 January 1979. Chart Set D.

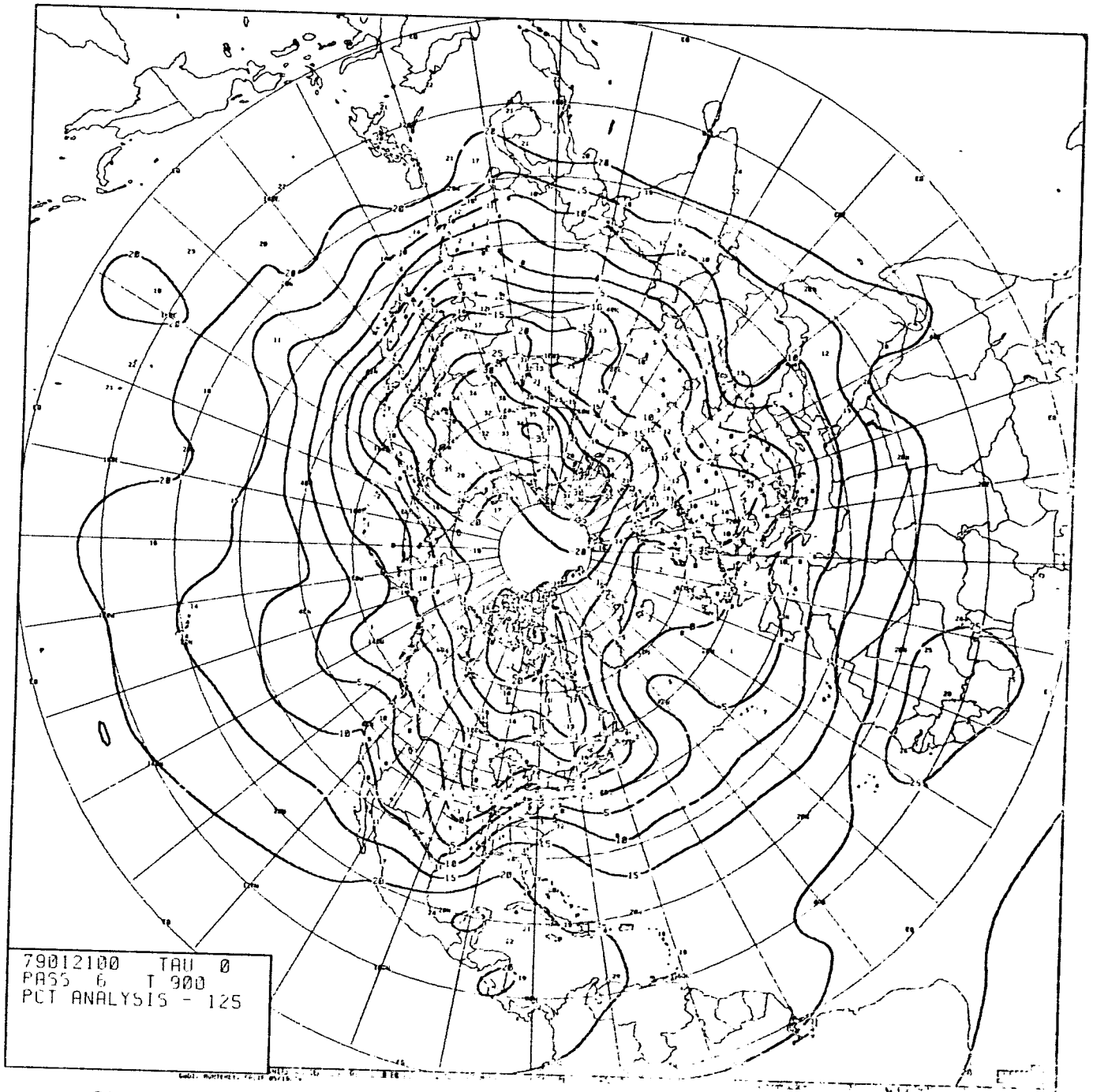

CHART IV-63: 900MB Temperature Analysis, 0000Z 21 January 1979. Chart Set D.

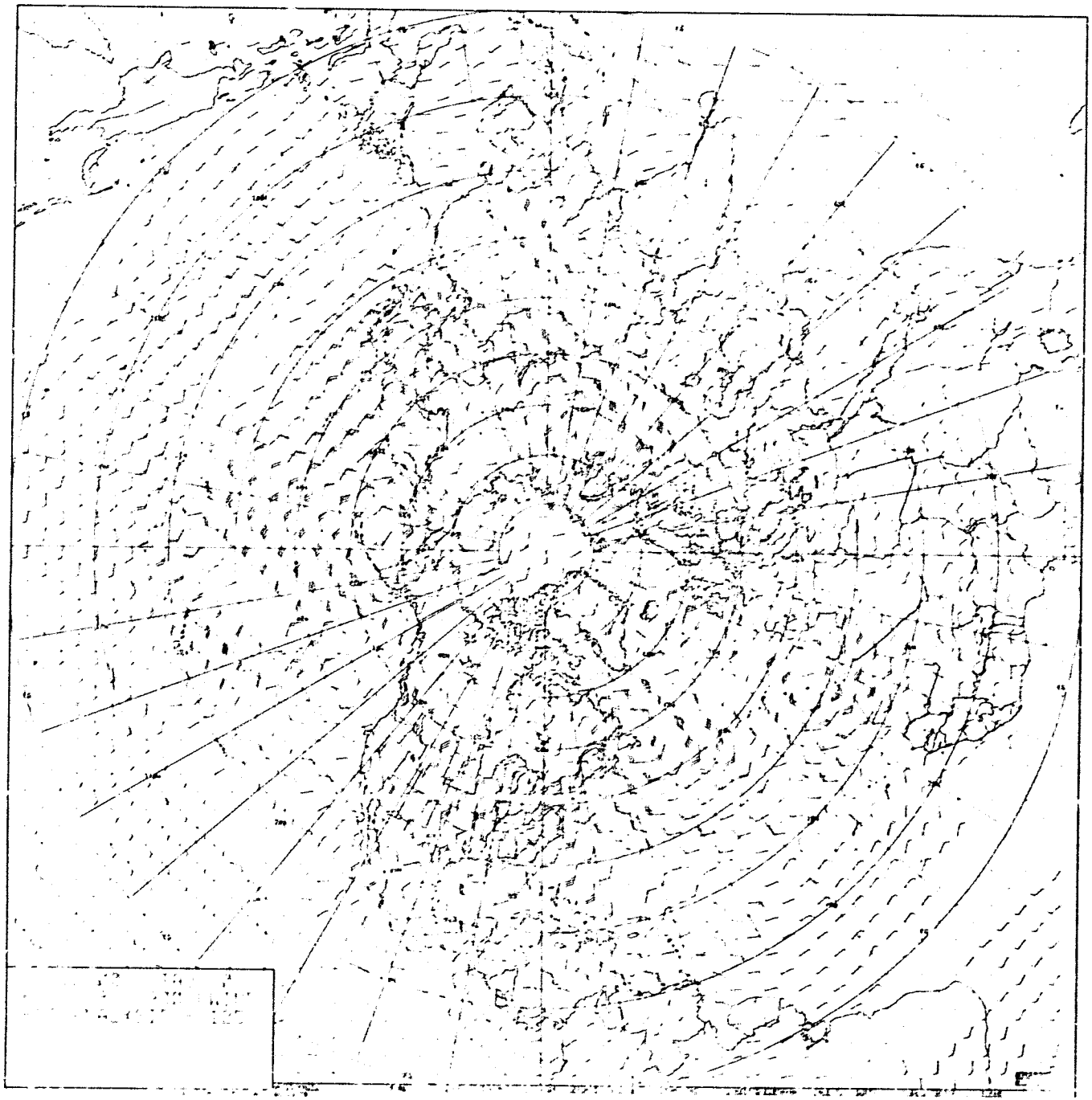

CHART IV-64: 900MB Wind Analysis, 0000Z 21 January 1979. Chart Set D.

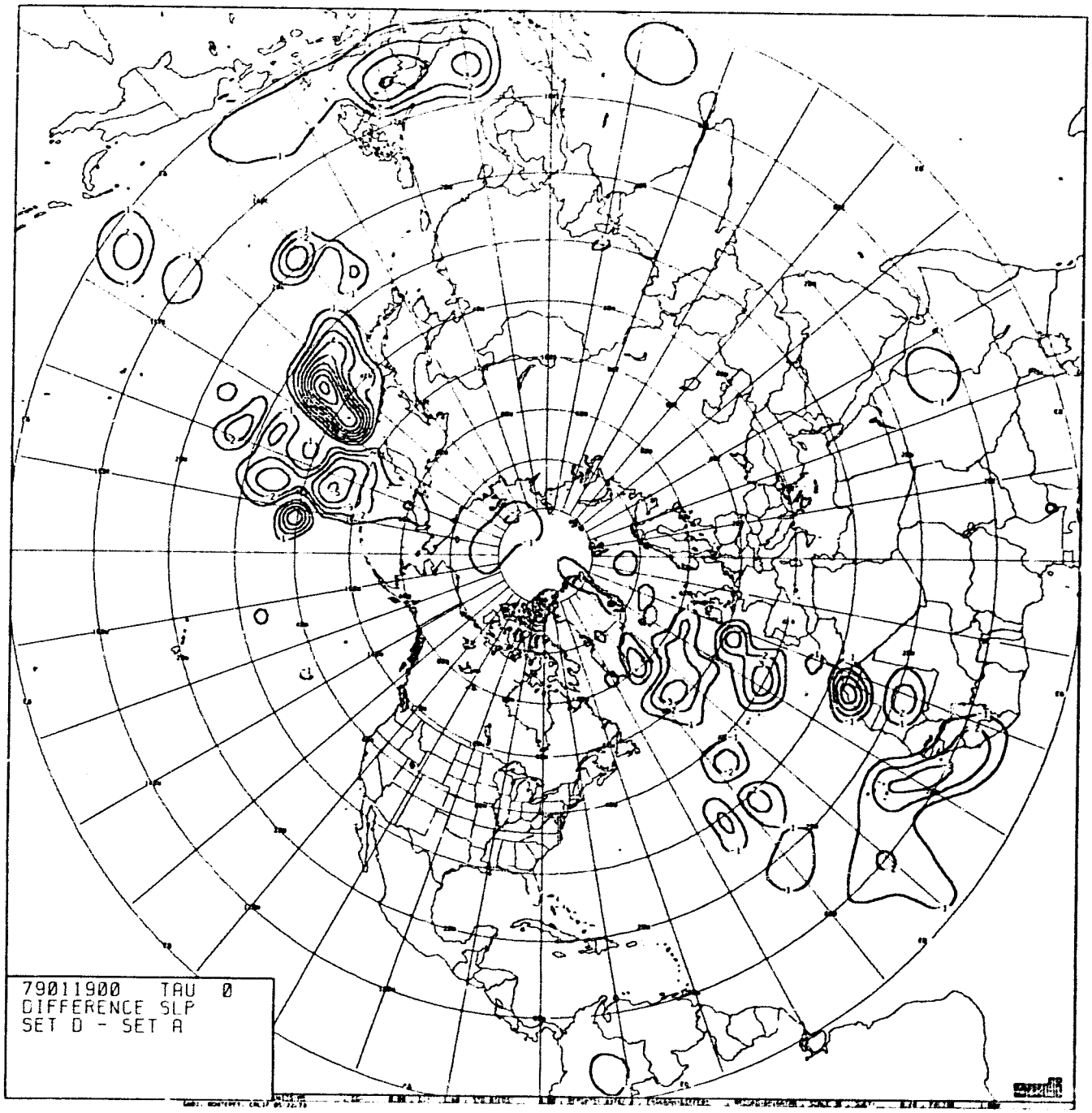

CHART IV-65: Surface Pressure Difference, 0000Z 19 January 1979. Chart Set D minus Chart Set A.

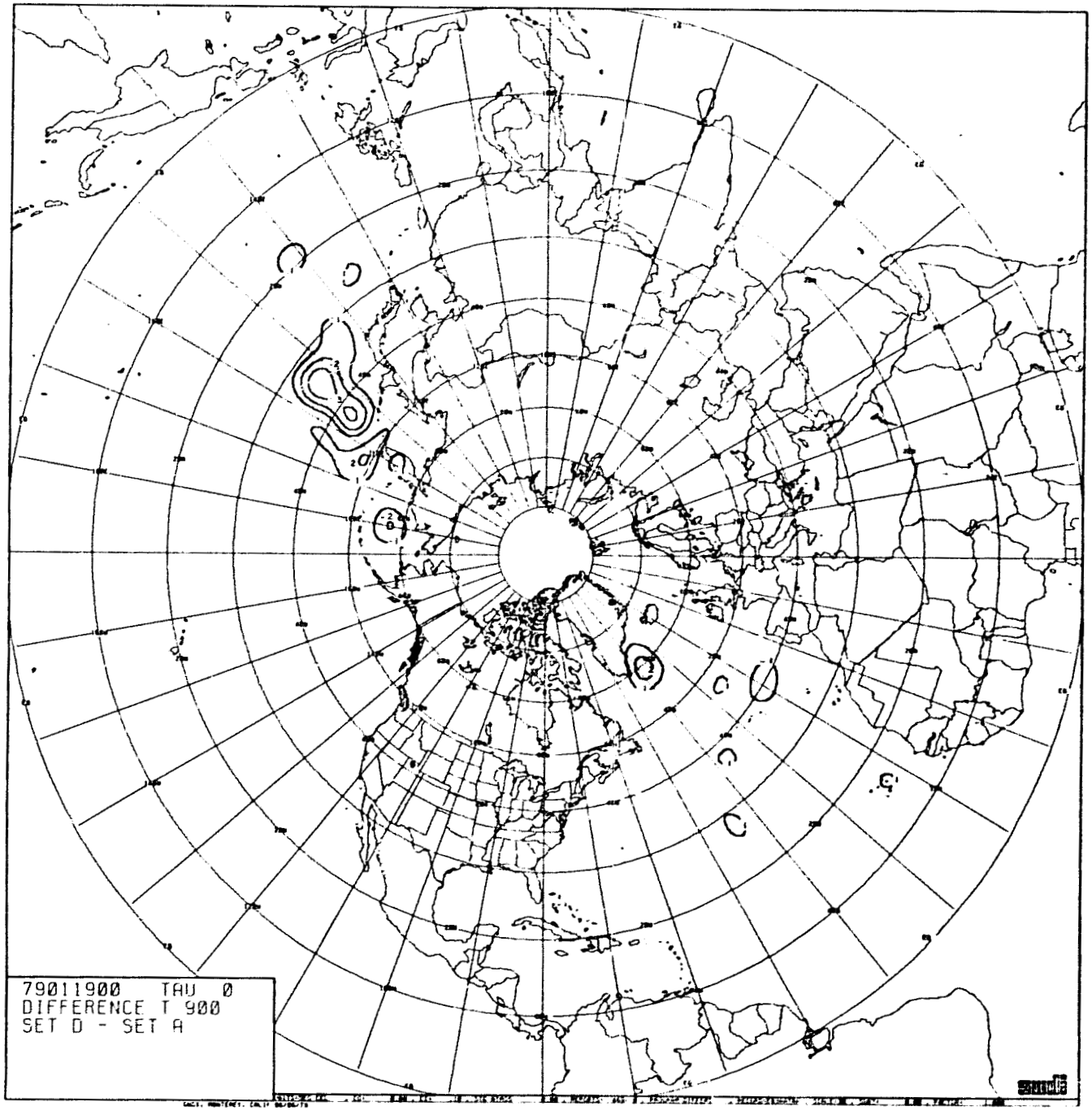

CHART IV-66: 900MB Temperature Difference, 0000Z 19 January 1979. Chart Set D minus Chart Set A.

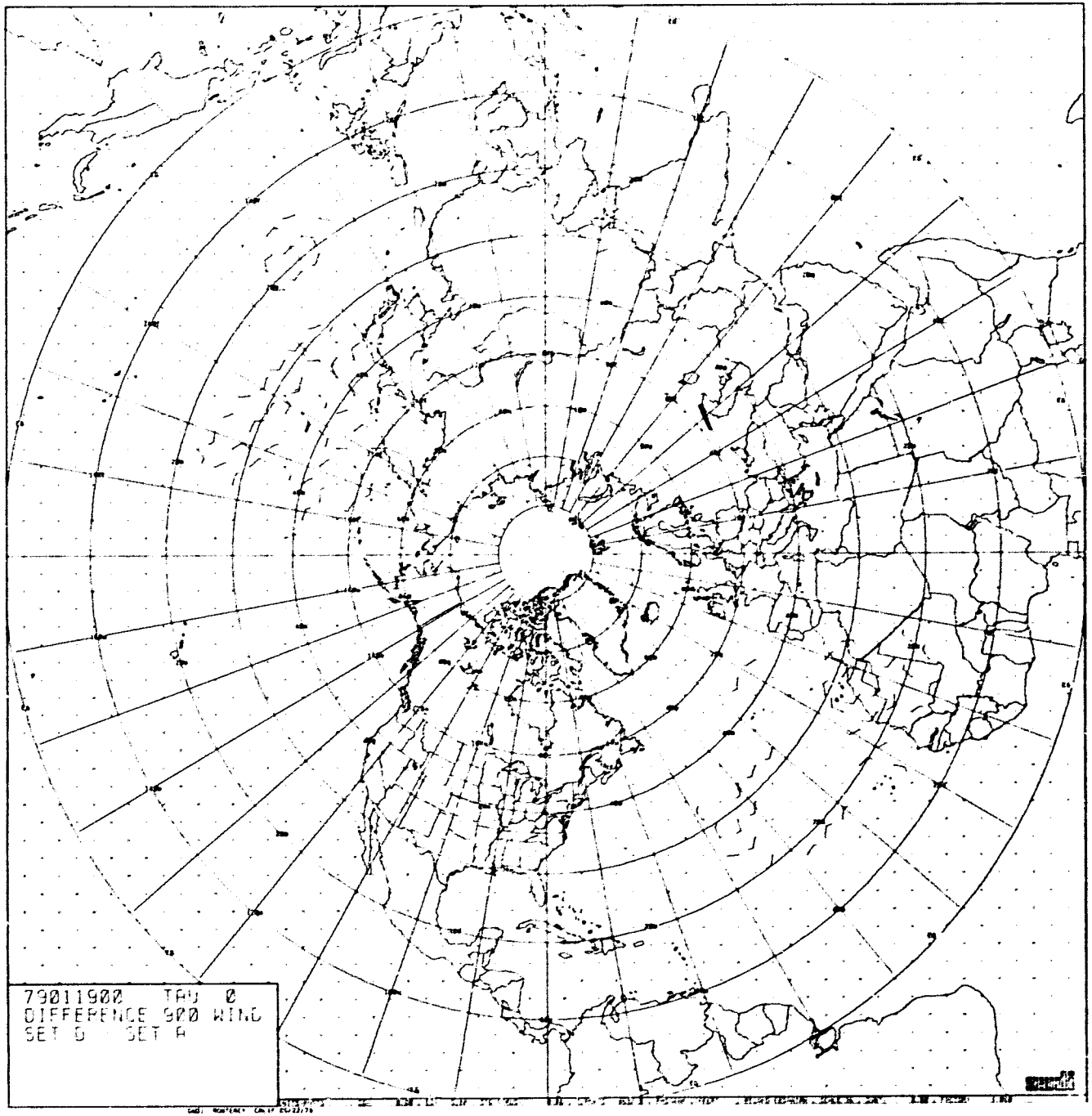

CHART IV-67: 900MB Wind Difference, 0000Z 19 January 1979. Chart Set D minus Chart Set A.

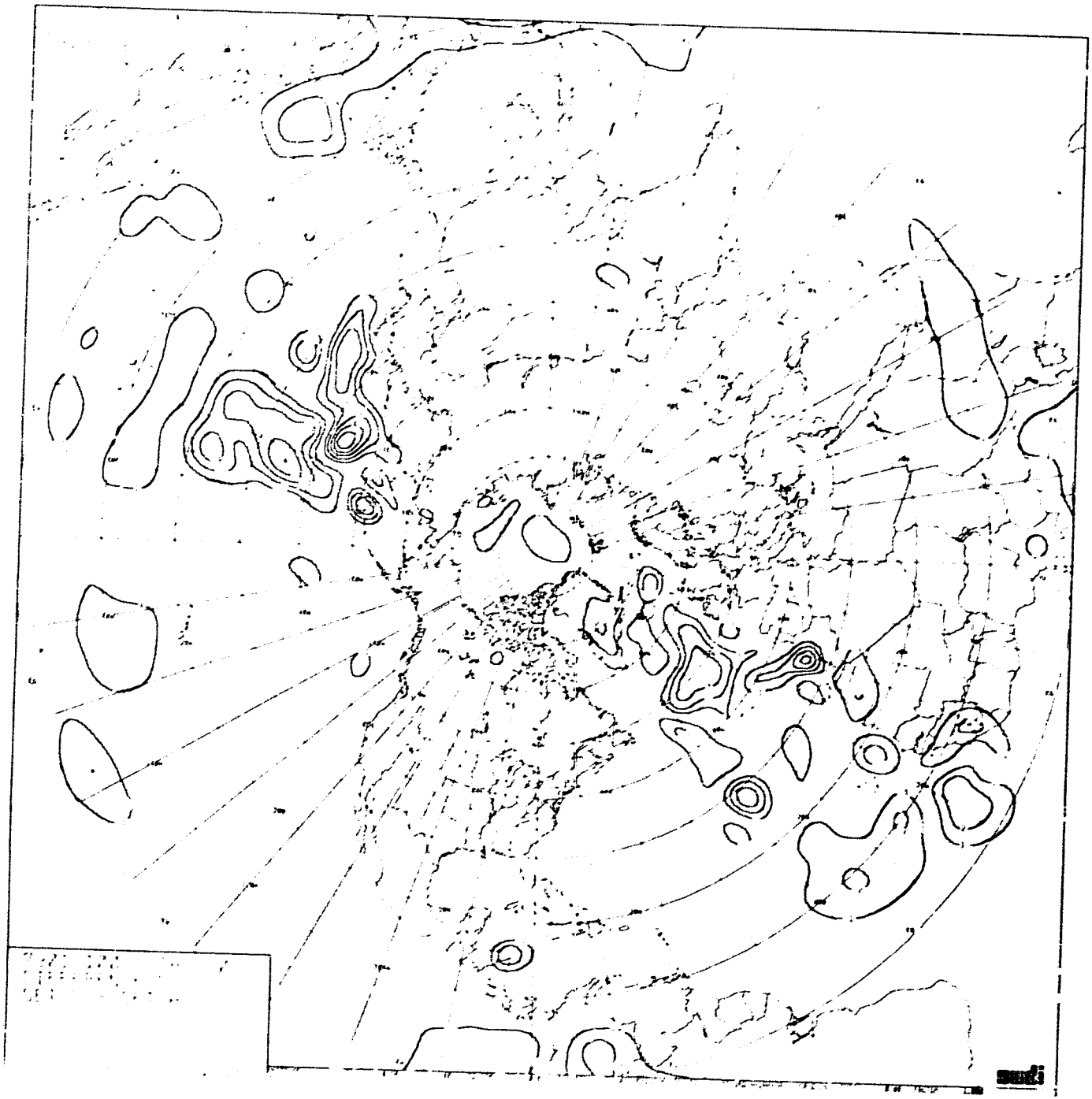

CHART IV-68: Surface Pressure (Cumulative) Difference, 0000Z 21 January 1979. Chart Set D minus Chart Set A.

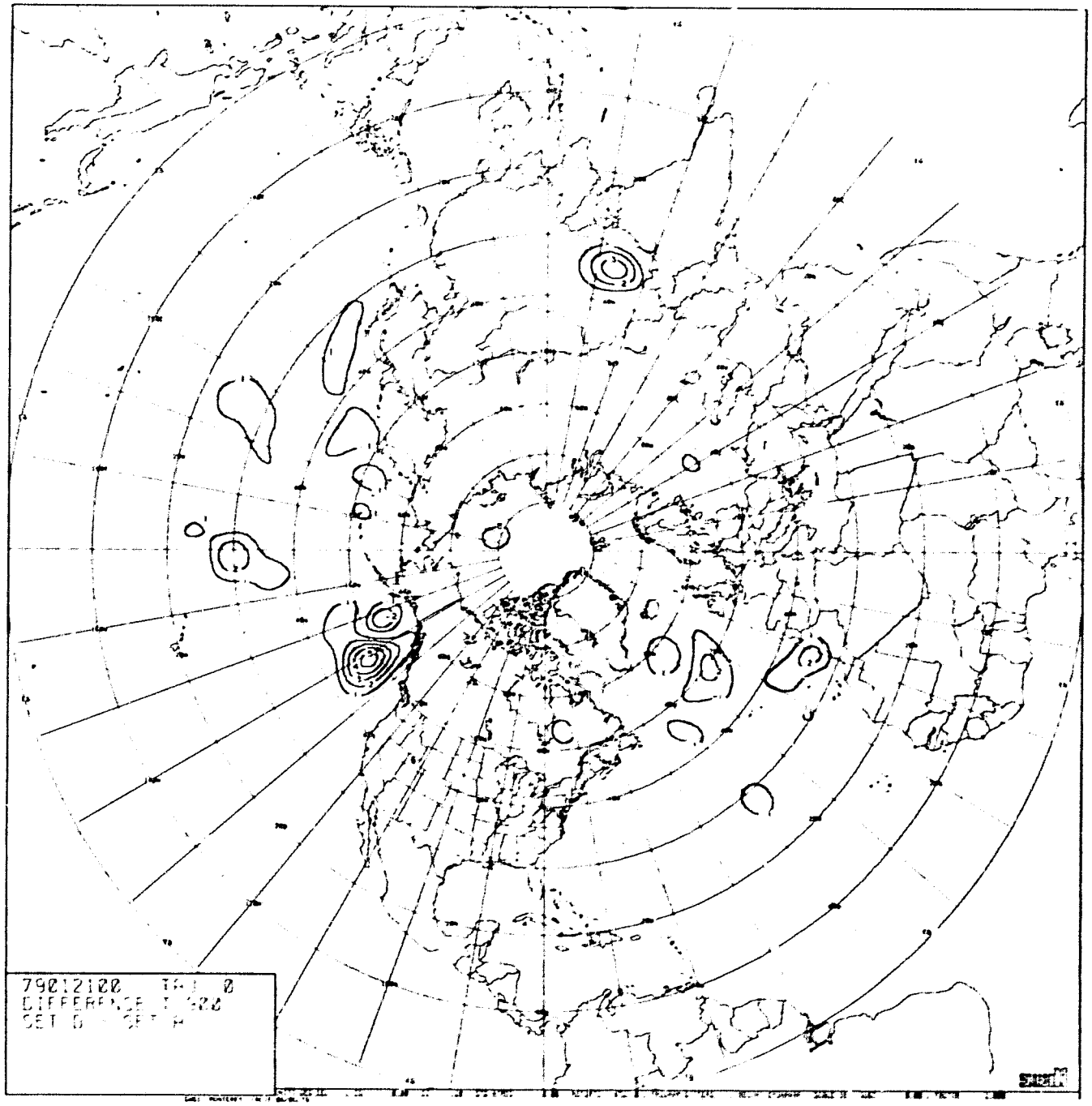

CHART IV-69: 900MB Temperature (Cumulative) Difference, 0000Z 21 January 1979. Chart Set D minus Chart Set A.

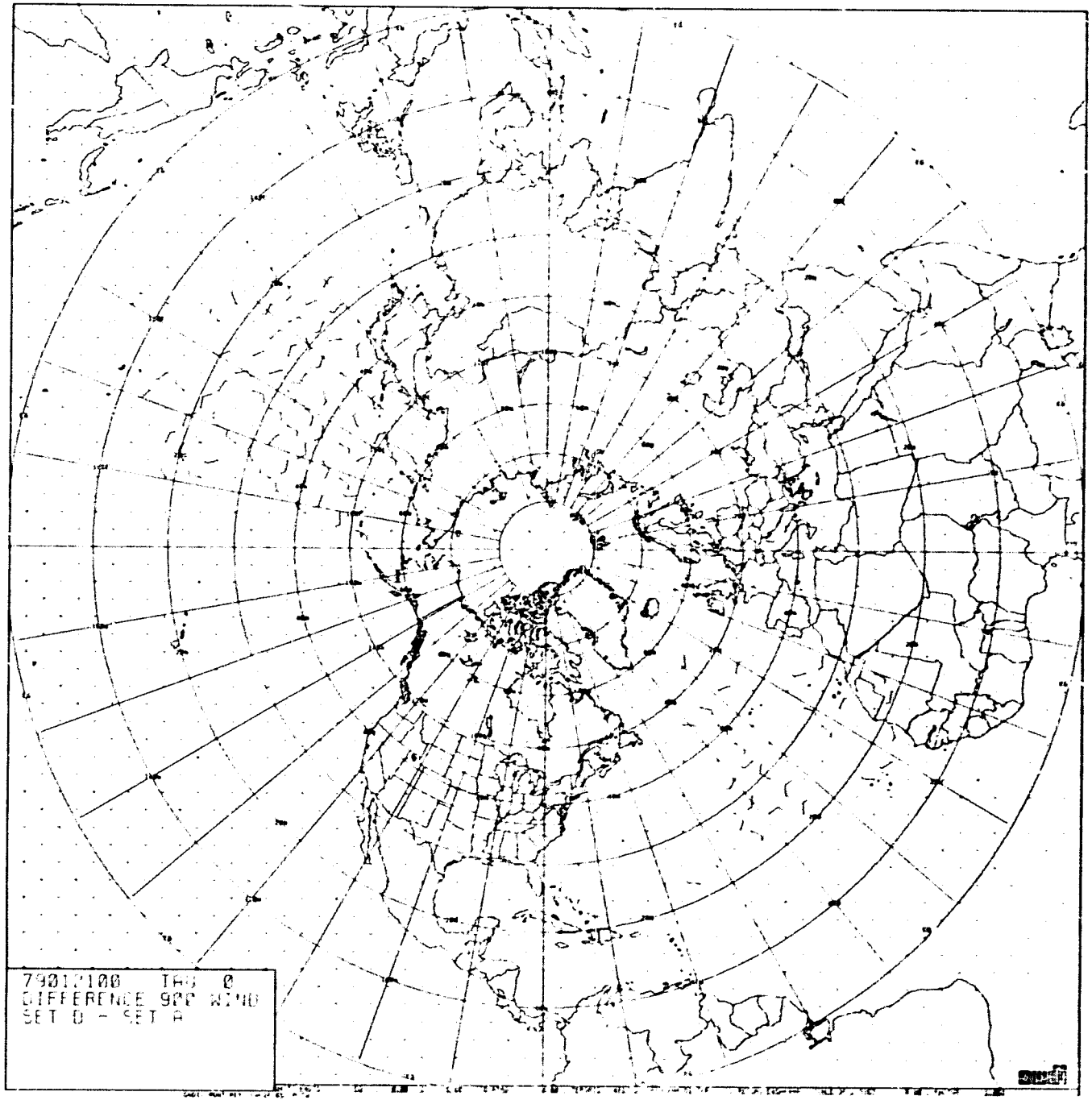

CHART IV-70: 900MB Wind (Cumulative) Difference, 0000Z 21 January 1979. Chart Set D minus Chart Set A.

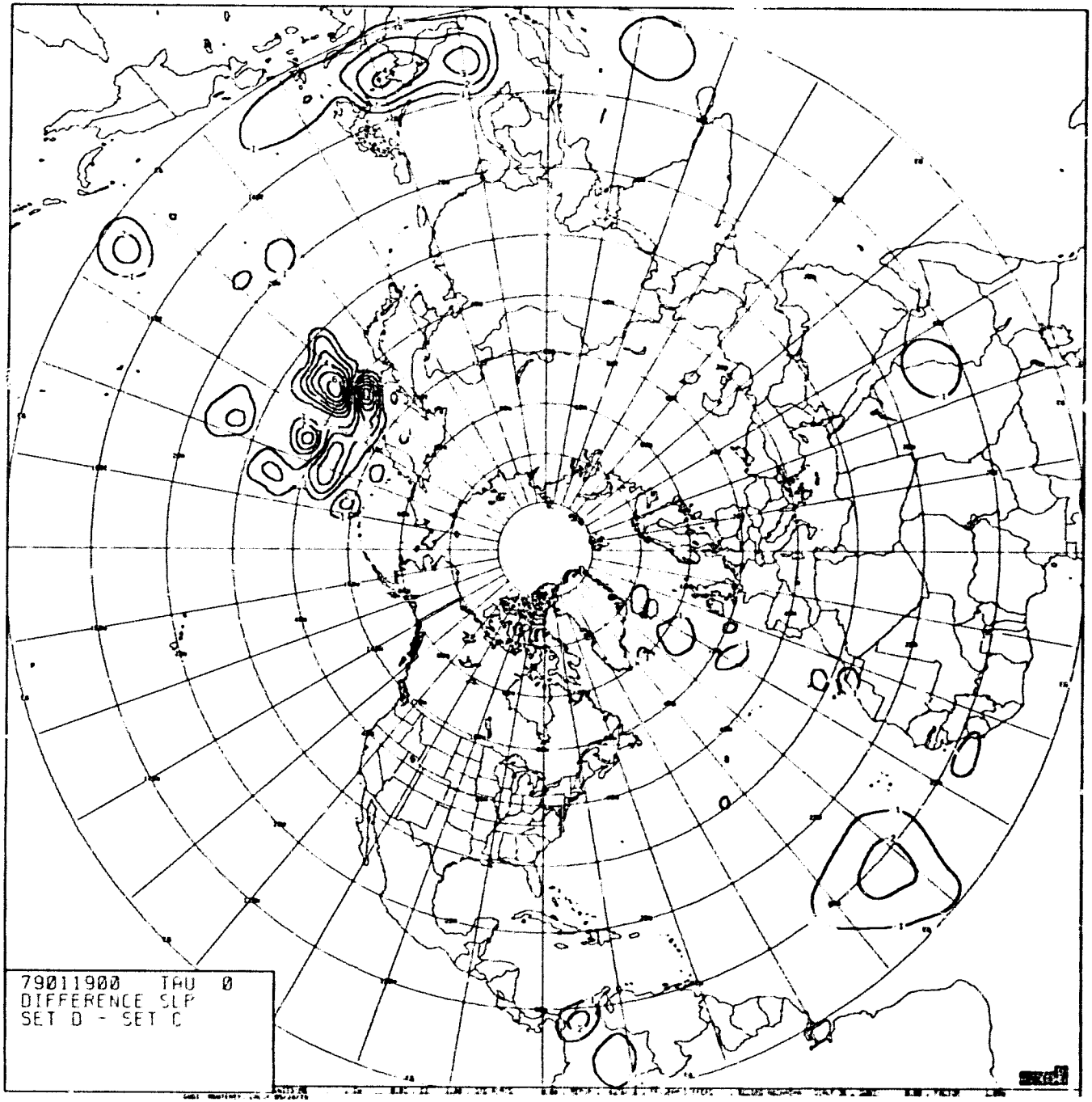

CHART IV-71: Surface Pressure Difference, 0000Z 19 January 1979. Chart Set D minus Chart Set C.

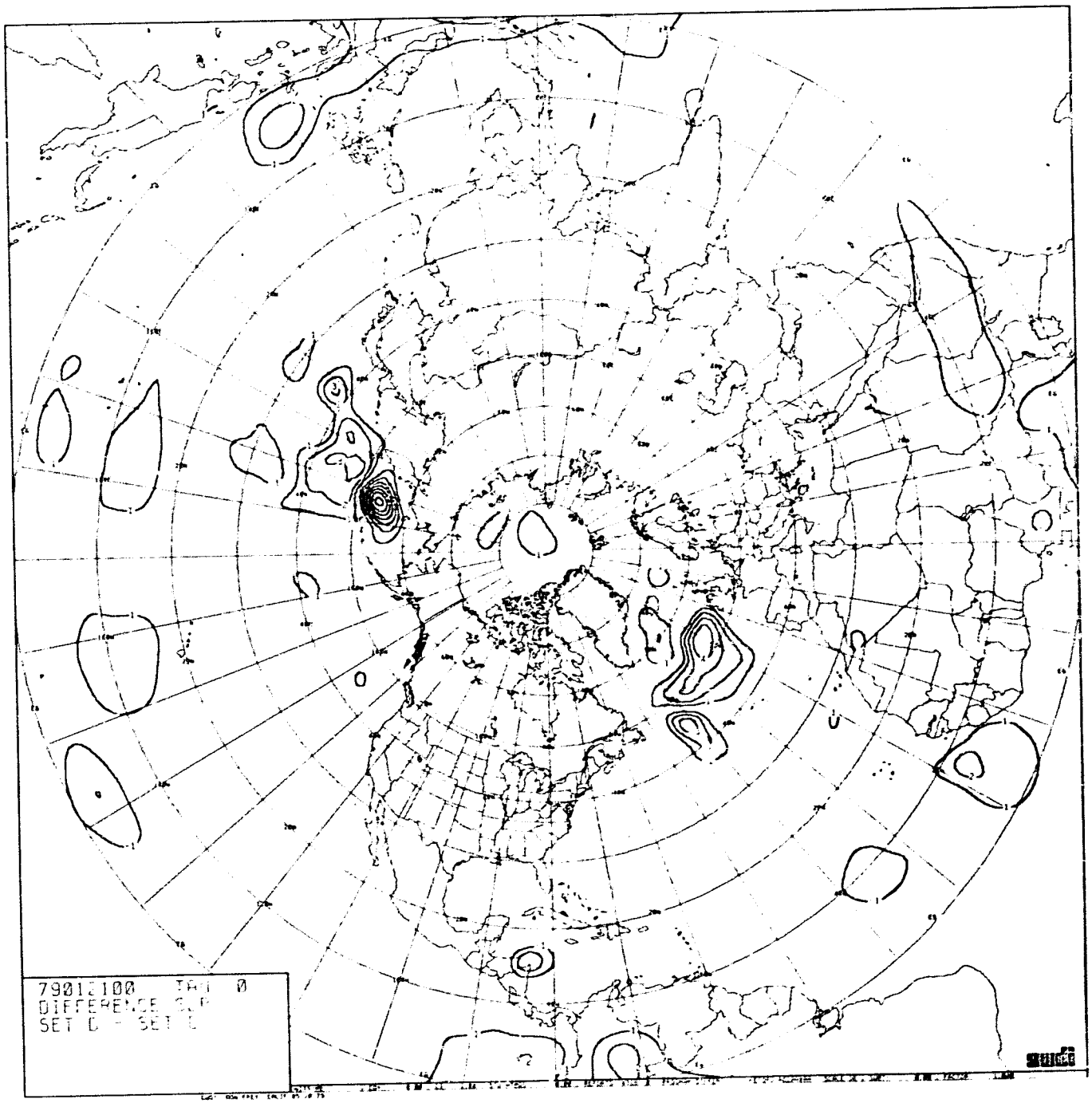

CHART IV-72: Surface Pressure (Cumulative) Difference, 0000Z 21 January 1979. Chart Set D minus Chart Set C.

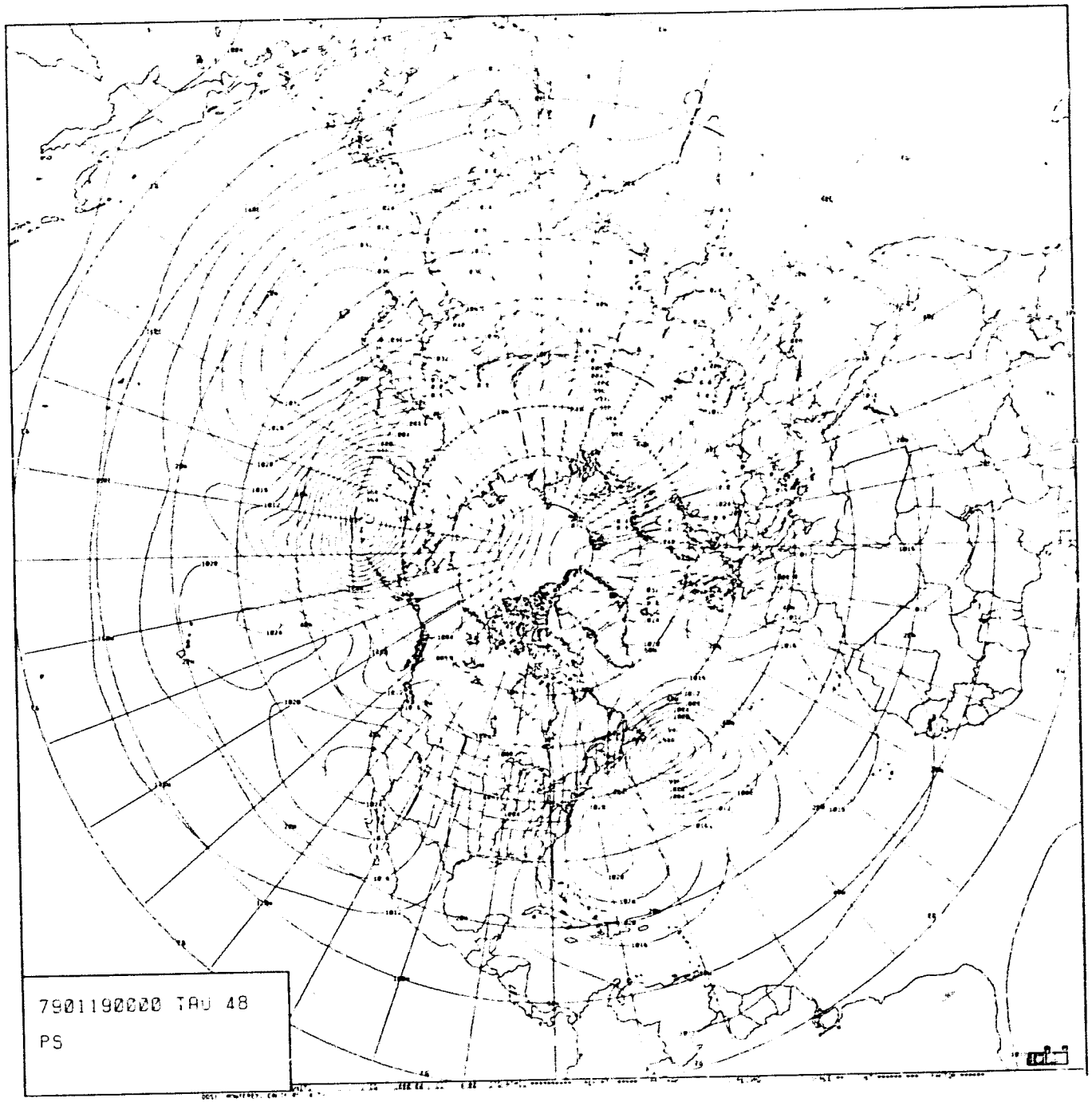

CHART IV-73: 48-Hour Surface Pressure Forecast from 0000Z 19 January 1979. Chart Set E.

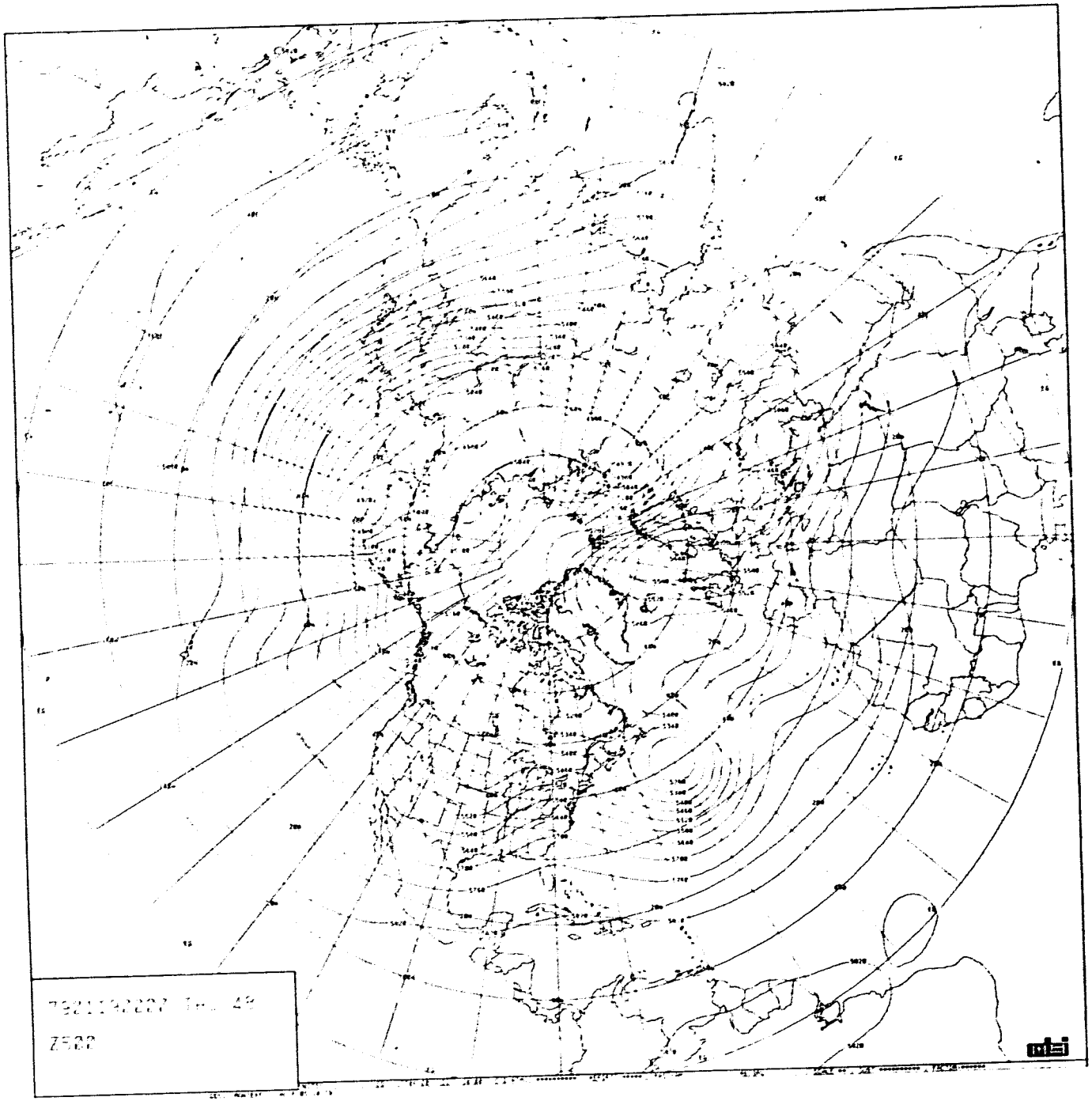

CHART IV-74: 48-Hour 500MB Height Forecast from 0000Z 19 January 1979. Chart Set E.

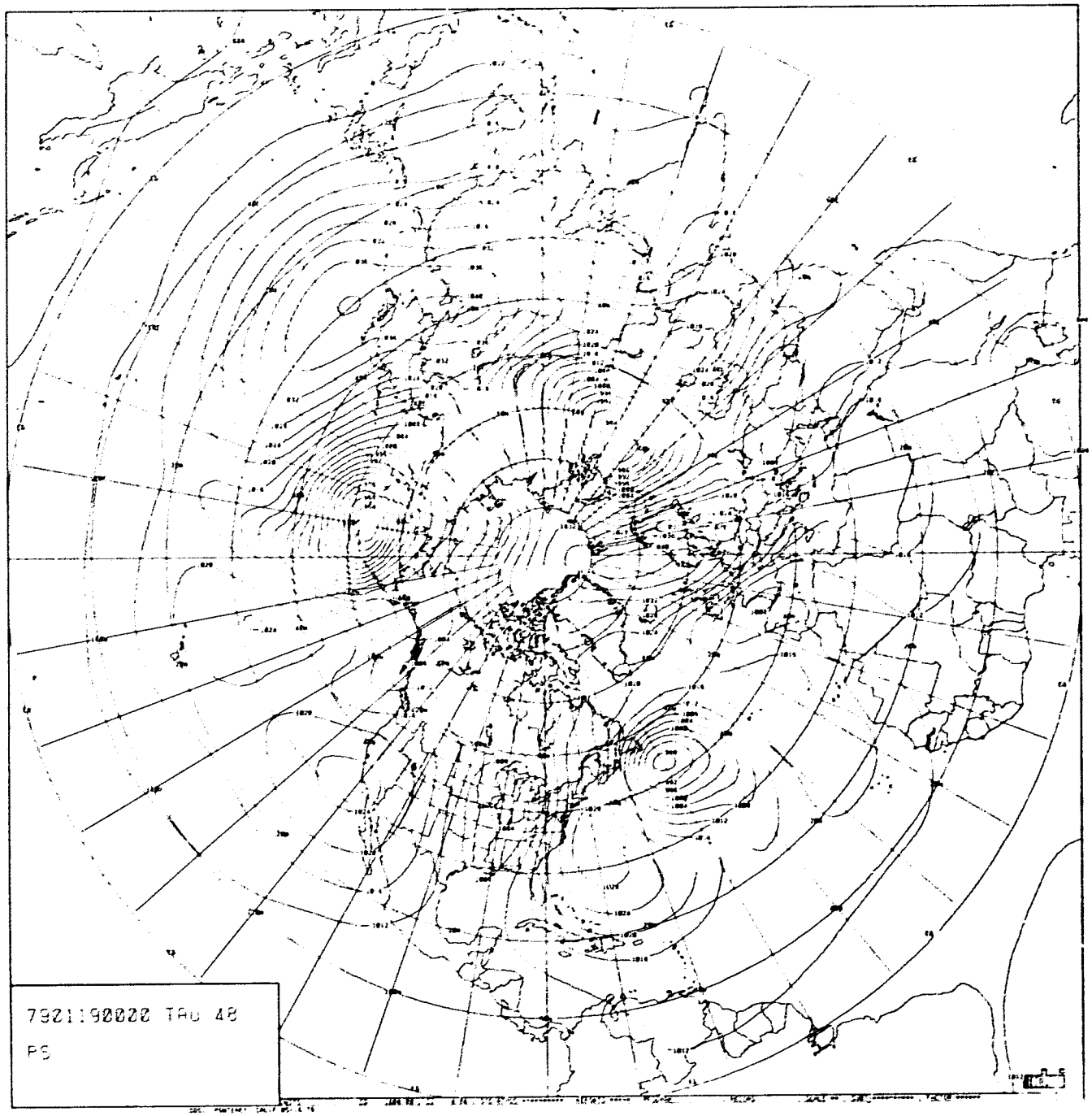

CHART IV-75: 48-Hour Surface Pressure Forecast from 0000Z 19 January 1979. Chart Set F.

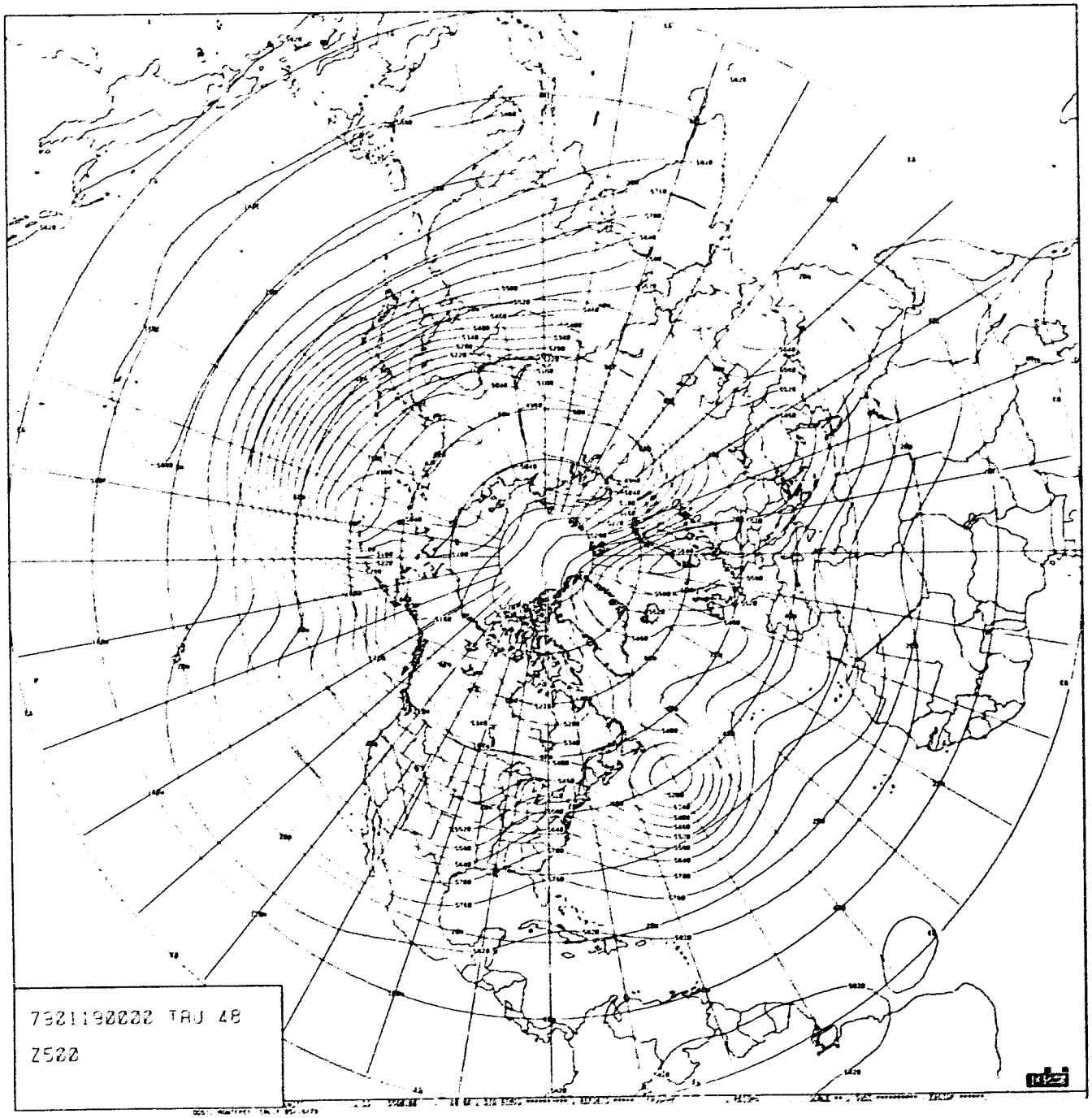

CHART IV-76: 48-Hour 500MB Height Forecast from 0000Z 19 January 1979. Chart Set F.

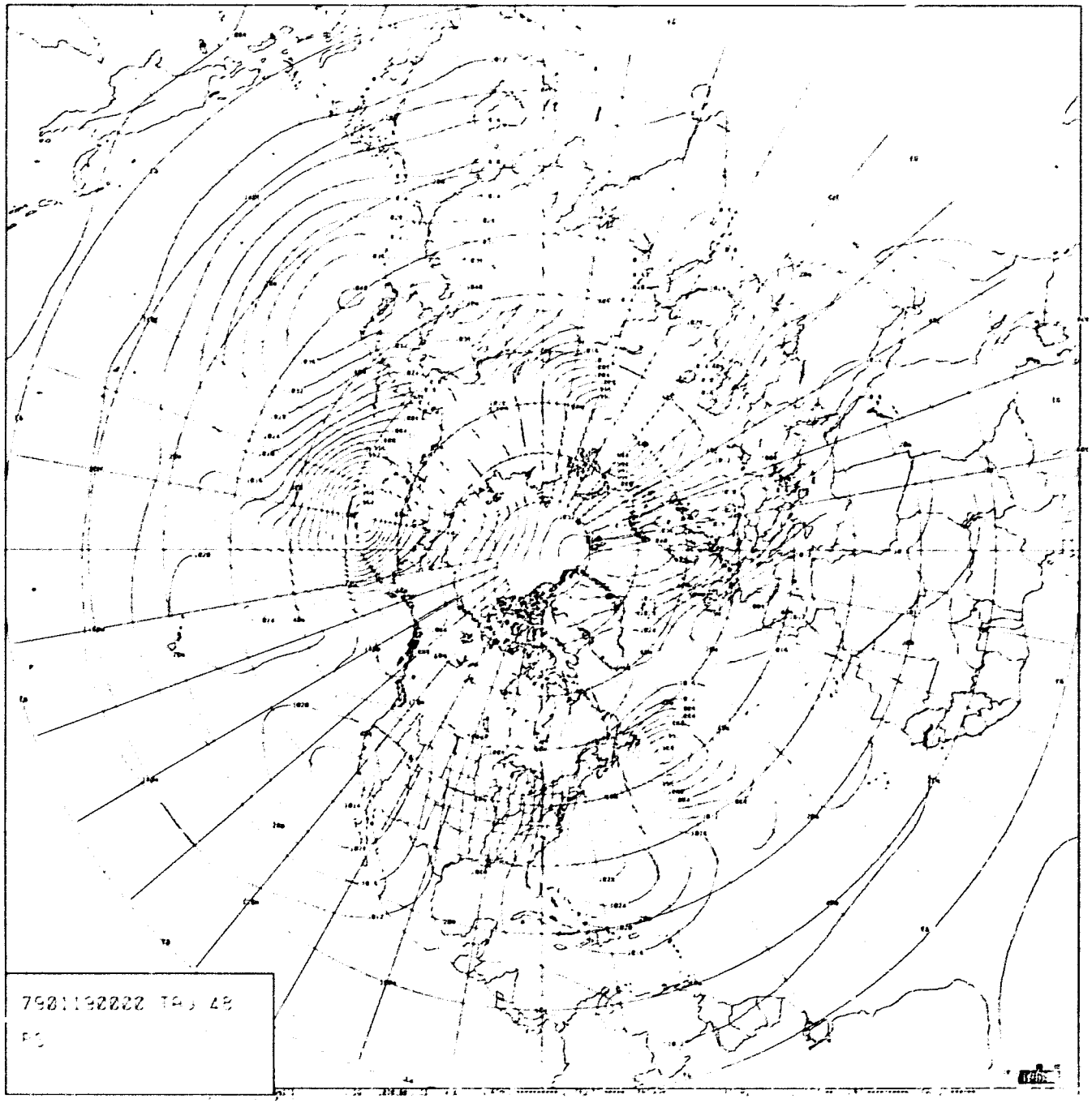

CHART IV-77: 48-Hour Surface Pressure Forecast from 0000Z 19 January 1979. Chart Set G1.

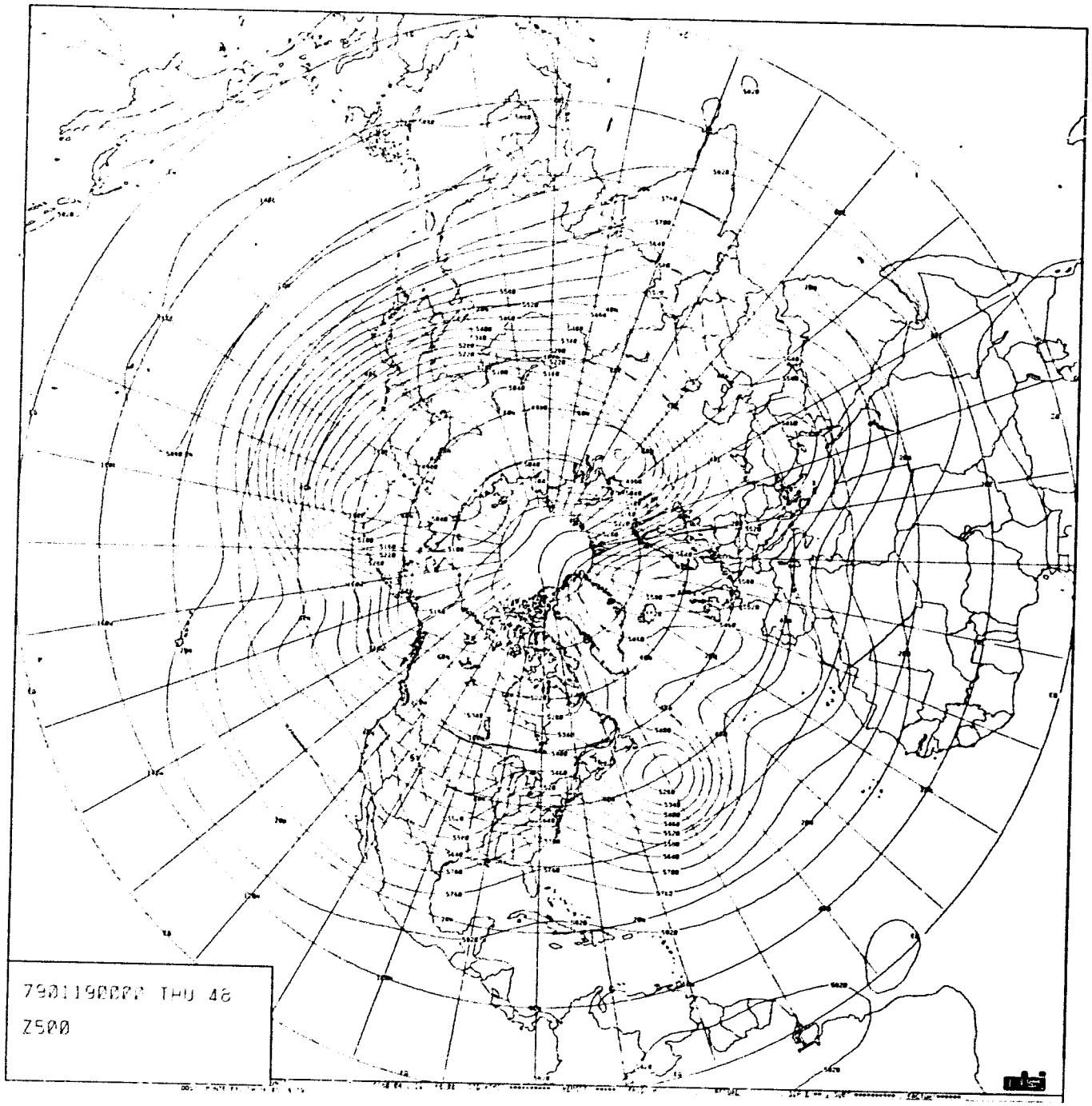

CHART IV-78: 48-Hour 500MB Height Forecast from 0000Z 19 January 1979. Chart Set G1.

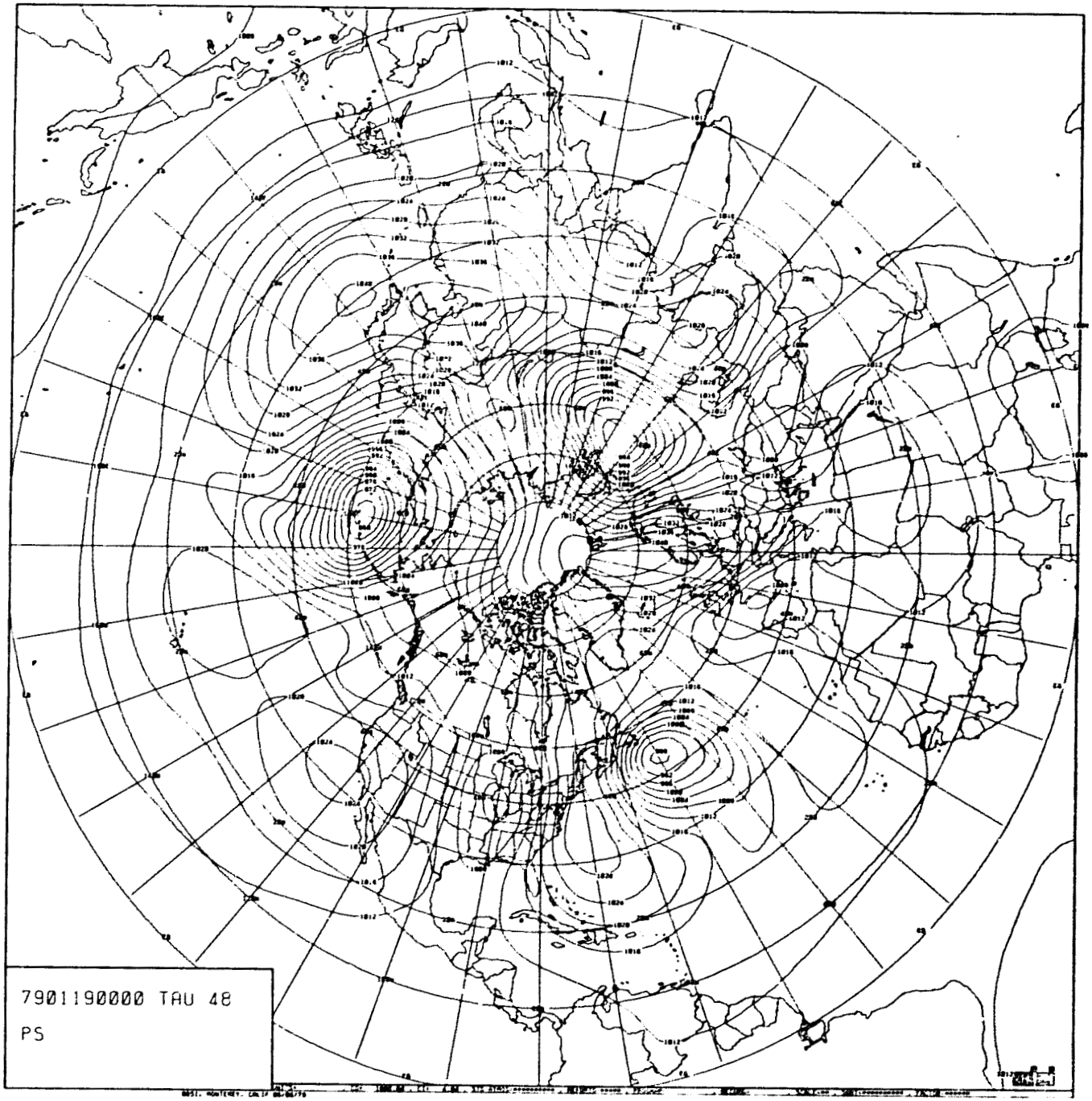

CHART IV-79: 48-Hour Surface Pressure Forecast from 0000Z 19 January 1979. Chart Set H1.

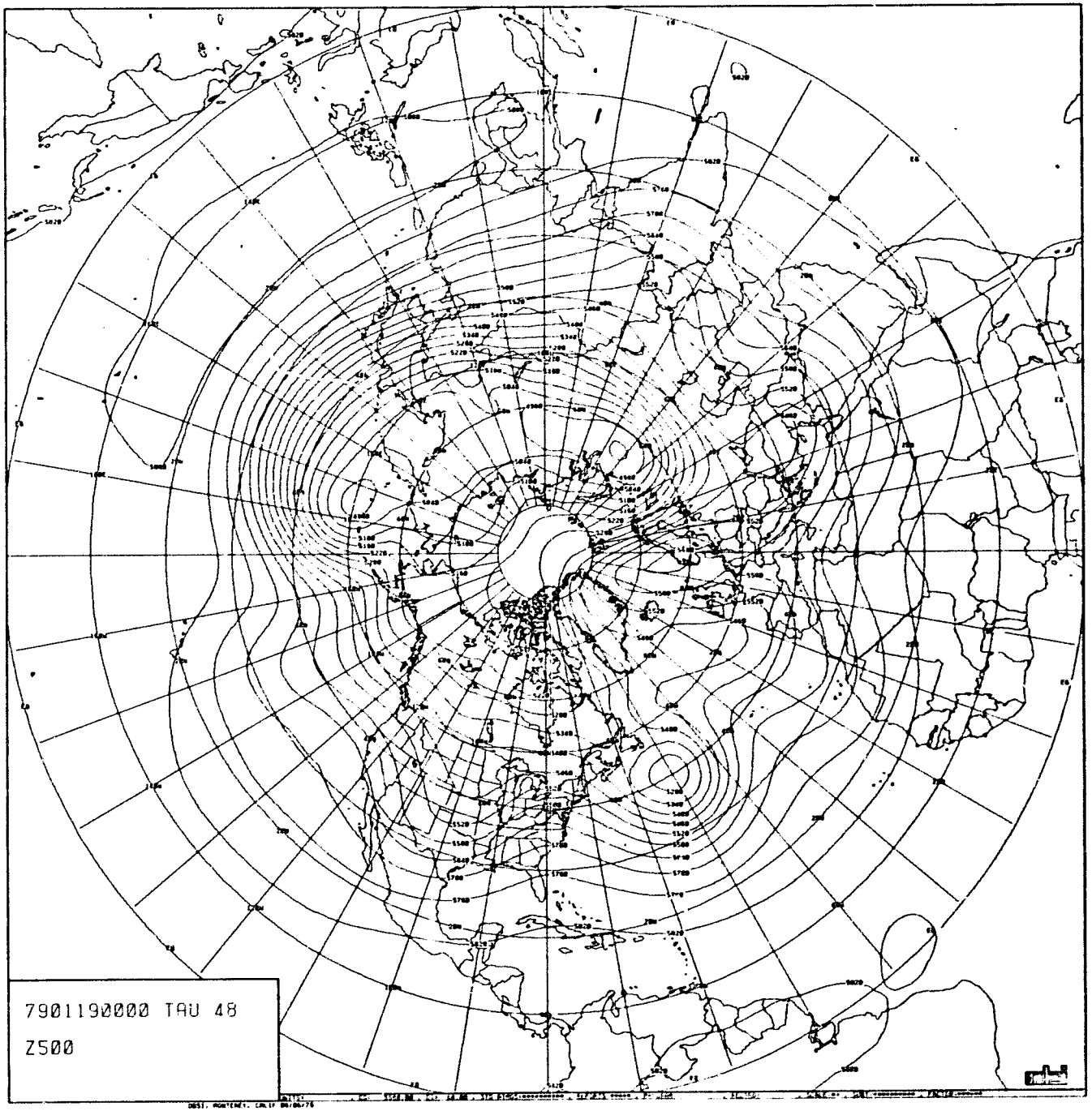

CHART IV-80: 48-Hour 500MB Height Forecast from 0000Z 19 January 1979. Chart Set H1.

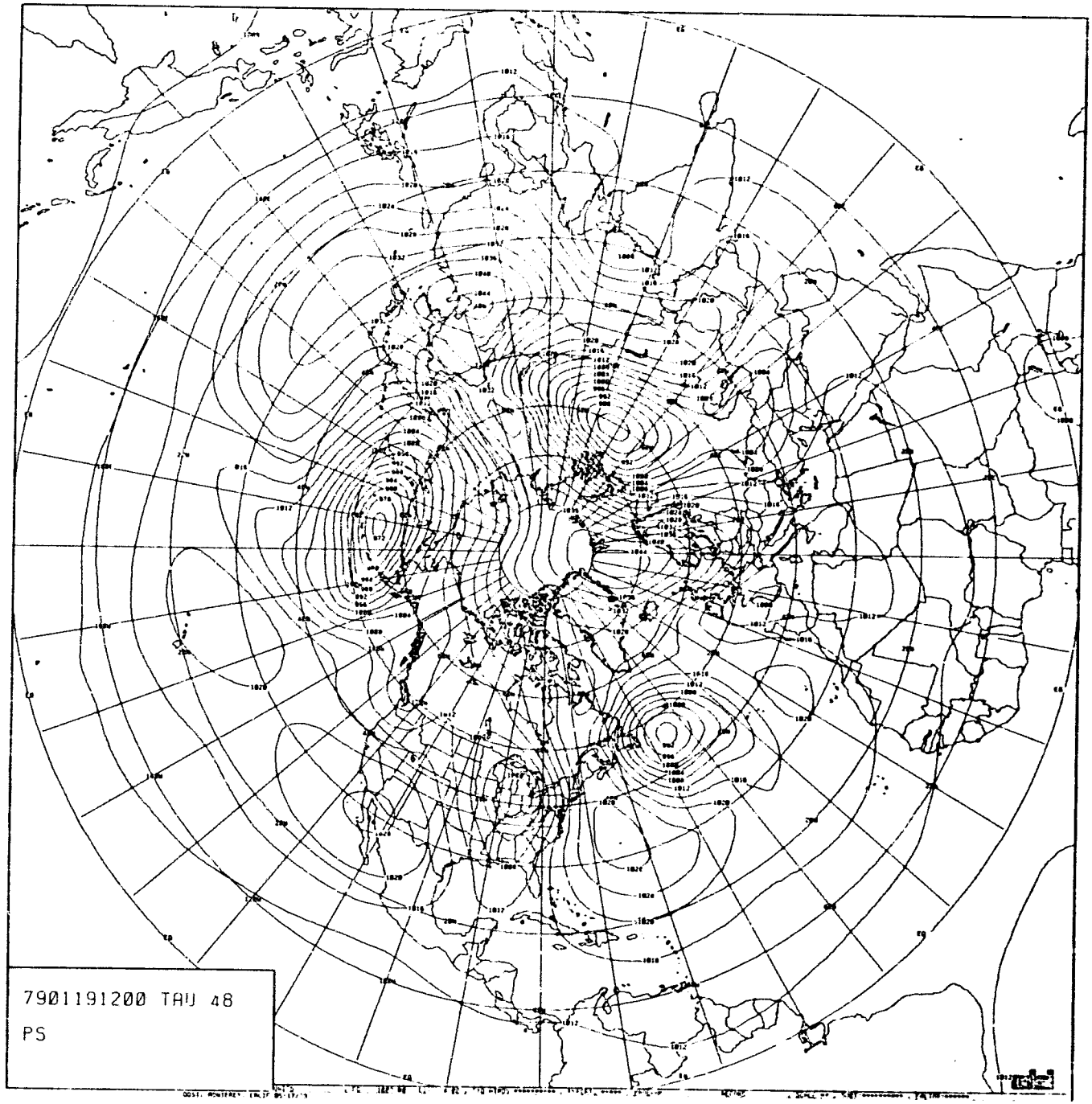

CHART IV-81: 48-Hour Surface Pressure Forecast from 1200Z 19 January 1979. Chart Set G2.

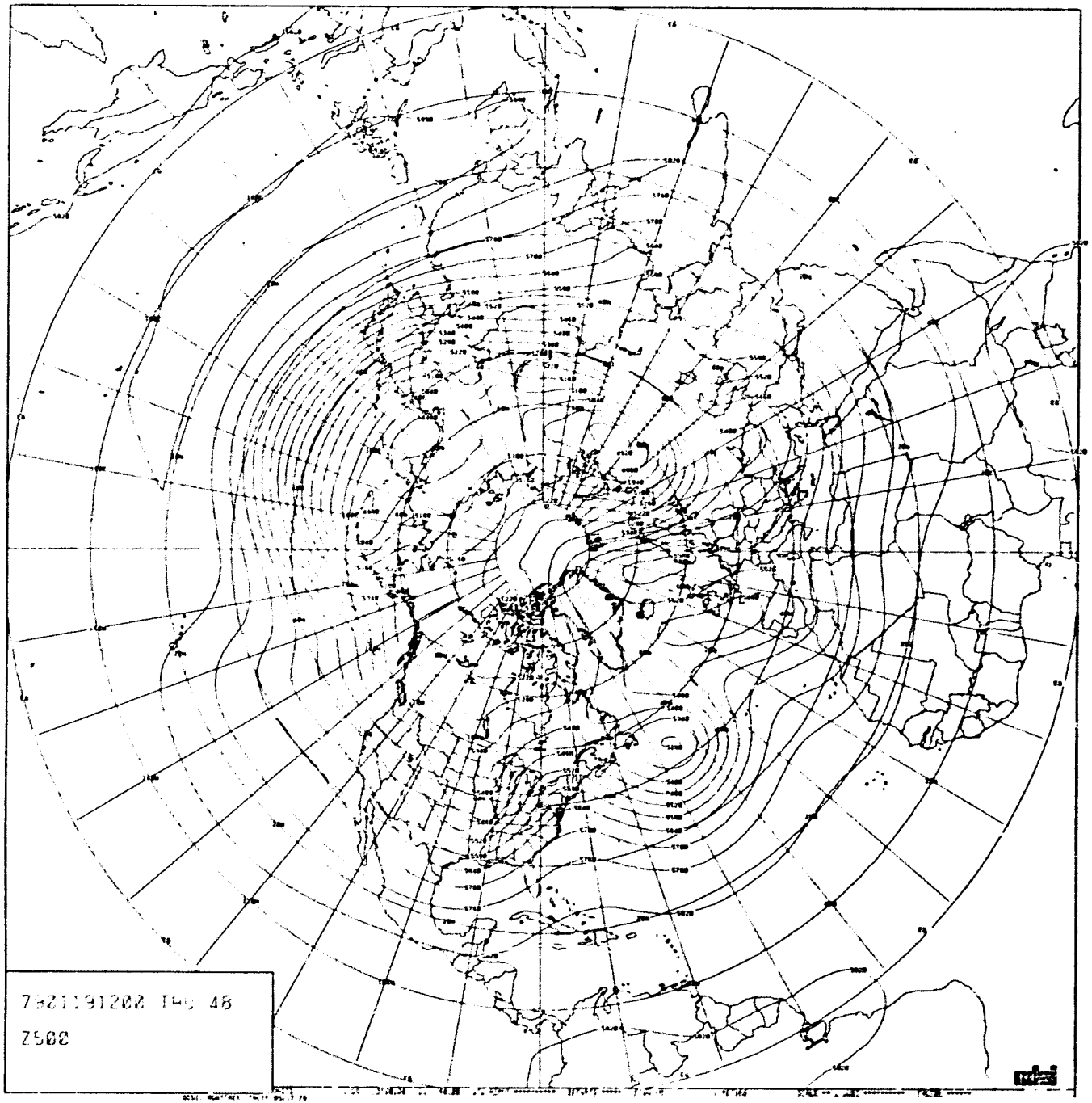

CHART IV-82: 48-Hour 500MB Height Forecast from 1200Z 19 January 1979. Chart Set G2.

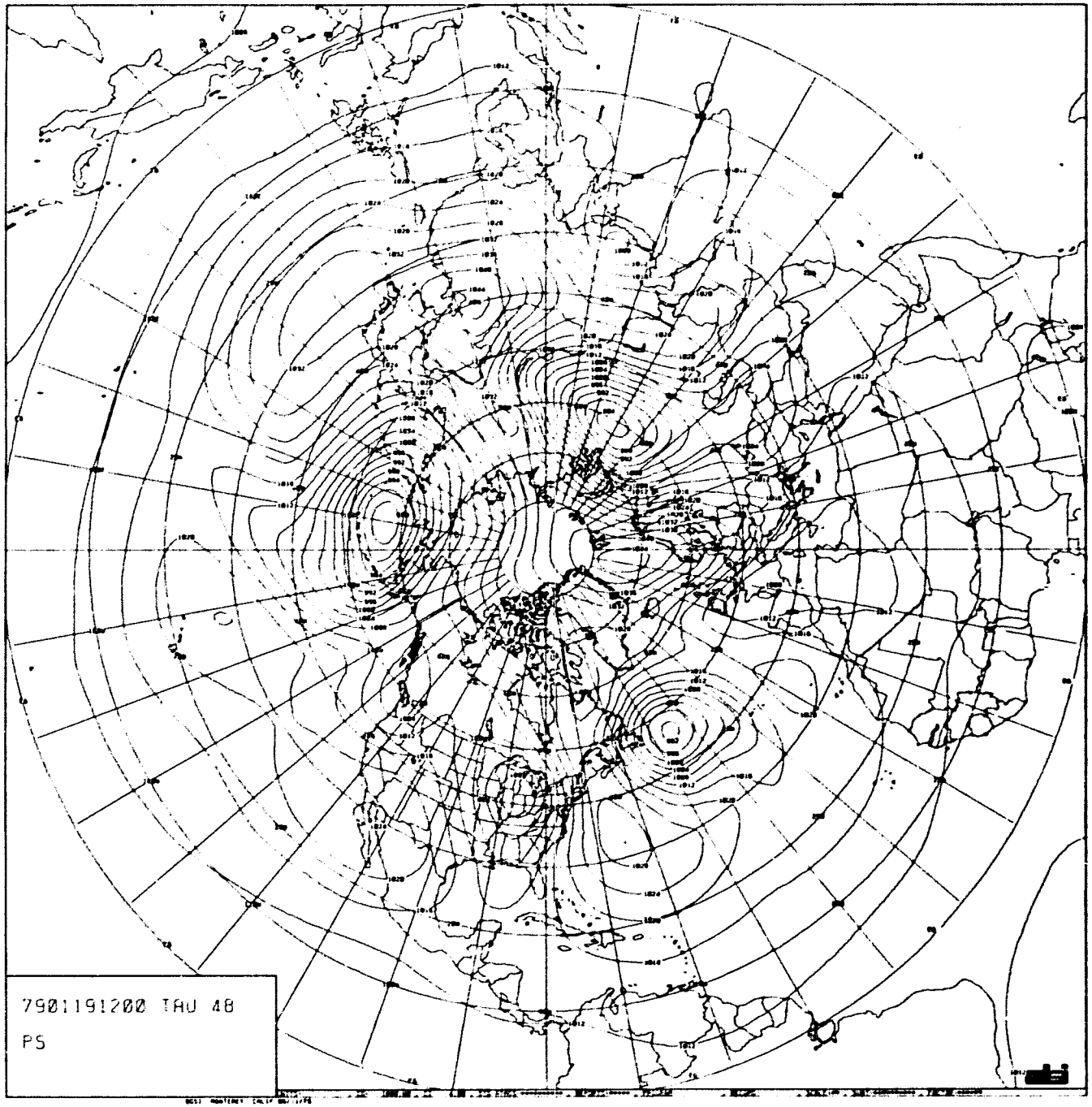

CHART IV-83: 48-Hour Surface Pressure Forecast from 1200Z 19 January 1979. Chart Set H2

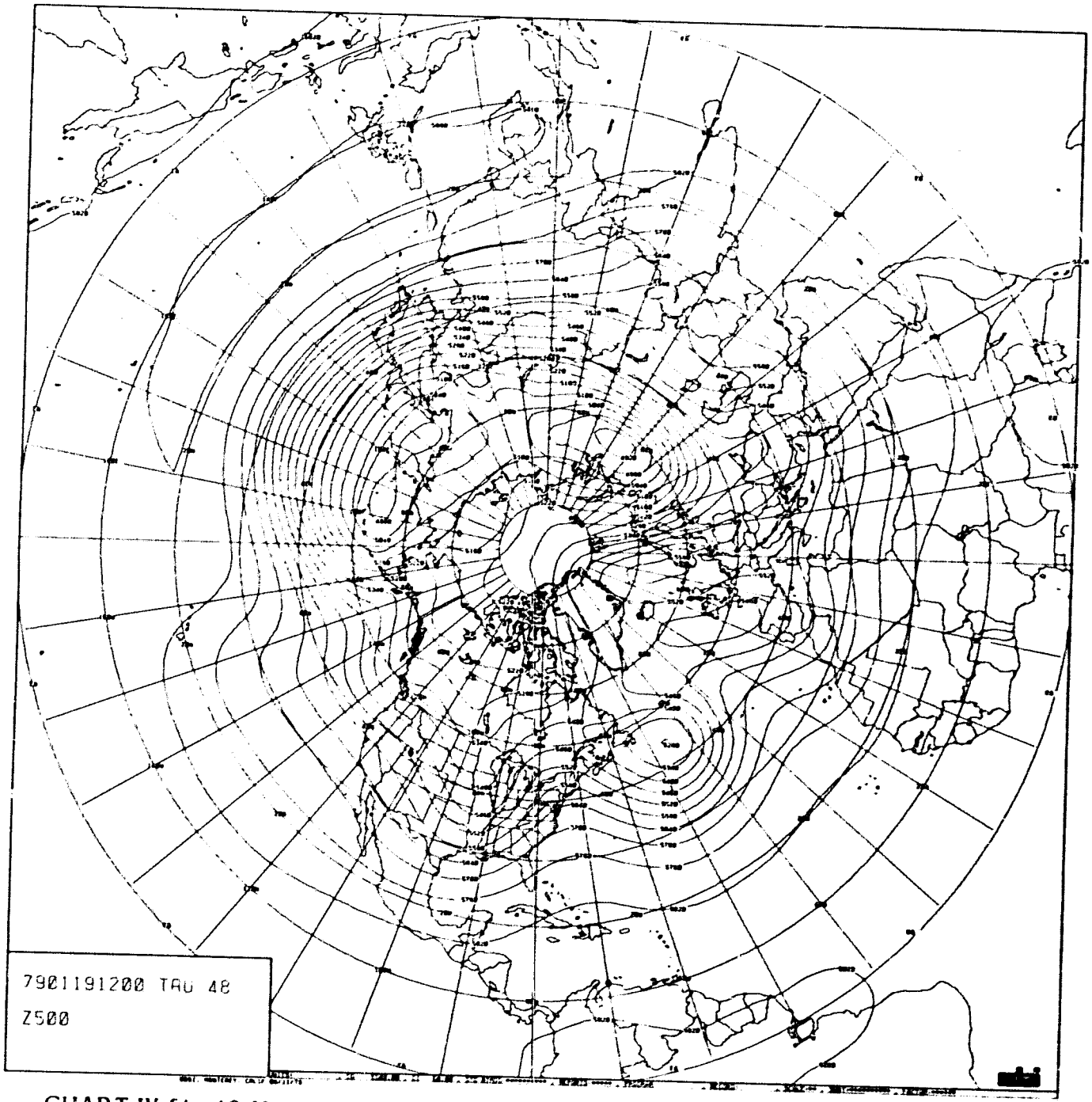

CHART IV-84: 48-Hour 500MB Height Forecast from 1200Z 19 January 1979. Chart Set H2.

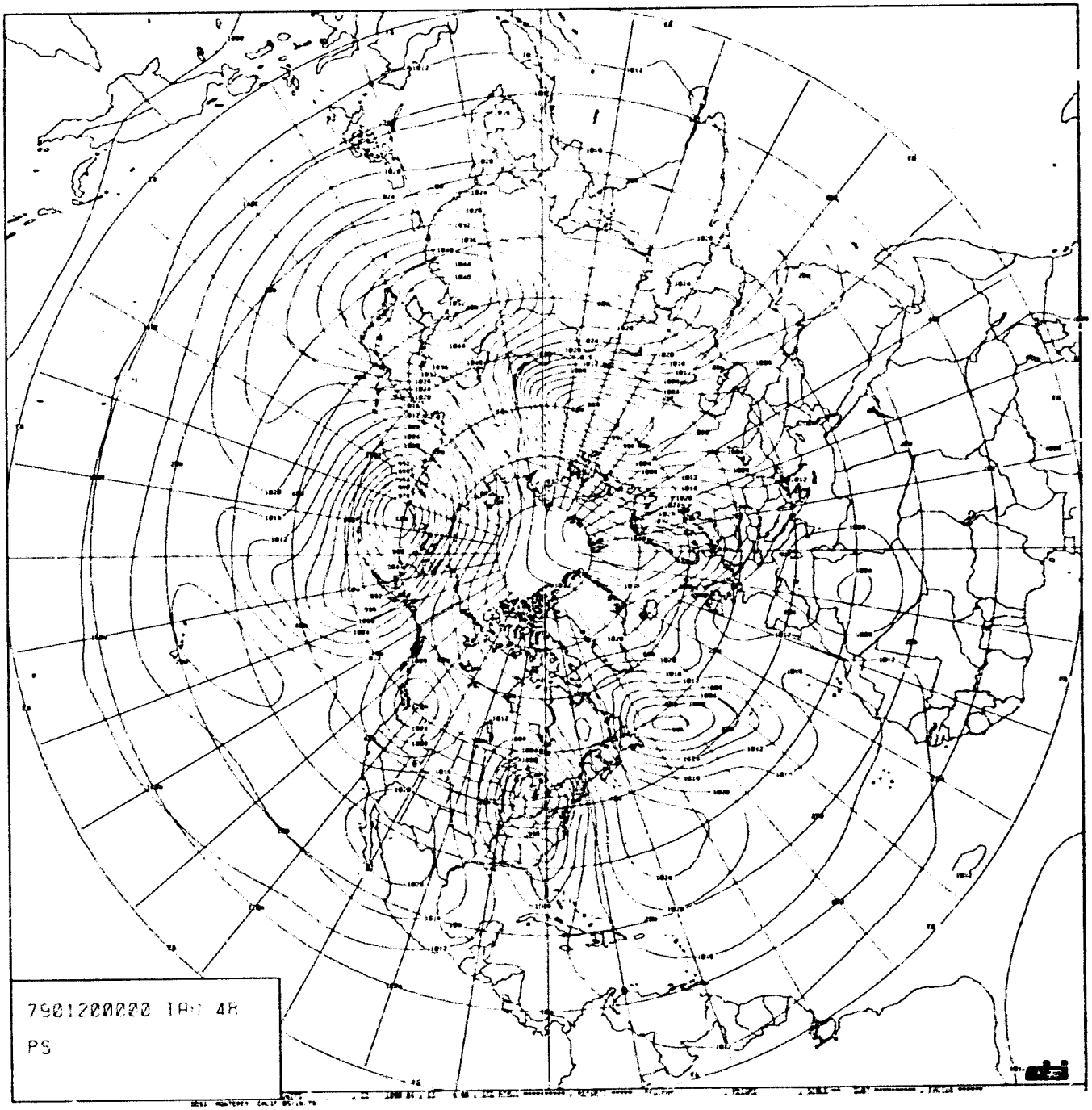

CHART IV-85: 48-Hour Surface Pressure Forecast from 0000Z 20 January 1979. Chart Set G3.

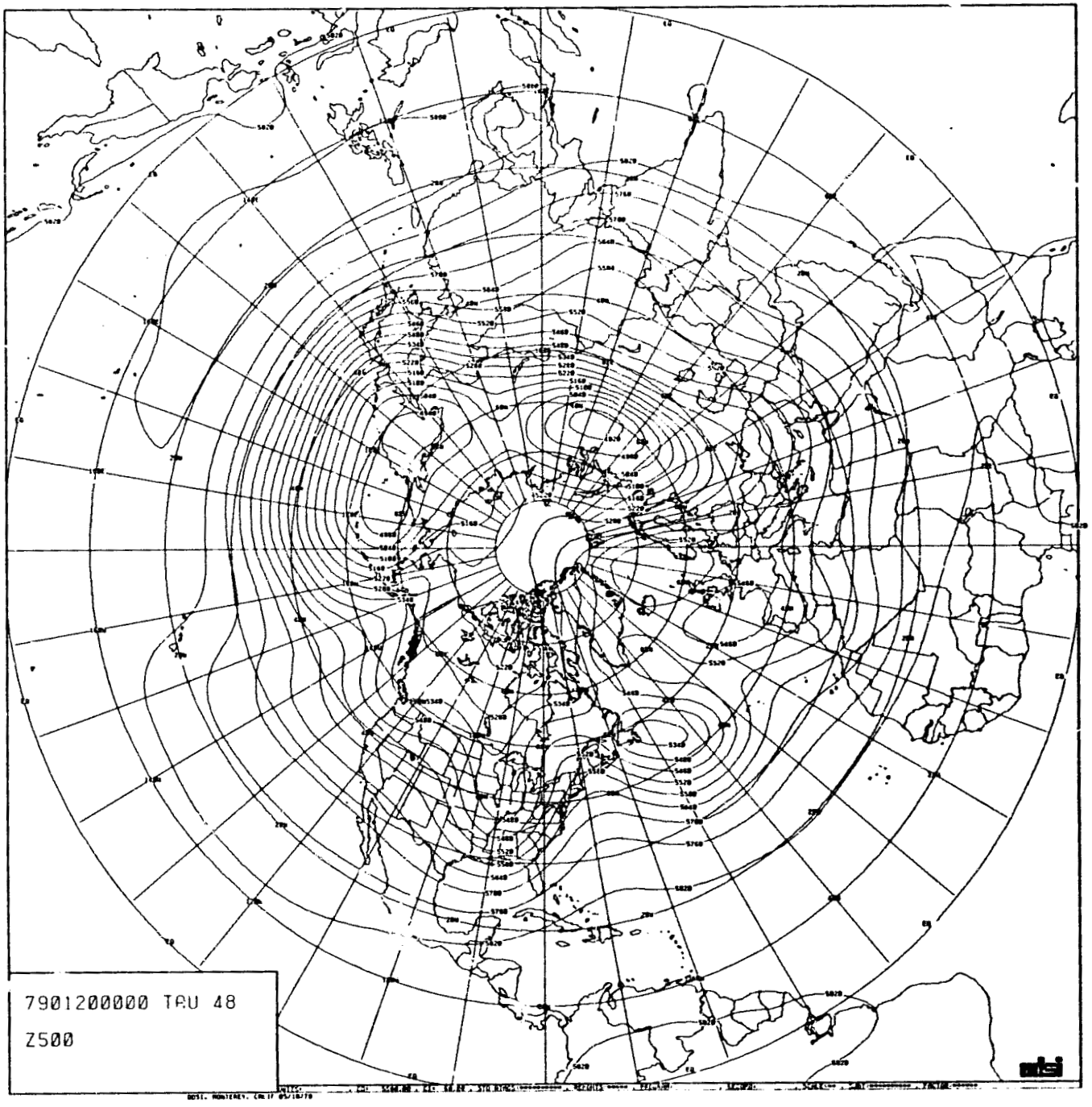

CHART IV-86: 48-Hour 500MB Height Forecast from 0000Z 20 January 1979. Chart Set G3.

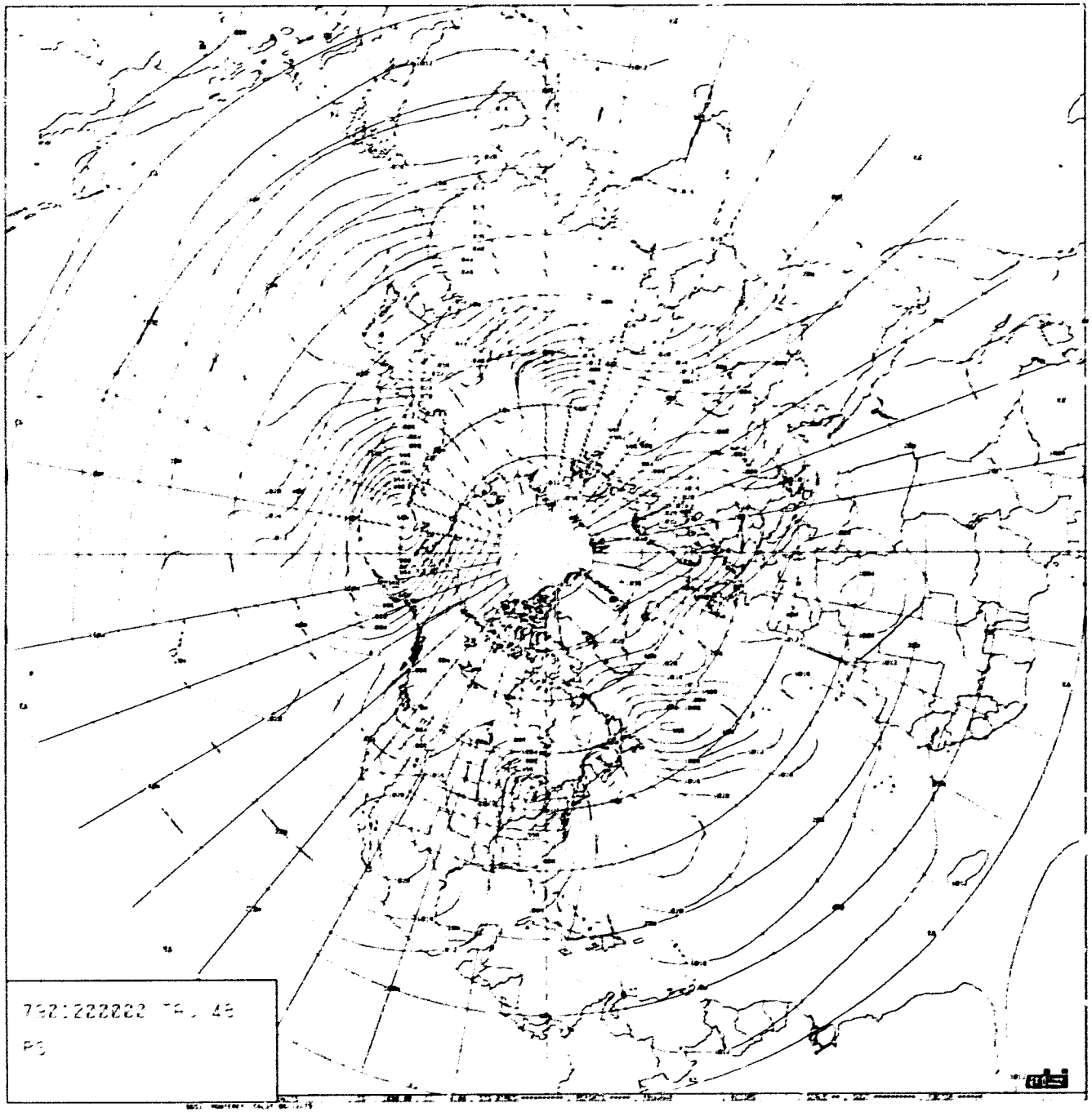

CHART IV-87: 48-Hour Surface Pressure Forecast from 0000Z 20 January 1979. Chart Set H3.

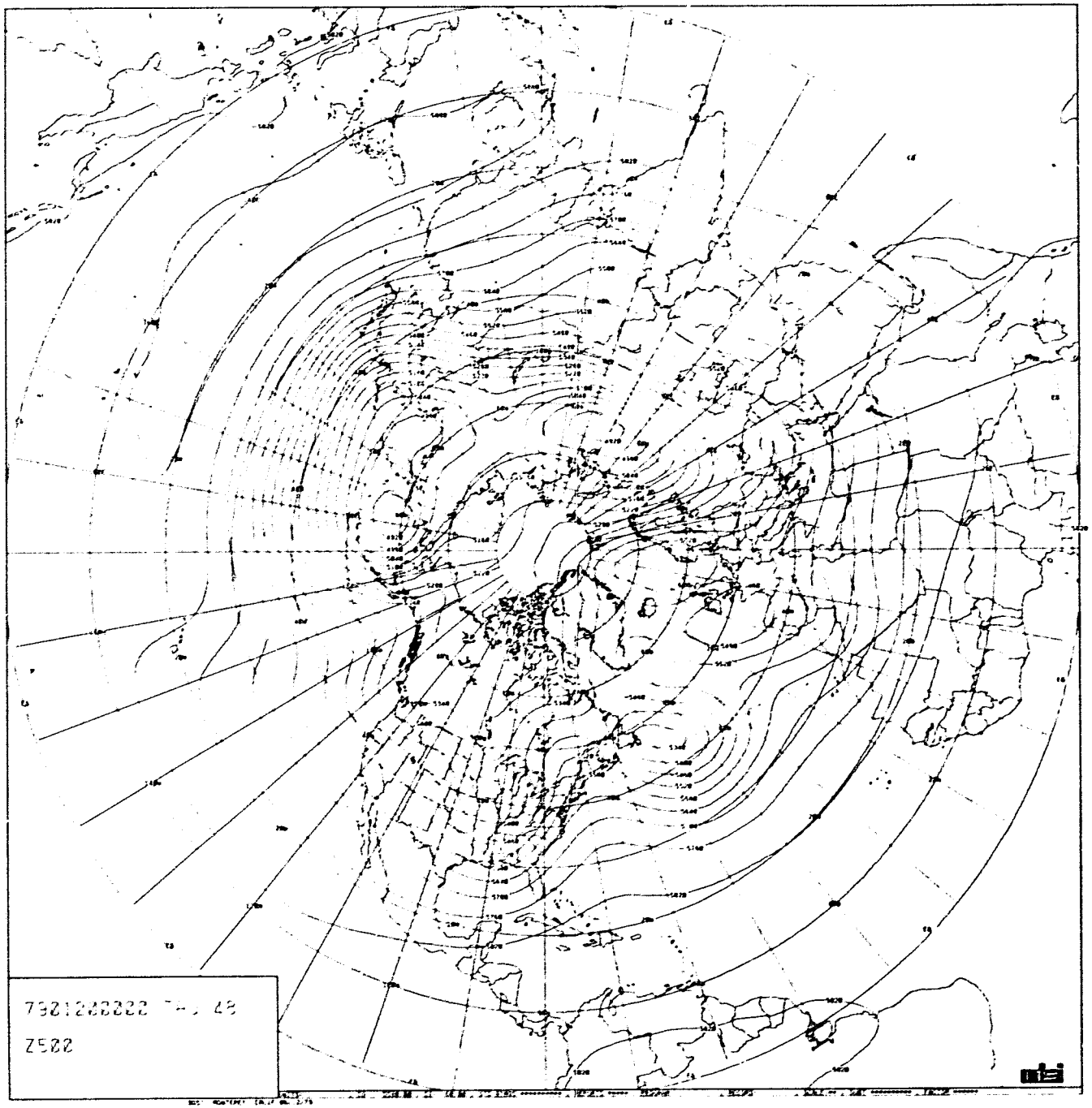

CHART IV-88: 48-Hour 500MB Height Forecast from 0000Z 20 January 1979. Chart Set H3.

TABLE V-1: RMS DIFFERENCES BETWEEN "SET A" AND "SET C" ANALYSES

PARAMETER	DATE*		
	JAN 19	JAN 20	JAN 21
PS (mbs)	0.62	0.67	0.55
ΔZ900 (m)	2.06	3.43	3.00
ΔT900 (^{o}C)	0.02	0.04	0.03
ΔU900 (m/sec)	0.46	0.71	0.55
ΔV900 (m/sec)	0.55	0.66	0.53
ΔZ250 (m)	0.96	2.37	1.92
ΔT250 (^{o}C)	0.02	0.03	0.05
ΔU250 (m/sec)	0.18	0.39	0.27
ΔV250 (m/sec)	0.22	0.40	0.28

*At 0000Z.

TABLE V-2: RMS DIFFERENCES BETWEEN "SET A" AND "SET D" ANALYSES

PARAMETER	DATE*		
	JAN 19	JAN 20	JAN 21
PS (mbs)	0.81	0.81	0.76
ΔZ900 (m)	3.23	2.78	2.84
ΔT900 (^{o}C)	0.03	0.04	0.04
ΔU900 (m/sec)	0.63	0.64	0.60
ΔV900 (m/sec)	0.76	0.65	0.63
ΔZ250 (m)	1.64	1.66	1.76
ΔT250 (^{o}C)	0.02	0.03	0.03
ΔU250 (m/sec)	0.21	0.28	0.28
ΔV250 (m/sec)	0.32	0.30	0.27

*At 0000Z.

TABLE V-3: NUMBER OF TEMPERATURE SOUNDINGS AVAILABLE FOR UPPER-AIR ANALYSES

Analysis Period	Number of Accepted Reports	
	Radiosondes/Rawinsondes*	SIRS
19/00	551	86
19/12	589	49
20/00	560	85
20/12	578	54
21/00	568	47

*Pieces of data at 500 MBS.

TABLE V-4: NUMBER OF CLOUD-MOTION VECTORS AVAILABLE FOR UPPER-AIR ANALYSES

Pressure Level	Date-Time of Analysis				
	19/00	19/12	20/00	20/12	21/00
900	180	72	106	156	118
700	1	3	0	3	4
500	3	4	7	18	1
400	7	2	8	10	9
300	22	7	22	39	20
250	25	20	26	20	10
200	22	5	5	12	6
Totals	260	113	172	255	168

TABLE V-5: NUMBER OF AIRCRAFT WIND REPORTS AVAILABLE FOR UPPER-AIR ANALYSES

Pressure Level	Date-Time of Analysis				
	19/00	19/12	20/00	20/12	21/00
850	3	0	0	0	1
700	2	3	2	1	2
500	4	2	1	4	4
400	21	9	17	12	21
300	176	151	123	142	214
250	447	372	464	356	488
200	312	255	322	245	256
Totals	965	792	929	760	986

TABLE V-6: RMS DIFFERENCES BETWEEN "SET A" AND "SET B" ANALYSES

PARAMETER	DATE*		
	JAN 19	JAN 20	JAN 21
PS (mbs)	0.00	0.11	0.10
ΔZ900 (m)	1.08	1.31	1.16
ΔT900 (^{o}C)	0.17	0.32	0.29
ΔU900 (m/sec)	0.65	0.63	0.78
ΔV900 (m/sec)	0.30	0.32	0.31
ΔZ250 (m)	13.7	17.5	15.8
ΔT250 (^{o}C)	0.11	0.22	0.26
ΔU250 (m/sec)	2.55	2.97	1.70
ΔV250 (m/sec)	1.78	2.72	1.90

*At 0000Z.

TABLE V-7: COMPUTER EXECUTION TIMES FOR TWO-DAY FORECASTS USING THE CDC CYBER 74 SYSTEM.

Model/Run Type	Computer Time (seconds)	
	CP	I/O
• Run E Static Initialization plus 2-day forecast	3,770	7,460
• Run F Six Orbits plus 2-day forecast	4,900	9,874
• Runs G1, G2, G3 Twelve Orbits plus 2-day forecast	6,020	12,200
• Runs H1, H2, H3 Twenty-four orbits w/ data assimilation	8,340	17,000

Note: Each Temperton "orbit" takes about 190 CP-seconds and about 400 seconds of I/O.

TABLE V-8: COMPARATIVE ERROR STATISTICS FOR 48-HOUR FORECASTS

Starting Time	Forecast Identifier	Sea-Level Pressure		500 MB Height	
		Mean	RMSE	Mean	RMSE
19/00Z	E	-0.22	4.99	-2.62	46.4
	F	-0.16	4.97	-2.52	46.2
	G1	-0.10	4.98	-2.04	46.3
	H1	0.01	5.01	-1.08	46.4
19/12Z	G2	0.02	5.26	-1.19	50.1
	H2	0.08	5.21	-0.65	49.2
20/00Z	G3	-0.01	5.33	3.55	50.0
	H3	0.04	5.27	3.42	48.6
19/00Z	H4	-0.17	4.99	-2.04	46.2

TABLE V-9: COMPARATIVE FORECAST MODEL PERFORMANCE FOR FOUR TYPES OF INITIALIZATION

Feature	Analyses		Forecast Run*			
	Initial	Verification	E	F	G1	H1
Japan Low	976	956	960 (960)	964 (961)	964 (962)	968 (966)
Asian Low	984	988	980 (979)	984 (981)	984 (981)	984 (981)
Newfoundland Low	996	984	988 (986)	988 (987)	988 (987)	988 (987)
U.S. Low	1008	992	1004 (1003)	1004 (1003)	1004 (1003)	1004 (1003)

*48-Hour Forecasts

VI. FIGURES

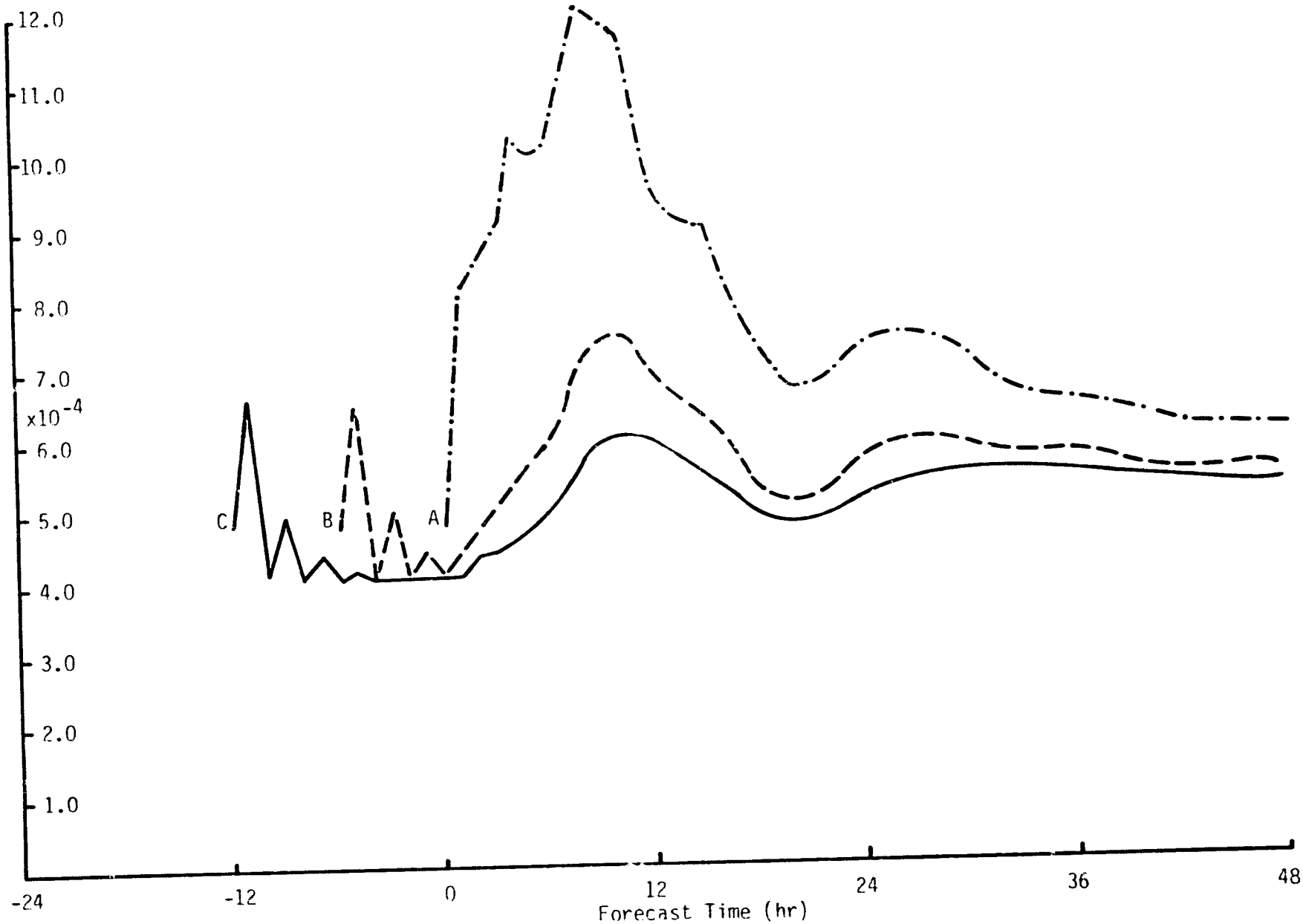

FIGURE VI-1: EFFECT OF INITIALIZATION ON RMS MASS DIVERGENCE AT SIGMA=0.9 LEVEL

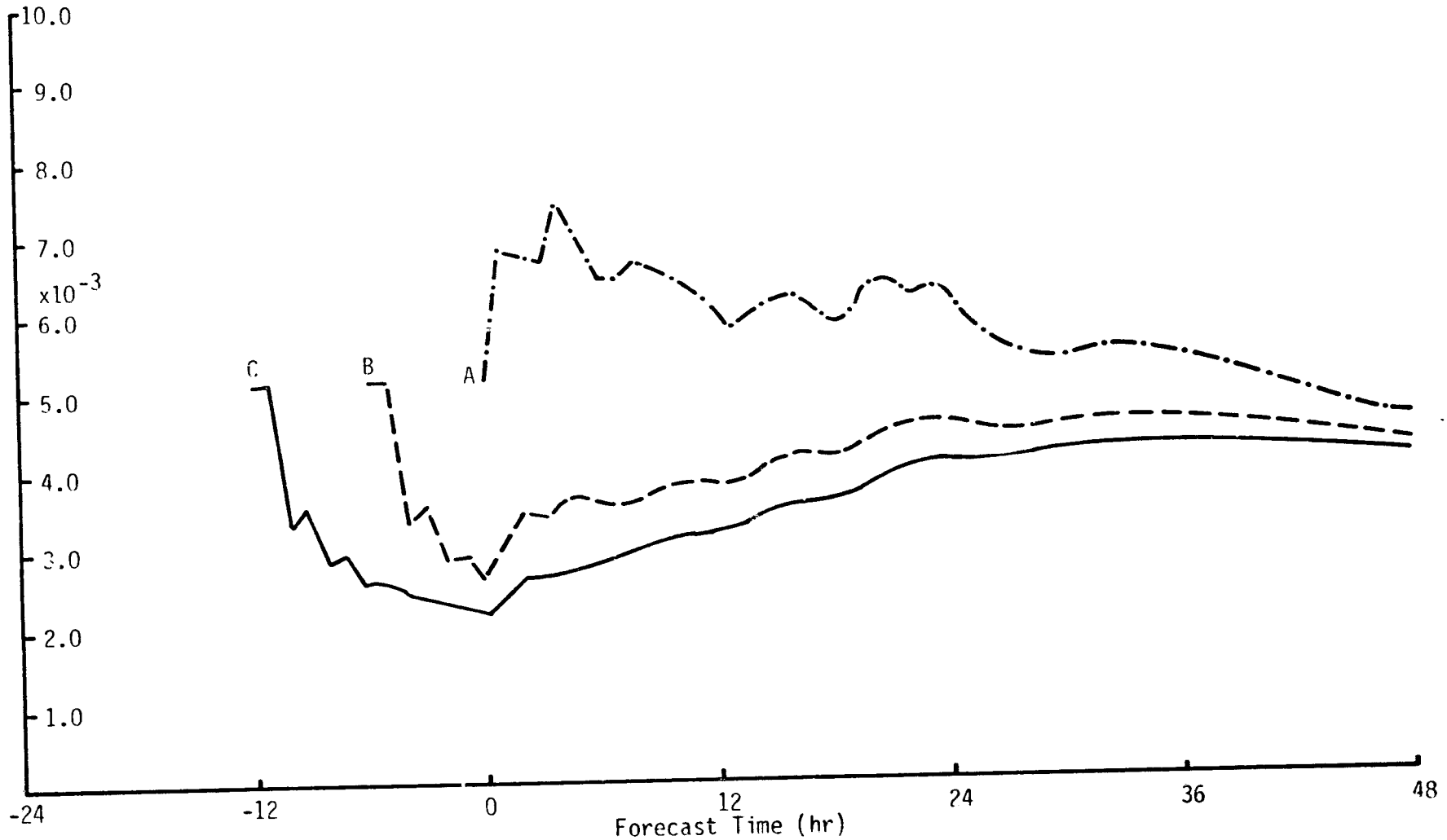

FIGURE VI-2: EFFECT OF INITIALIZATION ON RMS MASS DIVERGENCE AT SIGMA=0.7 LEVEL

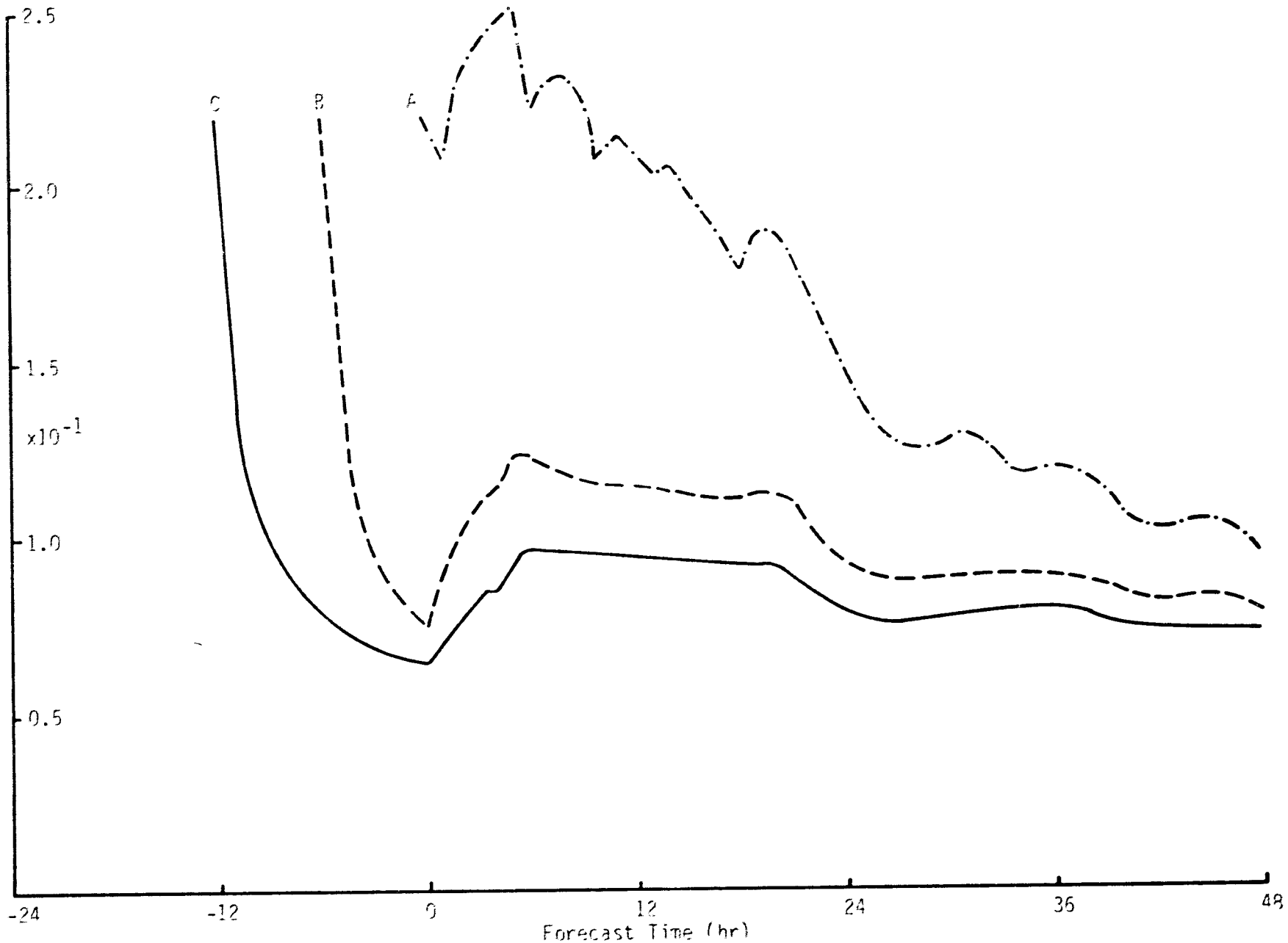

FIGURE VI-3: EFFECT OF INITIALIZATION ON RMS MASS DIVERGENCE AT SIGMA=0.5 LEVEL

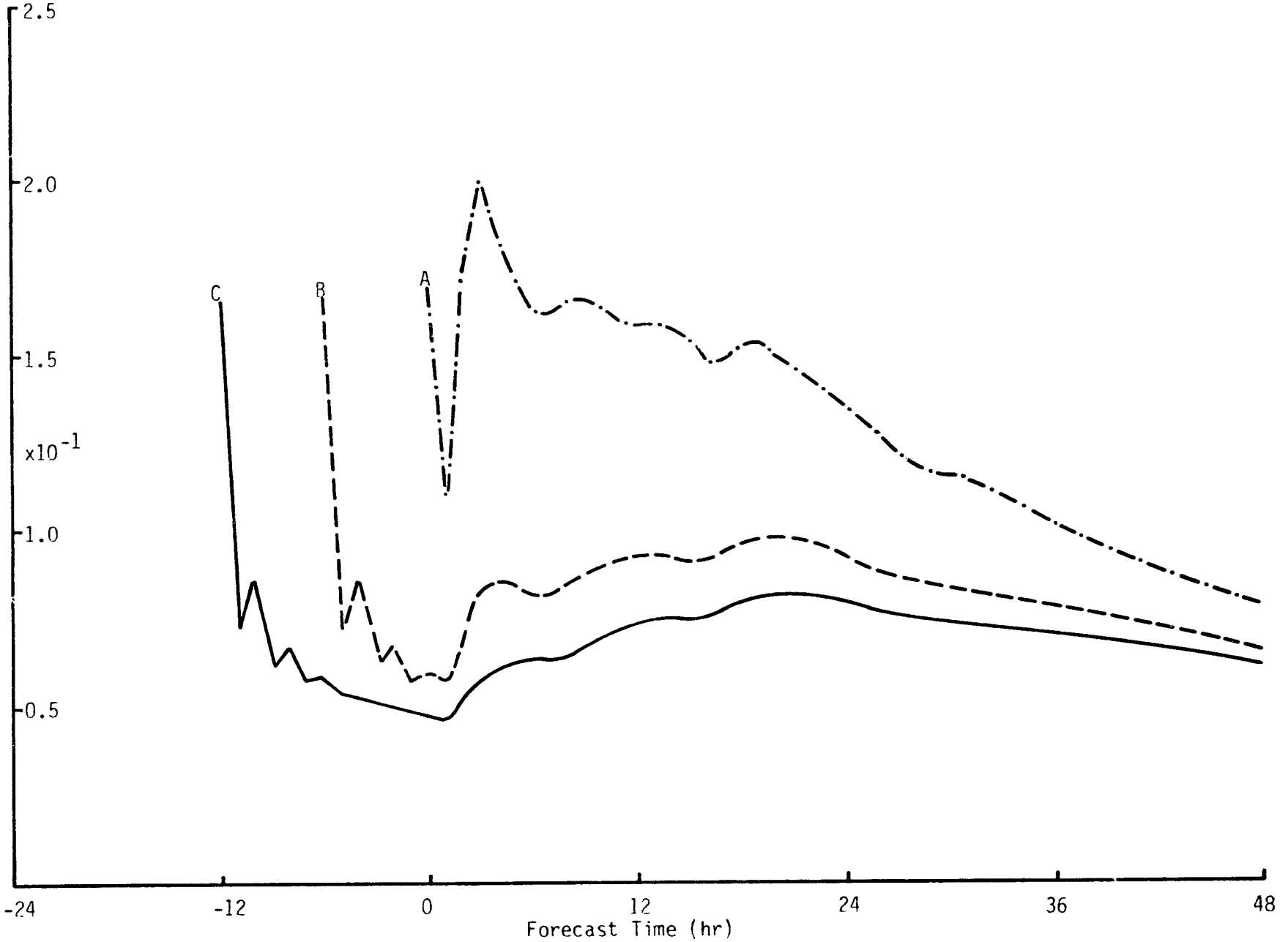

FIGURE VI-4: EFFECT OF INITIALIZATION ON RMS MASS DIVERGENCE AT SIGMA=0.3 LEVEL

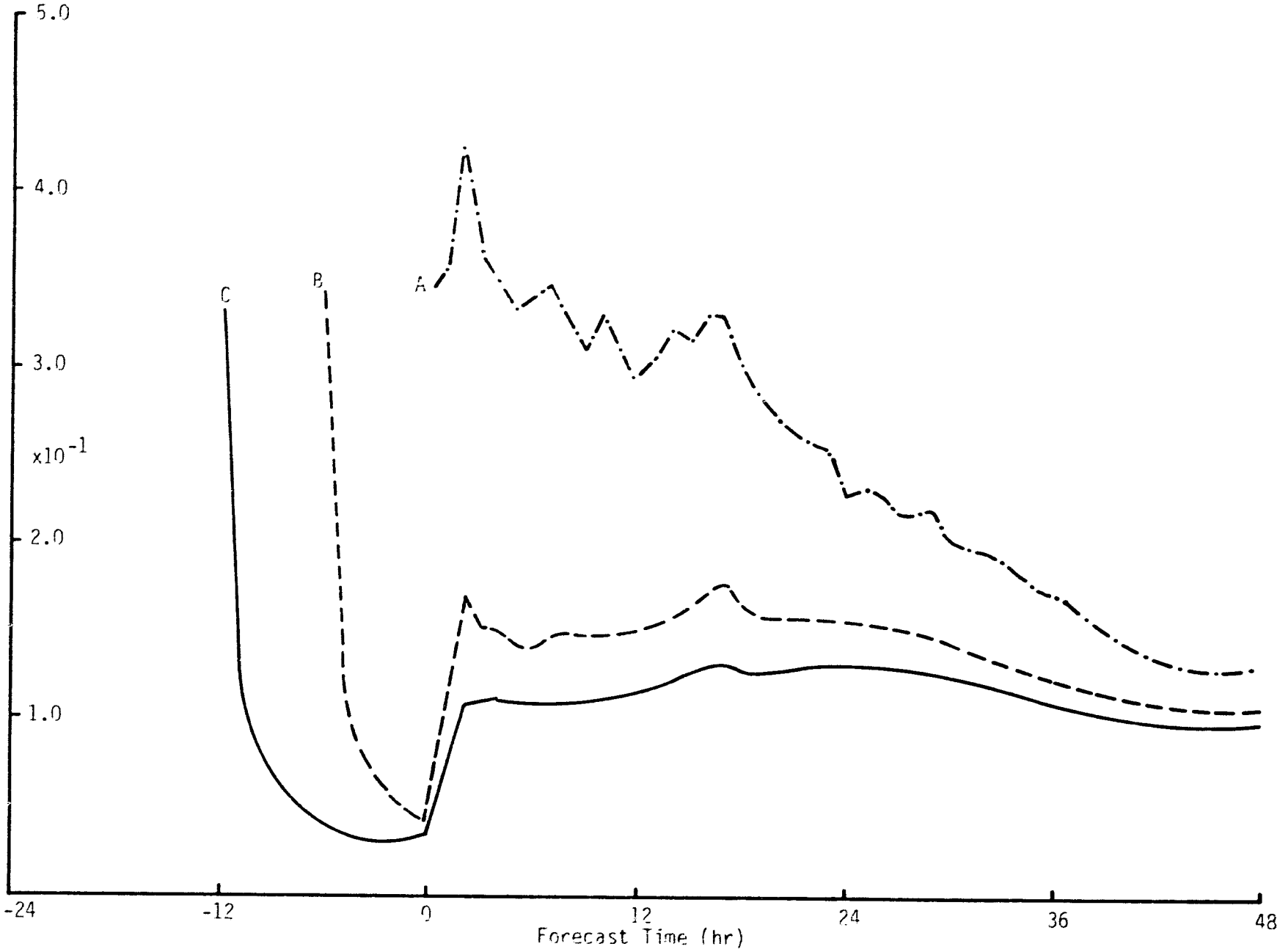

FIGURE VI-5: EFFECT OF INITIALIZATION ON RMS MASS DIVERGENCE AT SIGMA=0.1 LEVEL

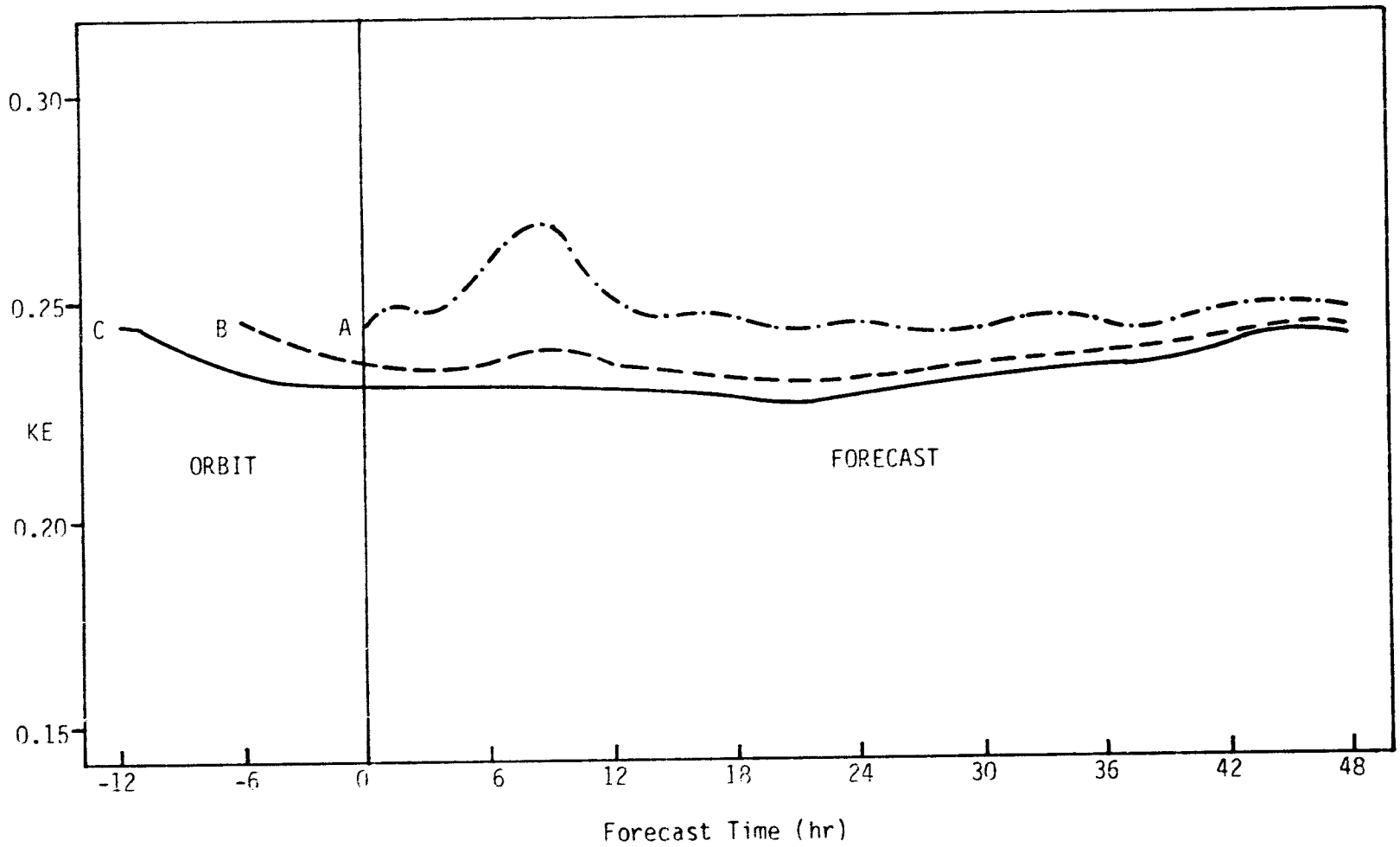

FIGURE VI-6: EFFECT OF INITIALIZATION ON LAYER MEAN KINETIC ENERGY AT SIGMA=0.9 LEVEL

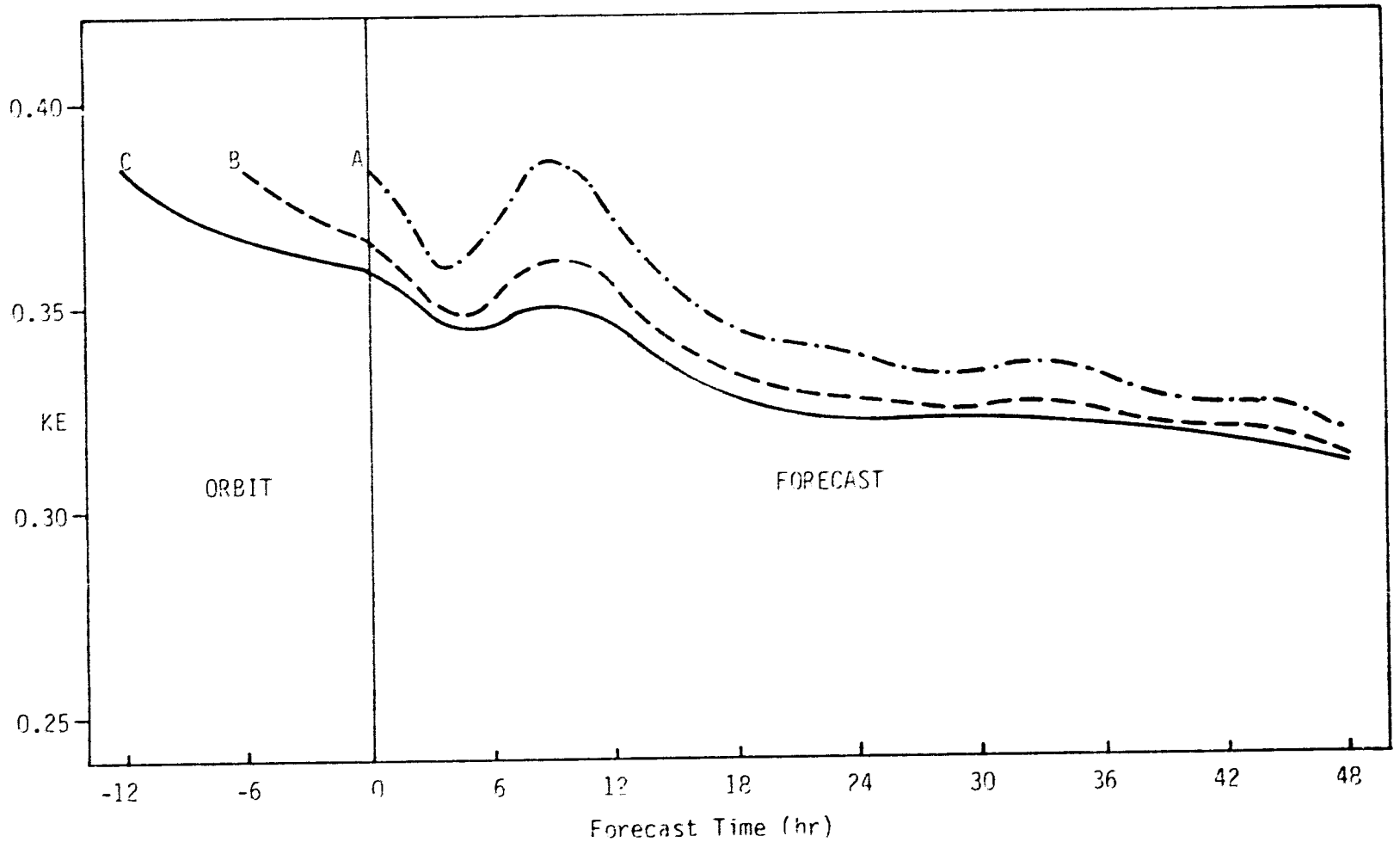

FIGURE VI-7: EFFECT OF INITIALIZATION ON LAYER MEAN KINETIC ENERGY AT SIGMA=0.7 LEVEL

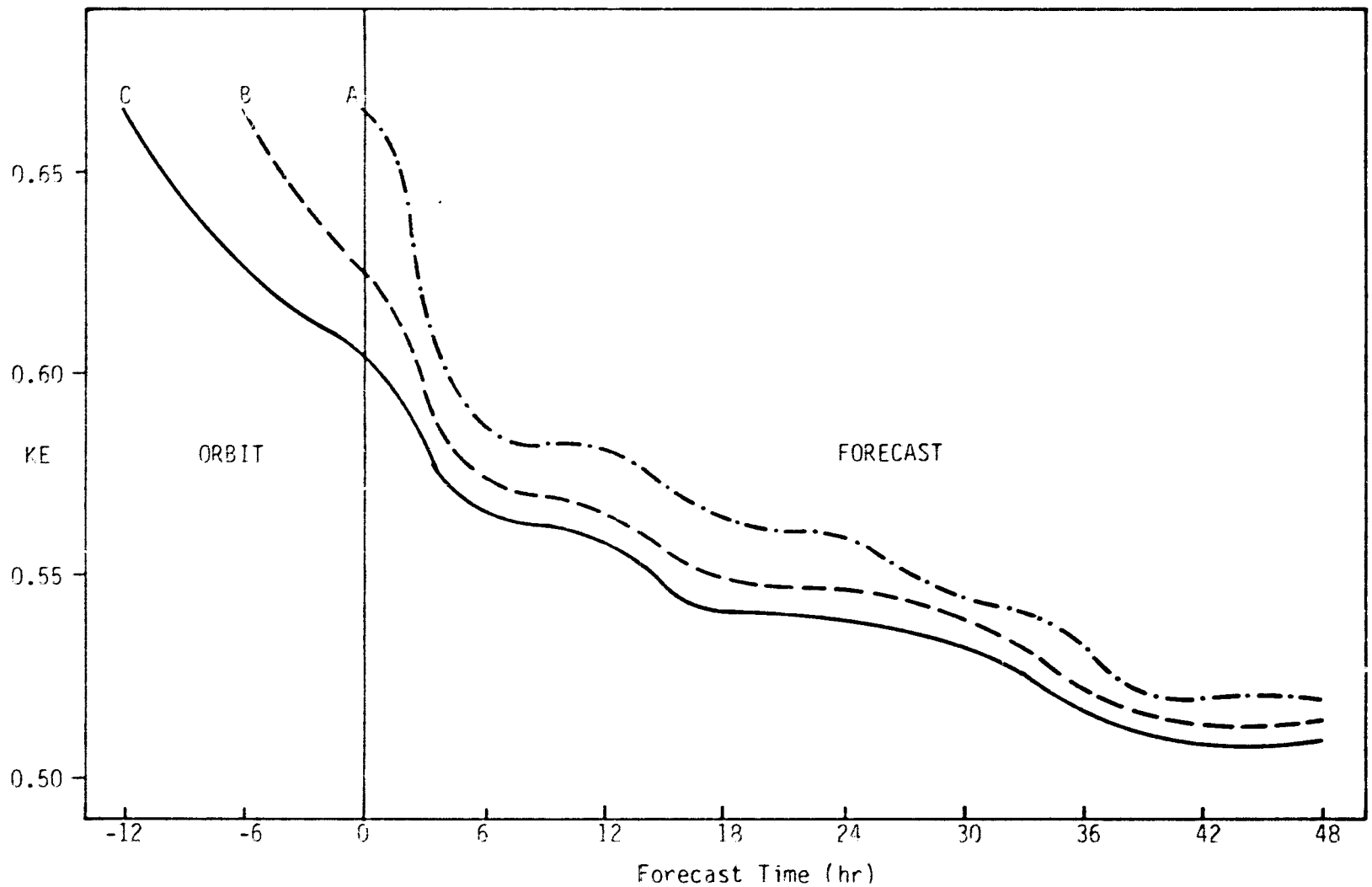

FIGURE VI-8: EFFECT OF INITIALIZATION ON LAYER MEAN KINETIC ENERGY AT SIGMA=0.5 LEVEL

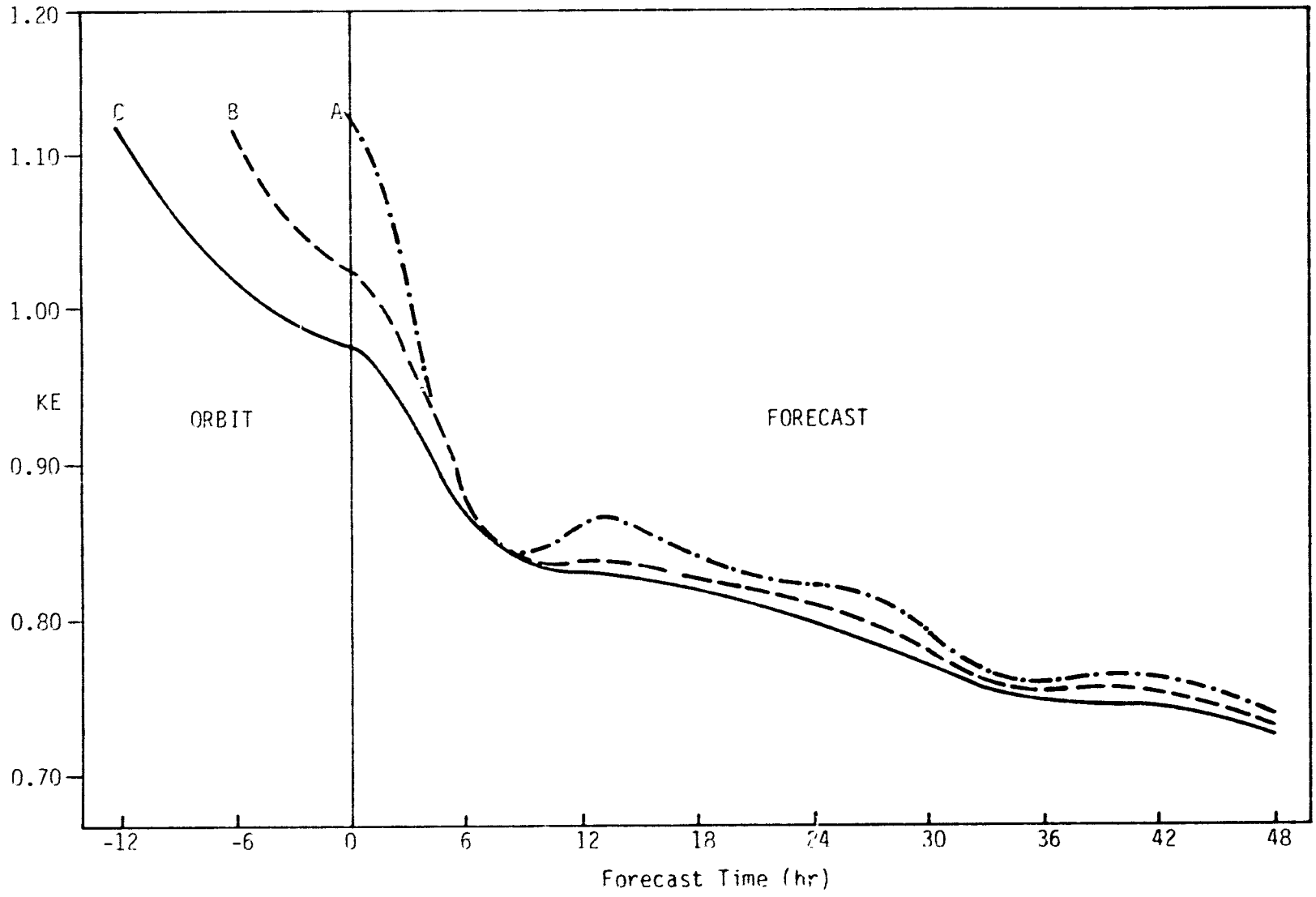

FIGURE VI-9: EFFECT OF INITIALIZATION ON LAYER MEAN KINETIC ENERGY AT SIGMA=0.3 LEVEL

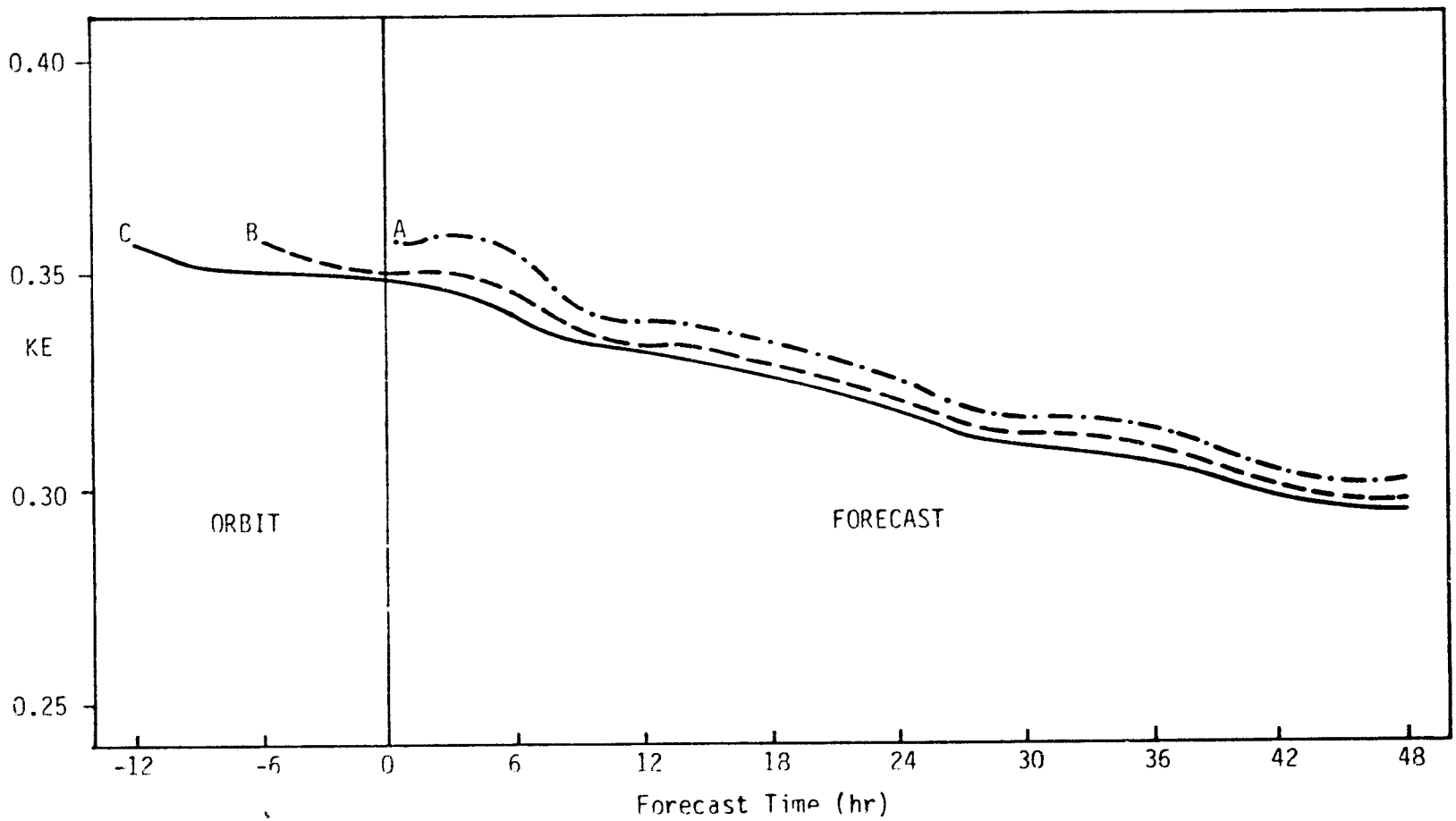

FIGURE VI-10: EFFECT OF INITIALIZATION ON LAYER MEAN KINETIC ENERGY AT SIGMA=0.1 LEVEL

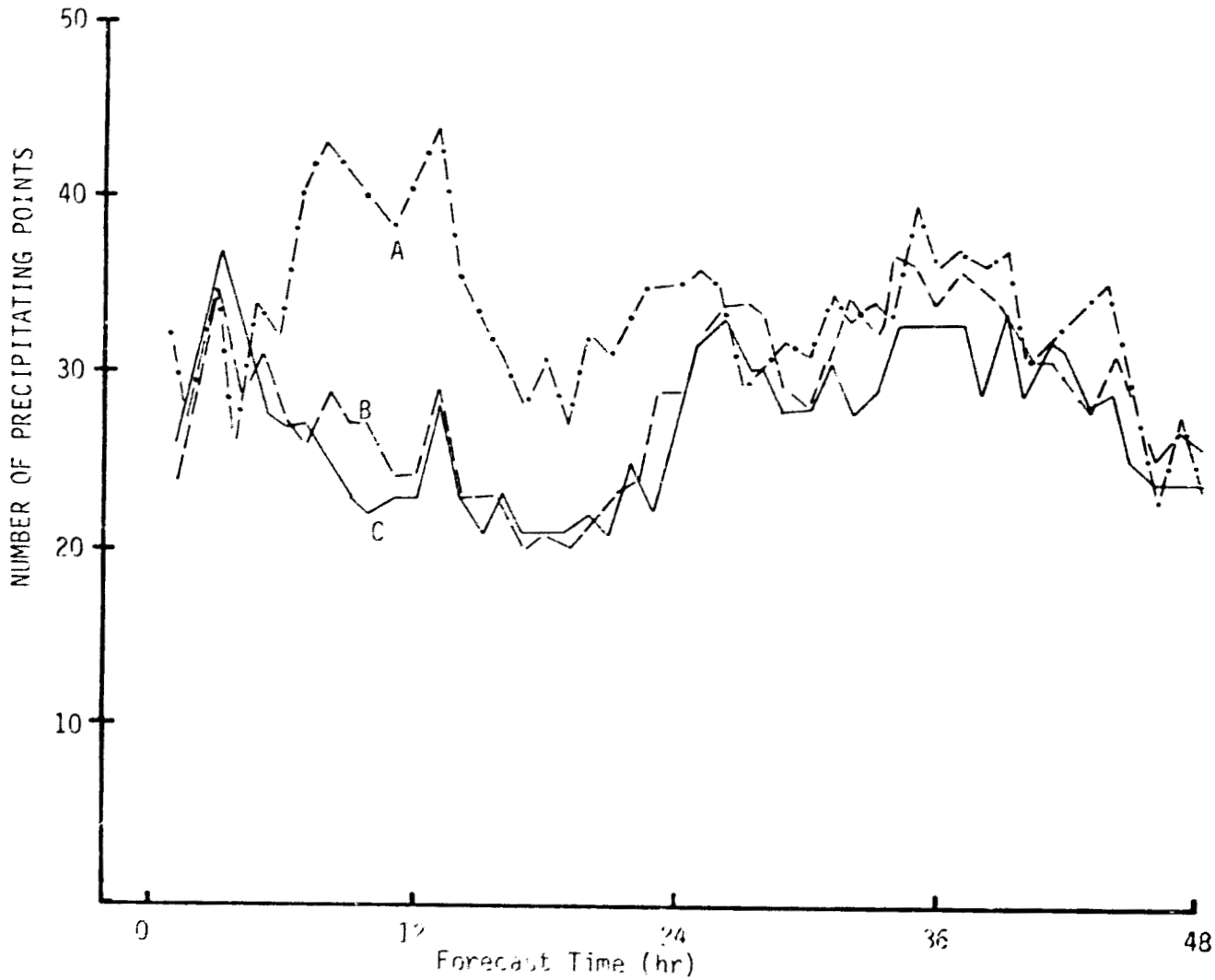

FIGURE VI-11: EFFECT OF INITIALIZATION ON CUMULUS SCALE PRECIPITATION MECHANISM

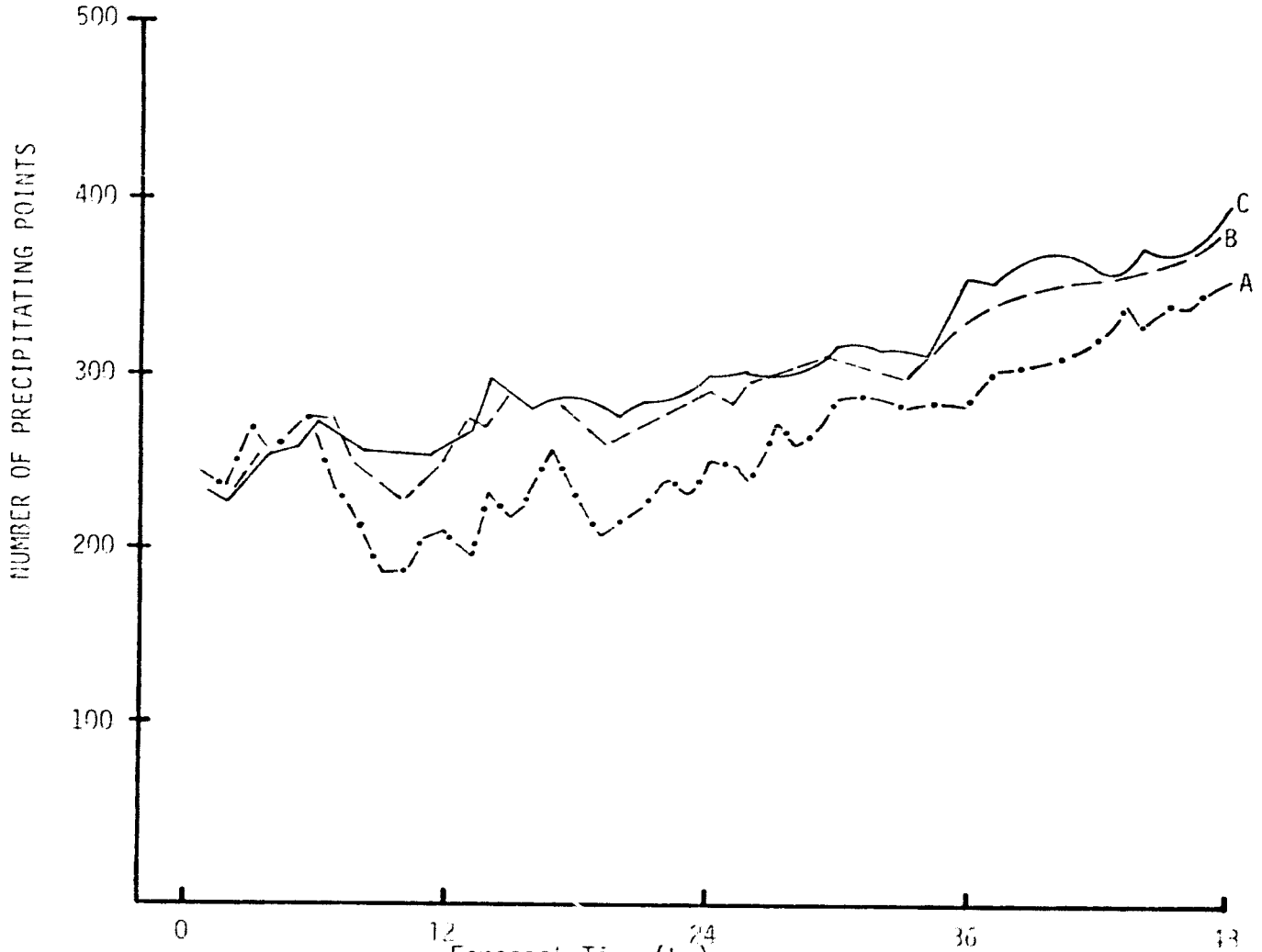

FIGURE VI-12: EFFECT OF INITIALIZATION ON LARGE SCALE PRECIPITATION MECHANISM

REFERENCES

Arakawa, Akio, 1966: "Computational Design for Long-Term Numerical Integration of the Equation of Fluid Motion: Two-Dimensional Incompressible Flow, Part I," Journal of Computational Physics, Vol. 1, No. 1, Academic Press Inc., New York, N. Y., January 1966, pp. 114-143.

Arakawa, Akio, Akira Katayama and Yale Mintz, 1969: "Numerical Simulation of the General Circulation of the Atmosphere," Proceedings of the WMO/IUGG Symposium on Numerical Weather Prediction, Tokyo, Japan, November 26 - December 4, 1968, Japan Meteorological Agency, Tokyo, March 1969, pp. IV-1 - IV-14.

Cressman, G. P., 1959: "An Operational Objective Analysis System," Monthly Weather Review, No. 10, pp. 367-374.

Gerrity, J. P., Jr. and S. H. Scolnick, 1971: "Some Comments on Robert's Time Filter for Time Integration," U.S. Dept. of Commerce NOAA, National Weather Service, Office Note 62, 9 pp.

Holl, M. M. and B. R. Mendenhall, 1972: "Fields by Information Blending, Sea-Level Pressure Version," U. S. Navy Fleet Numerical Weather Technical Note No. 72-2. Monterey, CA, 66 pp.

Holl, M. M. et al, 1963: "Linear Transforms for State-Parameter Structure," U. S. Navy Fleet Numerical Weather Central Report on Contract N228(62271)58264, Monterey, CA, 29 pp.

Kaitala, J. E., 1974: "Heating Functions and Moisture Source Terms in the FNWC Primitive Equation Models," unpublished manuscript, April 1974, 84 pp.

Kesel, Philip G. and Howard L. Lewit, 1974: "Primitive Equation Model: I. Moisture Initialization; II. PE Model Diagnostics," ODSI Final Technical Report, Contract No. N66314-74-C-1390, U. S. Navy Environmental Prediction Research Facility.

Kesel, Philip G. and Robert E. Wellck, 1975: "Data Assimilation Restorative-Iterative Model (RIMOD), ODSI Final Report for U. S. Navy Environmental Prediction Research Facility under Contract No. N00228-75-C-2120.

Kesel, Philip G., et al, 1976: "Atmospheric Analysis and Prediction Model Development," ODSI Final Report for Econ, Inc. under Contract NASW-2558, (in three volumes).

Kesel, Philip G., et al, 1977: "Atmospheric Model Development in Support of SEASAT," ODSI Final Report for JPL under Contract No. 954668, (in five volumes).

Kurihara, Yoshio, 1968: "Correspondence Note on Finite Difference Expressions for the Hydrostatic Relation and Pressure Gradient Force," Monthly Weather Review, Vol. 96, No. 9, September 1968, pp. 654-656.

Langland, R. A. and Pamela L. Stephens, 1978: "Atmospheric Analysis Modeling in Support of SEASAT," ODSI Final Report for GSFC under Contract No. NAS5-24469.

Langlois, W. C. and C. W. Kwok, 1969: "Description of the Mintz-Arakawa Numerical General Circulation Model," Numerical Simulation of Weather and Climate Technical Report No. 3, Dept. of Meteorology, Univ. of Calif., Los Angeles, 95 pp.

Lea, D. A., 1961: "Regression Equations for Vertical Extrapolation of Constant Pressure Surface Heights and Temperatures Between 200 mb and 30 mb," 191st meeting of the AMS, Chicago, Ill., March 1961.

Miyakoda, K. and Moyer, R. W., 1968: "A Method of Initialization for Dynamical Weather Forecasting," Tellus, 20, pp. 115-128.

Oliger, Joseph, Robert Wellck, Akira Kasahara and Warren Washington, 1970: "Description of NCAR Global Circulation Model," National Center for Atmospheric Research, NCAR-TN/STR-56.

Phillips, Norman A. 1957: "A Coordinate System Having Some Special Advantages for Numerical Forecasting," Journal of Meteorology, Vol. 14, No. 4, April 1957, pp. 184-185.

Robert, Andre J., 1966: "The Integration of a Low Order Spectral Form of the Primitive Meteorological Equations," Journal of the Meteorological Society of Japan, Serial 2, Vol. 44, No. 5, Tokyo, October 1966, pp 237-245.

Sasaki, Y., 1958: "An Objective Analysis Based on the Variational Method," Journal of the Meteorological Society of Japan, pp. 77-78.

Weigle, W. F., et al, 1973: "Development of FIB/UV-MED," U. S. Navy Environmental Prediction Research Facility Report on Contract N66314-73-C-1444, Monterey, CA, 38 pp.

APPENDICES

APPENDIX A

SCALAR ANALYSIS USING THE PATTERN-CONSERVING TECHNIQUE

I. INTRODUCTION

The goal of the PCT analysis is to blend the following information: the new data; the most recent past analysis (or forecast) value (the first guess); the gradients (of the first guess) in eight directions from each grid point; and the Laplacian (of the first guess). The relative importance of each piece of information is specified by an array of weights.

The desired blend is realized by minimizing the sum of the deviations of the various characteristics of the analysis from their counterparts in the first guess. The minimization is accomplished with an elementary application of the calculus of variations.

Information is spread spatially by the gradient and Laplacian terms. In a surface analysis, there are sometimes natural obstacles (mountain ridges, coastlines, etc.) beyond which an analyst would not allow a new observation to influence the analysis. This kind of constraint can be simulated in the objective analysis by reducing the weights of the gradients and Laplacian along the demarcation zone.

An analysis cycle consists of three major steps:

- Assemble the data at grid points.
- Solve the minimization equation.
- Re-evaluate the weight of each report.

In order to adequately evaluate the weight of each report, at least two cycles are required.

II. ASSEMBLY

We shall refer to the guess field as $P_{i,j}$ with weight $A_{i,j}$. On the first cycle, it is the first guess, and $A_{i,j}$ has a low and probably uniform value. On subsequent cycles, $P_{i,j}$ is the result of the previous cycle, but $A_{i,j}$ keeps its original value.

The purpose of the assembly procedure is to incorporate the observational data into the first guess field $P_{i,j}$, taking into account the subjective specification of each report's reliability (DWT) and its distance from the grid point. Grid points within a specified influence region of each observation are affected by that observation. The size and shape of the influence function are determined by the data density, analysis cycle number and first guess field shape (i.e., gradient and Laplacian), respectively. An information density field is used to produce a factor (FACT) which varies the basic radius of the influence for each observation between a minimum and maximum limit. In areas of dense data concentration, the influence radius is set to the minimum value so as not to spread a data report's influence so far that it interferes with the already well-specified observed values. However, if the observation is isolated, its influence is spread to the maximum allowed.

The assembly radius from an observation which includes all gridpoints to be influenced by that observation is calculated as:

$$\text{RADIUS} = \frac{\text{FACT} * \text{AMAP} * \text{RAD}}{\text{AMESH}}$$

where AMAP = map factor

AMESH = standard meshlength of the reference latitude

RAD = a multiple of AMESH

FACT = factor proportional to the information density

FACT is computed as follows:

$$\text{FACT} = \text{RADMAX} - \text{INFOFAC}_{(I,J)} * (\text{RADMAX} - \text{RADMIN})$$

where RADMAX = maximum allowable factor

RADMIN = minimum allowable factor

INFOFAC(I,J) = value of information density factor nearest observation location

The maximum allowed radius (RADMAX) is decreased with each cycle in order to better define progressively smaller scales.... in the manner used in Cressman analyses.

The basic influence function has a weight of one at its center (observation location), decreasing to zero at its maximum radius as determined by the information density. The fraction of the radius to which the weight value remains one (FRAC) varies between a minimum and maximum value determined by the curvature or gradients of the field. In systems such as cyclones, the curvature and gradients are large and an observation's full influence should not extend far from its location since it is less representative of the rapidly varying field. In anticyclones, these characteristics vary less rapidly, and it is acceptable to have the full weight of the observation included in the assembled fields at larger distances.

FRAC is computed as follows:

$$FRAC = 1.0 - SF$$

where $SF = \left(\frac{GRAD}{GRADMX}\right)$ or $\left(\frac{WTLAPL}{WTLAPLM}\right)$, whichever is greater

GRAD = maximum gradient at a gridpoint

GRADMAX = maximum gradient for the entire field.

WTLAPL = |Laplacian (I,J)|

WTLAPLM = Percentage of the maximum Laplacian for the entire field.

$$WTLAPL \leq WTLAPLM$$

$$GRAD < GRADMX$$

$$FRACMIN < FRAC < FRACMAX$$

As the first step in the assembly procedure, the guess field is interpolated at the observation location and the difference between the observation and the guess field determined (DIF). If DIF is greater than the gross tolerance for the parameter being analyzed, it is excluded from the assembly process in that analysis cycle. It may be included in some subsequent cycle(s).

Next, the value of the influence function appropriate to the distance of the grid point from the observation is computed (w), where:

$$w = 1.0 \text{ if } \frac{\text{distance}}{\text{RADIUS}} < \text{FRAC}$$

$$\text{otherwise } w = \frac{1.0 - \frac{\text{distance}}{\text{RADIUS}}}{1.0 - \text{FRAC}}$$

(For the upper air analyses, FRAC is set to a constant.)

For each gridpoint affected by the observation, a cumulative sum of the product (W*DWT)*W*DIF is computed at the appropriate I,J. Also, a field of the product W*DWT is accumulated. Once all observations have been processed, the assembled value is obtained by dividing the two fields at all grid points:

$$P_{I,J} = P_{I,J} + \frac{\sum_{K=1}^{NOBS} [W*DWT(K)]*W*DIF}{\sum_{K=1}^{NOBS} W*DWT(K)} \qquad \begin{matrix} \text{for } I=1,M \\ J=1,N \end{matrix}$$

P = assembled field value
NOBS = number of observations
DWT = data weight assigned to an observation

III. MINIMIZING THE ERROR FUNCTIONAL

TABLE A-1: PCT SCALAR CONSTRAINTS

Constraint	Weight
$P_{i,j}$ = Variable being analyzed (assembled value)	$A_{i,j}$
$\mu_{i,j}$ = y axis gradient = $P_{i,j+1} - P_{i,j}$ (computed from non-assembled value of first guess)	$B_{i,j}$
$\nu_{i,j}$ = x axis gradient = $P_{i+1,j} - P_{i,j}$ (computed from non-assembled value of first guess)	$C_{i,j}$
$\alpha_{i,j}$ = x-1,y+1 gradient = $P_{i-i,j+1} - P_{i,j}$ (computed from non-assembled value of first guess)	$E_{i,j}$
$\beta_{i,j}$ = x+1,y+1 gradient = $P_{i+1,j+1} - P_{i,j}$ (computed from non-assembled value of first guess)	$F_{i,j}$
$L_{i,j}$ = Laplacian = $P_{i+1,j} + P_{i-1,j} + P_{i,j+1} + P_{i,j-1} - 4P_{i,j}$ (computed from non-assembled value of first guess)	$D_{i,j}$

The first guess shapes μ, ν, α, β and L and their respective weights B, C, E, F and D have a constant value during the entire analysis. Within limits specified by the weights, we require the final analysis to have similar values of the constraints as the first guess field.

To effect this matching, we shall minimize the following integral:

$$I \equiv \iint [\qquad [A.1]$$

(a) $A_{i,j} (P^*_{i,j} - P_{i,j})^2 +$

(b) $B_{i,j} (P^*_{i,j+1} - P^*_{i,j} - u_{i,j})^2 +$

(c) $B_{i,j-1} (P^*_{i,j} - P^*_{i,j-1} - u_{i,j-1})^2 +$

(d) $C_{i,j} (P^*_{i+1,j} - P^*_{i,j} - v_{i,j})^2 +$

(e) $C_{i-1,j} (P^*_{i,j} - P^*_{i-1,j} - v_{i-1,j})^2 +$

(f) $E_{i,j} (P^*_{i-1,j+1} - P^*_{i,j} - \alpha_{i,j})^2 +$

(g) $E_{i+1,j-1} (P^*_{i,j} - P^*_{i+1,j-1} - \alpha_{i+1,j-1})^2 +$

(h) $F_{i,j} (P^*_{i+1,j+1} - P^*_{i,j} - \beta_{i,j})^2 +$

(i) $F_{i-1,j-1} (P^*_{i,j} - P^*_{i-1,j-1} - \beta_{i-1,j-1})^2 +$

(j) $D_{i,j} (P^*_{i+1,j} + P^*_{i-1,j} + P^*_{i,j+1} + P^*_{i,j-1} - 4P^*_{i,j} - L_{i,j})^2 +$

$]dxdy$

In the above, the starred quantities are the analysis values we are seeking. Each term is a departure from the desired matching of differential properties. Extra terms have been added to account for the effect of a changing $P^*_{i,j}$ on the differential properties computed at surrounding points. Their effect is to more closely couple neighboring grid points. See Figure A-1 for a depiction of the minimization stencil as it relates to the terms of equation [A.1]. To minimize the integral, we simply take the first variation with respect to $P^*_{i,j}$, and set it to zero (see equation [A.2]). The solution of the resulting equation will be the $P^*_{i,j}$ that will cause the integral to be minimized. The fact that each term is squared ensures a minimum as opposed to a maximum value.

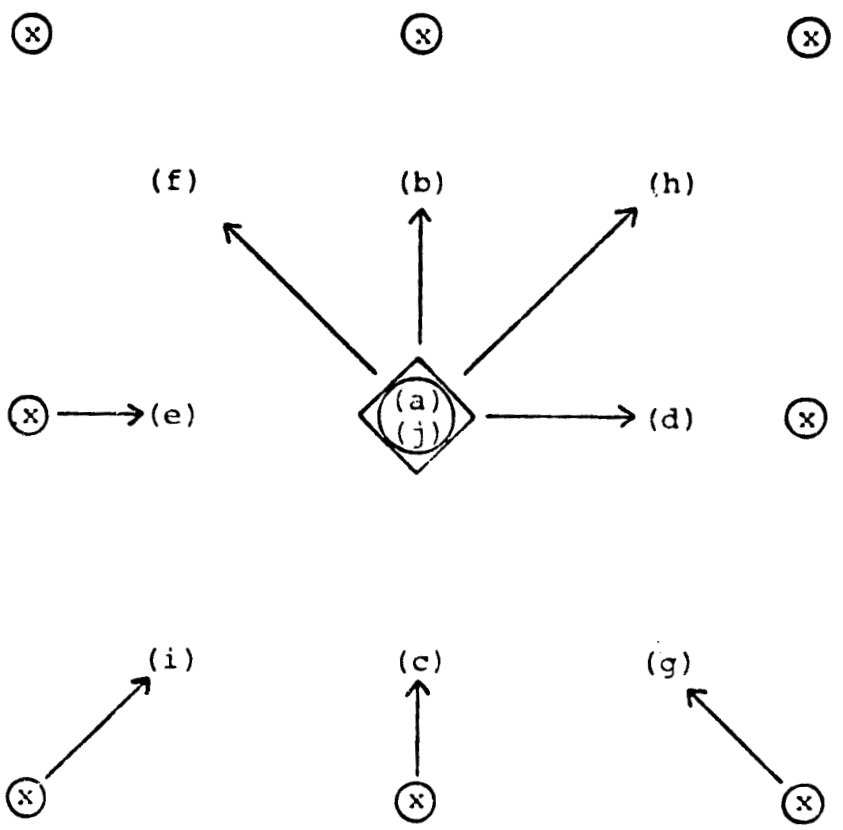

LEGEND: ( ) = constraint from Equation [A.1]

= difference

= gradient

= laplacian at grid point

= grid points

FIGURE A-1: SCALAR MINIMIZATION STENCIL

$$\frac{\delta I}{\delta P^*} = \iint [\ 2A_{i,j}\ (P^*_{i,j} - P_{i,j}) \qquad \text{[A.2]}$$

$$-2\ B_{i,j}\ (P^*_{i,j+1} - P^*_{i,j} - \mu_{i,j})$$

$$+\ 2\ B_{i,j-1}\ (P^*_{i,j} - P^*_{i,j-1} - \mu_{i,j-1})$$

$$-\ 2\ C_{i,j}\ (P^*_{i+1,j} - P^*_{i,j} - \nu_{i,j})$$

$$+\ 2\ C_{i-1,j}\ (P^*_{i,j} - P^*_{i-1,j} - \nu_{i-1,j})$$

$$-\ 2\ E_{i,j}\ (P^*_{i-1,j+1} - P^*_{i,j} - \alpha_{i,j})$$

$$+\ 2\ E_{i+1,j-1}\ (P^*_{i,j} - P^*_{i+1,j-1} - \alpha_{i+1,j-1})$$

$$-\ 2\ F_{i,j}\ (P^*_{i+1,j+1} - P^*_{i,j} - \beta_{i,j})$$

$$+\ 2\ F_{i-1,j-1}\ (P^*_{i,j} - P^*_{i-1,j-1} - \beta_{i-1,j-1})$$

$$-\ 8\ D_{i,j}\ (P^*_{i+1,j} + P^*_{i-1,j} + P^*_{i,j+1} + P^*_{i,j-1} - 4P^*_{i,j} - L_{i,j})$$

$$]\ dxdy \overset{\text{set}}{=} 0$$

The terms in $\frac{\delta I}{\delta P^*}$ can be grouped into three categories:

1. Those involving $P^*_{i,j}$.
2. Those involving P* at surrounding points.
3. Those not involving P*.

$$S_{i,j} P^*_{i,j} \left\{ \begin{array}{l} [\ A_{i,j} + B_{i,j} + B_{i,j-1} + C_{i,j} + C_{i-1,j} + E_{i,j} \\ \quad + E_{i+1,j-1} + F_{i,j} + F_{i-1,j-1} + 16\ D_{i,j}\ ]\ P^*_{i,j} \end{array} \right.$$

$$-H_{i,j} \begin{cases} - B_{i,j} P^*_{i,j+1} - B_{i,j-1} P^*_{i,j-1} - C_{i,j} P^*_{i+1,j} - C_{i-1,j} P^*_{i-1,j} \\ - E_{i,j} P^*_{i-1,j+1} - E_{i+1,j-1} P^*_{i+1,j-1} - F_{i,j} P^*_{i+1,j+1} \\ - F_{i-1,j-1} P^*_{i-1,j-1} - 4 D_{i,j} P^*_{i+1,j} - 4 D_{i,j} P^*_{i-1,j} \\ - 4 D_{i,j} P^*_{i,j+1} - 4 D_{i,j} P^*_{i,j-1} \end{cases}$$

$$-G_{i,j} \begin{cases} - A_{i,j} P_{i,j} + B_{i,j} \mu_{i,j} - B_{i,j-1} \mu_{i,j-1} + C_{i,j} \nu_{i,j} \\ - C_{i-1,j} \nu_{i-1,j} + E_{i,j} \alpha_{i,j} - E_{i+1,j-1} \alpha_{i+1,j-1} \\ + F_{i,j} \beta_{i,j} - F_{i-1,j-1} \beta_{i-1,j-1} + 4 D_{i,j} L_{i,j} \end{cases}$$

Note that all terms in S and G except $A_{i,j}$ in $S_{i,j}$ and $-A_{i,j} P_{i,j}$ in $G_{i,j}$ involve first-guess pattern information which is consistent during the analysis.

The minimization may be written as

$$S_{i,j} P^*_{i,j} - (G_{i,j} + H_{i,j}) = 0 \qquad [A.3]$$

In $H_{i,j}$, let us group together the coefficients of P* at each point.

$$
\begin{aligned}
-H_{i,j} = &+ (-C_{i-1,j} - 4\,D_{i,j})\,P^{*}_{i-1,j} \\
&+ (-C_{i,j} - 4\,D_{i,j})\,P^{*}_{i+1,j} \\
&+ (-E_{i,j})\,P^{*}_{i-1,j+1} \\
&+ (-B_{i,j} - 4\,D_{i,j})\,P^{*}_{i,j+1} \\
&+ (-F_{i,j})\,P^{*}_{i+1,j+1} \\
&+ (-F_{i-1,j-1})\,P^{*}_{i-1,j-1} \\
&+ (-B_{i,j-1} - 4\,D_{i,j})\,P^{*}_{i,j-1} \\
&+ (-E_{i+1,j-1})\,P^{*}_{i+1,j-1}
\end{aligned}
$$

Define:

$$
\begin{aligned}
X_{i,j} &\equiv C_{i,j} \\
Y_{i,j} &\equiv B_{i,j} \\
Z_{i,j} &\equiv -F_{i,j} \\
R_{i,j} &\equiv -E_{i+1,j}
\end{aligned}
$$

Note that X, Y, Z and R have a constant value during the analysis.

Then:

$$
\begin{aligned}
-H_{i,j} = &\; X_{i-1,j}\,P^{*}_{i-1,j} - X_{i,j}\,P^{*}_{i+1,j} \\
&+ R_{i-1,j}\,P^{*}_{i-1,j+1} - Y_{i,j}\,P^{*}_{i,j+1} \\
&+ Z_{i,j}\,P^{*}_{i+1,j+1} + Z_{i-1,j-1}\,P^{*}_{i-1,j-1} \\
&- Y_{i,j-1}\,P^{*}_{i,j-1} + R_{i,j-1}\,P^{*}_{i+1,j-1} \\
&- 4\,D_{i,j}(P^{*}_{i-1,j}+P^{*}_{i+1,j}+P^{*}_{i,j+1}+P^{*}_{i,j-1})
\end{aligned}
\qquad [A.4]
$$

The minimization equation [A.3] is solved by simultaneous over-relaxation. The matrices $S_{i,j}$ and $G_{i,j}$ may be computed initially except for the $A_{i,j}$ term and will not change throughout the analysis. Matrix $H_{i,j}$ must be recomputed for every iteration of the relaxation.

The relaxation proceeds as follows: At Point (i,j) the terms of the minimization equation are evaluated using the assembled P field for P*. In general, the equation is not satisfied and a residual is defined as

$$S_{i,j}\ P^{*\tau}_{i,j} - (G_{i,j} + H_{i,j}) \equiv R \qquad [A.5]$$

The superscript τ is an iteration counter. The value of $P^{*}_{i,j}$ is to be altered so that on the next iteration, the residual will be zero, provided $H_{i,j}$ does not change. Of course, $H_{i,j}$ will change, but if the equation is fairly well behaved, repetition of the procedure should lead to convergence on the correct solution.

$$S_{i,j}\ P^{*\tau+1}_{i,j} - (G_{i,j} + H_{i,j}) = 0 \qquad [A.6]$$

Subtracting [A.6] from [A.5],

$$S_{i,j}\ (P^{*\tau}_{i,j} - P^{*\tau+1}_{i,j}) = R \qquad [A.7]$$

and

$$P^{*\,\tau+1}_{i,j} = P^{*\,\tau}_{i,j} - \frac{R}{S_{i,j}}$$

Convergence can be hastened by increasing the correction term in [A.7] by a factor ALFA. The factor by which it is increased is called the over-relaxation coefficient. Equation [A.7] becomes:

$$P^{*\,\tau+1}_{i,j} = P^{*\,\tau}_{i,j} - \text{ALFA}\ \frac{R}{S_{i,j}} \qquad [A.8]$$

One iteration consists of making the correction [A.8] at every grid point. Testing has shown the convergence can be speeded up and unwanted solution noise decreased if the grid points are processed in a circular manner. Therefore, the field is scanned in a counter-clockwise circular sweep starting at the center and working toward the boundaries. Iterations are repeated until the maximum residual is less than a specified convergence criterion. The resulting P* field is the solution of equation [A.3].

IV. RE-EVALUATING THE DATA WEIGHTS

At the end of each cycle, the weight of each report is reevaluated. An observation will have its weight reduced if the report differs from the analysis value on the current scan by more than a subjectively determined amount. REVAL is the reevaluation parameter and CRIT, the critical value at which a report's weight is reduced. REVAL is calculated as:

$$REVAL = \frac{ABS(DIF)}{(ODWT*OFACT)}$$

and

$$OFACT = REFAC^{**}(FP-1.0)$$

where FP = scan number

REFAC = constant, reevaluation factor

ODWT = original data weight

DIF = difference between report and analyzed field value for that location.

If REVAL is less than CRIT, the observation retains its original weight, even though it may have been reduced another scan. If REVAL is greater than CRIT, then:

$$DWT = \frac{CONST * ODWT}{1. + REVAL}$$

where CONST = constant

ODWT = original data weight

DWT = new data weight

Notice that on any cycle, every data point may have its original weight restored, even if it had been reduced previously. In this way, a report that causes a large change in the analysis may have full effect if it is supported by data nearby.

APPENDIX B

WIND ANALYSIS USING THE PATTERN CONSERVING TECHNIQUE

I. INTRODUCTION

The essential feature of the pattern-conserving technique is that, while fitting new data, it tends to retain certain differential properties of the first-guess field. Some of the properties of the wind field we would like to conserve; e.g., vorticity and divergence, involve both scalar wind components.

The differential properties that we choose to conserve are the gradients of each wind component in eight directions from each grid point, the vorticity and the divergence. The same method is used here as in the scalar analysis, the main difference being that two minimization equations rather than one must be solved simultaneously.

The equations are simplified by using the staggered grid illustrated by Figure B-1 and defining the divergence, vorticity and gradients as in Table B-1 and Figure B-2. This arrangement causes certain matrices to be tridiagonal.

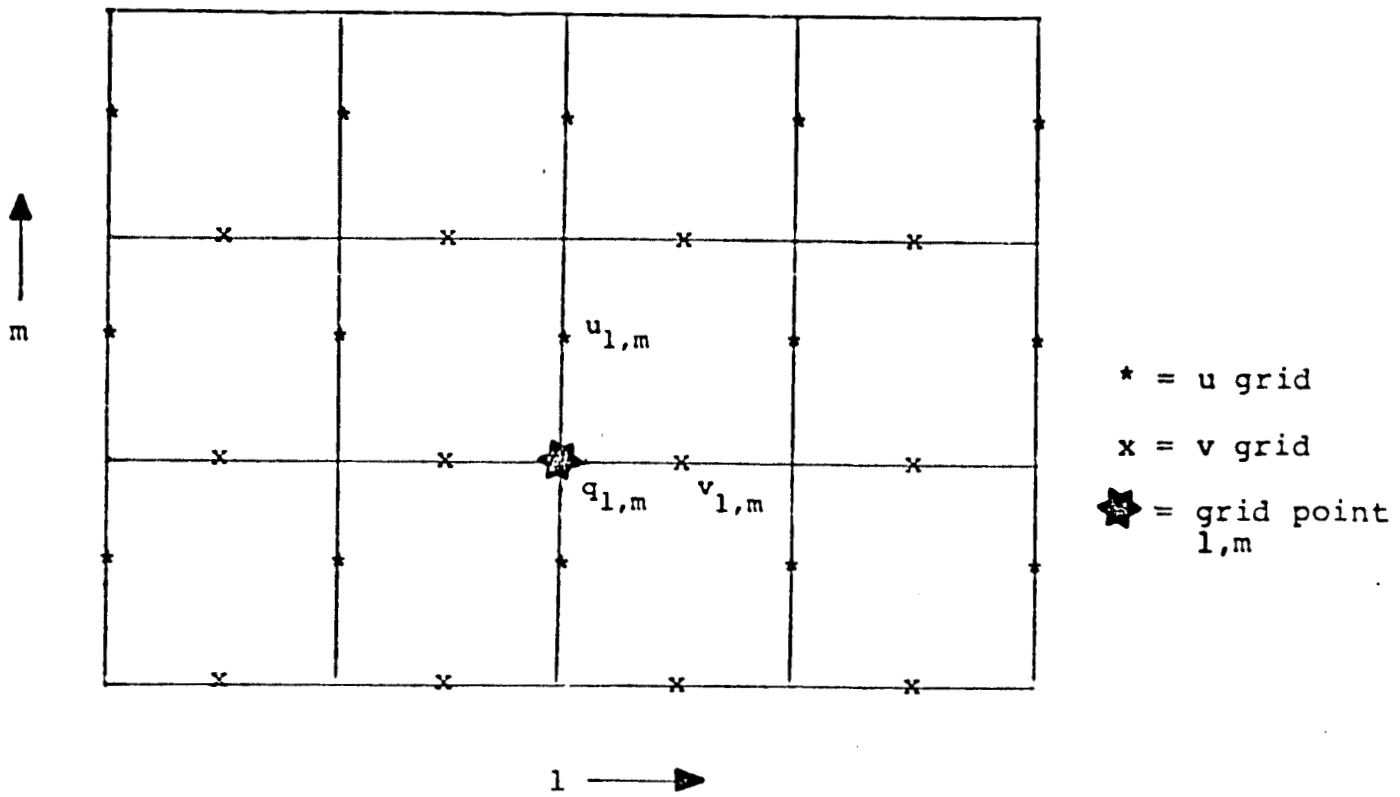

FIGURE B-1: STAGGERED u,v GRID

II. ASSEMBLY

The method of assembling data to grid points is similar to that in the scalar analyses. For the wind analysis, the u and v components are treated separately except for the gross reject criterion which is a function of the guess-field wind speed. The assembly radius for a particular report is based upon the cycle number and the information density at its location (as in the scalar analysis). The function which determines the weight of an observation is inversely proportional to both the local vorticity and to the relative distance between the observation and the grid point. Note that since the grid is staggered (Figure B-1), the individual wind components of an observation may be assembled to grid points with different weights.

III. MINIMIZING THE DEVIATIONS

The objective of the Pattern-Conserving Technique is to preserve the differential properties of the guess field. In the scalar analyses, it was found that to use the finite difference expressions centered about one grid point did not provide enough horizontal coupling. Accordingly, the integral was expanded to include the expressions for the surrounding grid points as well. In the wind analyses, this is not necessary because the particular differential properties and the staggered grid extend the influence of the observations more than in the scalar analyses and facilitate coupling.

TABLE B-1: PCT VECTOR CONSTRAINTS

Constraint	Weight
$u_{l,m}$ = Variable being analyzed (assembled value)	$A_{l,m}$
$v_{l,m}$ = Variable being analyzed (assembled value)	$\hat{A}_{l,m}$
$d_{l,m}$ = divergence = $\partial u/\partial x + \partial v/\partial y$	
$= u_{l+1,m} - u_{l,m} + v_{l,m+1} - v_{l,m}$ (Computed from non-assembled value of first guess.)	$D_{l,m}$
$q_{l,m}$ = vorticity = $\partial v/\partial x - \partial u/\partial y$	$Q_{l,m}$
$= v_{l,m} - v_{l-1,m} - u_{l,m} + u_{l,m-1}$ (Computed from non-assembled value of first guess.)	
$e_{l,m}$ = x-1,y+1 u gradient = $u_{l-1,m+1} - u_{l,m}$ (Computed from non-assembled value of first guess.)	$E_{l,m}$
$\hat{e}_{l,m}$ = x-1 y+1 v gradient = $v_{l-1,m+1} - v_{l,m}$ (Computed from non-assembled value of first guess.)	$\hat{E}_{l,m}$
$f_{l,m}$ = y axis u gradient = $u_{l,m+1} - u_{l,m}$ (Computed from non-assembled value of first guess.)	$F_{l,m}$
$\hat{f}_{l,m}$ = y axis v gradient = $v_{l,m+1} - v_{l,m}$ (Computed from non-assembled value of first guess.)	$\hat{F}_{l,m}$
$g_{l,m}$ = x+1,y+1 u gradient = $u_{l+1,m+1} - u_{l,m}$ (Computed from non-assembled value of first guess.)	$G_{l,m}$
$\hat{g}_{l,m}$ = x+1,y+1 v gradient = $v_{l+1,m+1} - v_{l,m}$ (Computed from non-assembled value of first guess.)	$\hat{G}_{l,m}$
$h_{l,m}$ = x axis u gradient = $u_{l+1,m} - u_{l,m}$ (Computed from non-assembled value of first guess.)	$H_{l,m}$
$\hat{h}_{l,m}$ = x axis v gradient = $v_{l+1,m} - u_{l,m}$ (Computed from non-assembled value of first guess.)	$\hat{H}_{l,m}$

We shall minimize the following integral:

$$I \equiv \iint \Big[$$

(a) $$A_{l,m}(u^*_{l,m} - u_{l,m})^2 \qquad [B.1]$$

(b) $$+ \hat{A}_{l,m}\,(v^*_{l,m} - v_{l,m})^2$$

(c) $$+ D_{l,m}(u^*_{l+1,m} \quad u^*_{l,m} + v^*_{l,m+1} - v^*_{l,m} - d_{l,m})^2$$

(d) $$+ Q_{l,m}(v^*_{l,m} - v^*_{l-1,m} - u^*_{l,m} + u^*_{l,m-1} - q_{l,m})^2$$

(e) $$+ E_{l,m}(u^*_{l-1,m+1} - u^*_{l,m} - e_{l,m})^2$$

(f) $$+ \hat{E}_{l,m}(v^*_{l-1,m+1} - v^*_{l,m} - \hat{e}_{l,m})^2$$

(g) $$+ F_{l,m}(u^*_{l,m+1} - u^*_{l,m} - f_{l,m})^2$$

(h) $$+ \hat{F}_{l,m}(v^*_{l,m+1} - v^*_{l,m} - \hat{f}_{l,m})^2$$

(i) $$+ G_{l,m}(u^*_{l+1,m+1} - u^*_{l,m} - g_{l,m})^2$$

(j) $$+ \hat{G}_{l,m}(v^*_{l+1,m+1} - v^*_{l,m} - \hat{g}_{l,m})^2$$

(k) $$+ H_{l,m}(u^*_{l+1,m} - u^*_{l,m} - h_{l,m})^2$$

(l) $$+ \hat{H}_{l,m}(v^*_{l+1,m} - v^*_{l,m} - \hat{h}_{l,m})^2$$

$$\Big] \, dxdy$$

The superscript (*) indicates the values we seek. The differential properties of the first-guess field are defined in Table B-1, and a depiction of the u component minimization stencil as it relates to the u terms of equation [B.1] is given in Figure B-2.

To minimize the integral we take the first variation with respect to $u^*_{l,m}$ and with respect to $v^*_{l,m}$, yielding the following two equations:

$$\frac{\delta I}{\delta u^*_{l,m}} = \iint [\, A_{l,m}(u^*_{l,m} - u_{l,m}) \qquad [B.2]$$
$$- D_{l,m}\,(u^*_{l+1,m} - u^*_{l,m} + v^*_{l,m+1} - v^*_{l,m} - d_{l,m})$$
$$- Q_{l,m}\,(v^*_{l,m} - v^*_{l-1,m} - u^*_{l,m} + u^*_{l,m-1} - q_{l,m})$$
$$- E_{l,m}\,(u^*_{l-1,m+1} - u^*_{l,m} - e_{l,m}) - F_{l,m}\,(u^*_{l,m+1} - u^*_{l,m} - f_{l,m})$$
$$- G_{l,m}\,(u^*_{l+1,m+1} - u^*_{l,m} - g_{l,m}) - H_{l,m}\,(u^*_{l+1,m} - u^*_{l,m} - h_{l,m})]\,dxdy \overset{\text{set}}{=} 0$$

$$\frac{\delta I}{\delta v^*_{l,m}} = \iint [\, \hat{A}_{l,m}\,(v^*_{l,m} - v_{l,m}) \qquad [B.3]$$
$$- D_{l,m}\,(u^*_{l+1,m} - u^*_{l,m} + v^*_{l,m+1} - v^*_{l,m} - d_{l,m})$$
$$+ Q_{l,m}\,(v^*_{l,m} - v^*_{l-1,m} - u^*_{l,m} + u^*_{l,m-1} - q_{l,m})$$
$$- \hat{E}_{l,m}\,(v^*_{l-1,m+1} - v^*_{l,m} - \hat{e}_{l,m}) - \hat{F}_{l,m}\,(v^*_{l,m+1} - v^*_{l,m} - \hat{f}_{l,m})$$
$$- \hat{G}_{l,m}\,(v^*_{l+1,m+1} - v^*_{l,m} - \hat{g}_{l,m}) - \hat{H}_{l,m}\,(v^*_{l+1,m} - v^*_{l,m} - \hat{h}_{l,m})]\,dxdy \overset{\text{set}}{=} 0$$

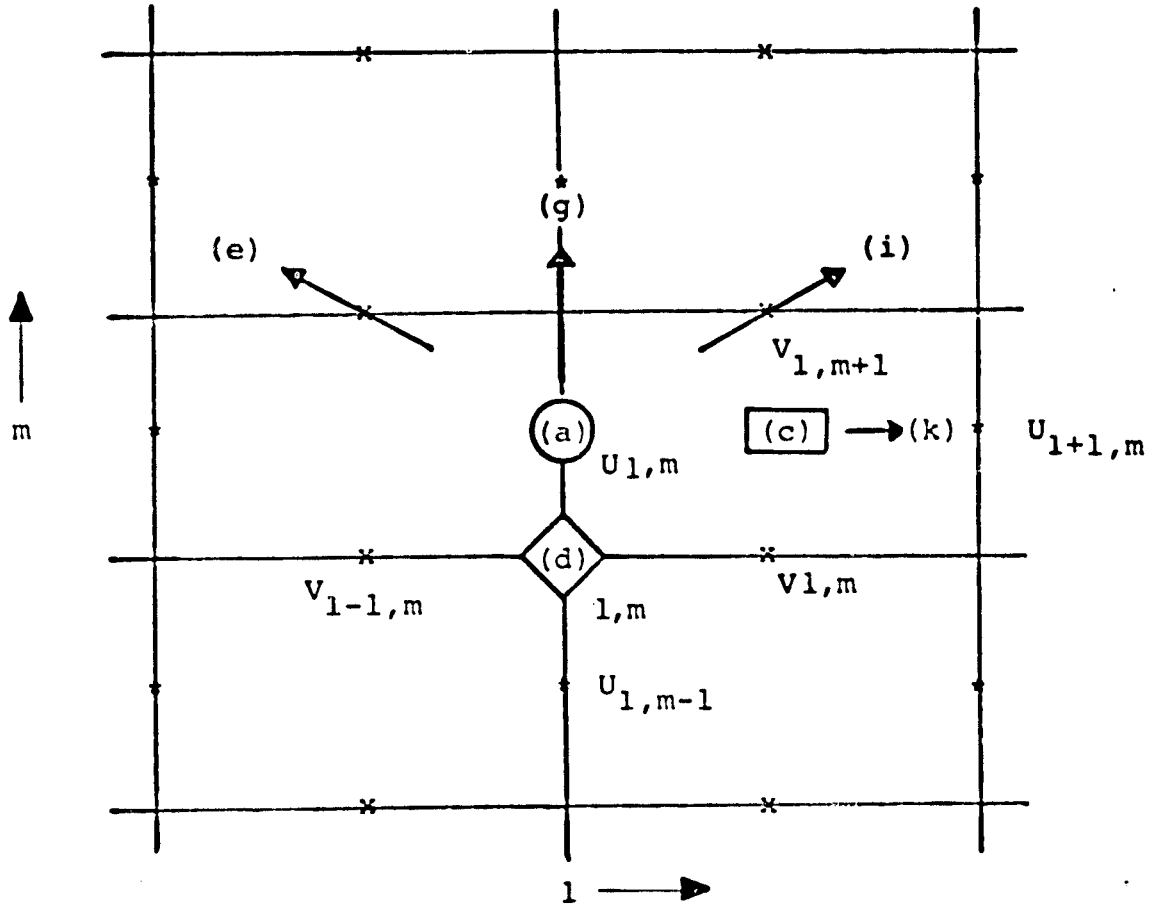

( ) = constraint from equation [B.1]

* = U grid points

x = V grid points

○ = difference

▭ = divergence

◇ = vorticity

→ = gradient

FIGURE B-2: U COMPONENT MINIMIZATION STENCIL

In equation [B.2] group terms involving 1) $u^*_{l,m}$; 2) u* at surrounding points; 3) v* and 4) everything else.

$$\iint [\overbrace{(A_{l,m} + D_{l,m} + Q_{l,m} + E_{l,m} + F_{l,m} + G_{l,m} + H_{l,m})}^{S_{l,m}} u^*_{l,m} \quad [B.4]$$

$$X_{l,m}\begin{cases} + (- D_{l,m} - H_{l,m})\, u^*_{l+1,m} + (-Q_{l,m})\, u^*_{l,m-1} \\ + (-E_{l,m})\, u^*_{l-1,m+1} + (-F_{l,m})\, u^*_{l,m+1} + (-G_{l,m})\, u^*_{l+1,m+1} \end{cases}$$

$$Y_{l,m}\ \{ + (D_{l,m} - Q_{l,m})\, v^*_{l,m} + (-D_{l,m})\, v^*_{l,m+1} + Q_{l,m}\, v^*_{l-1,m}$$

$$Z_{l,m}\begin{cases} - A_{l,m}\, u_{l,m} + D_{l,m}\, d_{l,m} + Q_{l,m}\, q_{l,m} + E_{l,m}\, e_{l,m} + F_{l,m}\, f_{l,m} \\ + G_{l,m}\, g_{l,m} + H_{l,m}\, h_{l,m}]\ dxdy = 0 \end{cases}$$

Group [B.3] similarly:

$$\iint [\overbrace{(\hat{A}_{l,m} + D_{l,m} + Q_{l,m} + \hat{E}_{l,m} + \hat{F}_{l,m} + \hat{G}_{l,m} + \hat{H}_{l,m})}^{\hat{S}_{l,m}} V^*_{l,m} \quad [B.5]$$

$$\hat{X}_{l,m}\begin{cases} + (-\hat{D}_{l,m} - \hat{F}_{l,m})\, V^*_{l,m+1} + (- Q_{l,m}) V^*_{l-1,n} + (-\hat{E}_{l,m})\, V^*_{l-1,m+1} \\ + (-\hat{G}_{l,m}) V^*_{l+1,m+1} + (-\hat{H}_{l,m})\, V^*_{l+1,m} \end{cases}$$

$$\hat{Y}_{l,m}\ \{ + (D_{l,m} - Q_{l,m})\, u^*_{l,m} - D_{l,m}\, u^*_{l+1,m} + Q_{l,m}\, u^*_{l,m-1}$$

$$\hat{Z}_{l,m}\begin{cases} - \hat{A}_{l,m}\, v_{l,m} + D_{l,m}\, d_{l,m} - Q_{l,m}\, q_{l,m} + \hat{E}_{l,m}\hat{e}_{l,m} + \hat{F}_{l,m}\, \hat{f}_{l,m} \\ + \hat{G}_{l,m}\, \hat{g}_{l,m} + \hat{H}_{l,m}\, \hat{h}_{l,m}]\ dxdy = 0 \end{cases}$$

Note that all terms in S and Z except $A_{l,m}$ in $S_{l,m}$ and $- A_{l,m}u_{l,m}$ in $Z_{l,n}$ involve first-guess information which is constant during the analysis. Similar conditions hold for $\hat{S}$ and $\hat{Z}$.

Equations [B.4] and [B.5] can be written in matrix form:

$$\underline{\underline{S}}_{l,m}\,\underline{u}^{*} + \underline{\underline{X}}_{l,m} + \underline{\underline{Y}}_{l,m} + \underline{\underline{Z}}_{l,m} = 0 \qquad [B.6]$$

$$\hat{\underline{\underline{S}}}_{l,m}\,\underline{v}^{*} + \hat{\underline{\underline{X}}}_{l,m} + \hat{\underline{\underline{Y}}}_{l,m} + \hat{\underline{\underline{Z}}}_{l,m} = 0 \qquad [B.7]$$

These equations must be solved simultaneously. The method of solution used is Liebmann successive over-relaxation. Using a first-guess for u* and v*, equation [B.6] is, in general, not satisfied. A residual is defined by:

$$\underline{\underline{S}}_{l,m}\,\underline{u}^{*\tau} + \underline{\underline{X}}_{l,m} + \underline{\underline{Y}}_{l,m} + \underline{\underline{Z}}_{l,m} = R \qquad [B.8]$$

The superscript τ is the iteration counter. We wish to find a next guess at $\underline{u}^{*}$ such that the residual is zero, if the values at surrounding points do not change.

$$\underline{\underline{S}}_{l,m}\underline{u}^{*\tau+1} + \underline{\underline{X}}_{l,m} + \underline{\underline{Y}}_{l,m} + \underline{\underline{Z}}_{l,m} = 0 \qquad [B.9]$$

Subtracting [B.9] from [B.8],

$$\underline{\underline{S}}_{l,m}\,(\underline{u}^{*\tau} - \underline{u}^{*\tau+1}) = R$$

and $$\underline{u}^{*\tau+1} = \underline{u}^{*\tau} - \frac{R}{\underline{\underline{S}}_{l,m}}\,. \qquad [B.10]$$

Convergence is more rapid if the correction in [B .10] is augmented by the inclusion of ALFA factor.

$$\underline{u}^{*\tau+1} = \underline{u}^{*\tau} - \text{ALFA}\ \frac{R}{\underline{S}_{l,m}} . \qquad [\ B.11]$$

At a particular grid point, u* is corrected by equation [B .11] and v* is then corrected in an analogous way. In computing R from equation [B .8] or from the analogous equation in v*, the latest estimate of both u* and v* at surrounding points is used. Some of them have been changed on the current iteration and some have not. As in the scalar analysis, the field is scanned in a counter-clockwise circular sweep starting at the center and working toward the boundaries.

During each iteration through the grid, the maximum residual is checked. When it becomes less than a prescribed convergence criterion, the equations are considered solved.

IV. RE-EVALUATING THE DATA WEIGHTS

The validity of wind reports is judged according to the vector difference between the reported wind and the analyzed wind. The analyzed wind is obtained by interpolation from the analysis fields. The reevaluation parameter (REVAL) is the same as its counterpart in the scalar analysis with the exception that DIF is the magnitude of the vector difference squared, i.e.

$$DIF = |\mathbb{V}_I - \mathbb{V}_R|^2$$

where $\mathbb{V}_I$ = interpolated analyzed wind

$\mathbb{V}_R$ = wind report

If REVAL is greater than a specified critical value, the weight is reevaluated in the same way as for the scalar analyses (see Section IV of Appendix A). Again, if REVAL is less than the critical value, a report is assigned its original weight, even if it has been reduced on a previous scan.

APPENDIX C

MASS STRUCTURE LINEAR TRANSFORMATIONS

I. INTRODUCTION

If an analysis of upper-air pressure heights and temperatures is to be used in initializing a forecast model, it is desirable for the heights and temperatures at grid points to be consistent with the hydrostatic equation. It will be shown in Section II that the heights, temperatures and layer stabilities can be interrelated through various linear transforms. It turns out that to close the equation set it is also necessary to specify a single height parameter and a single temperature parameter.

The vertical organization of height and temperature levels and stability layers to be used in the mass structure analysis is shown in Figure C-1. The stability parameter used here is defined as:

$$\sigma \equiv - \frac{p^2}{\rho} \frac{\partial \ln\theta}{\partial p} \qquad [\text{C.1}]$$

Other definitions are possible, as discussed by Holl et al (1963). This definition makes θ linear in $p^{-\kappa}$ ($\kappa \equiv R/Cp$), which is consistent with pseudo-adiabatic diagrams.

A limitation of this technique is that σ must be assumed to be constant in each of the layers labeled 1 - 10 in Figure C-1. If a serious departure from this condition occurs in a layer, the temperature above the layer will depart from the reported temperature, but will agree hydrostatically with the analyzed heights.

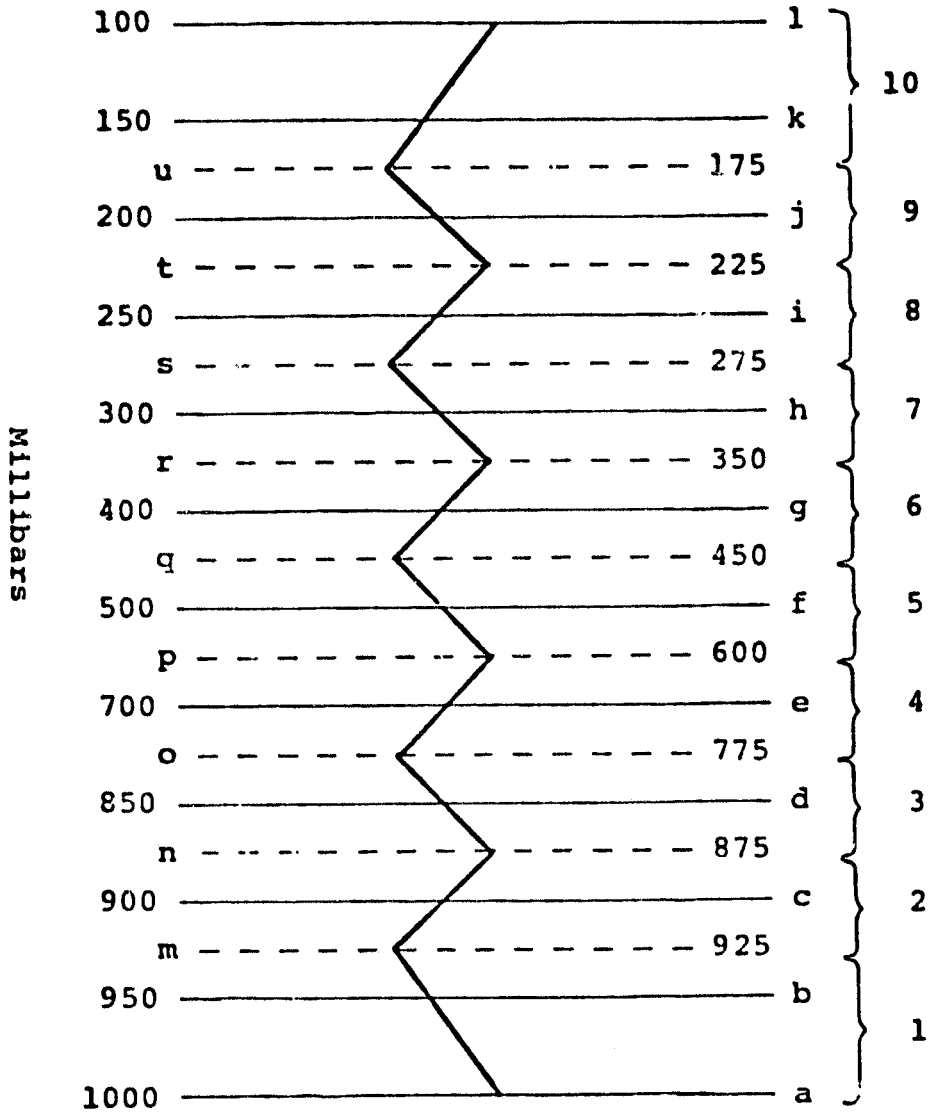

(12 levels, 10 layers)

FIGURE C-1: VERTICAL ORGANIZATION OF THE BASIC MASS STRUCTURE MODEL (DOES NOT SHOW THE STRATOSPHERIC EXTENSION).

II. DERIVATION OF THE TRANSFORMATIONS

The hydrostatic equation states

$$\frac{dz}{dp} = -\frac{1}{g\rho} = -\frac{RT}{pg} \qquad \text{where } \rho = \frac{p}{RT} \qquad [\ C.2\ ]$$

or

$$T = -\frac{pg}{R}\frac{dz}{dp}. \qquad [\ C.3\ ]$$

Potential temperature is defined as

$$\Theta \equiv T\left(\frac{p}{p_o}\right)^{-\kappa} \qquad \text{where } \kappa = R/_{Cp} \qquad [\ C.4\ ]$$

Therefore,

$$\Theta = -\frac{g}{R}\frac{dz}{dp}\, p^{1-\kappa}\, (P_o)^{\kappa}. \qquad [\ C.5\ ]$$

Defining $\eta \equiv 1-\kappa$,

$$\ln \Theta = \ln \frac{g}{R} + \ln\left(-\frac{dz}{dp}\right) + \eta \ln p + \kappa \ln P_o \qquad [\ C.6\ ]$$

and

$$\frac{d\ln\Theta}{dp} = \frac{d}{dp}\left[\ln\left(-\frac{dz}{dp}\right)\right] + \frac{\eta}{p} \qquad [\ C.7\ ]$$

and

$$-\frac{dz}{dp}\,\frac{d\ln\Theta}{dp} = -\frac{d^2z}{dp^2} - \frac{\eta}{p}\frac{dz}{dp}\ . \qquad [\ C.8\ ]$$

Substituting for ρ from the hydrostatic equation into [C.1] gives

$$\sigma = g\frac{dz}{dp}\, p^2\, \frac{d\ln\Theta}{dp} \qquad [\ C.9\ ]$$

and

$$\frac{d\ln\theta}{dp} = \frac{\sigma}{g \frac{dz}{dp} p^2} . \qquad [C.10]$$

Substituting [C.10] into [C.8]

$$\frac{d^2z}{dp^2} + \frac{n}{p} \frac{dz}{dp} = \frac{\sigma}{gp^2} . \qquad [C.11]$$

Multiplying by p^n

$$p^n \frac{d^2z}{dp^2} + np^{n-1} \frac{dz}{dp} = \frac{\sigma}{g} p^{n-2}. \qquad [C.12]$$

Let us define

$$\chi \equiv - p^n \frac{dz}{dp} . \qquad [C.13]$$

Then

$$\frac{d\chi}{dp} = - np^{n-1} \frac{dz}{dp} - p^n \frac{d^2z}{dp^2} . \qquad [C.14]$$

From [C.12] and [C.14]

$$- \frac{d\chi}{dp} = \frac{\sigma}{g} p^{n-2}. \qquad [C.15]$$

Integrating <u>within the layer</u> characterized by constant stability

$$- \chi + C_1 = \frac{\sigma}{g} \frac{1}{n-1} p^{n-1} + C_2 . \qquad [C.16]$$

Defining $M \equiv C_2 - C_1$

$$\chi = \frac{-\sigma}{g(\eta-1)}\, p^{\eta-1} + M. \qquad [\text{ C.17 }]$$

Integrating [C.17]

$$Z = C_3 - \int \frac{\chi}{p^{\eta}}\, dp. \qquad [\text{ C.18 }]$$

Substituting [C.17] into [C.18]

$$Z = C_3 + \int \left[\frac{\sigma}{g(\eta-1)}\, p^{-1} - Mp^{-\eta}\right] dp \qquad [\text{ C.19 }]$$

or

$$Z = C_3 + \frac{\sigma}{g(\eta-1)} \ln p - M\, \frac{1}{1-\eta}\, p^{1-\eta} + C_4 \qquad [\text{ C.20 }]$$

and finally

$$Z = N^* + M^*\, p^{\kappa} - \frac{\sigma}{g\kappa} \ln p \qquad [\text{ C.21 }]$$

where

$$N^* = C_3 + C_4$$

and

$$M^* = -\frac{M}{1-\eta}\,.$$

Equation [C.21] is the basic equation of the method relating pressure height to stability. We also need a relationship between the temperature and the stability. Taking the first derivative of equation [C.21] with respect to pressure,

$$\frac{dz}{dp} = M^*\, \kappa\, p^{\kappa-1} - \frac{\sigma}{g\kappa p}. \qquad [\text{ C.22 }]$$

Substituting [C.22] into [C.3]

$$T = -\frac{pg}{R}\left(M^* \kappa\, p^{\kappa-1} - \frac{\sigma}{g\kappa p}\right), \qquad [\text{ C.23 }]$$

or

$$T = \frac{\sigma}{R\kappa} - M^* \frac{g}{C_p}\, p^{\kappa}. \qquad [\text{ C.24 }]$$

Equation [C.24] is the basic equation of the method relating temperature to stability.

Equations [C.21] and [C.24] are the two model equations we need. They apply to each of the ten layers in Figure C-1. The N*, M* and σ in the ten layers make a total of 30 unknowns. Applying equation [C.21] to each mandatory level gives us twelve equations:

$$\begin{aligned}
N_1 + M_1 P_a^{\kappa} - \sigma_1 \beta_a &= Z_a \qquad [\text{ C.26 }]\\
N_1 + M_1 P_b^{\kappa} - \sigma_1 \beta_b &= Z_b\\
\vdots \quad &\quad \vdots \quad \vdots \quad \vdots\\
N_{10} + M_{10} P_k^{\kappa} - \sigma_{10} \beta_k &= Z_k\\
N_{10} + M_{10} P_1^{\kappa} - \sigma_{10} \beta_1 &= Z_1
\end{aligned}$$

where

$\beta_\eta \equiv \frac{1}{g\kappa} \ln p_\eta$ and the subscript (*) has been omitted.

Requiring continuity of height at the interface levels between each layer leads to nine more equations:

$$N_1 - N_2 + P_m^{\kappa} (M_1 - M_2) - \beta_m (\sigma_1 - \sigma_2) = 0 \qquad [\text{ C.27 }]$$

$$\vdots \qquad \vdots \qquad \vdots$$

$$N_9 - N_{10} + P_u^{\kappa} (M_9 - M_{10}) - \beta_u (\sigma_9 - \sigma_{10}) = 0$$

Requiring continuity of temperature at the interface levels gives, from equation [C.24], the remaining nine equations:

$$\alpha_m (M_1 - M_2) - (\sigma_1 - \sigma_2) = 0 \qquad [\text{ C.28 }]$$

$$\vdots \qquad \vdots$$

$$\alpha_u (M_9 - M_{10}) - (\sigma_9 - \sigma_{10}) = 0$$

where

$$\alpha_\eta \equiv g\kappa^2 P_\eta^{\kappa}.$$

The 30 equations in 30 unknowns may be written as a single matrix equation.

$$\underline{\underline{B}}\ \underline{C} = \underline{Z}'. \qquad [\text{ C.29 }]$$

The vector $\underline{Z}'$ is composed of the twelve mandatory level heights and 18 zeroes. The vector $\underline{C}$ is the 30-element column vector $\begin{pmatrix} \underline{N} \\ \underline{M} \\ \underline{\sigma} \end{pmatrix}$, where the ten elements of $\underline{N}$, and $\underline{M}$ and $\underline{\sigma}$ correspond to

the ten layers. Equation [C.29] is written out in Figure C-2. This can be represented in a partitioned form as

$$\begin{vmatrix} I_1 & I_2 & I_3 \\ H_1 & H_2 & H_3 \\ G_1 & G_2 & G_3 \end{vmatrix} \begin{vmatrix} \hat{N} \\ \hat{M} \\ \hat{\sigma} \end{vmatrix} = \begin{vmatrix} \hat{Z} \\ 0 \\ 0 \end{vmatrix} \qquad [C.30]$$

with the formal solution

$$\underline{C} = \underline{\underline{B}}^{-1} \underline{Z}'.$$

which can be represented in partitioned form as

$$\begin{vmatrix} \hat{N} \\ \hat{M} \\ \hat{\sigma} \end{vmatrix} = \begin{vmatrix} F_1 & F_2 & F_3 \\ E_1 & E_2 & E_3 \\ D_1 & D_2 & D_3 \end{vmatrix} \begin{vmatrix} \hat{Z} \\ 0 \\ 0 \end{vmatrix} \qquad [C.31]$$

In the analysis, we need a transformation to get stabilities from heights. That transformation is part of matrix $\underline{\underline{B}}^{-1}$, namely $\hat{\underline{\sigma}} = \underline{\underline{D}}_1 \hat{\underline{Z}}$.

We will also need a transform back to heights. For that problem, our set of 30 equations contains 32 unknowns (10 Ns, 10 Ms and 12 Zs). Two of the unknowns will have to be given in order to close the set.

The obvious choice for one of them is the 1000 mb height, since more data is available at the surface than in the upper air. Choosing the second parameter is more difficult. Since the temperature will be computed from the heights, the second parameter might be chosen as a reference for the temperature profile. We chose the thickness of the 1000 - 250 mb layer.

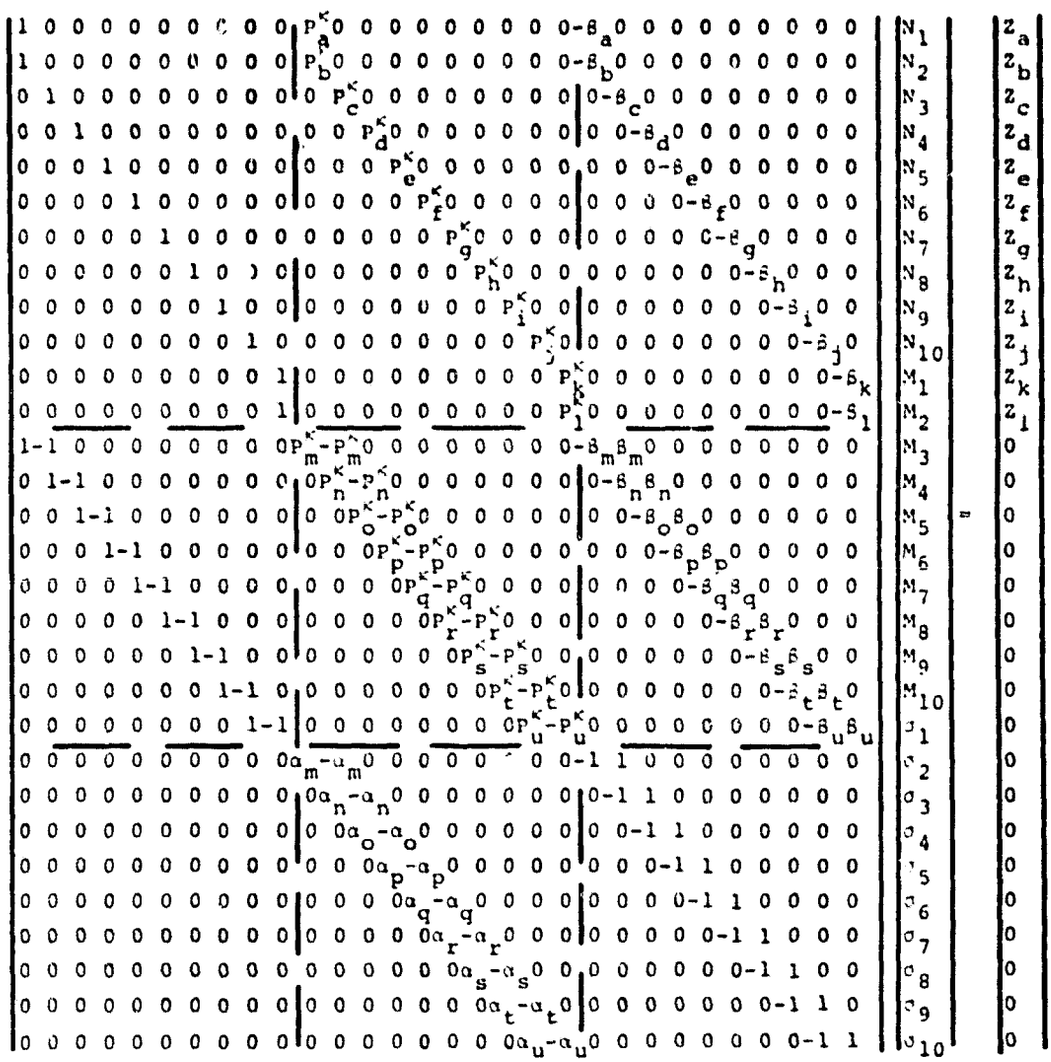

FIGURE C-2: $\underline{\underline{B}}\ \underline{C} = \underline{Z}'$

Define the 12-element column vector $\underline{\Sigma} \equiv \begin{pmatrix} Z_a \\ H \\ \underline{\sigma} \end{pmatrix}$,

where Z_a is the 1000 mb height and H is the 1000 - 250 mb thickness. We need the transformation $\underline{\Sigma} = \underline{\underline{D}}\ \underline{Z}$.

The last ten rows of matrix $\underline{\underline{D}}$ are the first twelve columns of the last ten rows of $\underline{\underline{B}}^{-1}$ (D_1 of [C.31]). The first two rows of $\underline{\underline{D}}$ are

100000000000

-100000001000.

Matrix $\underline{\underline{D}}^{-1}$ may be obtained by Gauss elimination, and the heights can be recovered using $\underline{Z} = \underline{\underline{D}}^{-1}\ \underline{\Sigma}$.

Let us repeat the sequence of operations. At grid points, matrix $\underline{\underline{D}}_1$ is used to convert twelve mandatory level heights to ten layer stabilities. The stabilities are limited to be greater than zero and less than a maximum value if necessary. Then matrix $\underline{\underline{D}}^{-1}$ is used to compute the mandatory level heights at the grid points.

The temperatures at the grid points can now be computed by simply substituting σ and M*, which are submatrices of $\underline{\underline{B}}^{-1}$, into [C.24]. In matrix form, $\underline{T} = \underline{\underline{Q}}\ \underline{\hat{Z}}$ where $\underline{T}$ comprises the twelve mandatory level temperatures, $\underline{\hat{Z}}$ the twelve mandatory level heights and $\underline{\underline{Q}}$ the matrix of [C.24] namely

$$\underline{\underline{D}}_1/R\kappa - \frac{g}{C_p}\, p^{\kappa}\, \underline{\underline{E}}_1. \qquad [\text{ C.32 }]$$

The temperatures and heights at the layer interface levels can be obtained by simply changing the pressures in the matrix coefficients. By proper substitution, the following matrix equation can be formulated:

$$\underline{F} = \underline{\underline{S}}\ \hat{\underline{Z}}$$

where

$$\underline{F} \equiv \begin{pmatrix} \underline{T}_i \\ \underline{Z}_i \end{pmatrix}$$

Vectors $\underline{T}_i$ and $\underline{Z}_j$ are the nine temperatures and heights at the layer interfaces.

APPENDIX D

RADIOSONDE CHECKER

Radiosonde soundings and satellite temperature/height profiles are known to occasionally contain errors due to a garbled transmission or errors in the actual workup of the sounding. The hydrostatic equation can be used as a check on whether reported values at successive levels in the sounding are reasonable. If levels are missing in the sounding, the hydrostatic equation can be used to approximate a value for them. In the current model the heights and temperatures at the 950 and 900 mb levels are analyzed. However, these are not mandatory levels for radiosonde reports, so all "observations" must be generated via this interpolation scheme.

The first part of the radiosonde checking program builds the working array. Significant, and then mandatory, level observations are read and duplicates are removed. The mandatory and significant level observations are then merged into an array in which pressure monotonically decreases (height increases). Tropopause and maximum wind data, if reported, are inserted at the appropriate level. Three major steps complete the process: the array is checked for hydrostatic consistency; heights are assigned to significant level reports; and missing levels are approximated (if possible).

In the first part of the hydrostatic consistency evaluation, the temperature lapse rate is checked using 3 degrees C per 100 meters as a gross measure. If the lapse rate at any level exceeds this, the level is flagged as missing and the check continues until the top of the sounding is reached. Next, an attempt is made to find the station level report to extract the pressure information. Generally, this is the first level reported in a significant level report. Knowing the station elevation, one can calculate the standard station pressure. This is compared to the reported station pressure and, if the two values differ significantly, it is assumed that the station level report is not available. If this is the case, the first reported mandatory level is used for the base height for the hydrostatic workup.

Given a surface pressure, height and temperature, one can calculate, using the hydrostatic equation, the height at the next pressure level if the pressure and temperature at that level are known. These heights are included in the significant level reports and changed in mandatory levels if the report does not appear to be consistent. Below 250 mb, the average height change required to make the sounding hydrostatically consistent is about 5 meters (in a sample size of approximately 450 soundings). Above 250 mb, the change varies from about 8 meters to 10 meters.

Next, missing information in the soundings is replaced by interpolated values. This includes heights, temperatures, dewpoint depression, wind direction and wind speed. The missing levels are interpolated in ln(p) wherever possible. Wind reports from both mandatory and significant levels are merged with tropopause and maximum wind reports.

Finally, the sounding data for the levels analyzed by the mass structure programs are extracted and written to the disk in a format compatible with the analysis input requirements.

APPENDIX E

STRATOSPHERIC HEIGHT-TEMPERATURE EXTRAPOLATION

The method for obtaining stratospheric height and temperature fields is based on the work of Lea (1961). The extrapolated values are given by equations of the form

$$Z=A_o+A_1 Z_{level-1}+A_2 T_{level-1} \quad \text{and}$$

$$T=A_3+A_4 Z_{level-1}+A_5 T_{level-1}.$$

In this manner, the 50 mb fields are extrapolated from the 100 mb height and temperature, 30 mb from the 50 mb, and the 10 mb from the 30 mb. The coefficients, which are a function of latitude and month, were obtained from empirical studies of selected rawinsonde stations. After the fields have been produced they are filtered.